

# **Construction of Ordered Self-Assembled Architectures from Peptide Foldamers Composed of Non-natural Amino Acids**

**A Thesis**

**Submitted in Partial Fulfillment of the  
Requirements of the Degree of**

**Doctor of Philosophy**

**By**

**Sanjit Dey**

**ID: 20143337**

**Research Supervisor: Prof. Hosahudya N. Gopi**



**Indian Institute of Science Education and Research, Pune**

**November 2022**

***“RS”***

***Dedicated to My Family, Teachers,  
and Friends***



# CERTIFICATE

This is to certify that the work incorporated in the thesis entitled “**Construction of Ordered Self-Assembled Architectures from Peptide Foldamers Composed of Non-natural Amino Acids**” submitted by **Sanjit Dey** carried out by the candidate at the Indian Institute of Science Education and Research (IISER), Pune, under my supervision. The work presented here or any part of it has not been included in any other thesis submitted previously for the award of any degree or diploma from any other University or Institution.

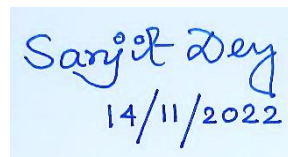
Date: 14/11/2022



**Prof. Hosahudya N. Gopi**  
(Research Supervisor)  
Professor, IISER-Pune  
Pune-411008, India

## Declaration

I hereby declare that the thesis entitled “**Construction of Ordered Self-Assembled Architectures from Peptide Foldamers Composed of Non-natural Amino Acids**” submitted for the degree of Doctor of Philosophy in Chemistry at the Indian Institute of Science Education and Research (IISER), Pune has not been submitted by me to any other University or Institution. This work was carried out at the Indian Institute of Science Education and Research (IISER), Pune, India under the supervision of Prof. Hosahudya N. Gopi.



Sanjit Dey  
14/11/2022

Date: 14/11/2022

**Sanjit Dey**

**ID: 20143337**

Senior Research Fellow

Department of Chemistry, IISER-Pune

Pune-411008

# Acknowledgment

*I would like to express my deepest gratitude to my Research Supervisor Prof. Hosahudya N. Gopi for his constant support, encouragement, and guidance throughout my doctoral program and for completing my dissertation. His guidance has helped me a lot during the time of research and writing of this thesis. I thank Prof. H. N. Gopi, not only for his valuable input and encouragement during my Ph.D. but also for his generous support in my personal life. I am very fortunate and happy to have had the opportunity to work under his supervision and in his laboratory.*

*My sincere thanks to our present Director Prof. Jayant B. Udgaonkar and former Director Prof. K. N. Ganesh for providing excellent infrastructure and research facilities. I would like to express great thanks and gratitude to the all members associated in “IISER-Pune Family”. I would like to acknowledge UGC-India for providing financial support during the last five years.*

*I am sincerely thankful to my research advisory committee members Prof. Seergazhi G. Srivatsan (IISER-Pune) and Dr. Chepuri V. Ramana (NCL-Pune) for their valuable suggestions during my RAC meetings which help me a lot to shape my research projects. I would like to express my sincere thanks to all chemistry faculties of IISER-Pune for their cooperation and help.*

*I am very fortunate to work with wonderful labmates. I would like to express great thanks to Dr. Sushil Benke, Dr. Rajkumar Misra, Dr. Rahi Masoom Reja, Dr. Kuruva Veeresh, and Dr. Anindita Adak for their guidance and support. I am lucky to have such a colleague. I would like to thank all my past and present lab mates Dr. Gigo, Dr. Rabibhushan, Sachin, DR. Puneeth, Manjeet, Souvik, Saikat, Souvik, Sandeep, Abhijit SA, Rajat, Vivek, Nithun, Devannand, and Manish. All are very hard-working, motivated, and supportive in maintaining the lab facilities and keeping the cheerful atmosphere in the lab during my doctoral research.*

*I am thankful to Mr. Nitin, Dr. Sandeep, Mr. Suresh, Mr. Rabindra, Mr. Mahesh, Mr. Yatish, Ms. Megha, Mr. Sandeep, Mr. Praveen, and other technical members of this department for their valuable technical support and help like XRD, NMR, MALDI-TOF/TOF, HRMS, SEM, AFM, TEM, CD, and others. I am very thankful to Mr. Mayuresh and Mr. Tushar for their administrative help.*

*The research and life journey will always be healthy, peaceful, and meaningful in terms of mental and physical even after a lot of ups and downs to resolve problems when you are surrounded by the good people. I am very fortunate to have such kind of wonderful people as “Friends” at IISER-Pune. I am thankful for all my chemistry batchmates (August PhD-2014). A very special thanks to my friends Ajay, Ashok, Balamurugan, Bappa, Chandan, Kamal, Madan, Ganesh, Shatruhan, Vinay, Farsha Ram, Saddam, Pabhan, Rahul, Mohan, Udaya, Neetu, Deepak, Debashis. The moments how we all spend will be as framed with me. Thank you all to be with me. Further, I would like to extend my special thanks to Dr. Dhruva, Dr. Sharad Chandrakant, Dr. Dinesh Pratapsinh, Dr. Sopan, Dr. Bijoyananda, Dr. Soumya, Dr. Shyama, Dr. Debanjan, Dr. Rahul, Dr. Arunava, Dr. Vijayakanth, Dr. Shammi, Dr. Satish, Dr. Dheeraj, Dr. Rishab and most importantly, last but not the least all past and present research scholars of this department for their kind support and valuable interactions.*

*I strongly feel it have difficult to complete my research journey as Ph.D. without support and encouragement and love from where I started my journey of education, Damughosa Board Prathomik School, Tajpur Ramcharan High School, Arambagh High School, Ramakrishna Mission Vivekananda Centenary College, and Presidency College. I am sincerely thankful to all my “Friends and Teachers” from the path of my educational journey.*

*I would like to thank Dr. Sudhanand Prasad Da, Dr. Mukesh Da, Dr. Ajit Da, Mr. Shivsakar Da, Mr. Ratheejit, Mr. Gopal, and Ms. Rimpa for their support and love.*

*I would like to express my deepest gratitude to my “Family Members” for their love, encouragement, support, and shown belief in me, my work, and my way of life. I am and will be always grateful to my family members (Mr. Kinkar Chandra Dey, Smt. Sankari Dey, Mr. Biswajit Dey, Smt. Priyanka Sarkar Dey, Mr. Bidi Ranjan Dey). I would also like to express my appreciation to all my village members in “Damughosa” for their love.*

*Finally, I would like to sign off with a prayer to “Thakur Sree Sree Anukulchandra” Ji for giving me the strength to keep understanding the “Philosophy of Life”.*

***Sanjit Dey***

# *Table of Contents*

Abbreviations .....	xiii
Abstract .....	xv
Synopsis.....	xvii
List of Publications .....	xxviii

## *Chapter 1*

### *General Introduction of Peptide Foldamers Composed of Non-natural Amino Acids*

1. Introduction:.....	2
1.1. Protein Structures:.....	2
1.2. Mimics of Protein Secondary Structures:.....	5
1.2.1. $\beta$ -Amino Acid Based Peptide Foldamers: .....	6
1.2.2. $\gamma$ -Amino Acid Based Peptide Foldamers: .....	8
1.2.3. $\beta$ - and $\gamma$ -Amino Acids Containing Heterogeneous Foldamers: .....	11
1.2.4. $\alpha,\beta$ -Unsaturated $\gamma$ -Amino Acids Based Peptide Foldamers:.....	14
2. Interactions of Peptides and Applications: .....	17
2.1. Peptide-Metals Interaction:.....	19
3. References:.....	20

# Chapter 2A

## *Effect of Substituents to Construct Achiral Double Helices: An Approach of Conformational Adaptation of Peptide Foldamer*

1. Introduction: .....	29
2. Object of the Present Work: .....	31
3. Results and Discussion: .....	32
3.1. Design and Synthesis of Peptides P1-P4: .....	32
3.2. Crystal Structure Analysis of Peptides (P1-P4): .....	34
3.2.1. Crystal Structure Analysis of Peptide (P1): .....	34
3.2.2. Crystal Structure Analysis of Peptide (P2): .....	36
3.2.3. Crystal Structure Analysis of Peptide (P3): .....	38
3.2.4. Crystal Structure Analysis of Peptide (P4): .....	40
4. Conclusion: .....	42
5. Experimental Section: .....	42
5.1. General Method: .....	42
5.2. Procedure for the Synthesis of Peptides: .....	43
5.2.1. Synthesis of Building Unit 1c: .....	43
5.2.2. Synthesis of Building Unit 2b: .....	43
5.2.3. Synthesis of Peptide(P1): .....	44
5.2.4. Synthesis of Peptide(P2): .....	45
5.2.5. Synthesis of Peptide(P3): .....	46
5.2.6. Synthesis of Peptide(P4): .....	48



6. Appendix:.....	54
6.1. ORTEP Diagrams:.....	54
A) ORTEP Diagram of Peptide(P1):.....	54
B) ORTEP Diagram of Peptide(P2):.....	55
C) ORTEP Diagram of Peptide(P3):.....	56
D) ORTEP Diagram of Peptide(P4):.....	57
6.2. Crystal Structure Information:.....	58
6.3. Torsion Angle Parameters:.....	59
7. References:.....	60
8. <sup>1</sup> H, <sup>13</sup> C NMR and Mass Spectra of Peptides P1-P4:.....	63

## *Chapter 2B*

### *Chirality Induction on Achiral Double Helices*

1. Introduction:.....	81
2. Results and Discussion:.....	81
2.1 Design and Synthesis of Peptides P5-P9:.....	81
2.2 Crystal Structure Analysis of Peptide P5:.....	82
2.3 Solution State Conformational Analysis of Peptides P6 and P7:.....	85
2.4 Circular Dichroism(CD) Spectroscopy of Peptides P6 and P7:.....	88
2.5. Crystal Structure Analysis of Chiral Double helix of Peptide P8:.....	89
2.6. Circular Dichroism(CD) Spectroscopy of Peptides P8 and P9:.....	91
3. Conclusion:.....	91
4. Experimental Section:.....	92

4.1. General Method: .....	92
4.2.1. Procedure for the Synthesis of Peptides (P5, P6, and P8):.....	92
4.2.2. Procedure for the Synthesis of Peptides (P7, P9):.....	94
4.3. Characterization of Peptides(P5-P7): .....	95
5. Appendix:.....	96
5.1 ORTEP Diagrams: .....	96
A) ORTEP Diagram of Peptide(P5):.....	96
B) ORTEP Diagram of Peptide(P8): .....	97
5.2. Crystal Structures Information: .....	98
6. References:.....	99
7. <sup>1</sup> H, and Mass Spectra of Peptides P5-P9: .....	100

## *Chapter 3*

### *Metal-Ions Tuned Structural Modulation of Metal-Helical Peptide Coordination Assemblies: Architectures from Porous Framework to Hierarchical Superhelix*

1. Introduction:.....	105
2. Object of the Present Work:.....	106
3. Results and Discussion: .....	107
3.1. Design and Synthesis of Peptides P1-P7:.....	107
3.2. Crystal Structure Analysis of Peptides P1, and P2:.....	108
3.3. Metal-Peptide Coordinated Supramolecular Assembly of Peptide P1:..	111
3.4. Metal-Peptide Coordinated Supramolecular Assembly of Peptide P2:..	117
3.5. Crystal Structure Analysis of Metal-Peptide Complexes:.....	122

4. Conclusion: .....	127
5. Experimental Section: .....	127
5.1. General Method: .....	127
5.2. Procedure for the Synthesis of Peptides: .....	128
5.2.1. Synthesis of Peptide(P1):.....	128
5.2.2. Synthesis of Peptide(P2):.....	130
5.3. Characterization of Peptides(P1-P2): .....	131
6. Appendix:.....	132
6.1. Crystallographic Information: .....	132
7. References:.....	135
8. <sup>1</sup> H, <sup>13</sup> C NMR and Mass Spectra of Peptides (P1-P2): .....	140

## *Chapter 4*

### *Metal Coordinated Supramolecular Polymers from the Minimalistic Hybrid Peptide Foldamers*

1. Introduction:.....	145
2. Object of the Present Work:.....	146
3. Results and Discussion: .....	147
3.1. Design and Synthesis of Peptides P1-P7:.....	147
3.2. Crystal Structure Analysis of Peptides P1, P2, P5, P6, and P7:.....	148
3.3. Solution State Conformational Analysis of Peptide P3:.....	152
3.3.1. TOCSY Spectrum of Peptide P3: .....	152
3.3.2. NH↔NH NOEs of Peptide P3: .....	153
3.3.3. C <sub>α</sub> H↔NH NOEs of Peptide P3:.....	153

3.3.4. NOEs Observed of Peptide P3: .....	154
3.4. Metal-Peptide Gelation Studies of Peptides P1- P7: .....	155
3.5. Investigation of Supramolecular Self-assemble Properties of Metal- Peptide Gel:.....	158
3.6. Circular Dichroism(CD) Analysis: .....	161
3.7. Viscoelastic Property of Peptide-Metallogel:.....	162
3.8. FT-IR Supports Extended Structures in Gel Matrix:.....	162
3.8. Metal-Peptide Coordinated Supramolecular Assembly: .....	163
4. Conclusion: .....	170
5. Experimental Section: .....	170
5.1. General Method: .....	170
5.2. Procedure for the Synthesis of Peptides: .....	171
5.2.1. Synthesis of Peptide(P1):.....	171
5.2.2. Synthesis of Peptide(P2):.....	173
5.2.3. Synthesis of Peptide(P3):.....	174
5.2.4. Synthesis of Peptide(P4):.....	174
5.2.5. Synthesis of Peptide(P5):.....	175
5.2.6. Synthesis of Peptide(P6):.....	175
5.2.7. Synthesis of Peptide(P7):.....	176
5.3. Characterization of Peptides(P1-P7): .....	176
6. Appendix:.....	180
6.1. Crystallographic Information: .....	180
7. References:.....	183
8. <sup>1</sup> H, <sup>13</sup> C NMR and Mass Spectra of Peptides (P1-P7): .....	186

## Abbreviations

ACN = Acetonitrile

AcOH = Acetic acid

Aib =  $\alpha$ -Amino isobutyric acid

aq. = Aqueous

AFM = Atomic Force Microscopy

Boc = tert-Butoxycarbonyl

(Boc)<sub>2</sub>O = Boc anhydride

Calcd. = Calculated

CD = Circular Dichroism

CIF = Crystallographic Information File

COSY = COrrelation SpectroscopY

d $\gamma$  = dehydro gamma

DBU = 1,8-Diazabicyclo(5.4.0)undec-7-ene

DCC = N, N' -Dicyclohexylcarbodiimide

DCM = Dichloromethane

DIPEA = Diisopropylethyl Amine

DMF = Dimethyl formamide

DMSO = Dimethyl Sulphoxide

EtOH = Ethanol

Et = Ethyl

EDC,HCl = N-(3-Dimethylaminopropyl)-N'-ethyl carbodiimide hydrochloride

EtOAc = Ethyl acetate

g = gram

h = hours

HBTU = 2-(1H-benzotriazole-1-yl)-1, 1, 3, 3-tetramethyluronium hexafluorophosphate

H-bond = Hydrogen bond

HOBt = Hydroxybenzotriazole

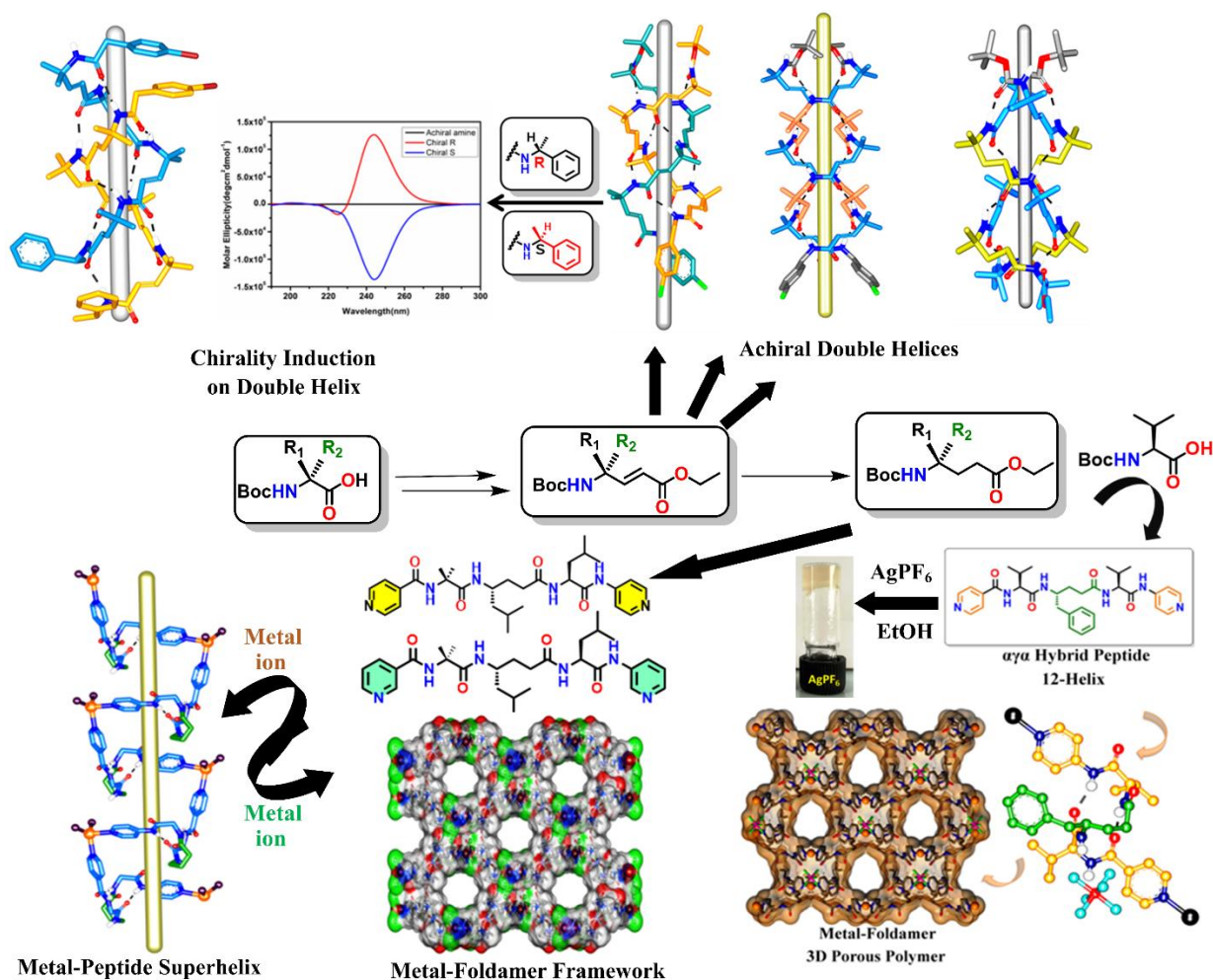
HOAt = 1-Hydroxy-7-azabenzotriazole

HCl = Hydrochloric acid  
IR = Infrared spectroscopy  
M = Molar  
MALDI-TOF/TOF = Matrix-Assisted Laser Desorption/Ionization-Time of Flight  
MeOH = Methanol  
mg = Milligram  
min = Minutes  
 $\mu\text{L}$  = Micro liter  
mL = Milliliter  
mM = Millimolar  
mmol = millimoles  
MS = Mass Spectroscopy  
N = Normal  
NHS = N-hydroxy succinimide  
NMP = N-methyl pyrrolidone  
NMR = Nuclear Magnetic Resonance  
NOE = Nuclear Overhauser Effect  
ORTEP = Oak Ridge Thermal-Ellipsoid Plot Program  
PG = Protecting Group  
ppm = Parts per million  
Py = Pyridine  
ROESY = **R**otating-frame nuclear **O**verhauser **E**ffect correlation **S**pectroscop**Y**  
RP- HPLC = Reversed Phase-High Performance Liquid Chromatography  
RT = Room Temperature  
SEM = Scanning Electron Microscopy  
TEM = Transmission Electron Microscopy  
TFA = Trifluoroacetic acid  
THF = Tetrahydrofuran  
UV = Ultraviolet-Visible Spectroscopy  
TOCSY = **T**otal **C**orrelation **S**pectroscop**Y**

# Abstract

Inspired by the functions of proteins and metalloproteins, extensive efforts have been made over the years to mimic their structures and functions using non-natural amino acid building blocks. The folded structures derived from the oligomers of beta, gamma, and delta amino acids and their mixed sequences along with alpha-amino acids offer a wide range of structural diversity with potential applications in biology and materials. In our previous studies, we have shown the remarkable beta-double helical structures from the homo-oligomers of 4,4-dimethyl substituted (*E*)-vinyllogous amino acids and stable helical structures from short sequences of alpha, gamma-hybrid peptides. However, understanding the requirement of amino acid residues and peptide sequences to form a double helical structure was an illusion. In the present study, we have revealed that the beta-double helical structures not confined to the oligomers 4,4-dimethyl substituted (*E*)-vinyllogous amino acids, even the mixed sequences composed of 3,3-dimethyl substituted  $\gamma$ -amino acid (Adb) along with 4,4-dimethyl substituted (*E*)-vinyllogous amino acids and also form artificial beta double-helical structures. In sharp contrast, replacing 3,3-dimethyl gamma-amino acids with 4,4-dimethyl gamma-amino acids also leads to double helical structures. The structural analysis of the double helix shows achiral in nature. Furthermore, we have examined the transformation of the achiral nature of the beta-double helices into chiral double helices by attaching chiral amines at the C-terminal of the peptides. Both single crystal structure and solution state analysis reveal that even after attaching a chiral amine, the peptide maintained its double helical nature, and chirality is induced throughout the peptide sequences. In contrast to the double helical structures, the  $\alpha\gamma\alpha$ -hybrid tripeptides composed of saturated gamma-amino acids gave stable helical structures in single crystals and solution state. We have examined these stable helical structures in the construction of various types of metal-coordinated ordered supramolecular architectures. We have used  $\text{Ag}^+$ ,  $\text{Cu}^{2+}$ ,  $\text{Zn}^{2+}$ , and  $\text{Cd}^{2+}$  ions to understand the helical structure organization in the presence of metal ions. The stable caged porous networks obtained in the presence of  $\text{ZnCl}_2$  have been further explored as hosts to encapsulate guest solvent molecules. On the other hand, the structural analysis of  $\text{CdI}_2$ -coordinated peptide reveals entirely different, remarkable left-handed superhelical architectures. Instructively, the hybrid tripeptide with valine residues forms metallogels in the presence of  $\text{Ag}^+$  and  $\text{Cu}^{2+}$  ions. The X-ray analysis of single crystals obtained from the gel matrix reveals that the helical structure is maintained during the self-assembly process. Overall, the sterically constrained chiral and achiral gamma-amino acids can be used

to construct different types of peptide foldamers. These secondary structure mimetics can be used to construct remarkably ordered supramolecular assemblies. The work presented here opens a new window to further explore these short helices and beta-double helices as new tools for the design of peptide-based biomaterials.





# Synopsis

## Chapter 1

### *General Introduction of $\beta$ - and $\gamma$ -peptide foldamers*

Proteins play a critical role in all biological events of living organisms. The functions of proteins mainly depend on their three-dimensional structures. The structure-function relationships of proteins have inspired chemists to construct protein structure mimetics using various types of unnatural building blocks.<sup>1</sup> Extensive efforts have been made in the literature to design protein structure mimetics using sterically constrained  $\alpha,\alpha$ -gem-dialkyl substituted  $\alpha$ -amino acids. In addition to the sterically constrained  $\alpha$ -amino acids, a variety of non-ribosomal amino acids as well as organic templates have been explored to construct the protein structure mimetics.<sup>2</sup> Among the different types of non-ribosomal amino acids and organic templates,  $\beta$ - and  $\gamma$ -amino acids have been extensively investigated to construct protein secondary structure mimetics (Foldamers).<sup>3</sup>

The  $\beta$ -amino acids are the backbone homologated analogs of  $\alpha$ -amino acids. These  $\beta$ -amino acids can be classified as  $\beta^3$ -,  $\beta^{3,3}$  and  $\beta^2$ -,  $\beta^{2,2}$ - and  $\beta^{2,3}$ - amino acids based on the position of amino acid side-chains.<sup>4</sup> In addition to the acyclic  $\beta^3$ - and  $\beta^2$ -amino acids, a variety of cyclic  $\beta$ -amino acids have been synthesized and utilized to design protein structure mimetics.<sup>5</sup> The  $\beta$ -peptides constructed from the  $\beta$ -amino acids have been shown to adopt various types of helical structures. Based on their intramolecular H-bonds, the  $\beta$ -peptide helices can be classified as  $C_{14}$ -,  $C_{12}$ -,  $C_{10}$ - and  $C_8$ -helices.<sup>6</sup> The numbers in the subscript indicate the total number of atoms involved in the one H-bond pseudo cycle. In addition, the  $\beta$ -peptide helices have also displayed different polarities compared to  $\alpha$ -peptide helices. The  $C_8$ - and  $C_{12}$ -helices of  $\beta$ -peptides have displayed the same hydrogen bonding directionality as  $\alpha$ -peptides ( $C \leftarrow N$ ), whereas  $C_{10}$ - and  $C_{14}$ - helices showed opposite H-bond directionality ( $N \leftarrow C$ ).<sup>7</sup> Another interesting feature of  $\beta$ -peptide foldamers is that, they also display mixed H-bonding consisting of opposite H-bond polarities within the same helix.<sup>8-10</sup>

$\gamma$ -Amino acids are homologated analogs of  $\beta$ -amino acids. The  $\gamma$ -amino acids can be recognized as  $\gamma^4$ -,  $\gamma^3$ -,  $\gamma^2$ -,  $\gamma^{4,4}$ -,  $\gamma^{3,3}$ -,  $\gamma^{2,2}$  and  $\gamma^{2,3,4}$ - amino acids based on the position of the side chain on the amino acid's backbone.<sup>11</sup> In comparison to  $\beta$ -amino acids  $\gamma$ -amino acids have

not been much explored, however many diverse structures can be expected from  $\gamma$ -amino acid oligomers. The groups Seebach and Hanessian showed the 14-helical conformations of the oligomers of  $\gamma^4$ -amino acids as well as 2, 3, and 4 substituted  $\gamma$ -amino acids.<sup>12,13</sup> In addition, Balaram and colleagues demonstrated C<sub>9</sub> helical conformations from  $\gamma^{3,3}$ -amino acid oligomers.<sup>14</sup>

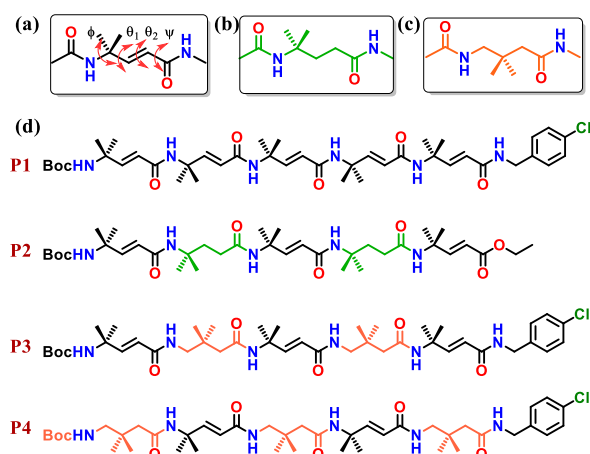
In contrast to the homo-oligomers of  $\beta$ - and  $\gamma$ -peptides, the mixed sequences consisting of  $\alpha$ -,  $\beta$ -, and  $\gamma$ -amino acids have attracted considerable attention. The advantage of the mixed sequences is that it provides an opportunity to design a variety of helices by varying the sequence patterns of different amino acids. Balaram and colleagues demonstrated a variety of hybrid helices in the combination of  $(\alpha\beta)_n$ - and  $(\alpha\gamma)_n$ -sequences.<sup>15,16</sup> Gellman and colleagues reported C<sub>11</sub>- C<sub>14/15</sub>- C<sub>11/11/12</sub>-helix and C<sub>10/11/11</sub> from  $\alpha$ ,  $\beta$ -hybrid peptides.<sup>17</sup> In addition, the same group reported 13-helices from  $\beta,\gamma$ -hybrid peptides.<sup>18</sup> The hybrid peptide foldamers have been explored to design antimicrobials,<sup>19</sup> p53-HDM2 inhibitors,<sup>20</sup> HIV inhibitors,<sup>21</sup> human cytomegalovirus entry inhibitors,<sup>22</sup> and in the field of supramolecular self-assembly.<sup>23</sup> Using theoretical calculations, Hofmann and colleagues predicted a range of helical structures available to 1:1 alternating  $\alpha$ - and  $\gamma$ - amino acids and also to the oligomers of (*E*)- and (*Z*)- $\alpha,\beta$ -unsaturated  $\gamma$ -amino acids.<sup>24,25</sup> We demonstrated the 12-helical structures from  $\alpha,\gamma$ -hybrid peptides composed of  $\alpha$ - and  $\gamma^3$ -amino acids.<sup>26</sup> Further, we showed the utilization of (*E*)- $\alpha,\beta$ -unsaturated  $\gamma$ -amino acids in the design of  $\beta$ -hairpins, multi-stranded  $\beta$ -sheets and the accommodation of (*Z*)-vinylogous amino acids in hybrid 12-helical structure.<sup>27-30</sup> In this thesis, we are demonstrating the utilization of geometrically constrained (*E*)-  $\alpha,\beta$  unsaturated  $\gamma$ -amino acids in the design of  $\beta$ - double helices, chiral double helices, substitution effects in the design of double helices, exploration of short  $\alpha,\gamma$ -hybrid peptides as templates to construct metal-helix-frameworks, metal-coordinated helical polymers, and metallogels.

## ***Chapter 2A***

### ***Effect of Substituents to Construct Achiral Double Helices: An Approach of Conformational Adaptation of Peptide Foldamer***

Double helices are the most important structural features of nucleic acids. The double helical structural motif plays a crucial role in the storage of genetic information in nucleic acids. The double helical structures are rarely observed in other natural biopolymers. In addition to DNA, naturally occurring gramicidin A and feglymycin adopt double helical conformations.<sup>31</sup> In

addition, synthetic analogues of gramicidin A, alternating L- and D-peptides,<sup>32</sup> oligomers of aromatic oligoamide,<sup>33</sup> and metal-coordinated aromatic oligoamides have been shown to adopt double helical conformations.<sup>34</sup> Recently, we demonstrated that oligomers composed of (*E*)  $\alpha,\beta$ -unsaturated 4,4-dialkyl  $\gamma$ -amino acids adopted double helical conformations, whereas  $\alpha,\beta$ -unsaturated  $\gamma$ -amino acid oligomers without dialkyl constraints at  $\gamma$ -position adopt  $\beta$ -sheet type structures in single crystals.<sup>35</sup> Encouraged by these fascinating double helical structures from  $\alpha,\beta$ -unsaturated  $\gamma$ -amino acids, we sought to investigate the necessity of the double bonds in dialkyl  $\gamma$ -amino acids in adopting double helical conformations. In this Chapter, we are reporting the conformational properties of 1:1 alternating unsaturated and saturated 4,4-dialkyl  $\gamma$ -amino acids (Aic) and 3,3-dialkyl  $\gamma$ -amino acids (Adb). We designed pentapeptides, **P1-P4** (Scheme 1), synthesized in the solution phase method and studied their conformations in single crystals.



**Scheme 1:** (a-c) The building block amino acid residues used. (d) Sequences of design peptides (**P1-P4**)

The X-ray diffracted single crystal structures of **P1-P4** are shown in Figure 1. The structural analysis revealed that **P1-P3** adopted double helical conformations. Peptide **P4** consisting of 3,3-dialkyl  $\gamma$ -amino acids at the N- and C- terminus of peptide adopted distorted double-helical conformation. The double helix structure is distorted at the terminals. In addition, all four peptides have displayed distinct H-bonding patterns in the double helical conformations. The torsion angles of  $\alpha,\beta$ -unsaturated 4,4-dialkyl  $\gamma$ -amino acid residue are consistent with the previously reported double helix structures.

Overall, the single crystal analysis of the peptides **P1-P4** revealed that the 4,4-dialkyl  $\gamma$ -amino acids (Aic) and 3,3-dialkyl  $\gamma$ -amino acids (Adb) can be accommodated into the  $\beta$ -

double helical conformation in combination with (*E*)- $\alpha,\beta$ -unsaturated 4,4-dialkyl  $\gamma$ -amino acid residues (dgAic). The (*E*)- $\alpha,\beta$ -unsaturated 4,4-dialkyl  $\gamma$ -amino acid residues are essential to induce double-helical conformation in  $\gamma$ -peptide foldamers.

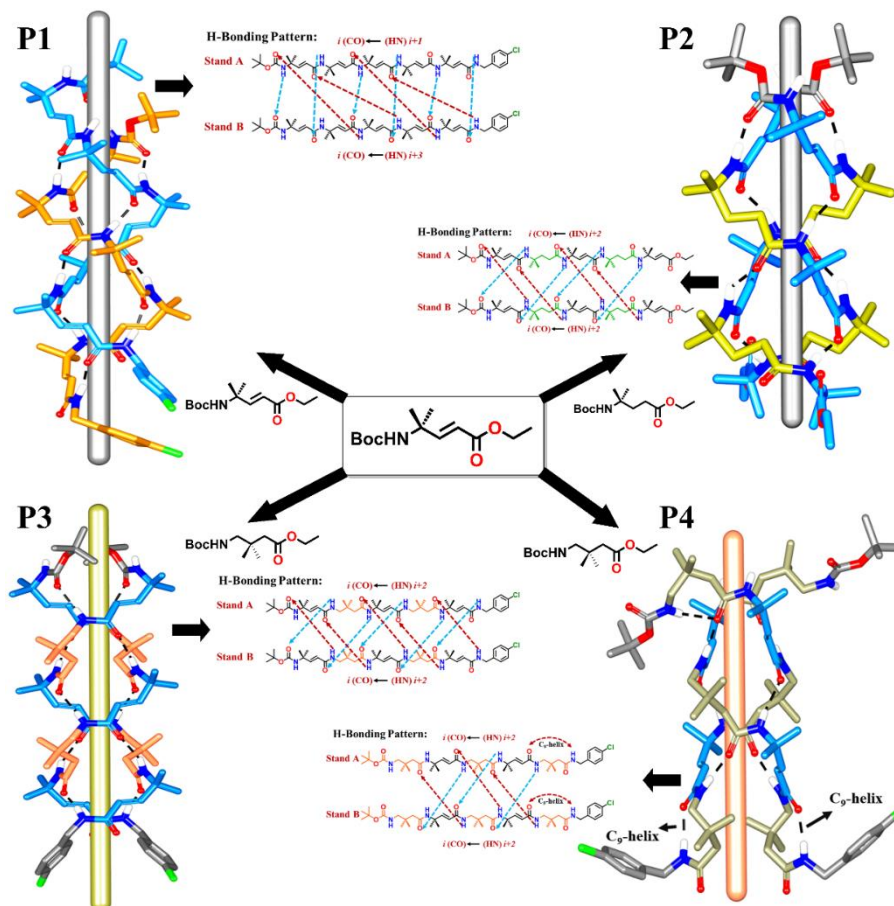


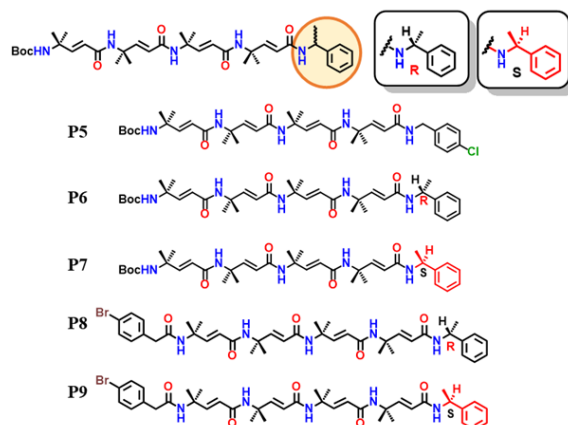
**Figure 1:** Single crystal structure of **P1-P4** (for clarity, pictorially rods are created along the central axis) and intermolecular hydrogen bonding pattern between two **strand A** and **strand B** are shown.

## Chapter 2B

### Chirality Induction on Achiral Double Helices

In the previous section 2A, we demonstrated the  $\beta$ -double helix conformations from the  $\gamma$ -peptides consisting of achiral (*E*)- $\alpha,\beta$ -unsaturated 4,4-dialkyl  $\gamma$ -amino acids. In addition, we have shown the accommodation of 4,4-dimethyl and 3,3-dimethyl  $\gamma$ -amino acids into the double helical conformations without deviating from the overall double helix fold. So far, the double helical structures reported from the  $\gamma$ -peptide foldamers are achiral in nature. In this context, we sought to investigate the possibilities of designing the chiral  $\beta$ -double helical structures. As the  $\gamma$ -peptide double helices consist of achiral amino acids, we hypothesized that

it may be possible to construct chiral double helices by coupling chiral amines at the C-terminus of the achiral peptides. To realize the hypothesis, peptides **P5-P9** were designed and synthesized. The sequences of these peptides are shown in Scheme 2. Out of these, we got the single crystals for the peptides **P5** and **P8**. The achiral **P5** and chiral **P8** adopted double helix conformations in single crystals, however with different H-bonding patterns. The crystal structures and the H-bonding patterns of **P5** and **P8** are shown in Figure 2.



**Scheme 2:** Sequences of design peptides **P5-P9** for chirality induction on the achiral double helix.

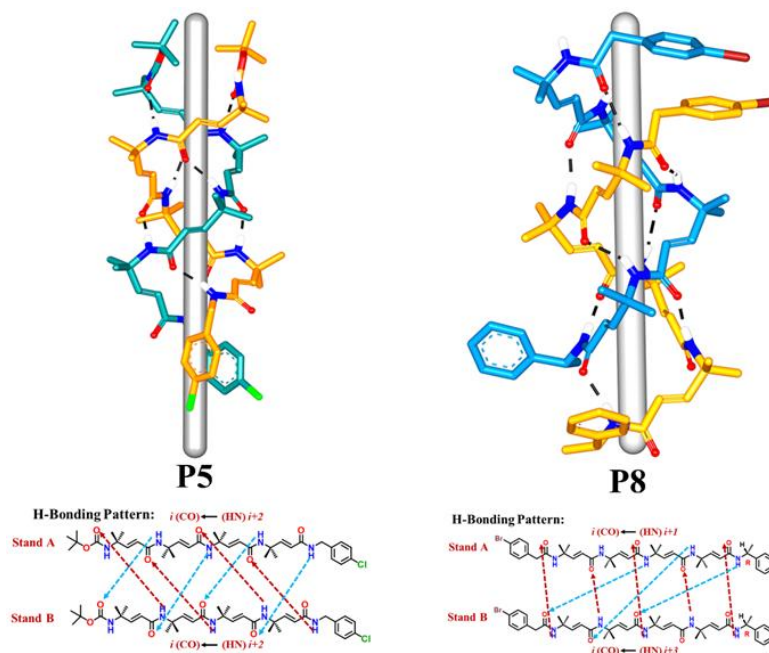


**Figure 2:** Single crystal structure of **P5** and **P8** (to get a better view of parallel  $\beta$ -double helices, pictorially rods are created along the central axis) and intermolecular hydrogen bonding pattern between two **strand A** and **strand B** are shown.

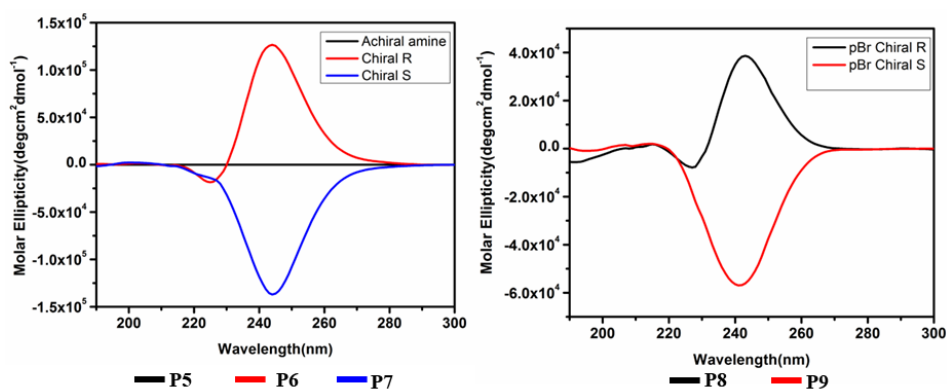


**Figure 3:** Circular Dichroism (CD) spectra of peptides **P5-P9** showing chirality induction.

Further, we subjected all peptides to circular dichroism spectroscopy to understand their solution conformations. The CD analysis revealed remarkable results on the chirality of the peptides. The peptides **P6** and **P8** coupled chiral (*R*) amine displayed CD maxima at around 245 nm, whereas **P7** and **P9** coupled with the chiral (*S*) amine displayed exactly opposite spectra with CD minima at around 245 nm. The achiral **P5** is CD inactive. The CD signatures of chiral double helices are shown in **Figure 3**.

The results reported here suggested that a single chiral atom can induce the chirality across the double helix. In addition, these results also advocated chiral double helices can be designed by introducing one chiral atom at the C-terminus of the achiral peptide.

### Chapter 3

#### *Metal-Ions Tuned Structural Modulation of Metal-Helical Peptide Coordination Assemblies: Architectures from Porous Framework to Hierarchical Superhelix*

Metal-coordinated supramolecular assembly of various organic and biomolecules represents a powerful approach for constructing discrete and well-defined three-dimensional architectures.<sup>36-38</sup> Recently, metal-coordinated peptide architectures are gaining momentum due to their close resemblance to native biological systems.<sup>39-40</sup> In this chapter, we investigated the formation of metal coordinated architectures from  $\alpha\gamma\alpha$ -hybrid tripeptide 12-helices containing terminal 4- or 3-pyridyl groups in combination with  $Zn^{2+}$  and  $Cd^{2+}$  metal ions. The sequences of  $\alpha\gamma\alpha$ -hybrid tripeptides and metal-coordinated single crystal structures are shown in **Figure 4**.

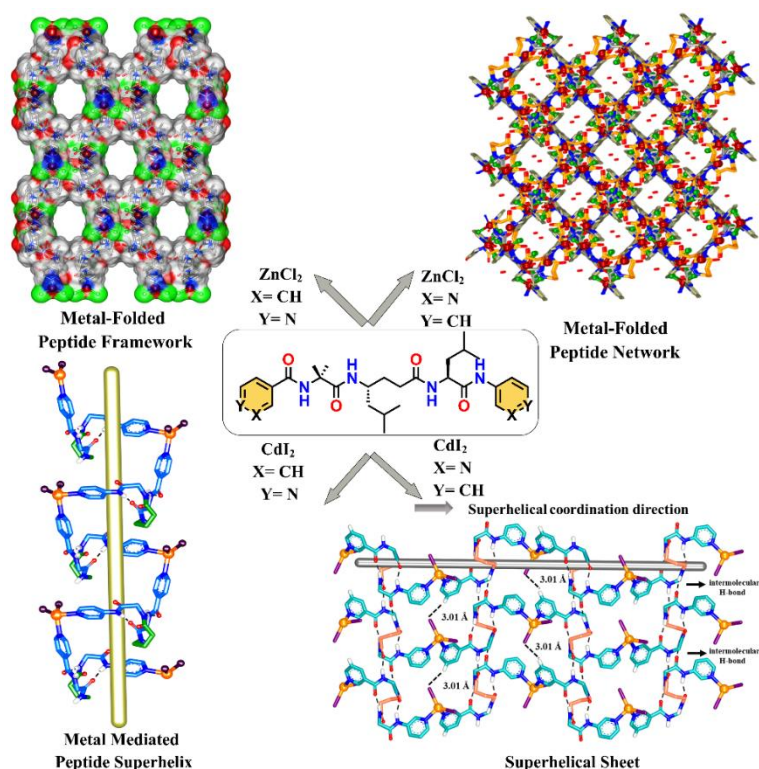


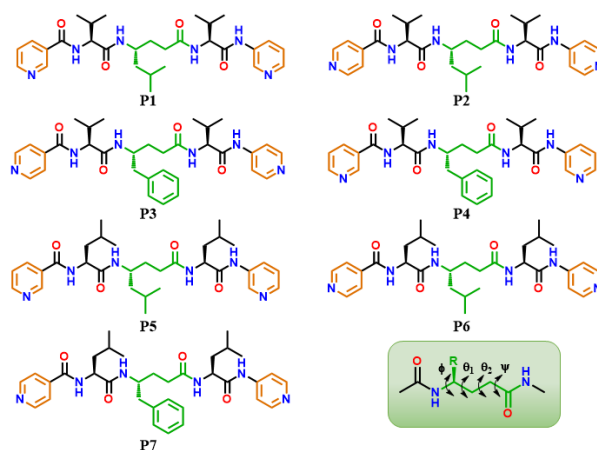
**Figure 4:** Metal-coordinated structural architectures of  $\alpha\gamma\alpha$ -hybrid tripeptides.

The X-ray diffracted single-crystal structure analysis revealed that the peptide helix terminated with 4-pyridyl groups displayed a stable porous framework upon coordinating with  $\text{ZnCl}_2$ . These porous frameworks have been further explored to encapsulate guest molecules. Interestingly, the positional isomeric ligand, the peptide helix terminated with 3-pyridyl groups upon coordination with  $\text{ZnCl}_2$  revealed a different coordination assembly with low porosity. On the other hand, the single-crystal structural analysis of  $\text{CdI}_2$ -coordinated peptide helices displayed remarkable right-handed superhelical architectures. However, the superhelical architecture from the helix containing 3-pyridyl groups further assembled into new hierarchical superhelical  $\beta$ -sheet type structural motifs stabilized by intermolecular H-bonds. The short helical peptide ligands displayed an intriguing variety of ordered structural architectures in combination with different metal ions.

## Chapter 4

### *Metal-Coordinated Supramolecular Polymers from the Minimalistic Hybrid Peptide Foldamers*

Availing the peptide folded architectures to design metal-coordinated frameworks and cages is restricted due to the scarcity of readily accessible short and stable secondary structures. The secondary structures,  $\alpha$ -helix and  $\beta$ -sheets, play significant roles in stabilizing tertiary folds of proteins. Designing such helical structures from the short sequences of peptides without having any steric restrictions is exceptionally challenging. In this chapter, we reveal the short  $\alpha,\gamma$ -hybrid tripeptide sequences that manifest stable helical structures without having any sterically constrained amino acids. These short hybrid tripeptides fold into helices even in the presence of two typically  $\beta$ -sheet favoring Val residues. The sequences of peptides **P1-P7** are given in Scheme 3.



**Scheme 3:** The sequences of design peptides **P1-P7** and torsion parameters of  $\gamma$ -amino acid are shown.

The hybrid helix consisting of terminal pyridine units coordinates with the metal ions and drives the helical polymerization. Depending on the sequence and the position of N in pyridine moieties, these peptides form selective metallogels with  $\text{Ag}^+$  and  $\text{Cu}^{2+}$  ions. The X-ray diffracted analysis of the peptide single crystals obtained from the gel matrix reveals that the helical structure is maintained during the self-assembly process shown in Figure 5. Further, by varying the counter anion, a 3D helical crystalline coordination polymer with permanent porosity is generated. The findings reported here can be used to design new functional metal-foldamer coordinated polymers.



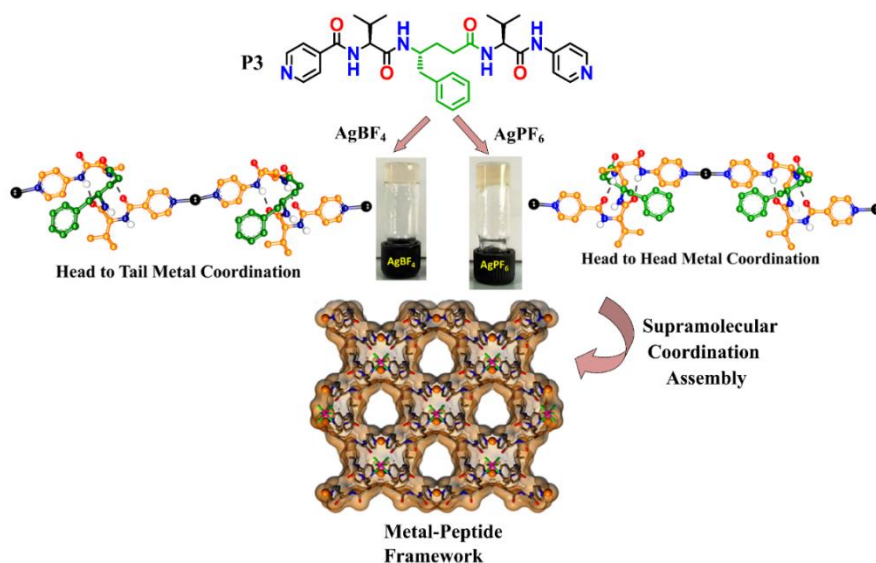


**Figure 5:** Effect of the counter anion of  $\text{Ag}^+$  ion with **P3** and coordination assembly.

Overall, we explored the utilization of unnatural  $\gamma$ -amino acids to design protein secondary structures and examined their supramolecular architectures.

### References:

1. (a) Seebach, D.; Beck, A. K.; Bierbaum, D. J. *Chem. Biodiversity* **2004**, *1*, 1111. Cheng, R. P.; Gellman, S. H.; DeGrado, W. F. *Chem. Rev.* **2001**, *101*, 3219
2. (a) Karle, I. L.; Balaram, P. *Biochemistry*, **1990**, *29*, 6747. (b) Karle, I. L. *Acc. Chem. Res.* **1999**, *32*, 693.
3. (a) Hecht, S.; Huc, I. *Foldamers: Structure, Properties and Applications*; Wiley-VCH: Weinheim, **2007**.
4. a) Seebach, D.; Matthews, J. L. *Chem. Commun.*, **1997**, 2015. (b) Seebach, D.; Gardiner, J. *Acc. Chem. Res.*, **2008**, *41*, 1366. (c) Hintermann, T.; Gademann, K.; Jaun, B.; Seebach, D. *Helv. Chim. Acta.* 1998, *81*, 893. (d) Hanessian, S.; Luo, X.; Schaum, R.; Michnick, S. *J. Am. Chem. Soc.* **1998**, *120*, 8569.
5. Gellman, S. H. *Acc. Chem. Res.* **1998**, *31*, 173.
6. Venkatraman, J.; Shankaramma, S. C.; Balaram, P. *Chem. Rev.* **2001**, *101*, 3131
7. Martinek, T. A.; Fulop, F. *Chem. Soc. Rev.*, **2012**, *41*, 687.
8. Horne, W. S.; Gellman, S. H. *Acc. Chem. Res.*, **2008**, *41*, 1399
9. Mándity, I. M.; Weber, E.; Martinek, T. A.; Olajos, G.; Tóth, G. K.; Vass, E.; Fülöp, F. *Angew. Chem., Int. Ed.* **2009**, *48*, 2171.

10. Baldauf, C.; Günther, R.; Hofmann, H. -J.; *Helv. Chim. Acta*, **2003**, *86*, 2573.
11. Vasudev, P. G., Chatterjee, S., Shamala, N., Balaram, P. *Chem. Rev.*, **2011**, *111*, 657.
12. (a)Hintermann, T.; Gademann, K.; Seebach, D. *Helv. Chim. Acta*. **1998**, *81*, 893.  
(b)Arvidsson, P. I.; Rueping, M.; Seebach, D. *Chem. Commun.* **2001**, 649
13. Hanessian, S.; Luo, X.; Schaum, R.; Michnick, S. *J. Am. Chem. Soc.* **1998**, *120*, 8569.
14. Vasudev, P. G.; Shamala, N.; Ananda, K.; Balaram, P. *Angew. Chem., Int. Ed.* **2005**, *44*, 4972.
15. Vasudev, P. G.; Chatterjee, S.; Shamala, N.; Balaram, P. *Acc. Chem. Res.* **2009**, *42*, 1628.
16. Vasudev, P. G.; Chatterjee, S.; Ananda, K.; Shamala, N.; Balaram, P. *Angew. Chem., Int. Ed.* **2008**, *47*, 6430.
17. (a)Giuliano, M. W.; Horne, W. S.; Gellman, S. H. *J. Am. Chem. Soc.* **2009**, *131*, 9860.  
(b) Price, J. L.; Horne, W. S.; Gellman, S. H. *J. Am. Chem. Soc.* **2010**, *132*, 12378
18. Guo, L.; Almeida, A. M.; Zhang, W.; Reidenbach, A. G.; Choi, S. H.; Guzei, I. A.; Gellman, S. H. *J. Am. Chem. Soc.* **2010**, *132*, 7868
19. (a) Epand, R. F.; Raguse, T. L.; Gellman, S. H., Epand, R. M. *Biochemistry*, **2004**, *43*, 9527. (b) Hamuro, Y.; Schneider, J. P.; DeGrado, W. F. *J. Am. Chem. Soc.*, **1999**, *121*, 12200.
20. Kritzer, J. A.; Lear, J. D.; Hodsdon, M. E.; Schepartz, A. *J. Am. Chem. Soc.* **2004**, *126*, 9468.
21. Stephens, O. M.; Kim, S.; Welch, B. D.; Hodsdon, M. E.; Kay, M. S.; Schepartz, A. *J. Am. Chem. Soc.* **2005**, *127*, 13126.
22. English, E. P.; Chumanov, R. S.; Gellman, S, H.; Compton, T. *J. Biol. Chem.* **2006**, *28*, 2661.
23. Kim, J.; Kwon, S.; Kim, S. H.; Lee, C.-K.; Lee, J. -H.; Cho, S. J.; Lee, H. -S.; Ihee, H. *J. Am. Chem. Soc.* **2012**, *134*, 20573.
24. Baldauf, C.; Gunther, R.; Hofmann, H. J. *Helv. Chim. Acta.* **2003**, *86*, 2573.
25. Baldauf, C.; Gunther, R.; Hofmann, H. -J. *J. Org. Chem.* **2006**, *71*, 1200.
26. Jadhav, S. V.; Bandyopadhyay, A.; Gopi, H. N. *Org. Biomol. Chem.* **2013**, *11*, 509
27. Bandyopadhyay, A.; Mali, S. M.; Lunawat, P.; Raja, K. M. P.; Gopi, H. N. *Org. Lett.* **2011**, *13*, 4482
28. Bandyopadhyay, A.; Misra, R.; Gopi, H. N. *Chem. Commun.* **2016**, *52*, 4938.
29. Ganesh Kumar, M.; Thombare, V. J.; Katariya, M. M.; Veeresh, K.; Raja, K. M.P; Gopi, H. N. *Angew. Chem. Int. Ed.* **2016**, *55*, 7847

30. Kumar, M. G.; Benke, S. N.; Raja, K. M. P.; Gopi, H. N. *Chem. Commun.*, **2015**, 51, 13397.
31. (a) Ketchum, R. R.; Hu, W.; Cross, T. A. *Science* **1993**, 261, 1457. (b) Bunkóczi, G.; Vértesy, L.; Sheldrick, G. M. *Angew. Chem. Int. Ed.* **2005**, 44, 1340
32. Benedetti, E.; Di Blasio, B.; Pedone, C.; Lorenzi, G. P.; Tomasic, L.; Gramlich, V. *Nature*, **1979**, 282, 630.
33. Berl, V.; Huc, I.; Khoury, R. G.; Krische, M. J.; Lehn, J. -M. *Nature* **2000**, 407, 720
34. Tanaka, Y.; Katagiri, H.; Furusho, Y. Yashima, E. *Angew. Chem., Int. Ed.*, **2005**, 44, 3867.
35. (a) Misra, R.; Dey, S.; Reja, R. M.; Gopi, H. N. *Angew. Chem. Int. Ed.* **2018**, 57, 1057. (b) Veeresh, K.; Singh, M.; Gopi, H. N. *Org. Biomol. Chem.* **2019**, 17, 9226.
36. Zhou, H.-C.; Long, J. R.; Yaghi, O. M. *Chem. Rev.* **2012**, 112, 673.
37. Zhou, H.-C.; Kitagawa, S. *Chem. Soc. Rev.* **2014**, 43, 5415.
38. McConnell, A. J.; Wood, C. S.; Neelakandan, P. P.; Nitschke, J. R. *Chem. Rev.* **2015**, 115, 7729
39. Churchfield, L. A.; Tezcan, F. A. *Acc. Chem. Res.* **2019**, 52, 345.
40. Misra, R.; Saseendran, A.; Dey, S.; Gopi, H. N. *Angew. Chem. Int. Ed.* **2019**, 58, 2251

## List of Publications

1. **Dey, S.**; Misra, R.; Saseendran, A.; Pahan, S.; Gopi, H. N. Metal-Coordinated Supramolecular Polymers from the Minimalistic Hybrid Peptide Foldamers. *Angew. Chem. Int. Ed.* **2021**, *60*, 9863-9868.
2. Misra, R.; **Dey, S.**; Reja, R. M.; Gopi, H. N. Artificial  $\beta$ -Double Helices from Achiral  $\gamma$ -Peptides. *Angew. Chem. Int. Ed.* **2018**, *57*, 1057-1061.
3. Misra, R.; Saseendran, A.; **Dey, S.**; Gopi, H. N. Metal-Helix Frameworks from Short Hybrid Peptide Foldamers. *Angew. Chem. Int. Ed.* **2019**, *58*, 2251-2255.
4. **Dey, S.**; Roy, S.; Gopi, H. N. Effect of Substituent and Chirality Induction on Achiral Double Helix: An Approach of Conformational Adaptation of Peptide Foldamer. Manuscript Submitted.
5. **Dey, S.**; Roy, S.; Puneeth Kumar, DR.; Nalawade, S. A.; Singh, M.; Mahapatra, S.P.; Gopi, H. N. Metal-Ions Tuned Structural Modulation of Metal-Helical Peptide Coordination Assemblies: Architectures from Porous Framework to Hierarchical Superhelix. Manuscript Submitted.
6. Misra, R.; George, G.; Reja, R. M.; **Dey, S.**; Ragothama, R.; Gopi, H. N. Structural insight into hybrid peptide  $\epsilon$ -helices. *Chem. Commun.* **2020**, *56*, 2171-2173.
7. Kumar, S.; Mishra, K. K.; Singh, S. K.; Borish, K.; **Dey, S.**; Sarkar, B.; Das, A. Observation of a weak intra-residue C5 hydrogen-bond in a dipeptide containing Gly-Pro sequence. *J. Chem. Phys.* **2019**, *151*, 104309-9.
8. Kumar, S.; Borish, K.; **Dey, S.**; Nagesh, J.; Das, A. Sequence-dependent folding motifs of the secondary structures of Gly-Pro and Pro-Gly containing oligopeptides. *Phys. Chem. Chem. Phys.*, **2022**, *24*, 18408-18418.

# *Chapter 1*

## *General Introduction of Peptide Foldamers Composed of Non-natural Amino Acids*

## 1. Introduction:

In all living organisms, several biological functions are exhibited by various biomolecules namely nucleic acids, lipids, carbohydrates, and proteins. Among them, proteins and metalloproteins are the utmost important biomolecules<sup>1</sup>. The three-dimensional structural architectures of proteins are mainly responsible to serve various biological functions. Naturally occurring 20 amino acids have been used to generate numerous proteins with definite three-dimensional structures and functions. Misfolding or conformational changes in proteins lead to various diseases including Alzheimer's disease, cystic fibrosis, Parkinson's disease, diabetes, Parkinson's disease, and others<sup>2</sup>. Therefore, an understanding of protein and its structural property relationship is an essential requirement.

### 1.1. Protein Structures:

The Protein structures are classified at four levels, primary, secondary, tertiary, and quaternary structures. The four different types of levels of protein structures are represented in Figure 1.

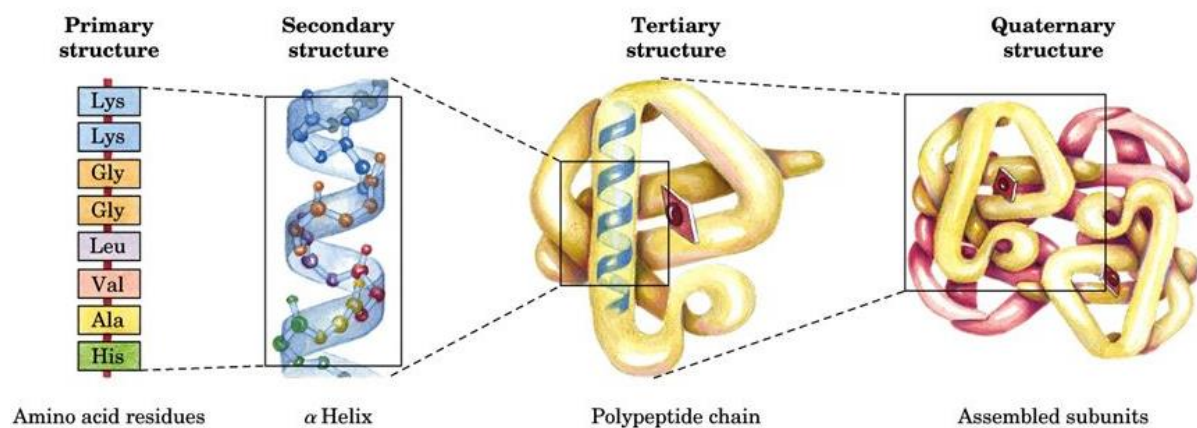


**Figure 1:** Schematic representation of protein in four different levels.

**Primary structure:** The primary structure of protein signifies the number and sequence of amino acid residues in the polypeptide backbone. This polypeptide backbone motif can fold into more ordered definite secondary structures.

**Secondary structures:** The stable folded conformational arrangement of protein secondary structures is classified into helices,  $\beta$ -sheets, and reverse turns. In 1951, Linus Pauling and colleagues designated the structures of  $\alpha$ -helix and  $\beta$ -sheet<sup>3</sup>. The secondary structures are stabilized by the hydrogen bonding between the NH and CO groups of the polypeptide chains. In proteins, the secondary structure units are connected by loosely structured peptides called loops. The loop region connects two adjacent anti-parallel  $\beta$ -strands called reverse turns. In

their pioneering work, G. N. Ramachandran and colleagues<sup>4</sup> established a plot known as the Ramachandran plot, to find out the stable secondary structures using torsional parameters of amino acids in the peptide chains. The Ramachandran plot for various types of protein secondary structures has shown in Figure 2.

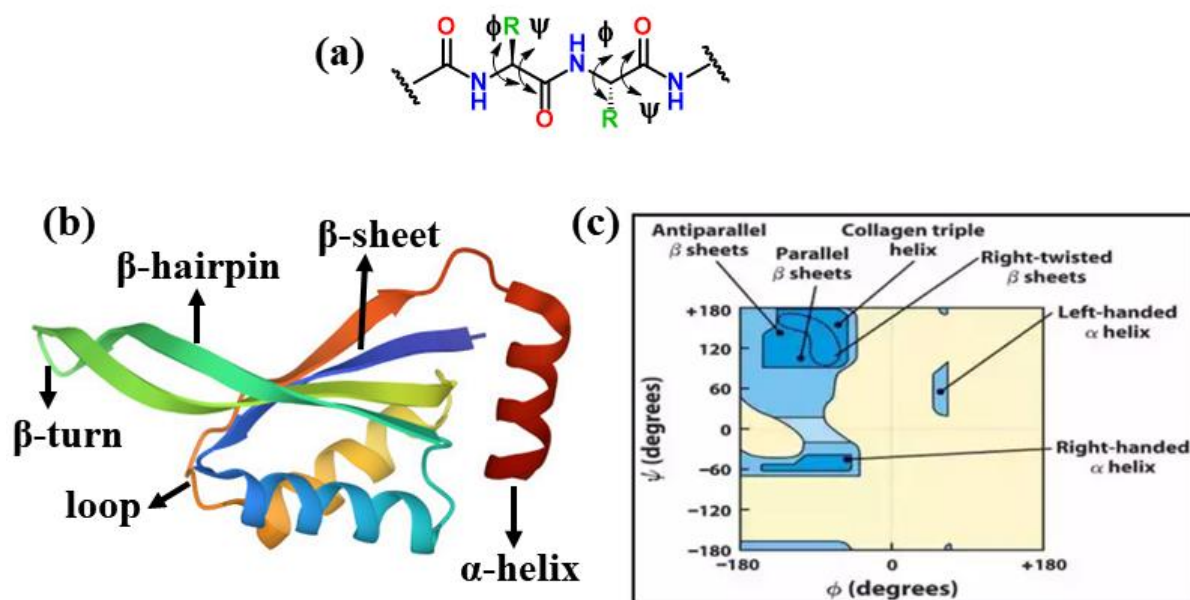
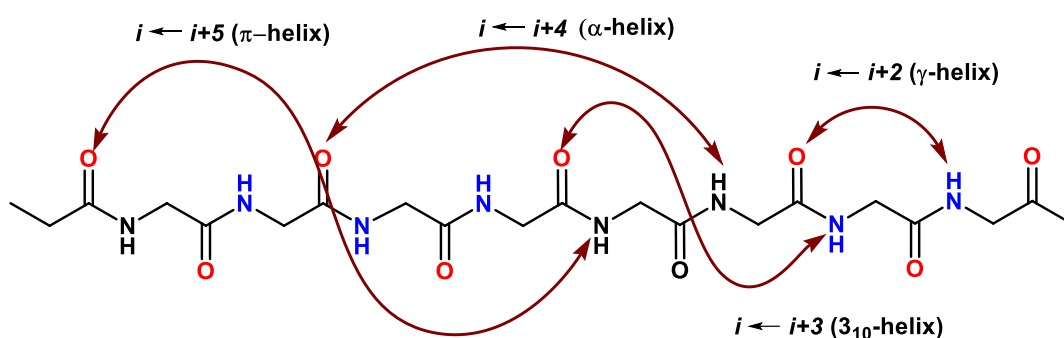


**Figure 2:** (a) Torsional angles  $\phi$  and  $\psi$  on peptide backbone of  $\alpha$ -amino acids (a) Different protein secondary structural elements (PDB code: 10.2210/pdb1P1L/pdb) (c) Classical Ramachandran plot and the allowed region for the torsional angles of different secondary structures.

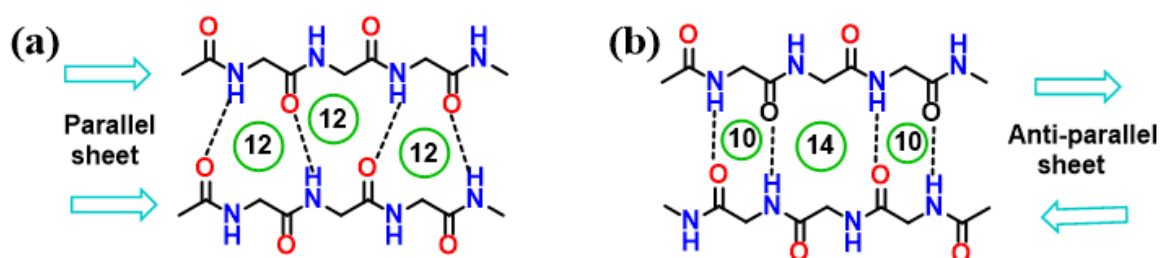
**Helices:** Helices are the major part of protein secondary structures. The helical stabilization in proteins or peptides occurs by intermolecular hydrogen bonding between CO and NH groups of polypeptide backbone ( $\text{CO} \cdots \text{HN}$ ). Depending on the number of atoms involved in the hydrogen-bonded pseudo-cycle and the number of residues per helical turn, different helical structures are classified into 2.2<sub>7</sub>-helix (or  $\gamma$ -helix), 3.0<sub>10</sub>, 3.6<sub>13</sub> (or  $\alpha$ -helix) and 4.4<sub>16</sub>-helix (or  $\pi$ -helix). In 1951, Linus Pauling suggested that the  $\alpha$ -helical structure is stabilized by 13-membered intramolecular hydrogen bonds and contains 3.6 amino acid residues per helical turn and noted by 3.6<sub>13</sub>( $\alpha$ -helix). These C<sub>13</sub> H-bonds form between the CO group of  $i$  amino acid and the NH group of ( $i+4$ ) amino acid like ( $i \leftarrow i+4$ ) of the polypeptide backbone.  $\alpha$ -helical structures are classified into right-handedness(P) and left-handedness(M) respectively. Generally,  $\alpha$ -helix is denoted as 3.6<sub>13</sub>-(P)-helix with the average torsion parameters  $\phi = -60^\circ$

and  $\psi = -45^\circ$  in the Ramachandran plot. Unlike  $\alpha$ -helical structures, rarely involved  $3.0_{10}$ -helical structures (or  $3.0_{10}$ -(*P*)-helix) are stabilized by 10-membered hydrogen bonding pseudo-cycles forms H-bond between the CO group of *i* amino acid and NH group of (*i*+3) amino acids like (*i*←*i*+3) of the polypeptide backbone. The average torsion parameters for  $3.0_{10}$ -helical structures are  $\phi = -49^\circ$  and  $\psi = -26^\circ$ . Similarly,  $\pi$ -helix is termed as  $4.4_{16}$ -(*P*)-helix ( $\phi = -55^\circ$ ,  $\psi = -70^\circ$ ) and  $\gamma$ -helix as  $2.2_7$ -helix ( $\phi = -70^\circ$ ,  $\psi = 70^\circ$ ). The schematic representation of the different types of H-bonding in different helical structures is shown in Scheme 1.



**Scheme 1:** Representation of H-bonding pattern in different helices.

**$\beta$ -Sheets:**  $\beta$ -Sheets are the second most abundant structural elements in proteins. In 1930, William Astbury proposed a  $\beta$ -sheet structure. However, in 1951, Linus Pauling and Robert Corey<sup>5</sup> came up with advanced structural information on  $\beta$ -sheet structures. The torsion parameters  $\phi$  and  $\psi$  values are found to be within the structurally allowed region in the upper left quadrant of the Ramachandran Map. Depending on the directionality of the  $\beta$ -strands in polypeptide backbone,  $\beta$ -sheets are classified into (i) parallel  $\beta$ -sheets and (ii) anti-parallel  $\beta$ -sheets as shown in Scheme 2.



**Scheme 2:** Representation of H-bonding pattern and directionality of polypeptide chains in  $\beta$ -sheet structures, (a) Parallel  $\beta$ -sheets (b) Anti-parallel  $\beta$ -sheets.

**Reverse Turns:** Reverse turns are also considered a major class of secondary structures in proteins. They signify a change in the polypeptide chain's site orientation. Depending on the



number of residues involved in the reverse turn, they are classified into  $\alpha$ -turn<sup>6a</sup> (5 amino acid residues),  $\beta$ -turn<sup>6b</sup> (4 amino acid residues),  $\pi$ -turn<sup>6c</sup> (6 amino acids),  $\gamma$ -turn (3 amino acids)<sup>6d</sup>. Out of these types,  $\beta$ -turns are largely found in the protein structures. Based on the dihedral angles  $\phi$  and  $\psi$  of  $i+1$  and  $i+2$  residues,  $\beta$ -turns are divided into type I, II, and III as well as their mirror images type I', II' and III' turns respectively.<sup>6e</sup>

**Tertiary structures:** The tertiary structures are the 3D-dimensional folding patterns of the polypeptide chain. The secondary structure units of the polypeptide along with the loosely structured loops together form compact three-dimensional structures. Different electrostatic interactions such as  $\pi$ - $\pi$  stacking, ionic interactions, and hydrophobic interactions help to fold the polypeptide into a tertiary structure.

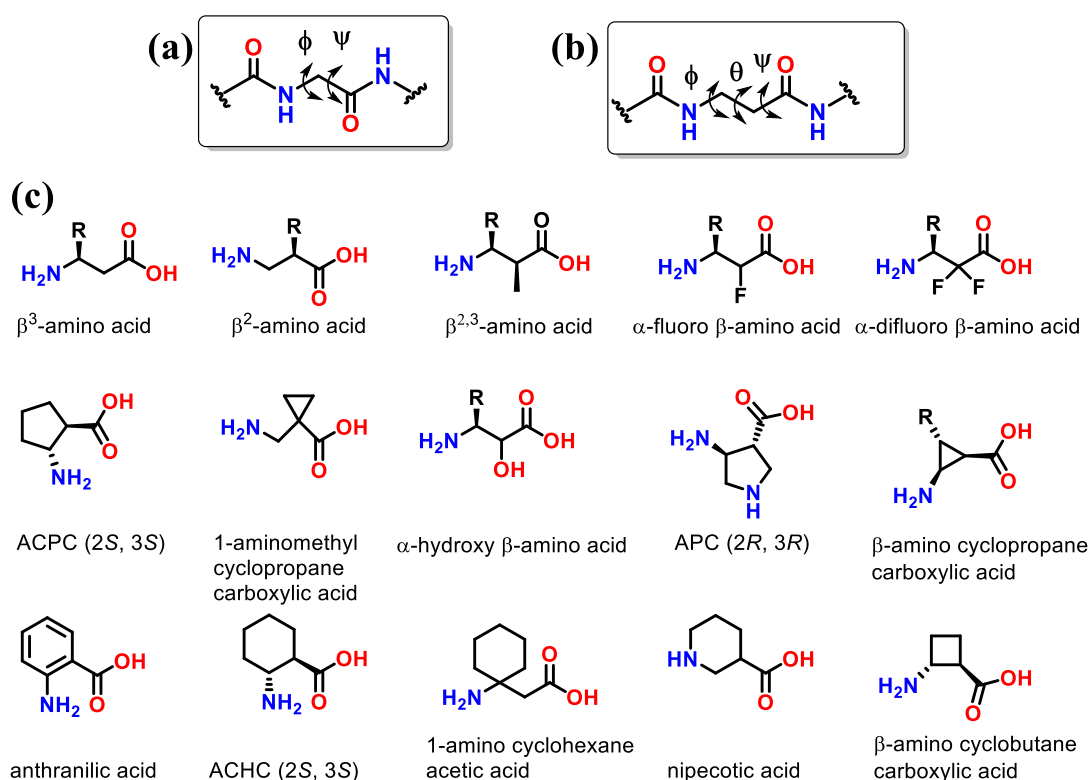
**Quaternary structure:** The combination or association of multiple subunits of a protein are closely arranged to form quaternary structures. Each part of the protein tertiary unit is held together with the help of electrostatic interaction to form a quaternary structure.

## 1.2. Mimics of Protein Secondary Structures:

The understanding of the structural and functional properties of proteins attracted chemists to design protein structure mimetics using non-natural amino acid building blocks. Over the past several decades, a considerable effort has been made to design folded architectures from  $\alpha$ -amino acid units.<sup>7</sup> The *de novo* design and mimicking of protein secondary structures have been utilized to develop various functional biomaterials and biologically impactful peptide-based drug molecules. However, due to limitations (e.g. proteolysis, protein-protein interaction, activity) of naturally occurring amino acid-based peptides or proteins, a variety of non-natural amino acid building blocks and the organic template have been used to construct a variety of protein secondary structures and studied their functions.<sup>8</sup> In addition to the non-natural amino acids and organic templates, oligomers of  $\beta$ - and  $\gamma$ -amino acids have been well-explored in design protein secondary structure mimetics and their structural properties have been studied<sup>8</sup>. These non-natural  $\beta$ - and  $\gamma$ -amino acid-based foldamers provide a unique opportunity to design and construct protein structure mimetics from the mixed sequences such as  $\alpha,\beta$ -,  $\alpha,\gamma$ - and  $\beta,\gamma$ -sequences.

### 1.2.1. $\beta$ -Amino Acid Based Peptide Foldamers:

The term “Foldamers” was coined by Prof. Samuel H. Gellman and he states that “*any oligomer which can adopt a rigid conformation in solution.*”<sup>8a</sup> In foldamers, molecules can adopt any structure or geometry to attain the most stable conformation and its minimum energy state.  $\beta$ -Amino acids are homologated versions of  $\alpha$ -amino acid with an extra  $-\text{CH}_2$  group in between amine( $-\text{NH}_2$ ) and carboxyl( $-\text{COOH}$ ) groups of  $\alpha$ -amino acids. It is due to this additional  $-\text{CH}_2$  group,  $\beta$ -amino acids give an extra torsional angle  $\theta$ , in addition to  $\phi$  and  $\psi$  angles of  $\alpha$ -amino acids. The local torsion angles and different types of  $\beta$ -amino acids reported in the literature are shown in Scheme 3. As the  $\beta$ -amino acids have additional  $-\text{CH}_2$ , they can be functionalized further. Therefore, depending on the position of the side chain,  $\beta$ -amino acids can be classified as  $\beta^3$ - and  $\beta^2$ -amino acids. The development of protein-folded secondary structures in combination with  $\beta$ -amino acids leads not only to an increase in the repertoire of the folded secondary structures but also shows greater proteolytic stability *in vivo* conditions.<sup>9</sup>



**Scheme 3:** Presentation of the torsional variables for (a)  $\alpha$  and (b)  $\beta$ - amino acid. (c) list of  $\beta$ -amino acids used in the peptide of foldamers.

In their pioneering work, Seebach<sup>10</sup> and Gellman<sup>11</sup> reported using acyclic and cyclic chiral  $\beta$ -amino acids based on a variety of folded architectures. Gellman and co-workers used cyclic

*trans*-2-amino cyclopentanecarboxylic acid (ACPC) and *trans*-2-aminocyclohexanecarboxylic acid (ACHA) to construct folded architectures. The oligomer of ACPC and ACHA has been shown to adopt 12- and 14-helical conformations, respectively. In continuation, Sharma and co-workers reported the 10/12 or 12/10 mixed helical structures from carbo- $\beta$ -amino acid.<sup>12</sup> In addition, the groups of Atkins<sup>13</sup> and Fulop<sup>14</sup> also designed and studied the conformations of the oligomers of various cyclic  $\beta$ -amino acids. The helical structures of  $\beta$ -peptides are shown in Figure 3.

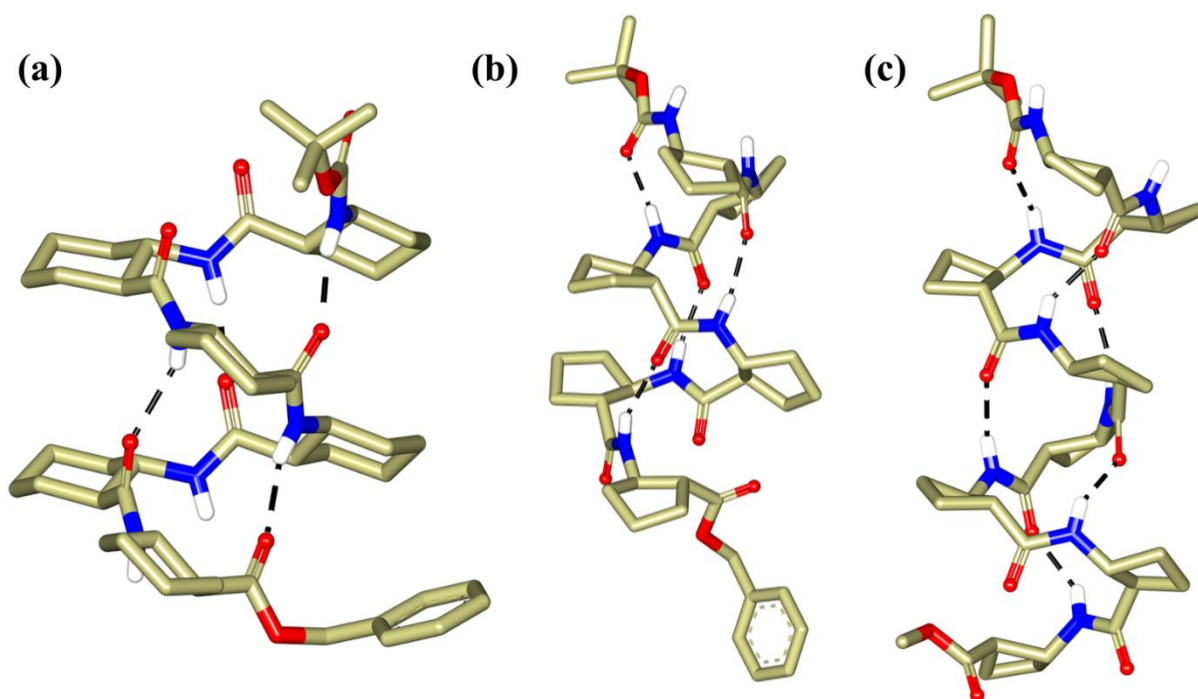


**Figure 3:** Helical structures of  $\beta$ -peptides, (a) 14-helix derived from the *trans*-ACHA  $\beta$ -amino acid<sup>11a</sup> (b) 12-helix formed derived from *trans*-ACPC  $\beta$ -amino acid<sup>11b</sup> (c) 12-helix constructed from cyclobutane  $\beta$ -amino acid<sup>13</sup>.

The structural folded analysis of  $\beta$ -amino acid-based peptides shows a completely different H-bonding pattern as compared to  $\alpha$  amino acid-based peptides.  $\beta$ -peptides form organized secondary structures like helices, sheets, and turns. Depending on the folding and H-bonding pattern of the  $\beta$ -residues in the polypeptide chain the  $\beta$ -peptide helices can be categorized as C<sub>8</sub>-, C<sub>10</sub>-, C<sub>12</sub>-, and C<sub>14</sub>-helices.<sup>15-17</sup> Extensive theoretical calculation by Hoffman and colleagues<sup>18</sup> suggested the different types of helical structures available to the  $\beta$ -peptides. The different H-bonded helices are shown in Figure 4.

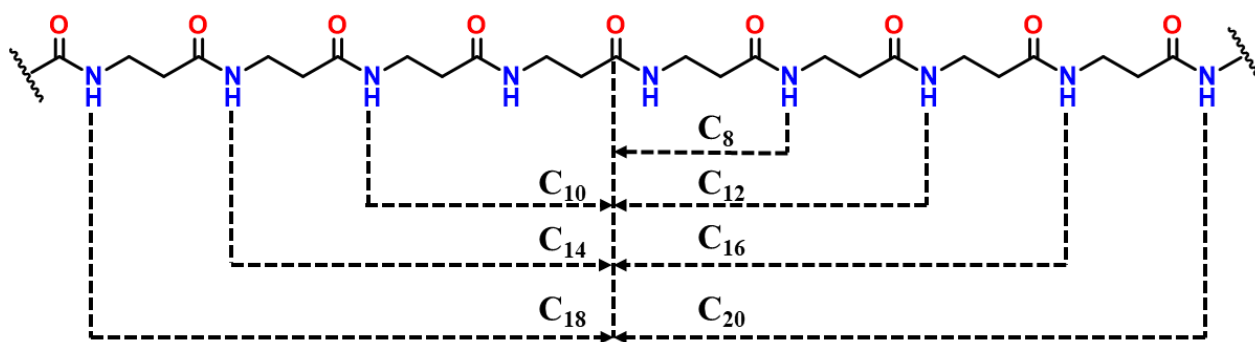
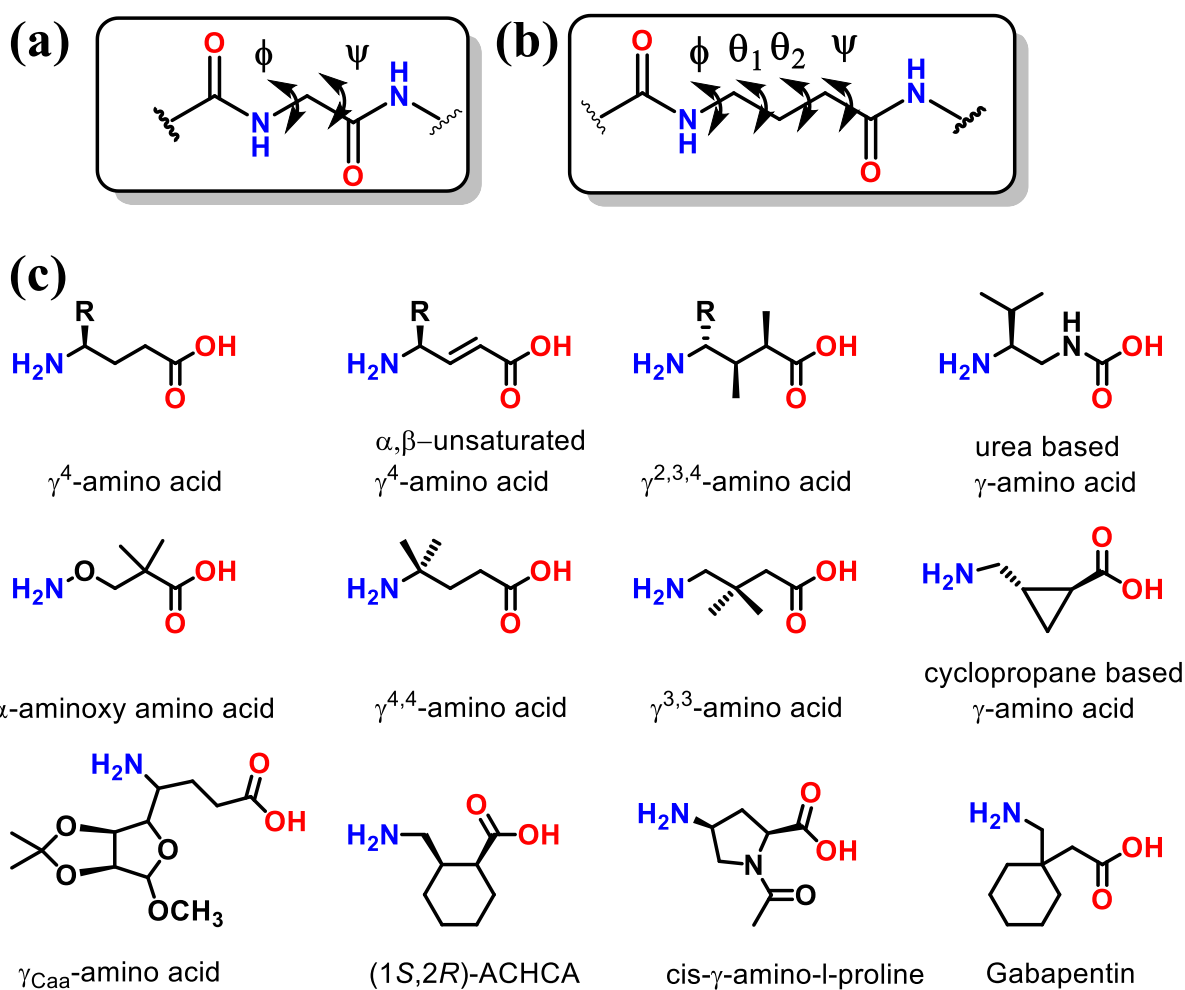


**Figure 4:** H-bonding patterns observed of  $\beta$ -peptide-based foldamer.

In addition to the helical diversity observed in  $\beta$ -peptides, the directionality of H-bonding patterns is also different. The  $C_8$  and  $C_{12}$  helices showed  $N(i+3) \rightarrow C(i)$  H-bonding direction which is similar to the  $\alpha$ -helix, whereas  $C_{10}$  and  $C_{14}$  helices showed  $N(i) \rightarrow C(i+2)$  in opposite H-bonding direction. Along with the helical structures,  $\beta$ -sheets (both parallel and antiparallel),  $\beta$ -hairpin structures from  $\beta$ -amino acids have also been reported.<sup>19-21</sup> The distinct differences in  $\beta$ -sheets types of structures formed by  $\alpha$ -amino-acid and  $\beta$ -amino-acid is the directionality of H-bonding between  $NH \dots O=C$ . In the case of the  $\alpha$ -amino acid based peptides, H-bonds in  $\beta$ -sheets alternate in direction, whereas in the case of the  $\beta$ -peptides the H-bonds in  $\beta$ -sheets are in the same direction.

### 1.2.2. $\gamma$ -Amino Acid Based Peptide Foldamers:

$\gamma$ -Amino acids are homologated analogs of  $\beta$ -amino acids and double homologated species of  $\alpha$ -amino acids. It is having two additional  $-\text{CH}_2$  groups between  $C^\alpha$  and  $\text{C}=\text{O}$  carbon and provides extra backbone torsion angles  $\theta_1$  ( $C^\beta-C^\alpha$ ) and  $\theta_2$  ( $C^\gamma-C^\beta$ ) along with  $\phi$  and  $\psi$ . As  $\gamma$ -amino acids consist of two additional  $-\text{CH}_2-$  groups in the backbone, it is expected they will produce higher structural diversity compared to  $\alpha$ - and  $\beta$ -peptides. In comparison, the  $\gamma$ -amino acids based foldamers have not been much explored, probably, due to the challenges in synthesis and isolation of stereochemically pure  $\gamma$ -amino acids. The various types of  $\gamma$ -amino acids used as building units in the design of  $\gamma$ -peptide foldamers are shown in Scheme 4.



**Scheme 4:** Presentation of the torsional variables for (a)  $\alpha$  and (b)  $\gamma$ - amino acid. (c) list of  $\gamma$ -amino acids used in the peptide of foldamers.

In the year 1998, Seebach and Hanessian groups reported that the homo-oligomers of monosubstituted  $\gamma^4$  and disubstituted  $\gamma^{2,4}$ -amino acids form a stable right-handed 14-helical conformation in the solution stabilized by H-bonds between CO and NH group in  $i$  to  $i+3$  residues.<sup>22</sup> Subsequently, Seebach and colleagues showed a stable 14-helical conformation using trisubstituted homo-oligomer of  $\gamma^{2,3,4}$ -amino acids in the single crystal structure.<sup>23</sup> Later, Hofmann and colleagues using *ab initio* MO theoretical calculations, reported various types of helical structures available to the  $\gamma$ -peptides.<sup>24</sup> The different H-bonding structures of  $\gamma$ -peptides are shown in Figure 5. They have proposed that out of all possible helices,  $C_{14}$ - and  $C_9$ - helices are the most stable ones. The predicted  $C_9$ -helices were realized by Sharma and colleagues using alternating C-linked carbo- $\gamma^4$ -amino acid and  $\gamma$ -aminobutyric acid (GABA).<sup>25</sup>

Gellman and colleagues reported the 14-helical conformation from homo-oligomers of cyclic  $\gamma$ -amino acids in a single crystal.<sup>26</sup> The single crystal structures of 14- and 9-helices obtained from  $\gamma$ -peptide foldamers are shown in Figure 6.

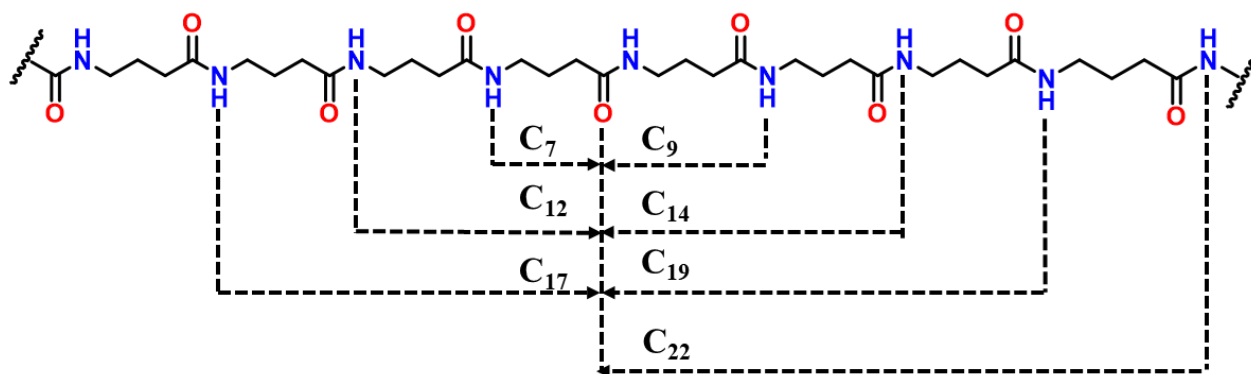


**Figure 5:** Types of H-bonding patterns observed of  $\gamma$ -peptide-based foldamer.

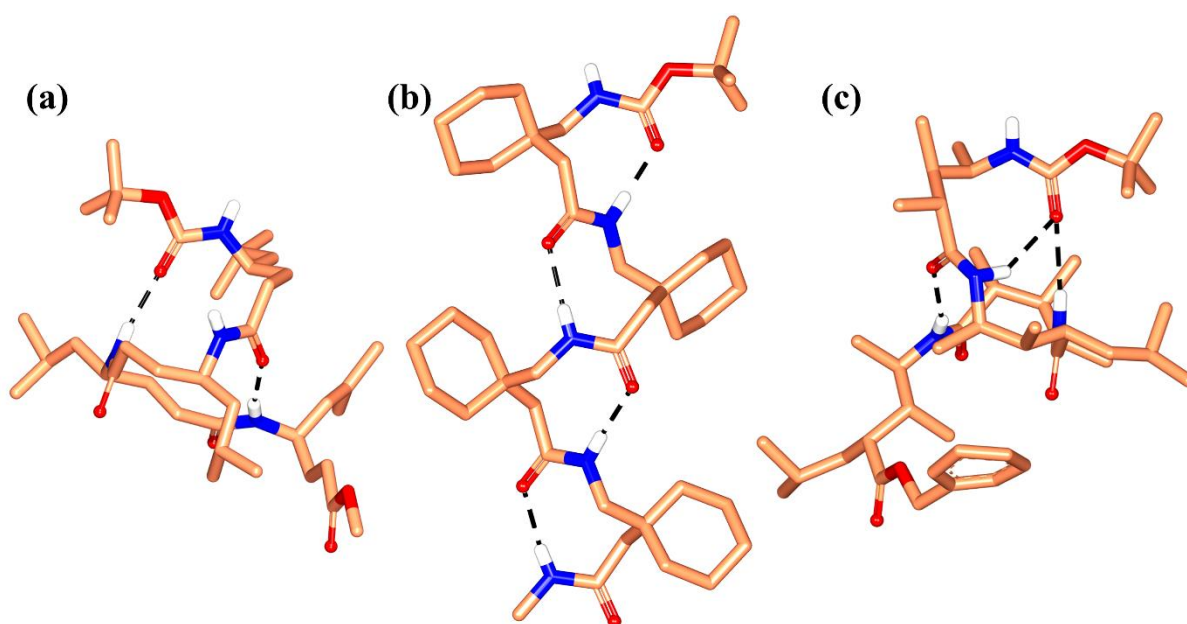


**Figure 6:** (a)  $C_{14}$  helix of  $\gamma$ -peptide<sup>27a</sup> (b)  $C_9$  helix of  $\gamma$ -peptide composed with gabapentin oligomer<sup>27b</sup> (c)  $C_{14}$  helix of the  $\gamma^{2,3,4}$ -oligomer peptide<sup>23</sup>.

In continuation, Balaram and colleagues reported the formation of 14-helical structures by  $\gamma^4$ -amino acid homo-oligomers consisting of proteinogenic side chains ( $\gamma^4$ Leu,  $\gamma^4$ Ile, and  $\gamma^4$ Val) and also reported  $C_9$  helical conformations from the oligomers gabapentin (3, 3-dialkyl- $\gamma$ -amino acid) in single crystals. The  $C_9$  helical structure is stabilized by the H-bonds between  $i$  and  $i + 2$  residues.<sup>27</sup> Smith and colleagues investigated the conformational properties of  $\gamma$ -

peptides consisting of cyclopropane  $\gamma$ -amino acids. These peptides have been shown to adopt a parallel sheet structure using a bifurcated H-bond between the CO and NH group and one CH of the cyclopropane ring.<sup>28</sup> Further, the same group has utilized cyclopropane  $\gamma$ -peptides in the design of non-peptidic reverse turn of  $\beta$ -hairpins.<sup>29</sup> Along with cyclic and acyclic  $\gamma$ -amino acids, backbone heteroatoms such as O (Oxygen) and N (Nitrogen) containing  $\gamma$ -amino acids are also reported. Yang and colleagues reported 8-helical conformations from  $\alpha$ -aminoxy peptides and 9-helices and turns in the case of  $\beta$ -aminoxy peptides.<sup>30</sup> In addition, Guichard and colleagues reported the 14-helical conformations from  $\gamma$ -peptide oligoureas.<sup>31</sup> Further, Millard and colleagues reported both single crystal and solution state 9-helices from the oligomers of thiazole backbone based  $\gamma$ -amino acids.<sup>32</sup>

### 1.2.3. $\beta$ - and $\gamma$ -Amino Acids Containing Heterogeneous Foldamers:

A variety of substituted  $\beta$ - and  $\gamma$ -amino acids have been derived to construct diverse helical structures. Balaram and colleagues developed the hybrid peptide structures by inserting  $\beta$ -amino acids and higher homologous amino acids into  $\alpha$ -peptide helices and  $\beta$ -hairpin structures.<sup>33</sup> In addition, hybrid peptides were further explored by other groups.<sup>34</sup> Using quantum mechanical calculation, Hofmann and colleagues proposed that 9-, 11/9-, 9/11-, 11-, 12/13-, 15/14-, 16/18- and 18/16- helical structures can be produced from  $\alpha,\beta$ -hybrid peptides.<sup>35</sup> Gellman and colleagues reported peptide sequences of  $\alpha$ ,  $\beta$ -hybrid peptides containing constrained *trans*-ACPC amino acids and Aib residues having the ability to form both 11-helix and 14/15-helical structures.<sup>36</sup> In addition, Gellman and co-workers reported the 11/11/12 and 10/11/11-helical foldamer of 1:2 and 2:1  $\alpha,\beta$ -hybrid peptides.<sup>37a</sup> Fulop and colleagues reported the effect of stereochemical patternings in the design of  $\alpha,\beta$ -hybrid peptides, which has the ability to adopt different helical structures.<sup>37b</sup> However, similar results have also been reported by Sharma and co-workers.<sup>37c-f</sup> In addition to these secondary structural mimetics, Gellman and co-workers reported helix bundle quaternary structures in hybrid  $\alpha/\beta$ -peptide foldamers.<sup>37g-h</sup> Different types of  $\alpha,\beta$ -hybrid peptide foldamers are shown in Figure 7.

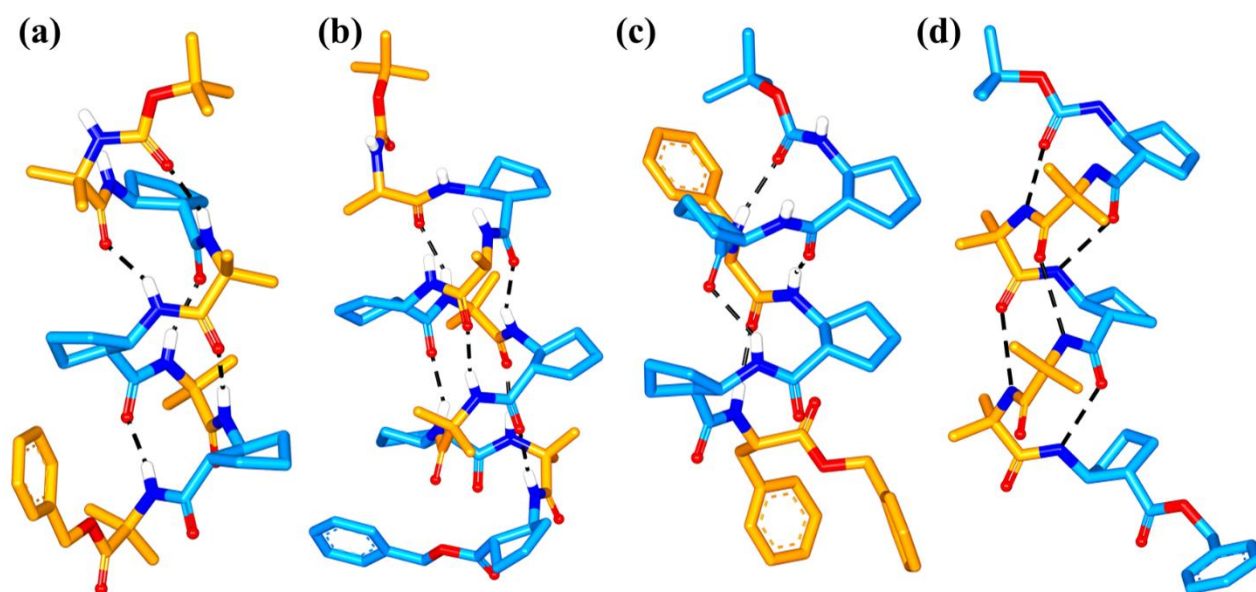


**Figure 7:** (a)  $C_{11}$  helix from  $\alpha,\beta$ -hybrid peptide of Aib and ACPC residues.<sup>36b</sup> (b) 14/15-helical structure from  $\alpha,\beta$ -hybrid peptide of Ala, ACPC, and Aib residues.<sup>36c</sup> (c) 10/11/11-helical structure of 2:1  $\alpha,\beta$ -hybrid peptide.<sup>37a</sup> (d) 12/11/11-helical structure of 1:2  $\alpha,\beta$ -hybrid peptide.<sup>37a</sup>

Similar to the mixed  $\alpha,\beta$ - hybrid peptide,  $\alpha,\gamma$ -hybrid peptide foldamers have also been explored in the literature. Hofmann and co-workers projected a variety of helices available to 1:1 alternating  $\alpha$ - and  $\gamma$ - amino acids. Among the various helix types, they suggested that the 12-helix is the most stable helix followed by 12/10- or 18/20- helices.<sup>24b</sup> In continuation, Balaram and co-workers reported stable 12-helix from the  $\alpha,\gamma$ -hybrid peptide consisting of 1:1 Aib and gabapentin(Gpn) residues,<sup>38a</sup> and also from 1:1  $\alpha$ -and  $\gamma^4$ -amino acids.<sup>38b</sup> In both cases, the helical structures formed intramolecular H-bond between  $i$  and  $i+3$  residues. Further, Sharma and co-workers reported several  $\alpha,\gamma$ -hybrid peptide 12/10-helices composed of L-Ala and  $\gamma$ -Caa (C-linked carbo- $\gamma$ -amino acid) in the solution state.<sup>39a</sup> Further, Balaram and co-workers reported the single crystal structure of 12/10-helix.<sup>39b,c</sup> In continuation, Gellman and co-workers group reported utilization of cyclic  $\gamma$ -amino acids to construct various  $\alpha/\gamma$ -peptide foldamers.<sup>40</sup> Further, Balaram and co-workers utilized the  $\gamma$ -amino acids to design  $\beta$ -turns as well in the  $\beta$ -hairpins.<sup>41</sup> Different types of  $\alpha,\gamma$ -hybrid peptide foldamers are shown in Figure 8.



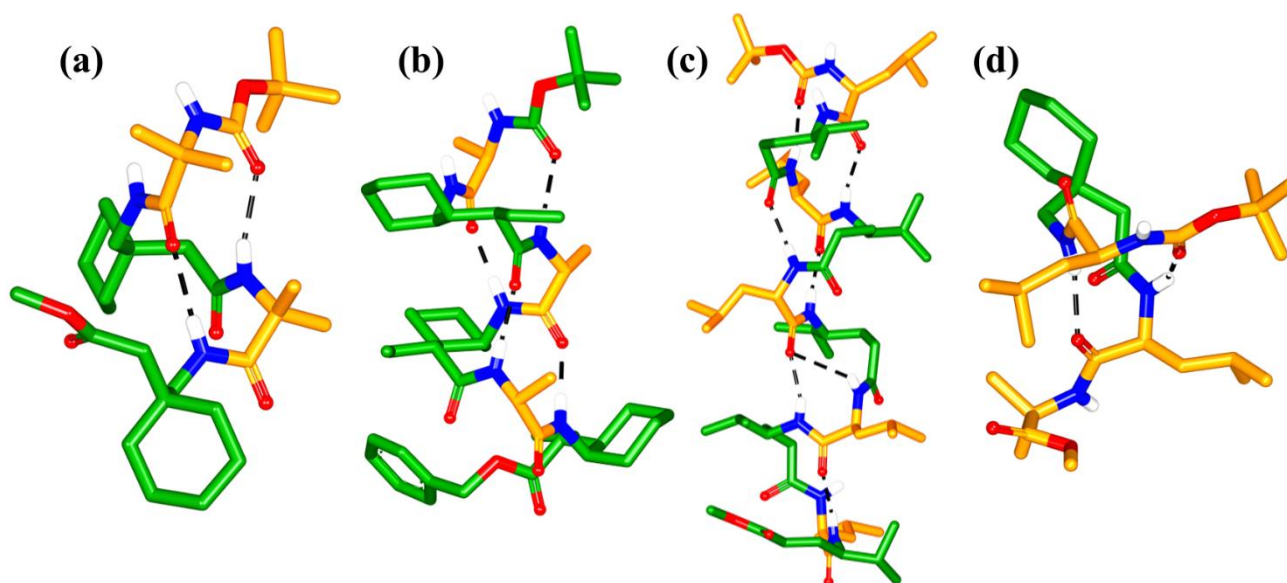


**Figure 8:** (a) 12-helix of  $\alpha,\gamma$ -hybrid peptide foldamer.<sup>38a</sup> (b) 12-helix of  $\alpha,\gamma$ -hybrid peptide foldamer composed of <sup>D</sup>Ala and EtACHA residues.<sup>40b</sup> (c) 12-helix of  $\alpha,\gamma$ -hybrid peptide foldamer composed of leu and  $\gamma$ -Val residues.<sup>39c</sup> (d) 10/12-helix of  $\alpha\gamma\alpha$  with Leu, Gpn, and Aib residues.<sup>39</sup>

Furthermore, there are very few reports on  $\beta,\gamma$ -hybrid peptide foldamers. However, Hofmann and co-workers performed systematic quantum calculations and proposed stable 11-, 13-, mixed 11/13-, or 20/22- helices in combination with  $\beta,\gamma$ -hybrid peptide and the H-bonding pattern.<sup>24b</sup> These structures are shown in Figure 9.

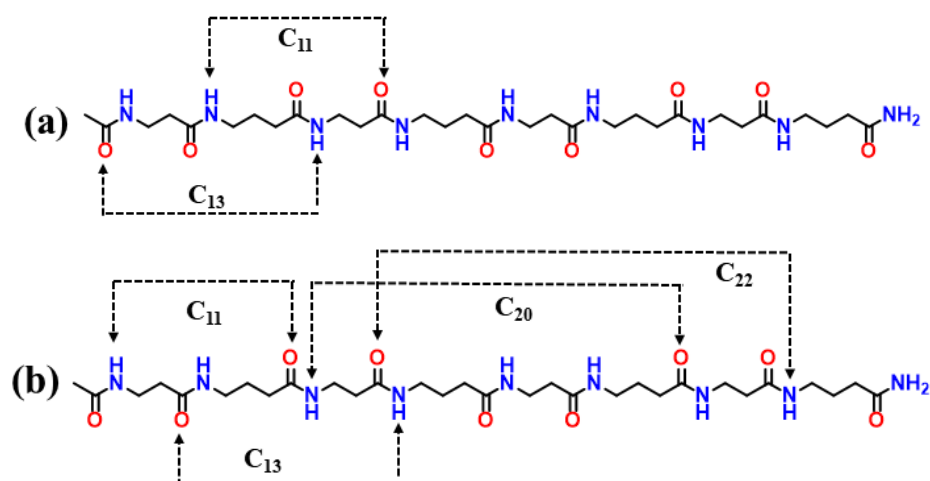
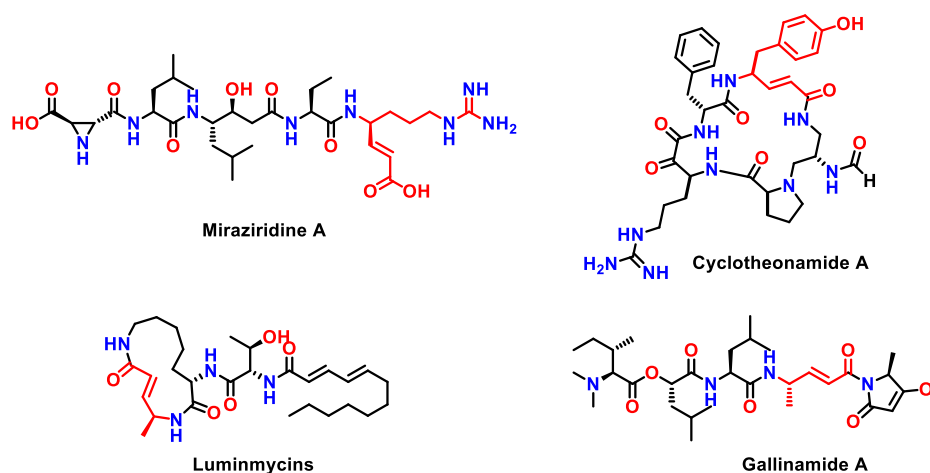


**Figure 9:** Examples of  $\beta,\gamma$  hybrid peptide helices. a) H-bonding pattern of 11 and 13 helix b) H-bonding pattern in mixed helices: 11/13 helix or in 20/22 helix.

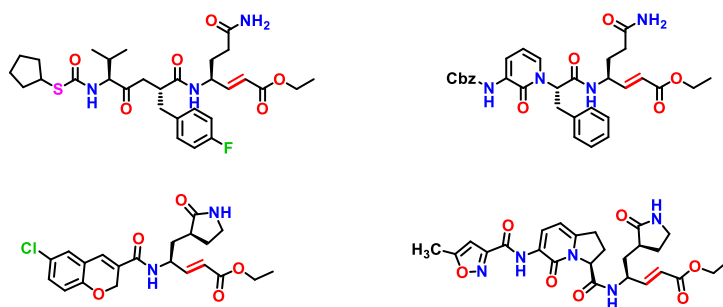
Balaram and co-workers reported a short  $\beta$ ,  $\gamma$ -hybrid tripeptide composed of Boc- $\beta$ Leu-Gpn-Val-OMe that adopted 13-helix in a single crystal structure.<sup>42</sup> The  $\beta$ ,  $\gamma$ -hybrid peptide showed similar helical parameters as that of  $\alpha$ -helix. Therefore, the  $\beta$ ,  $\gamma$ -hybrid peptides have a unique opportunity to mimic  $\alpha$ -helical peptides. Aitken and co-workers reported the formation of 9/8 ribbon from  $\beta,\gamma$ -hybrid peptides. They also showed the utility of the choice of amino acid residues peptide sequence and hence 9/8 ribbon structure transform into 13-helix by using unconstrained  $\gamma$ -amino acids with  $\gamma^4$ -amino acids in the  $\beta,\gamma$ -hybrid peptides.<sup>43</sup>

#### 1.2.4. $\alpha,\beta$ -Unsaturated $\gamma$ -Amino Acids Based Peptide Foldamers:

$\alpha,\beta$ -Unsaturated (vinylogous amino acids) are the analogs of  $\gamma^4$ -amino acids consisting of CH=CH- unit between C $_{\alpha}$ H and CO of  $\alpha$ -amino acids. The (*E*)- $\alpha,\beta$ -unsaturated  $\gamma$ -amino acids are frequently found in the peptide natural products. These non-ribosomal amino acids were found in peptides like Cyclotheonamides (A, B, C, D, E) which act as potent inhibitors for serine protease and bovine  $\beta$ -trypsin,<sup>44</sup> Gallinamide A,<sup>45</sup> and Miraziridine A.<sup>46</sup> The natural peptide products containing (*E*)- $\alpha,\beta$ -unsaturated  $\gamma$ -amino acids, and various synthetic vinylogous amino acid based peptide inhibitors for serine and cysteine proteases<sup>47</sup> are shown in Scheme 5-6.



**Scheme 5:** Chemical structures of naturally available cyclic and linear peptides containing  $\alpha,\beta$ -unsaturated  $\gamma$ -amino acid.



**Scheme 6:**  $\alpha,\beta$ -unsaturated  $\gamma$ -amino acids containing synthetic protease inhibitors.

Schreiber and colleagues<sup>48</sup> reported  $\beta$ -sheet type of conformation from (*E*)-vinylogous dipeptide. In continuation, Chakraborty and colleagues reported the utility of (*E*)-vinylogous amino acids to induce  $\beta$ -turn in  $\beta$ -hairpins structures.<sup>49</sup> In continuation, Hofmann and colleagues studied ab initio MO theory calculations and predicted various helical structures from (*E*)- and (*Z*)-vinylogous homo-oligomers.<sup>50</sup> A systematic computational analysis reveals that peptides composed of (*E*)-vinylogous amino acids adopt helices starting from 14- to 27-membered H-bond pseudo cycles with sufficient pore diameter. These pores can be used to design helical nanotubes and peptide-based ion channels. Further, peptides composed of (*Z*)-vinylogous amino acid oligomers favor helices with smaller H-bonded pseudo cycles such as 9 and 12-helices. These structures are shown in Figure 10.

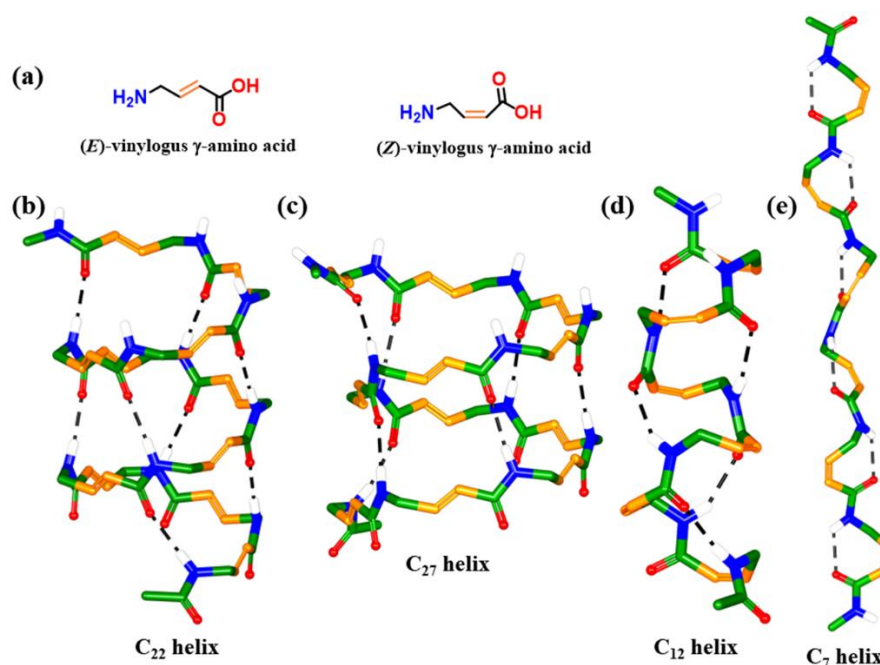


**Figure 10:** (a) (*E*)- and (*Z*)-vinylogous  $\gamma$ -amino acids. (b-d) Theoretically, stable structures of  $C_{22}$ -,  $C_{27}$ -,  $C_{12}$ - and  $C_7$ -helices composed of homo-oligomers of (*E*)-vinylogous  $\gamma$ -amino acids and (*Z*)-vinylogous  $\gamma$ -amino acids.<sup>50</sup>

Previously, we have shown the utilization of (*E*)-vinylogous  $\gamma$ -amino acids in the design of stable  $\beta$ -hairpins structures,<sup>51</sup> miniature  $\beta$ -meanders,<sup>52</sup> and multiple  $\beta$ -sheet structures.<sup>53</sup> In addition, our group has also designed and studied conformations of  $\alpha,\gamma$ -hybrid peptide foldamers consisting of (*Z*)-vinylogous  $\gamma$ -amino acids.<sup>54</sup> Recently, we have reported the transformation of an unstructured peptide containing (*E*)-vinylogous  $\gamma$ -amino acids to  $\alpha,\gamma$ -short hybrid tripeptide 12-helical structure through base-mediated double bond migration. This study shows the transformation of (*E*)-vinylogous  $\gamma$ -amino acid unit into (*Z*)-vinylogous  $\gamma$ -amino acid and the incorporation of carbon-carbon cis double bonds into 12-helix.<sup>55</sup> Some of these structures are shown in Figure 11.

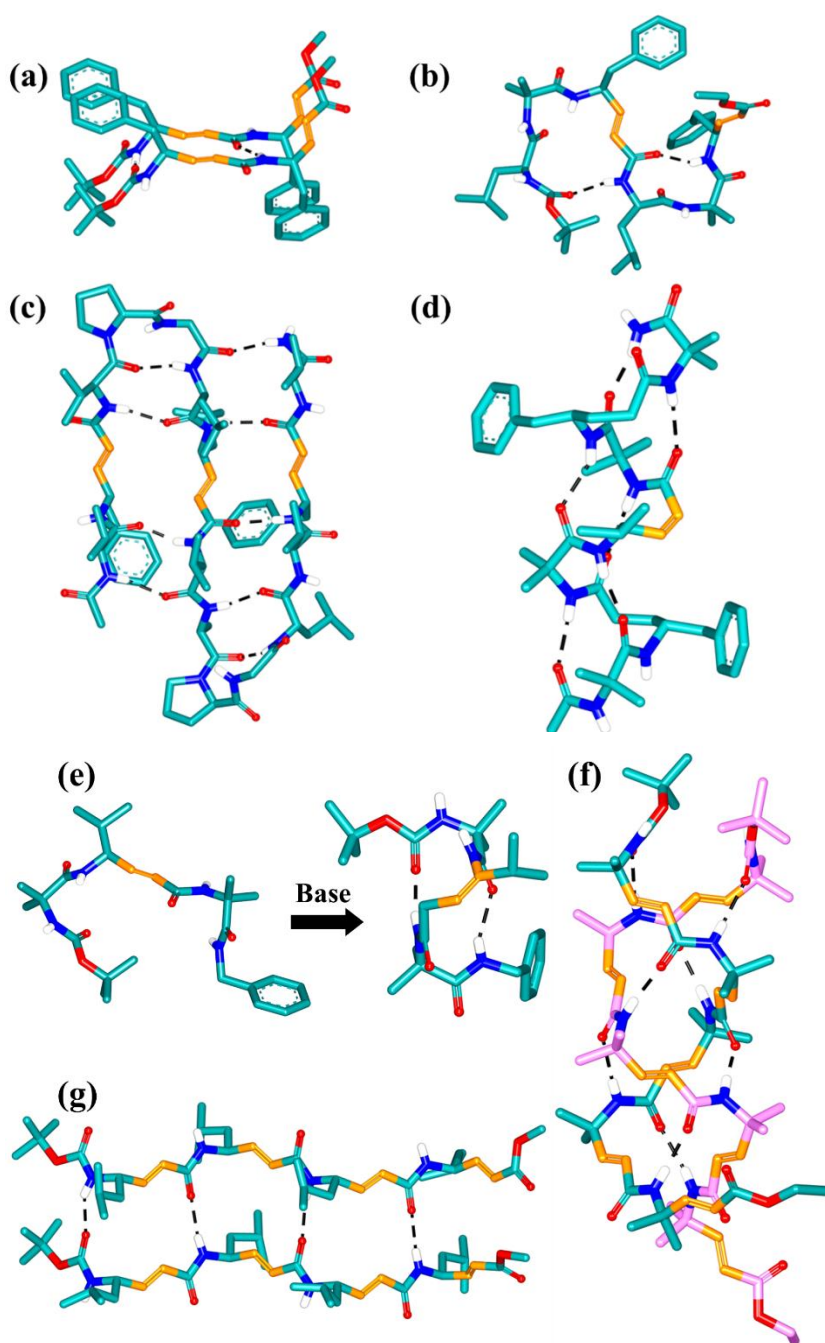


**Figure 11:** Vinylogous  $\gamma$ -amino acids based peptide foldamer. (a) Extended sheet of (*E*)-vinylogous  $\gamma$ -Phe dipeptide.<sup>48</sup> (b)  $\beta$ -meanders type secondary structures of the  $\alpha\gamma$ -hybrid peptide of (*E*)-vinylogous  $\gamma$ -Phe, Aib and Leu.<sup>52</sup> (c) Three stranded  $\beta$ -sheets comprising (*E*)-vinylogous amino acids.<sup>53</sup> (d)  $\alpha,\gamma$ - hybrid peptides containing (*Z*)-vinylogous  $\gamma^4$ -amino acids in C<sub>12</sub>-helical structure.<sup>54</sup> (e) Conformational change (*E*)-vinylogous  $\gamma$ -amino acid unit into (*Z*)-vinylogous  $\gamma$ -amino acid unit in 12-helical  $\alpha,\gamma$ -short hybrid tripeptide.<sup>55</sup> (f)  $\beta$ -double helical structure composed of homo-oligomer of (*E*)-vinylogous  $\gamma^{4,4}$ -amino acid.<sup>56</sup> (g) Extended sheet of (*E*)-vinylogous  $\gamma$ -Leu tripeptide.<sup>57</sup>

Recently we have also reported the  $\beta$ -double-helical structures from the homo-oligomers of 4,4-gem-dimethyl  $\alpha,\beta$ -unsaturated  $\gamma$ -amino acids.<sup>56,57</sup> Replacement of dialkyl with monoalkyl groups leads to the parallel  $\beta$ -sheet structure. Crystal structures of various  $\alpha,\beta$ -unsaturated  $\gamma$ -amino acid foldamers are shown in Figure 11.

In the present study, we have revealed that the beta-double helical structures not confined to the oligomers 4,4-dimethyl substituted (*E*)-vinylogous amino acids, even the mixed sequences composed of 3,3-dimethyl substituted  $\gamma$ -amino acids (Adb) along with 4,4-dimethyl substituted (*E*)-vinylogous amino acids can also form artificial beta double-helical structures. Furthermore, we have examined the transformation of the achiral nature of the beta-double helices into chiral double helices by attaching chiral amines at the C-terminus of the peptides.

## 2. Interactions of Peptides and Applications:

To carry out biological functions, molecular interaction<sup>58</sup> between the biomolecules (DNA-RNA interaction, protein-protein interaction, and protein-DNA or protein-RNA interaction) are the key factors. Among them, protein-protein interactions play the most significant role in various functions. Proteins/peptides/amino acids play a fundamental role in the origin of life and are also the central dogma of biology. Inspired by the functions of proteins, extensive efforts have been made over the years to mimic their structures and functions using natural and non-natural amino acid building blocks. The folded structures derived from the oligomers of  $\beta$ ,  $\gamma$ , and  $\delta$ - amino acids and their mixed sequences along with  $\alpha$ -amino acids offer a wide range of structural diversity with potential applications in biology and materials e.g antimicrobials,<sup>59</sup> p53-HDM2 inhibitors,<sup>60</sup> HIV inhibitors,<sup>61</sup> human cytomegalovirus entry inhibitors<sup>62</sup> and in the field of supramolecular self-assembly.<sup>63</sup> The amino acid residues in the peptide backbone motif

show conformational adaptation to form a 3D structural architecture (helix or sheet) via the interaction between hydrogen-bond donors and acceptors.<sup>64</sup> Indeed, the ability of peptides to adopt such well-ordered structures leads to properties known as peptide self-assembly. Peptide self-assembly has been observed even in dipeptide as well as longer sequences.<sup>65</sup> The diverse nature of the assembly of peptides is controlled by kinetics and thermodynamics.<sup>66</sup> Various supramolecular non-covalent interactions including H-bonding, electrostatic,  $\pi$ - $\pi$  stacking hydrophobic, and van der Waals interactions are the key factors to control the self-assembly of peptides. However, some external entities like physical and chemical stimuli (e.g., temperature, pH, metal ions, and chemical accompaniments) can also influence the assembling properties of peptides. However, the functional amino acid residues in the peptide sequences themselves provide additional self-assembly properties. As peptides have the ability to form self-assembled properties which display several interactions and functions with other molecular components (i. e., sugar, nucleic acids). This leads to a wide application of peptides. Some of these interactions and applications are shown in Figure 12. Out of these interactions, my research work focused on peptide-metal interactions.

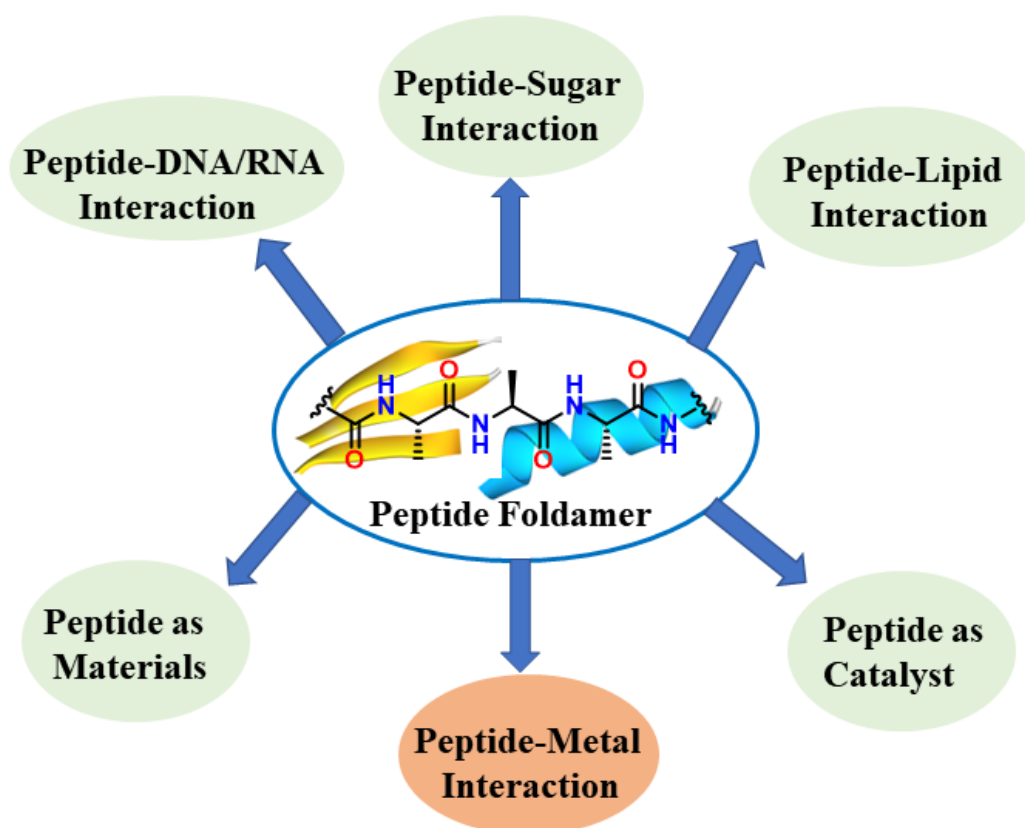


**Figure 12:** Diverse applications of peptides

## 2.1. Peptide-Metals Interaction:

Metal ions play pivotal roles in biological systems, including catalytic, oxidative reactions, and electron transfer, transport proteins. In metalloenzymes and metalloproteins, the active site consists of the folded structural unit of peptides and metal ions.<sup>67</sup> In their pioneering work, Szostak reported that peptides containing side arm acidic residue Asp and Glu, could have chelation ability with  $Mg^{2+}$  ion and thus protect against degradation of RNA molecules by  $Mg^{2+}$  ions.<sup>68</sup> In the classic DNA binding Zn-finger motifs, Zn plays a crucial role in providing a specific folding of polypeptide motif into a compact domain by binding to Cys/His residues, and also zinc metal ion plays significant structural functions and catalytic properties within many zinc-containing metalloproteins and enzymes.<sup>69</sup> The iron-sulfur (FeS) proteins are essential for basic processes in life. FeS proteins such as ferredoxin (Fd) allow  $CO_2$  fixation. A diversity of cysteine-containing tripeptides was shown to stabilize iron-sulfur clusters.<sup>70</sup> The coordination of metal ions with peptides leads to a conformational change in peptides. In addition, Ghadiri and colleagues have shown that the peptide with His residues can transform a random coil into an  $\alpha$ -helical structure upon binding the imidazole side chains and a tetraammineruthenium (II) moiety.<sup>71</sup> Synthetic peptides represent an alternative and attractive class of ligands that can encompass the properties of both small molecules and proteins. In addition to the attractive features of peptides such as diverse functional groups, lipophilicity, polarity, and charge, various metal coordinating sites have been introduced and studied the ordered self-assembling properties of peptides.<sup>72</sup> Metal coordination is an important force to direct the ordered association of peptide molecules. The advantage of this strategy is that the functional properties of peptides and metal ions can be explored to design novel self-assembled peptide-based materials and also metalloprotein mimetics. Recently, Fujita and colleagues showed the metal-dictated knotted networks from the short peptides.<sup>73</sup> In their pioneering work, the groups of Chmielewski<sup>74</sup> and Conticello<sup>75</sup> have studied the protein-like architectures from metal-mediated supramolecular assemblies of collagen and coiled-coil peptides. In the present study, we have explored the utilization of short hybrid  $\alpha\gamma\alpha$  tripeptide folded units to construct various metal-coordinated structural architectures.

### 3. References:

1. Linderstrom-Lang, K. U.; Schellman, J. A. (1959), *The Enzymes*, (P. D. Boyer, Ed.), Vol. 1, 2<sup>nd</sup> ed., pp. 443-510. Academic Press, New York.
2. Chaudhuri, T. K.; Paul, S. *FEBS J.* **2006**, *273*, 1331
3. Pauling, L.; Corey, R. B.; Branson, H. R. *Proc. Nat. Acad. Sci. USA*, **1951**, *37*, 205.
4. Ramachandran, G. N.; Sasisekaran, V. *Adv. Protein Chem.* **1968**, *23*, 283.
5. Pauling, L.; Corey, R. B. *Proc. Nat. Acad. Sci. USA*, **1951**, *37*, 729.
6. (a) Pavone, V.; G Gaeta, G.; Lombardi, A.; Natri, F.; Maglio, O.; Isernia, C.; Saviano, M. *Biopolymers* **1996**, *38*, 705. (b) Nataraj, D., Srinivasan, N., Sowdhamini, R.; Ramakrishnan, C. *Curr. Sci.* **1995**, *69*, 434. (c) Dasgupta, B.; Chakrabarti, P. *BMC Struct Biol* **2008**, *8*, 39. (d) Matthews, B. W. *Macromolecules* **1972**, *5*, 818. (e) Venkatachalam, C. M. *Biopolymers* **1968**, *6*, 1425.
7. (a) Marshall, G. R.; Bosshard, H. E. *Circ. Res.* **1972**, *31*, 143. (b) Ramachandran, G. N.; Chandrasekaran, R. *Progress in Peptide Research*. Lande, S. Ed.; Gordon & Breach: New York, 1972; Vol. II (Proceedings of the Second American Peptide Symposium, Cleveland, 1970), p 195. (c) Toniolo, C.; Benedetti, E. *ISI Atlas Sci. Biochem.* **1988**, *1*, 225. (d) Bosch, R.; Schmitt, H.; Jung, G.; Winter, W. *Biopolymers* **1985**, *24*, 961. (e) Toniolo, C.; Benedetti, E. *Trends Biochem. Sci.* **1991**, *16*, 350. (f) Karle, I. L.; Balaram, P. *Biochemistry* **1990**, *29*, 6747. (g) Marshall, G. R.; Hodgkin, E. E.; Langs, D. A.; Smith, G. D.; Zabrocki, J.; Leplawy, M. T. *Proc. Natl. Acad. Sci. U.S.A.* **1990**, *87*, 487. (h) Karle, I. L. *Acc. Chem. Res.* **1999**, *32*, 693. (i) Kaul, R.; Balaram, P. *Bioorg. Med. Chem.* **1999**, *7*, 105. (j) Balaram, P. *J. Pept. Res.* **1999**, *54*, 195. (k) Venkatraman, J.; Shankaramma, S. C.; Balaram, P. *Chem. Rev.* **2001**, *101*, 3131.
8. (a) Gellman, S. H. *Acc. Chem. Res.* **1998**, *31*, 173. (b) Frackenhohl, J.; Arvidsson, P. I.; Schreiber, J. V.; Seebach, D. *ChemBioChem* **2001**, *2*, 445. (c) Goodman, C. M.; Choi, S.; Shandler, S.; DeGrado, W.F. *Nat. Chem. Biol.* **2007**, *3*, 252.



9. (a) Frackenpohl, J.; Arvidsson, P. I.; Schreiber, J. V.; Seebach, D. *ChemBioChem* **2001**, *2*, 445. (b) Goodman, C. M.; Choi, S.; Shandler, S.; DeGrado, W.F. *Nat. Chem. Biol.* **2007**, *3*, 252.
10. (a) Hintermann, T.; Gademann, K.; Jaun, B.; Seebach, D. *Helv. Chim. Acta*, **1998**, *81*, 983. (b) Seebach, D.; Beck, A. K.; Bierbaum, D. J. *Chem. Biodiv.* **2004**, *1*, 1111.
11. (a) Appella, D. H.; Christianson, L. A.; Karle, I. L.; Powell, D. R.; Gellman, S. H. *J. Am. Chem. Soc.* **1996**, *118*, 13071. (b) Appella, D. H.; Christianson, L. A.; Karle, I. L.; Powell, D. R.; Gellman, S. H. *J. Am. Chem. Soc.* **1999**, *121*, 6206. (c) Appella, D. H.; Christianson, L. A.; Klein, D. A.; Richards, M. A.; Powell, D. R.; Gellman, S. H. *J. Am. Chem. Soc.* **1999**, *121*, 7574. (d) Krauthauser, S.; Christianson, L. A.; Powell, D. R.; Gellman, S. H. *J. Am. Chem. Soc.* **1997**, *119*, 11719.
12. (a) Sharma, G. V. M.; Reddy, R.; Krishna, P. R.; Ravi Sankar, A.; Narsimulu, K., Kumar, S. K.; Jayaprakash, P.; Jagannadh, B.; Kunwar, A. C. *J. Am. Chem. Soc.* **2003**, *125*, 13670. (b) Sharma, G. V. M.; Chandramouli, N.; Choudhary, M.; Nagendar, P.; Ramakrishna, K. V. S.; Kunwar, A. C.; Schramm, P.; Hofmann, H. -J. *J. Am. Chem. Soc.* **2009**, *131*, 17335.
13. Fernandes, C.; Faure, S.; Pereira, E.; They, V.; Declerck, V.; Guillot, R.; Aitken, D. *J. Org. Lett.* **2010**, *12*, 3606.
14. (a) Fulop, F.; Forro, E.; Toth, G. K. *Org. Lett.* **2004**, *6*, 4239. (b) Martinek, T. A.; Fulop, F. *Chem. Soc. Rev.* **2012**, *41*, 687.
15. (a) Gellman, S. H. *Acc. Chem. Res.* **1998**, *31*, 173. (b) Hill, D. J.; Mio, M. J.; Prince, R. B.; Hughes, T. S.; Moore, J. S. *Chem. Rev.* **2001**, *101*, 3893. (c) Cheng, R. P.; Gellman, S. H.; DeGrado, W. F. *Chem. Rev.* **2001**, *101*, 3219. (d) Venkatraman, J.; Shankaramma, S. C.; Balaram, P. *Chem. Rev.* **2001**, *101*, 3131. (e) Seebach, D.; Beck, A. K.; Bierbaum, D. J. *Chem. Biodiversity* **2004**, *1*, 1111. (f) Hecht, S.; Huc, I. *Foldamers: Structure, Properties and Applications*; Wiley-VCH: Weinheim, **2007**. (g) Seebach, D.; Gardiner, J. *Acc. Chem. Res.* **2008**, *41*, 1366. (h) Cummings, C. G.; Hamilton, A. D. *Curr. Opin. Chem. Biol.* **2010**, *14*, 341.
16. (a) Petersson, E. J.; Schepartz, A. *J. Am. Chem. Soc.* **2008**, *130*, 821. (b) Price, J. L.; Horne, W. S.; Gellman, S. H. *J. Am. Chem. Soc.* **2010**, *132*, 12378.

17. (a) Arvidsson, P. I.; Rueping, M.; Seebach, D. *Chem. Commun.* **2001**, 649. (b) Appella, D. H.; Christianson, L. A.; Klein, D. A.; Powell, D. R.; Huang, X. L.; Barchi J. J.; Gellman, S. H. *Nature* **1997**, 387, 381. (c) Seebach, D.; Schreiber, V. J.; Abele, S.; Daura, X.; Gunsteren, F. W. *Helv. Chim. Acta* **2000**, 83, 34. (d) Daura, X.; Bakowies, D.; Seebach, D.; Fleischhauer, J.; Van Gunsteren, W. F.; Kruger, P. *Eur. Biophys. J.* **2003**, 32, 661. (e) Hetenyi, A.; Mandity, I. M.; Martinek, T. A.; Toth, G. K.; Fulop, F. *J. Am. Chem. Soc.* **2005**, 127, 547. (f) Threlfall, R.; Davies, A.; Howarth, N.M.; Fisher, J.; Cosstick, R. *Chem. Commun.* **2008**, 585. (g) Rua, F.; Boussert, S.; Parella, T.; Diez-Perez, I.; Branchadell, V.; Giralt, E.; Ortuno, R. M. *Org. Lett.* **2007**, 9, 3643. (h) Arvidsson, P. I.; Ryder, N. S.; Weiss, H. M.; Gross, G.; Kretz, O.; Woessner, R.; Seebach, D. *ChemBioChem* **2003**, 4, 1345. (i) Mandity, I. M.; Weber, E.; Martinek, T. A.; Olajos, G.; Toth, G. K.; Vass E.; Fulop, F. *Angew. Chem., Int. Ed.* **2009**, 48, 2171. (j) Seebach, D.; Abele, S.; Gademann, K.; Jaun, B. *Angew. Chem., Int. Ed.* **1999**, 38, 1595. (k) Martinek, T. A.; Toth, G. K.; Vass, E.; Hollosi, M.; Fulop, F. *Angew. Chem., Int. Ed.* **2002**, 41, 1718. (l) Martinek, T. A.; Mandity, I. M.; Fulop, L.; Toth, G. K.; Vass, E.; Hollosi, M.; Forro, E.; Fulop, F. *J. Am. Chem. Soc.* **2006**, 128, 13539.
18. Günther, R., Hofmann, H.-J. & Kuczera, K. Searching for periodic structures in  $\beta$ -peptides. *J. Phys. Chem. B* **2001**, 105, 5559.
19. Krauthauser, S.; Christianson, L. A.; Powell, D. R.; Gellman S. H. *J. Am. Chem. Soc.* **1997**, 119, 11719.
20. Chung, Y. J.; Huck, B. R.; Christianson, L. A.; Stanger, H. E.; Krauthauser, S.; Powell, D. R.; Gellman S. H. *J. Am. Chem. Soc.* **2000**, 122, 3995.
21. Karle, I.; Gopi, H. N.; Balaram P. *Proc. Natl. Acad. Sci., USA*, **2002**, 99, 5161.
22. (a) Hintermann, T.; Gademann, K.; Jaun, B.; Seebach, D. *Helv. Chim. Acta.* **1998**, 81, 893. (b) Hanessian, S.; Luo, X.; Schaum, R.; Michnick, S. *J. Am. Chem. Soc.* **1998**, 120, 8569.
23. Seebach, D.; Brenner, M.; Rueping, M.; Schweizer, B.; Jaun, B. *Chem. Commun.* **2001**, 207.

24. (a) Baldauf, C.; Gunther, R.; Hofmann, H. J. *Helv. Chim. Acta.* **2003**, *86*, 2573. (b) Baldauf, C.; Gunther, R.; Hofmann, H. -J. *J. Org. Chem.* **2006**, *71*, 1200.
25. Vasudev, P. G.; Shamala, N.; Ananda, K.; Balaram, P. *Angew. Chem., Int. Ed.* **2005**, *44*, 4972.
26. Guo, L.; Zhang, W.; Reidenbach, A.G.; Giuliano, M.W.; Guzei, I.A.; Spencer, L.C.; Gellman, S. H., *Angew. Chem. Int. Ed.* **2011**, *50*, 5843.
27. (a) Basuroy, K.; Dinesh, B.; Reddy, M. B. M.; Chandrappa, S.; Raghothama, S.; Shamala, N.; Balaram, P. *Org. Lett.* **2013**, *15*, 4866. (b) Vasudev, P. G.; Shamala, N.; Ananda, K.; Balaram, P. *Angew. Chem., Int. Ed.* **2005**, *44*, 4972.
28. Khurram, M.; Qureshi, N.; Smith, M. D. *Chem. Commun.* **2006**, 5006.
29. Kothari, A.; Khurram, M.; Qureshi, N.; Beck, E. M.; Smith, M. D. *Chem. Commun.* **2007**, 2814.
30. (a) Lee, X.; Yang, D. *Chem. Commun.* **2006**, 3367. (b) Chen, F.; Zhu, N.-Y.; Yang, D. *J. Am. Chem. Soc.* **2004**, *126*, 15980.
31. Pendem, N.; Nelli, Y. R.; Douat, C.; Fischer, L.; Laguerre, M.; Ennifar, E.; Kauffman, B.; Guichard, G. *Angew. Chem. Int. Ed.* **2013**, *52*, 4147.
32. Mathieu, L.; Legrand, B.; Deng, C.; Vezenkov, L.; Wenger, E.; Didierjean, C.; Amblard, M.; Averlant-Petit, M. C.; Masurier, N.; Lisowski, V.; Martinez, J.; Maillard, L. T. *Angew. Chem. Int. Ed.* **2013**, *52*, 6006
33. (a) Roy, R. S.; Karle, I. L.; Raghothama, S.; Balaram, P. *Proc. Natl. Acad. Sci. USA* **2004**, *101*, 16478. (b) Karle, I. L.; Pramanik, A.; Banerjee, A.; Bhattacharjya, S.; Balaram, P. *J. Am. Chem. Soc.* **1997**, *119*, 9087.
34. (c) De Pol, S.; Zorn, C.; Klein, C. D.; Zerbe, O.; Reiser, O. *Angew. Chem., Int. Ed.* **2004**, *43*, 511. (d) Hayen, A.; Schmitt, M. A.; Ngassa, F. N.; Thomasson, K. A.; Gellman, S. H. *Angew. Chem., Int. Ed.* **2004**, *43*, 505. (e) Schmitt, M. A.; Choi, S. H.; Guzei, I. A.; Gellman, S. H. *J. Am. Chem. Soc.* **2005**, *127*, 13130. (f) Schmitt, M. A.; Choi, S. H.; Guzei, I. A.; Gellman, S. H. *J. Am. Chem. Soc.* **2006**, *128*, 4538.
35. Baldauf, C.; Günther, R.; Hofmann, H.-J. *Peptide Science.* **2006**, *84*, 408.

36. (a) Hayen, A.; Schmitt, M. A.; Ngassa, F. N.; Thomasson, K. A.; Gellman, S. H. *Angew. Chem., Int. Ed.* **2004**, *43*, 505. (b) Schmitt, M. A.; Choi, S. H.; Guzei, I. A.; Gellman, S. H. *J. Am. Chem. Soc.* **2005**, *127*, 13130. (c) Choi, S. H.; Guzei, I. A.; Spencer, L. C.; Gellman, S. H. *J. Am. Chem. Soc.* **2008**, *130*, 6544.
37. (a) Schmitt, M. A.; Choi, S. H.; Guzei, I. A.; Gellman, S. H. *J. Am. Chem. Soc.* **2006**, *128*, 4538. (b) Mándity, I. M.; Weber, E.; Martinek, T. A.; Olajos, G.; Tóth, G. K.; Vass, E.; Fülöp, F. *Angew. Chem., Int. Ed.* **2009**, *48*, 2171. (c) Sharma, G. V. M.; Reddy, K. R.; Krishna, P. R.; Sankar, A. R.; Narasimulu, K.; Kumar, S. K.; Jayaprakash, P.; Jagannadh, B.; Kunwar, A. C. *J. Amer. Chem. Soc.* **2003**, *125*, 13670. (d) Sharma, G. V. M.; Reddy, K. R.; Krishna, P. R.; Sankar, A. R.; Jayaprakash, P.; Jagannadh, B.; Kunwar, A. C. *Angew. Chem., Int. Ed.* **2004**, *43*, 3961. (e) Sharma, G. V. M.; Nagendar, P.; Krishna, P. R.; Ramakrishna K. V. S.; Jayaprakash, P.; Kunwar, A. C. *Angew. Chem., Int. Ed.* **2005**, *44*, 5878. (f) Sharma, G. V. M.; Subash, V.; Narasimulu, K.; Sankar, A. R.; Kunwar, A. C. *Angew. Chem. Int. Ed.* **2006**, *45*, 8207. (g) Horne, W. S.; Price, J. L.; Keck, J. L.; Gellman, S. H. *J. Am. Chem. Soc.* **2007**, *129*, 4178. (h) Giuliano, M. W.; Horne, W. S.; Gellman, S. H. *J. Am. Chem. Soc.* **2009**, *131*, 9860.
38. (a) Ananda, K.; Vasudev, P. G.; Sengupta, A.; Raja, K. M. P.; Shamala N.; Balaram, P. *J. Am. Chem. Soc.* **2005**, *127*, 168. (b) Jadhav, S. V.; Bandyopadhyay, A.; Gopi, H. N. *Org. Biomol. Chem.* **2013**, *11*, 509.
39. (a) Sharma, G. V. M.; Jadhav, V. B.; Ramakrishna, K. V. S.; Jayaprakash, P.; Narsimulu, K.; Subash, V.; Kunwar, A. C. *J. Am. Chem. Soc.* **2006**, *128*, 14657. (b) Vasudev, P. G.; Chatterjee, S.; Ananda, K.; Shamala, N.; Balaram, P.; *Angew Chem Int Ed*, **2008**, *41*, 6430. (c) Sonti, R.; Dinesh, B.; Basuroy, K.; Raghothama, S.; Shamala, N.; Balaram; P. *Org. Lett.*, **2014**, *16*, 1656.
40. (a) Guo, L.; Zhang, W.; Guzei, I. A.; Spencer, L. C.; Samuel H. Gellman, S. H. *Org. Lett.* **2012**, *14*, 2582. (b) Guo, L.; Chi, Y.; Almeida, A. M.; Guzei, I. A.; Parker, B. K.; Gellman, S. H. *J. Am. Chem. Soc.* **2009**, *131*, 16018.
41. Chatterjee, S.; Vasudev, P. G.; Raghothama, S.; Ramakrishnan, C.; Shamala, N.; Balaram, P. *J. Am. Chem. Soc.* **2009**, *131*, 5956.

42. Vasudev, P. G.; Ananda, K.; Chatterjee, S.; Aravinda, S.; Shamala, N.; Balaram, P. *J. Am. Chem. Soc.* **2007**, *129*, 4039.
43. (a) Grison, C. M.; Robinab, S.; Aitken D. J.; *Chem. Commun.*, **2015**, *51*, 16233. (b) Grison, C. M.; Robin, S.; Aitken, D. J. *Chem. Commun.*, **2016**, *52*, 7802.
44. Hagihara, M.; Schreiber, S. L. *J. Am. Chem. Soc.* **1992**, *114*, 6570.
45. Linington, R. G.; Clark, B. R.; Trimble, E. E.; Almanza, A.; Uren, L.-D.; Kyle, D. E.; Gerwick, W. H. *J. Nat. Prod.* **2009**, *72*, 14.
46. Nakao, Y.; Fujita, M.; Warabi, K.; Matsunaga, S.; Fusetani, N. *J. Am. Chem. Soc.* **2000**, *122*, 10462.
47. (a) Hanzlik, R. P.; Thompson, S. A. *J. Med. Chem.* **1984**, *27*, 711. (b) Bastiaans, H. M. M.; Van der Baan, J. L.; Ottenheijm, H. C. J. *J. Org. Chem.* **1997**, *62*, 3880. (c) Liu, S.; Hanzlik, R. P. *J. Med. Chem.* **1992**, *35*, 1067. (d) Kong, J.-S.; Venkatraman, S.; Furness, K.; Nimkar, S.; Shepherd, T. A.; Wang, Q. M.; Aube, J.; Hanzlik, R. P. *J. Med. Chem.* **1998**, *41*, 2579. (e) Schaschke, N.; Sommerhoff, C. P. *ChemMedChem* **2010**, *5*, 367.
48. Hagihara, M.; Anthony, N. J.; Stout, T. J.; Clardy, J.; Schreiber, S. L. *J. Am. Chem. Soc.* **1992**, *114*, 6568.
49. Chakraborty, T. K.; Ghosh, A.; Kumar, S. K.; Kunwar, A. C. *J. Org. Chem.* **2003**, *68*, 6459.
50. Baldauf, C.; Gunther, R.; Hofmann, H.-J. *J. Org. Chem.* **2005**, *70*, 5351.
51. Bandyopadhyay, A.; Mali, S. M.; Lunawat, P.; Raja, K. M. P.; Gopi, H. N. *Org. Lett.* **2011**, *13*, 4482.
52. Bandyopadhyay, A.; Gopi, H. N. *Org. Lett.* **2012**, *14*, 2770.
53. Bandyopadhyay, A.; Misra, R.; Gopi, H. N. *Chem. Commun.* **2016**, *52*, 4938.
54. Ganesh Kumar, M.; Thombare, V. J.; Katariya, M. M.; Veeresh, K.; Raja, K. M. P.; Gopi, H. N. *Angew. Chem. Int. Ed.* **2016**, *55*, 1.
55. Veeresh, K.; Gopi, H. N. *Org. Lett.* **2019**, *21*, 4500.

56. Misra, R.; Dey, S.; Reja, R. M.; Gopi, H. N. *Angew. Chem. Int. Ed.* **2018**, *57*, 1057.
57. Veeresh, K.; Singh, M.; Gopi, H. N. *Org. Biomol. Chem.* **2019**, *17*, 9226.
58. (a) Bonetta, L. *Nature* **2010**, *468*, 851. (b) Rual, J. F.; Venkatesan, K.; Hao, T.; Hirozane-Kishikawa, T.; Dricot, A.; Li, N.; Berriz, G. F.; Gibbons, F. D.; Dreze, M.; Ayivi-Guedehoussou, N. *Nature* **2005**, *437*, 1173. (c) Cafarelli, T. M.; Desbuleux, A.; Wang, Y.; Choi, S. G.; De Ridder, D.; Vidal, M. *Curr. Opin. Struct. Biol.* **2017**, *44*, 201.
59. (a) Epanand, R. F.; Raguse, T. L.; Gellman, S. H., Epanand, R. M. *Biochemistry*, **2004**, *43*, 9527. (b) Hamuro, Y.; Schneider, J. P.; DeGrado, W. F. *J. Am. Chem. Soc.*, **1999**, *121*, 12200.
60. Kritzer, J. A.; Lear, J. D.; Hodsdon, M. E.; Schepartz, A. *J. Am. Chem. Soc.* **2004**, *126*, 9468.
61. Stephens, O. M.; Kim, S.; Welch, B. D.; Hodsdon, M. E.; Kay, M. S.; Schepartz, A. *J. Am. Chem. Soc.* **2005**, *127*, 13126.
62. English, E. P.; Chumanov, R. S.; Gellman, S. H.; Compton, T. *J. Biol. Chem.* **2006**, *28*, 2661.
63. Kim, J.; Kwon, S.; Kim, S. H.; Lee, C.-K.; Lee, J. -H.; Cho, S. J.; Lee, H. -S.; Ihee, H. *J. Am. Chem. Soc.* **2012**, *134*, 20573.
64. (a) Runnels, C. M.; Lanier, K. A.; Williams, J. K.; Bowman, J. C.; Petrov, A. S.; Hud, N. V.; Williams, L. D. *J. Mol. Evol.* **2018**, *86*, 598. (b) Rose, G. D.; Fleming, P. J.; Banavar, J. R.; Maritan, A. *Proc. Natl. Acad. Sci. U. S. A.* **2006**, *103*, 16623.
65. (a) Reches, M.; Gazit, E. *Science* **2003**, *300*, 625. (b) Frederix, P. W.; Scott, G. G.; Abul-Haija, Y. M.; Kalafatovic, D.; Pappas, C. G.; Javid, N.; Hunt, N. T.; Ulijn, R. V.; Tuttle, T. *Nat. Chem.* **2015**, *7*, 30. (c) Reches, M.; Porat, Y.; Gazit, E. *J. Biol. Chem.* **2002**, *277*, 35475.
66. (a) Wang, J.; Liu, K.; Xing, R.; Yan, X. *Chem. Soc. Rev.* **2016**, *45*, 5589. (b) Whitesides, G. M.; Grzybowski, B. *Science* **2002**, *295*, 2418.

67. (a) Bartnikas, T. B.; Gitlin, J. D. *Nat. Struct. Biol.* **2001**, *8*, 733. (b) Vallee, B. L.; Williams, R. *Proc. Natl. Acad. Sci. U. S. A.* **1968**, *59*, 498.
68. Ring, D.; Wolman, Y.; Friedmann, N.; Miller, S. L. *Proc. Natl. Acad. Sci. U. S. A.* **1972**, *69*, 765.
69. (a) Kluska, K.; Adamczyk, J.; Krężel, A. *Coord. Chem. Rev.* **2018**, *367*, 18. (b) Lee, S. J.; Michel, S. L. *J. Acc. Chem. Res.* **2014**, *47*, 2643. (c) Krizek, B. A.; Amann, B. T.; Kilfoil, V. J., Merkle, D. L., Berg, J. M. *J. Am. Chem. Soc.* **1991**, *113*, 4518.
70. Scintilla, S.; Bonfio, C.; Belmonte, L.; Forlin, M.; Rossetto, D.; Li, J.; Cowan, J. A.; Galliani, A.; Arnesano, F.; Assfalg, M.; *Chem. Commun.* **2016**, *52*, 13456.
71. Ghadiri, M. R.; Fernholz, A. K. *J. Am. Chem. Soc.* **1990**, *112*, 9633.
72. (a) Zou, R., Wang, Q.; Wu, J., Wu, J., Schmuck, C., Tian, H. *Chem. Soc. Rev.* **2015**, *44*, 5200. (b) Ousaka, N., Takeyama, Y., Iida, H., Yashima, E. *Nat. Chem.* **2011**, *3*, 856.
73. (a) Sawada, T., Matsumoto, A., Fujita, M. *Angew. Chem. Int. Ed.* **2014**, *53*, 7228. (b) Inomata, Y., Sawada, T., Fujita, M. *Chem* **2020**, *6*, 294. (d) Sawada, T., Fujita, M. *Chem* **2020**, *6*, 1861.
74. (a) Przybyla, D. E., Chmielewski, J. *J. Am. Chem. Soc.* **2008**, *130*, 12610. (b) Nepal, M., Sheedlo, M. J., Das, C., Chmielewski, J. *J. Am. Chem. Soc.* **2016**, *138*, 11051.
75. (a) Dublin, S. N., Conticello, V. P. *J. Am. Chem. Soc.* **2008**, *130*, 49.

## *Chapter 2A*

*Effect of Substituents to Construct Achiral  
Double Helices: An Approach of Conformational  
Adaptation of Peptide Foldamer*



## 1. Introduction:

Double-helices are the most important structural features of nucleic acids.<sup>1</sup> The double-helical structural motif plays a crucial role in storing genetic information in nucleic acids. In DNA the two nucleic acid strands are intertwined through intermolecular H-bonds of base pairs of the opposite strands.<sup>2</sup> The double helical structures are unique to nucleic acids. The double helical structures are rarely observed in other natural biopolymers. Nevertheless, the natural peptide antibiotic gramicidin A produced by the *Bacillus Brevis* adopts the double-helical conformation.<sup>3</sup> The interesting feature of gramicidin A is that it consists of alternative L- and D-amino acids. In addition, this peptide consists of fully hydrophobic amino acids. The structural studies revealed environment-dependent structural heterogeneity of gramicidin A. In organic solvents, the gramicidin A adopted a left-handed, antiparallel  $\beta$ -double helix and also a right-handed parallel  $\beta$ -double helix conformation.<sup>4</sup> However, in the presence of Cs<sup>+</sup> ions in a methanol-chloroform solvent mixture, it converges into a right-handed anti-parallel double helix with ions bound.<sup>5</sup> No definite structure was observed in 1:1 DMSO-acetone solvents.<sup>6</sup> In ethanol, four different structures, parallel  $\beta$ <sup>5,6</sup> double helices differing only in hydrogen bond registry, a right-handed parallel  $\beta$ <sup>5,6</sup> double helix and a left-handed anti-parallel  $\beta$ <sup>5,6</sup> double helix were observed. Single anti-parallel double helical structures were observed in benzene-ethanol solvent combinations and also in X-ray diffracted single crystal structures.<sup>7,8</sup> Along with the  $\beta$ -double helical conformations, the peptide also adopts a single-stranded beta-helix structure in the lipid bilayer.<sup>9</sup> As the peptide consists of alternating L- and D-amino acids, it displays no net dipole. The single-strand  $\beta$ -helix of gramicidin A is stabilized by the intramolecular H-bonds, two single  $\beta$ -helices form head-to-head and tail-to-tail dimers in lipids.<sup>10</sup> These dimer structures serve as membrane channels to transport the ions. These membrane channels are uncharged and highly cation-specific. In addition to the experimental observations, the theoretical studies also suggested that wide-bore helical structures of gramicidin A wound around a helical axis.<sup>11</sup> In addition to the gramicidin A, another naturally occurring peptide antibiotic feglymycin, isolated from *Streptomyces* sp. consisting of unnatural amino acids with alternating L- and D-configurations adopted a  $\beta$ -double-helical conformation.<sup>12</sup> It also adopts the beta-double helical structure similar to the gramicidin A. The two strands are intertwined by intermolecular H-bonds. In comparison to gramicidin A, feglymycin functions as an ion transporter, not as a membrane channel.<sup>13</sup> The peptide feglymycin showed weak antibacterial activity against Gram-positive bacteria, however,

showed strong inhibitory activity in HIV syncytia formation in vitro.<sup>14</sup> The double helical structures of nucleic acids, gramicidin A, and feglymycin are shown in Figure 1.

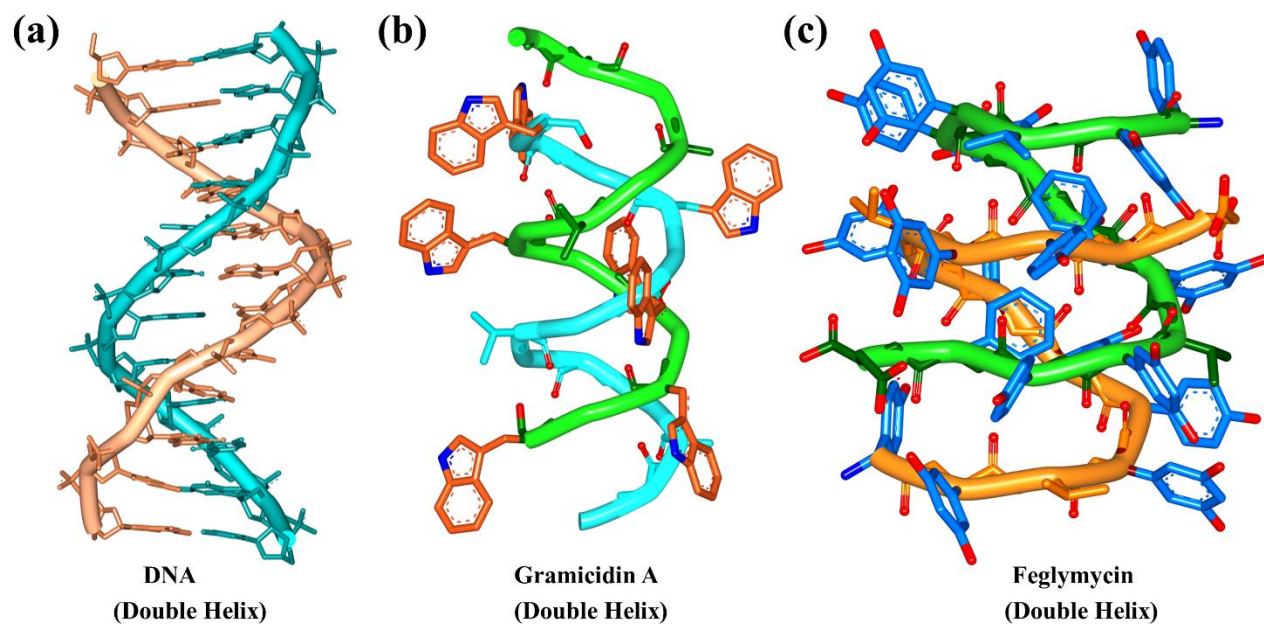


**Figure 1:** Different types of double helical structures of (a) Nucleic acids (PDB: 1BNA), (b) Gramicidin A(PDB: 1AV2), and (c) Feglymycin<sup>12</sup>.

Based on the structural information of gramicidin A and feglymycin, efforts have been made in the literature to design double helical structures from peptide sequences composed of the alternating L and D-amino acids. Benedetti and colleagues reported the first crystal structure of the  $\beta$ -double helix from the synthetic peptide composed of alternating L- and D-amino acids.<sup>15</sup> In addition to the alternating L- and D-peptides,<sup>16</sup> Lehn and Huc and colleagues reported the double helical structure from the oligomers consisting of aromatic oligoamide.<sup>17</sup> The double helical structure in aromatic oligoamides is stabilized by  $\pi$ - $\pi$  stacking and H-bonds between the  $\beta$ -strands. In addition, a variety of aromatic oligoamides have shown to adopt double helical conformations through metal coordination, H-bonding, ionic bonding and van der Waals interactions.<sup>18, 19</sup> Further, double helical structures have also been reported from 1:1 alternating electron-rich 1,5-dialkoxy-naphthalene (DAN) and electron-deficient 1,4,5,8-naphthalene-tetracarboxylic diimides (NDI).<sup>20</sup> Further, Yashima and colleagues reported the double helix structures derived from the meta-terphenyl derivatives and these structures are stabilized through amidinium-carboxylate salt bridges.<sup>21a-c</sup> The representative double helical structures observed in the L, D-peptides, aromatic oligoamides, organic templates and metal-coordinated<sup>21d</sup> double helical structures are shown in Figure 2.

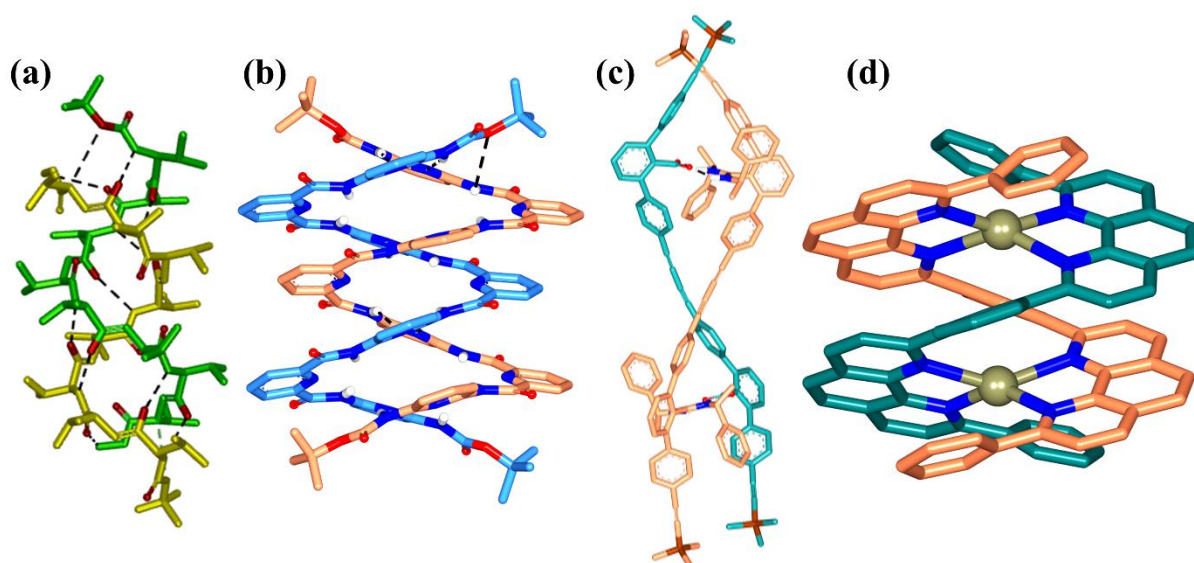


**Figure 2:** Representation of double helical structures observed in the (a) L, D-peptides<sup>15</sup>, (b) Aromatic oligoamides,<sup>17a</sup> (c) organic templates<sup>21a</sup>, and (d) Metal-coordinated aromatic ligand<sup>21d</sup>.

## 2. Object of the Present Work:

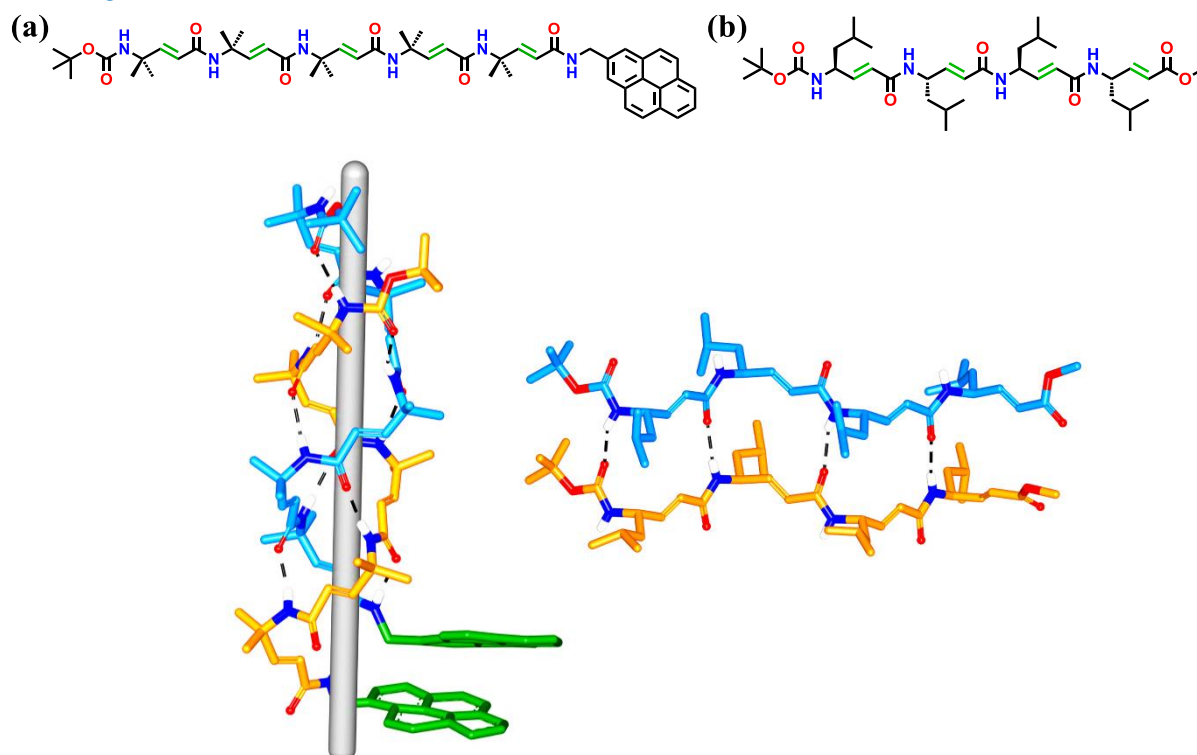


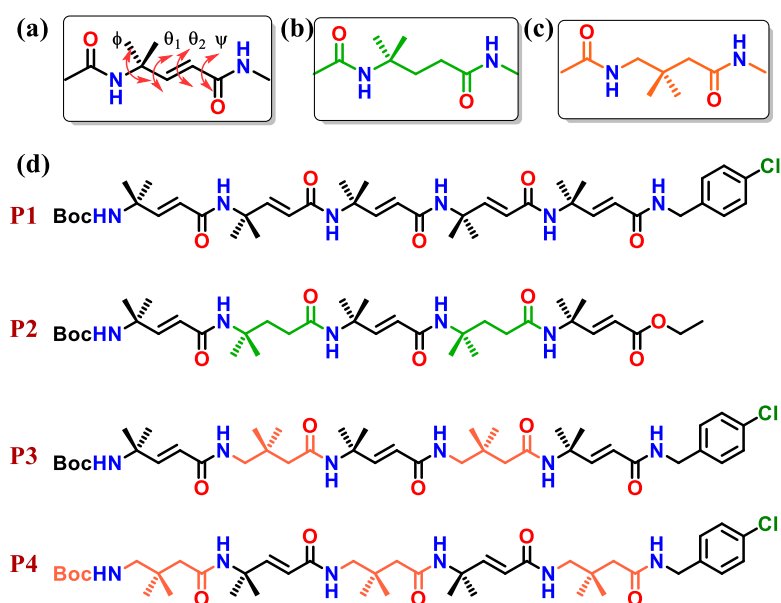
**Figure 3:** (a) The double-helical structure<sup>22a</sup> and (b)  $\beta$ -structures of  $\alpha$ ,  $\beta$ -unsaturated  $\gamma$ -amino acids<sup>22b</sup>.

We have been interested in the conformational analysis of peptides composed of non-natural  $\gamma$ -amino acids. Recently, we demonstrated that oligomers composed of (*E*)- $\alpha,\beta$ -unsaturated 4,4-dialkyl  $\gamma$ -amino acids adopted double helical conformations in single crystals.<sup>22</sup> Interestingly, these oligomers adopt  $\beta$ -sheet type structures after removing the dialkyl constraints at  $\gamma$ -positions. The double helical structures and  $\beta$ -structures of (*E*)- $\alpha,\beta$ -unsaturated  $\gamma$ -amino acids are shown in Figure 3. Encouraged by these fascinating double helical structures from (*E*)- $\alpha,\beta$ -unsaturated  $\gamma$ -amino acids, we sought to investigate the necessity of the double bonds in dialkyl  $\gamma$ -amino acids in adopting double helical conformations. In this Chapter, we are reporting the conformational properties of 1:1 alternating unsaturated and saturated 4,4-dialkyl  $\gamma$ -amino acids (Aic) and 3,3-dialkyl  $\gamma$ -amino acids (Adb). We designed pentapeptides, **P1-P4** (Scheme 1), synthesized in the solution phase method, and studied their conformations in single crystals.

### 3. Results and Discussion:

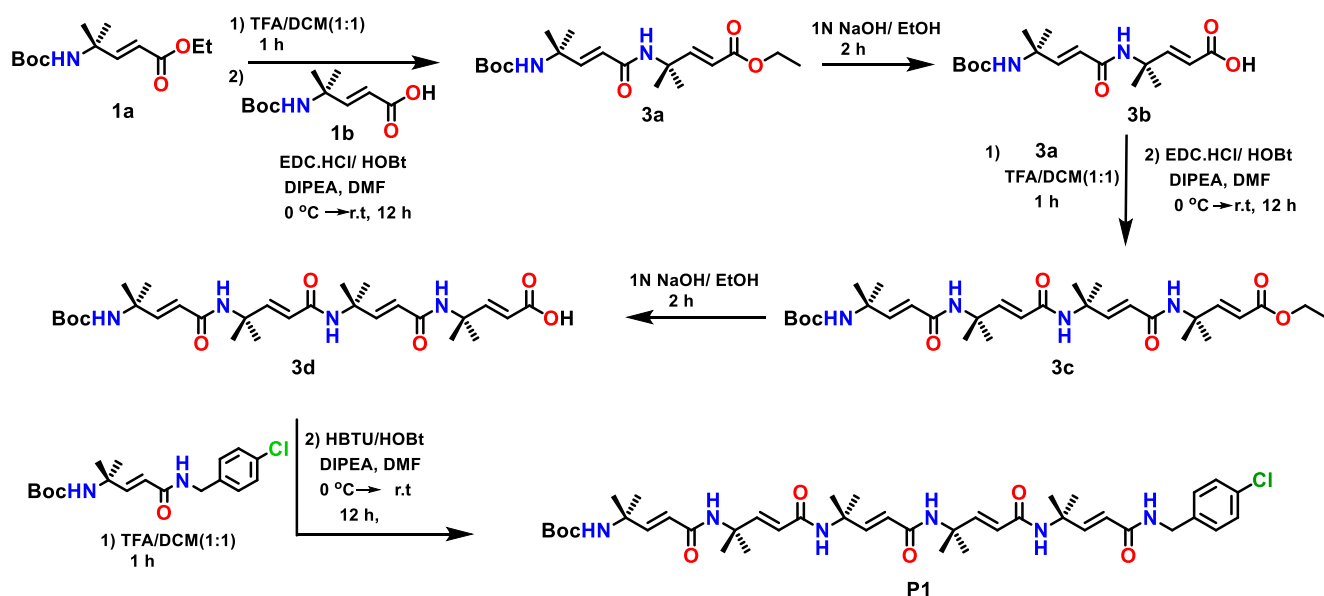
#### 3.1. Design and Synthesis of Peptides (P1-P4):

In order to understand the conformational properties of peptides composed of 1:1 alternating (*E*)- $\alpha,\beta$ -unsaturated 4,4-dialkyl  $\gamma$ -amino acids and 4,4-dialkyl  $\gamma$ -amino acids and 3,3-dialkyl  $\gamma$ -amino acids, we designed pentapeptides, **P1-P4**. The sequences of these peptides are shown in Scheme 1.



**Scheme 1:** (a-c) The building blocks amino acid residue used. (d) Sequences of design peptides (**P1-P4**)

Peptide **P1** is an oligomer of (*E*)- $\alpha,\beta$ -unsaturated 4,4-dimethyl  $\gamma$ -amino acids. Peptide **P2** consists of alternating (*E*)- $\alpha,\beta$ -unsaturated 4,4-dimethyl  $\gamma$ -amino acids and 4,4-dimethyl  $\gamma$ -amino acids. Peptide **P3** consists of alternating (*E*)- $\alpha,\beta$ -unsaturated 4,4-dimethyl  $\gamma$ -amino acids and 3,3-dimethyl  $\gamma$ -amino acids. Peptide **P4** consists of alternating 3,3-dimethyl  $\gamma$ -amino acids and  $\alpha,\beta$ -unsaturated 4,4-dimethyl  $\gamma$ -amino acids. The C-terminal of peptides **P1**, **P3**, and **P4** are coupled with 4-chlorobenzylamine. The peptide **P2** is an ethyl ester. The *N*-terminus of all peptides were protected by the Boc group. The (*E*)- $\alpha,\beta$ -unsaturated 4,4-dimethyl  $\gamma$ -amino acid, and 3,3-dimethyl  $\gamma$ -amino acids were synthesized as reported earlier.<sup>23,24</sup> All four peptides were synthesized in the solution phase method. The combination of EDC.HCl and HOBt were used as coupling agents in the peptide synthesis. The Boc groups were deprotected using 50% TFA in DCM. The ethyl esters were hydrolyzed using 1N NaOH. Peptides, **P1-P3**, were synthesized using the (2+2+1) coupling strategy, whereas peptide **P4** was synthesized using the (2+3) coupling strategy. Interestingly, we found that the extension of peptides from the C-terminus was relatively easier than the *N*-terminus. Several attempts were made to extend the tetrapeptide to pentapeptide from the *N*-terminus, however, always obtained relatively poor yields of the pentapeptide. The schematic representation of the synthesis of peptide **P1** is shown in Scheme 2.



**Scheme 2:** Synthesis of pentapeptide **P1**

All other peptides were synthesized using the same strategy as shown in Scheme 2. All peptides were isolated in good yields and subjected to structural analysis.

## 3.2. Crystal Structure Analysis of Peptides (P1-P4):

### 3.2.1. Crystal Structure Analysis of Peptide (P1):

As X-ray diffracted single crystal structures give unambiguous structural information, we subjected all four peptides for crystallization in various solvent combinations. The single crystals of peptide **P1** were obtained from the slow evaporation of peptide solution in the  $\text{CHCl}_3$  and n-heptane solvents mixture. The X-ray diffracted single crystal structure of peptide **P1** is shown in Figure 4a. Similar to the tetrapeptides reported earlier,<sup>21</sup> the peptide **P1** adopted double-helical conformation in single crystals.

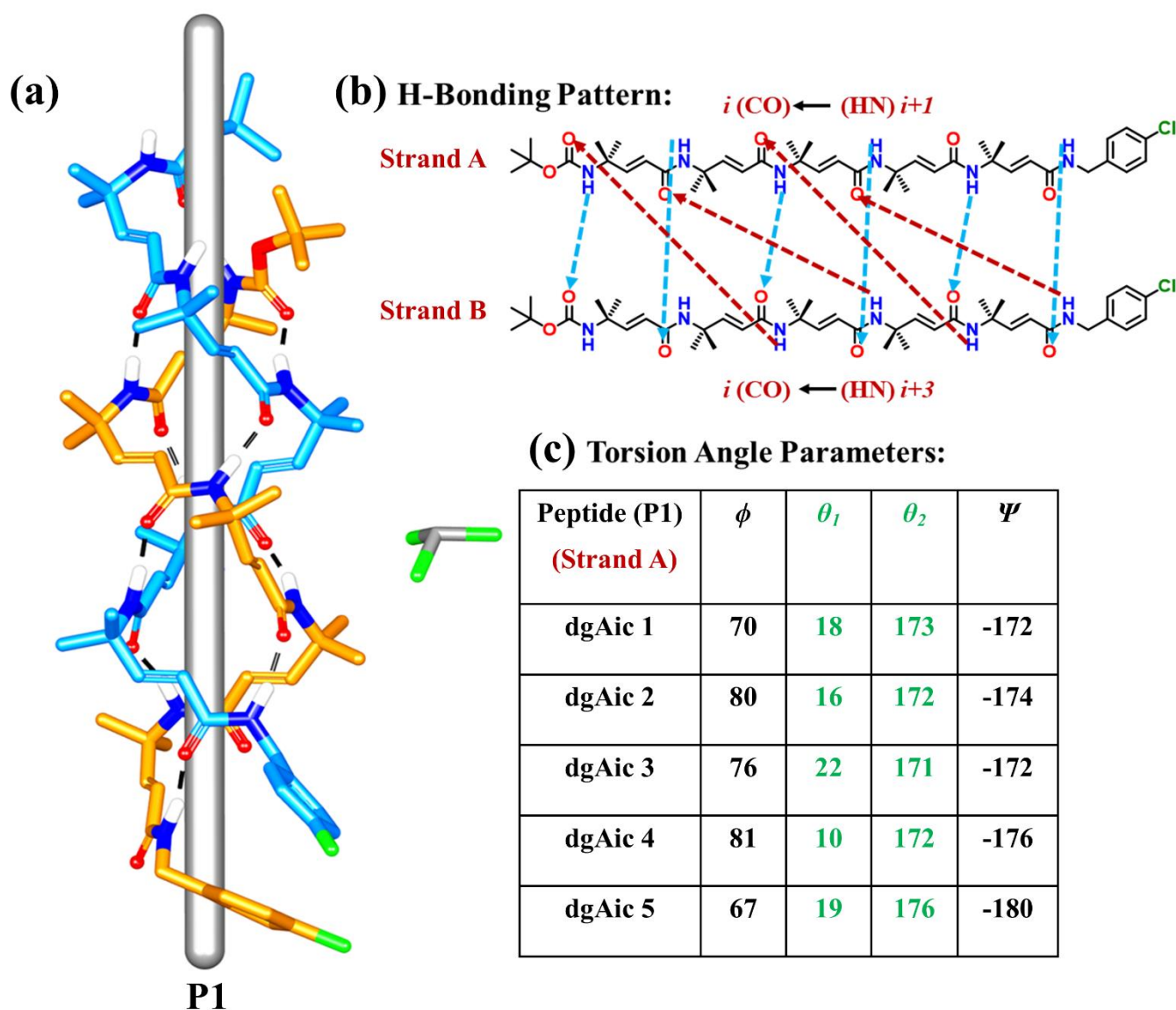


**Figure 4:** (a) Single crystal structure of **P1**. To get a better view of parallel  $\beta$ -double helices, pictorially rods are created along the central axis. (b) Intermolecular hydrogen bonding patterns between two strand A and strand B and (c) Torsion angle parameters (strand A) are shown.

The two peptide strands in the double helix are held together by ten intermolecular H-bonds between strand A and strand B. The donor amide CO group in residue  $i$  of strand B is involved in the H-bond with the amide NH group of the residue  $i+1$  in strand A ( $i \rightarrow i+1$ ). Additionally, the amide CO group of the residue  $i$  in strand A is involved in the H-bond with the amide NH group of the residue  $i+3$  in strand B. The structure has displayed a unique pattern of H-bonds. More importantly, no amide NH or CO groups along the strands are exposed for the H-bonds with other strands, except the N-terminal amide NH of strand B and the C-terminal amide CO of strand A. The intermolecular H-bonds between strand A and strand B are depicted in Figure 4b. The H-bond parameters of the **P1** double-helix are tabulated in Table 1. The parameters of the observed H-bonds are within the limits of standard H-bonds parameters reported in the literature.<sup>25</sup>

**Table 1:** The H-bond parameters of the **P1** double helix are tabulated.

<b>Donor (D)</b>	<b>Acceptor (A)</b>	<b>D...A (Å)</b>	<b>DH...A (Å)</b>	<b>NH...O (deg)</b>
<b>N1</b>	<b>O2</b>	<b>2.98</b>	<b>2.12</b>	<b>173</b>
<b>N2</b>	<b>O3</b>	<b>2.79</b>	<b>1.94</b>	<b>173</b>
<b>N3</b>	<b>O4</b>	<b>2.81</b>	<b>1.95</b>	<b>177</b>
<b>N4</b>	<b>O5</b>	<b>2.79</b>	<b>1.95</b>	<b>166</b>
<b>N5</b>	<b>O6</b>	<b>2.73</b>	<b>1.88</b>	<b>169</b>
<b>N6</b>	<b>O7</b>	<b>2.80</b>	<b>1.97</b>	<b>167</b>
<b>N9</b>	<b>O9</b>	<b>2.85</b>	<b>2.01</b>	<b>164</b>
<b>N10</b>	<b>O10</b>	<b>2.89</b>	<b>2.03</b>	<b>173</b>
<b>N11</b>	<b>O11</b>	<b>2.81</b>	<b>1.95</b>	<b>172</b>

The torsion angles of  $\gamma$ -residues can be analyzed using torsion parameters  $\phi$ ,  $\theta_1$ ,  $\theta_2$  and  $\psi$  as depicted in Figure 4c. As the  $\theta_2$  represents the *trans*-carbon-carbon double bond, the torsion value will be always  $\pm 180^\circ$  or closer to  $180^\circ$ . The careful structure analysis of **P1** revealed that  $\phi$  it has an average value of  $68^\circ \pm 12^\circ$ . Further, the value of  $\theta_1$  is closer to  $0^\circ$ . Interestingly, both torsion angles  $\theta_2$  and  $\psi$  adopted the extended conformation with values closer to  $180^\circ$ . Being achiral in nature, we observed two molecules in the asymmetric unit with opposite signs in the

torsion angles. The observed sign of torsion parameters is +, +, +, - or -, -, -, or +. The observed torsion parameters of **P1** are consistent with the previously reported results from our laboratory.<sup>20</sup> Overall, the structural analysis suggested that the **P1** adopted a double helical conformation with similar H-bond and torsion angles as reported earlier.

### 3.2.2. Crystal Structure Analysis of Peptide (**P2**):

The single crystals of peptide **P2** were obtained after the slow evaporation of the peptide solution in the CHCl<sub>3</sub> and xylene solvents. The X-ray diffracted single crystal structure of peptide **P2** is shown in Figure 5a. Fascinatingly, the hybrid peptide **P2** consisting of both dgAic and Aic residues adopted the  $\beta$ -double helix conformation in single crystals. The Aic residues are nicely accommodated into the  $\beta$ -double helix conformation. The double-helix structure is stabilized by eight inter-strand H-bonds. The C-terminal residues are distorted away from the canonical  $\beta$ -double helical structure due to the lack of terminal amide NH groups.

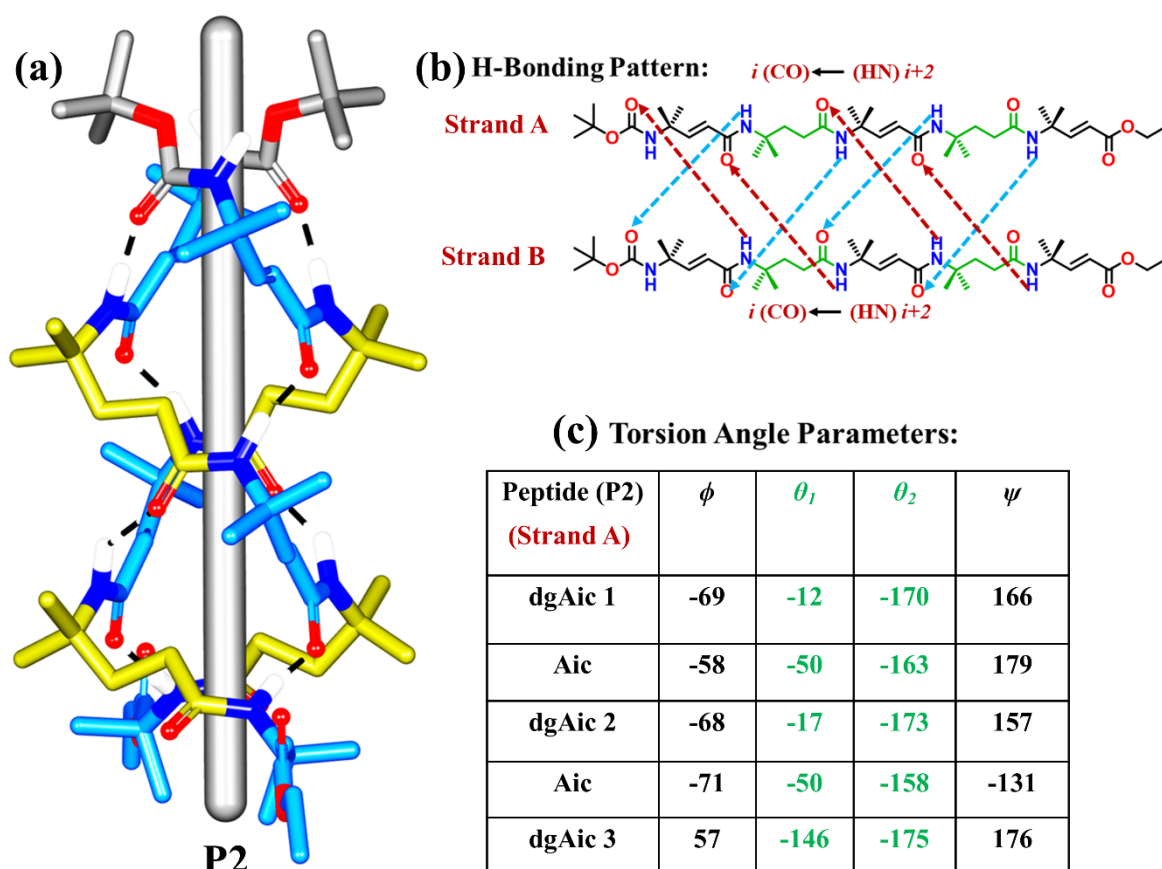


**Figure 5:** (a) Single crystal structure of **P2**. To get a better view of parallel  $\beta$ -double helices, pictorially rods are created along the central axis. (b) Intermolecular hydrogen bonding patterns between two strand A and strand B and (c) Torsion angle parameters (strand A) are shown.



The donor amide CO group in residue  $i$  of strand B is involved in the H-bonding with the amide NH group of residue  $i+2$  in strand A ( $i \rightarrow i+2$ ). Similarly, the amide CO group of residue  $i$  in strand A is involved in the H-bonding with the amide NH group of residue  $i+2$  in strand B ( $i \rightarrow i+2$ ). The H-bonding pattern observed in the **P2** is different from the H-bonding pattern observed in the crystal structure of **P1**. The N-terminal Boc-amide NH groups and C-terminal ester CO groups are not involved in the inter-strand H-bonding interactions, however, they are involved in the intermolecular H-bonds with other  $\beta$ -double helices. The schematic representation of the inter-strand H-bonds observed in **P2** is shown in Figure **5b**. The H-bond parameters of the **P2** double helix are tabulated in Table 2. The parameters of the observed H-bonds are within the limits of standard H-bonds parameters.

**Table 2:** The H-bond parameters of the **P2** double-helix are tabulated.

<b>Donor (D)</b>	<b>Acceptor (A)</b>	<b>D...A (Å)</b>	<b>DH...A (Å)</b>	<b>NH...O (deg)</b>
<b>N17</b>	<b>O18</b>	<b>2.90</b>	<b>2.04</b>	<b>174</b>
<b>N12</b>	<b>O26</b>	<b>2.90</b>	<b>2.05</b>	<b>171</b>
<b>N18</b>	<b>O19</b>	<b>2.87</b>	<b>2.07</b>	<b>155</b>
<b>N13</b>	<b>O27</b>	<b>2.88</b>	<b>2.06</b>	<b>155</b>
<b>N19</b>	<b>O20</b>	<b>2.89</b>	<b>2.13</b>	<b>147</b>
<b>N14</b>	<b>O28</b>	<b>2.91</b>	<b>2.17</b>	<b>144</b>
<b>N20</b>	<b>O21</b>	<b>2.89</b>	<b>2.04</b>	<b>174</b>
<b>N15</b>	<b>O29</b>	<b>2.90</b>	<b>2.04</b>	<b>174</b>

Careful structural analysis of **P2** revealed a very interesting pattern of torsion angle parameters. The dgAic residues displayed similar torsion angle parameters as observed in the crystal structure of **P1**. The average torsion angle parameters are  $\phi = -70^\circ \pm 3^\circ$ ,  $\theta_1 = -0^\circ \pm 17^\circ$ ,  $\theta_2 = -173^\circ \pm 5^\circ$ , and  $\psi = +162^\circ \pm 5^\circ$ . In contrast to dgAic residues, the Aic residues displayed different torsion angle parameters. The average torsion angle parameters are  $\phi = -65^\circ \pm 8^\circ$ ,  $\theta_1 = -50^\circ \pm 2^\circ$

$\theta_2 = -160^\circ \pm 5^\circ$ , and  $\psi = +162^\circ \pm 5^\circ$ . Interestingly, in dgAic the  $\theta_1$  generally takes the value close to  $0^\circ$ , however, in Aic,  $\theta_1$  takes the value  $-50^\circ \pm 2^\circ$ . The torsion angles of C-terminal residues were not included in the calculation of average torsion angles. The torsion angles of the peptide **P2** are given in Figure 5c. Overall these results suggested that Aic residues can be accommodated into the  $\beta$ -double helix conformation without much deviation from the overall double helix structure.

### 3.2.3. Crystal Structure Analysis of Peptide (P3):

The single crystals of peptide **P3** were obtained after the slow evaporation of the peptide solution in the EtOAc and n-hexane solvent mixture. The X-ray diffracted single crystal structure of peptide **P3** is shown in Figure 6a.

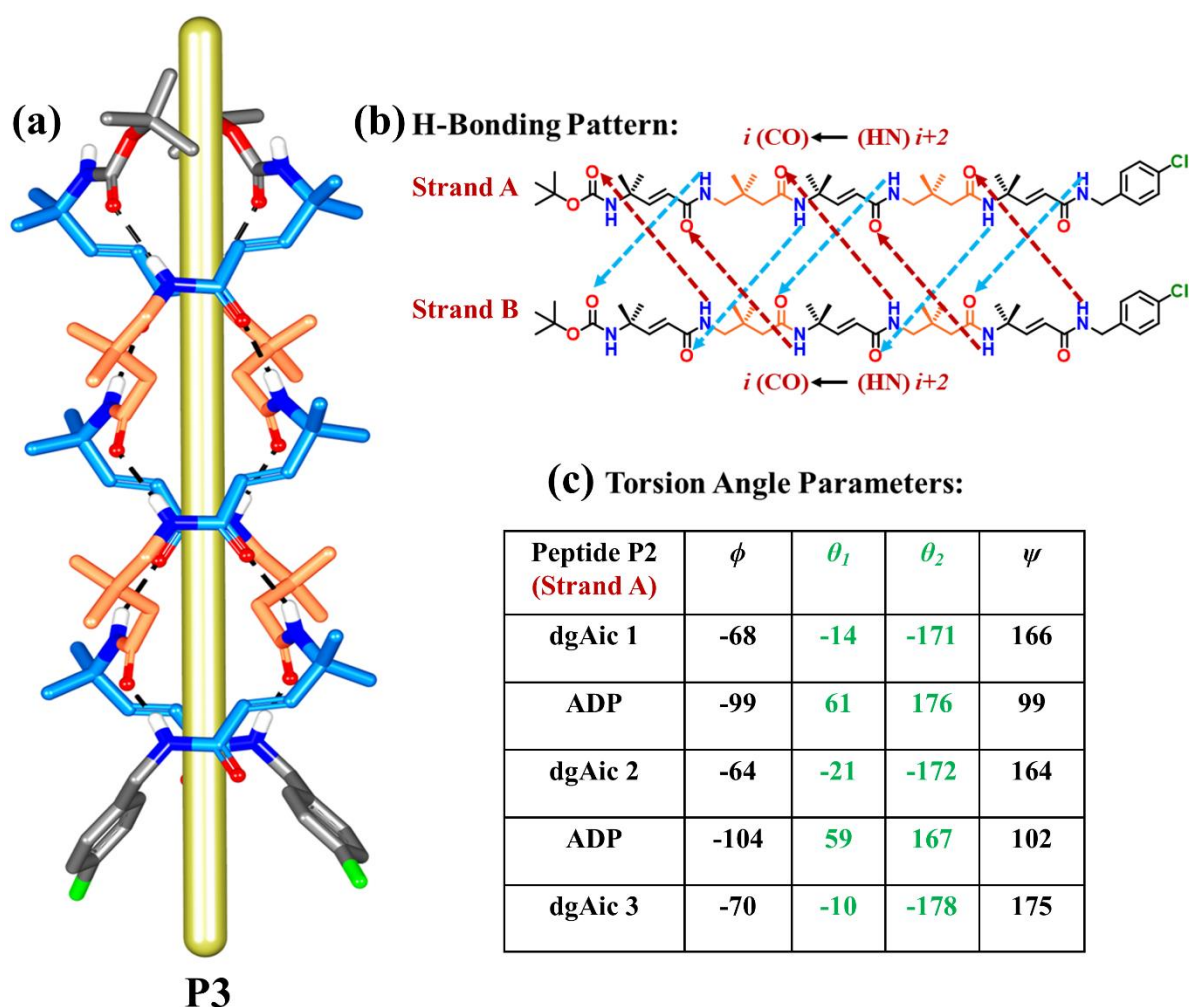


**Figure 6:** (a) Single crystal structure of **P3**. To get a better view of parallel  $\beta$ -double helices, pictorially rods are created along the central axis. (b) Intermolecular hydrogen bonding patterns between two strand A and strand B and (c) Torsion angle parameters (strand A) are shown.

Interestingly, the hybrid pentapeptide **P3** consisting of alternating dgAic and Adb residues adopted  $\beta$ -double helix conformation in single crystals. The Adb residues are nicely accommodated into the double helix conformation. The peptide strands A and B are intertwined through inter-strand H-bonds and the  $\beta$ -double helix structure is stabilized by ten inter-strand H-bonds. The donor amide CO group in residue  $i$  of strand B is involved in the H-bonding with the amide NH group of the residue  $i+2$  in strand A ( $i \rightarrow i+2$ ). Similarly, the amide CO group of the residue  $i$  in strand A is involved in the H-bonding with the amide NH group of the residue  $i+2$  in strand B ( $i \rightarrow i+2$ ). The H-bond pattern observed in **P3** is different from the H-bond pattern observed in the crystal structure of **P1**. The schematic representation of the inter-strand H-bonds observed in **P3** is shown in Figure 6b. The H-bond parameters of the **P3** double helix are tabulated in Table 3. The parameters of the observed H-bonds are within the limits of standard H-bonds parameters.

**Table 3:** The H-bond parameters of the **P3** double-helix are tabulated.

<b>Donor (D)</b>	<b>Acceptor (A)</b>	<b>D...A (Å)</b>	<b>DH...A (Å)</b>	<b>NH...O (deg)</b>
<b>N2</b>	<b>O2</b>	<b>2.90</b>	<b>2.07</b>	<b>165</b>
<b>N3</b>	<b>O3</b>	<b>3.00</b>	<b>2.14</b>	<b>173</b>
<b>N4</b>	<b>O4</b>	<b>2.90</b>	<b>2.04</b>	<b>175</b>
<b>N5</b>	<b>O5</b>	<b>2.99</b>	<b>2.17</b>	<b>159</b>
<b>N6</b>	<b>O6</b>	<b>2.78</b>	<b>1.98</b>	<b>153</b>

The crystal structure analysis of **P3** revealed an interesting pattern of torsion angles. The dgAic residues displayed similar torsion angle values as that of the residues observed in the structure of **P1**. The average torsion angles of the dgAic residues in the double helix **P3** are  $\phi = -68^\circ \pm 5^\circ$ ,  $\theta_1 = -0^\circ \pm 20^\circ$ ,  $\theta_2 = -174^\circ \pm 5^\circ$ , and  $\psi = +169^\circ \pm 5^\circ$ . In contrast to dgAic residues, the 3,3-dimethyl  $\gamma$ -amino acid(Adb) residues displayed entirely different torsion angles. The average torsion angles are  $\phi = -102^\circ \pm 3^\circ$ ,  $\theta_1 = 60^\circ \pm 2^\circ$ ,  $\theta_2 = 172^\circ \pm 5^\circ$ , and  $\psi = +101^\circ \pm 2^\circ$ . Instructively, the torsion angles  $\phi$  and  $\psi$  displayed are  $-101^\circ$  and  $+102^\circ$ , respectively. The  $\theta_1$  generally takes the value close to  $0^\circ$ , however in the case of Adb,  $\theta_1$  takes the value  $60^\circ \pm 2$  and adopted the gauche

conformation along the N-C $\gamma$ -C $\beta$ -C $\alpha$  bond. The torsion angle  $\theta_2$  displayed a value close to 180°. Interestingly, only  $\phi$  displayed the -ve sign and the other torsion angles displayed the +ve sign. The torsion angles of the peptide **P3** are given in Figure 6c. Overall these results suggested that Adb residues can be accommodated into the double-helix structure without much deviation from the overall double-helix conformation.

### 3.2.4. Crystal Structure Analysis of Peptide (P4):

As peptide **P3** nicely accommodated saturated Adb residues into the double-helix, we sought to investigate whether or not Adb can be accommodated at the N- and C- termini of the peptide instead of unsaturated residues. For that, we have designed peptide **P4** which was synthesized. The single crystals of peptide **P4** were obtained after the slow evaporation of the peptide solution in the EtOAc and n-hexane solvents.

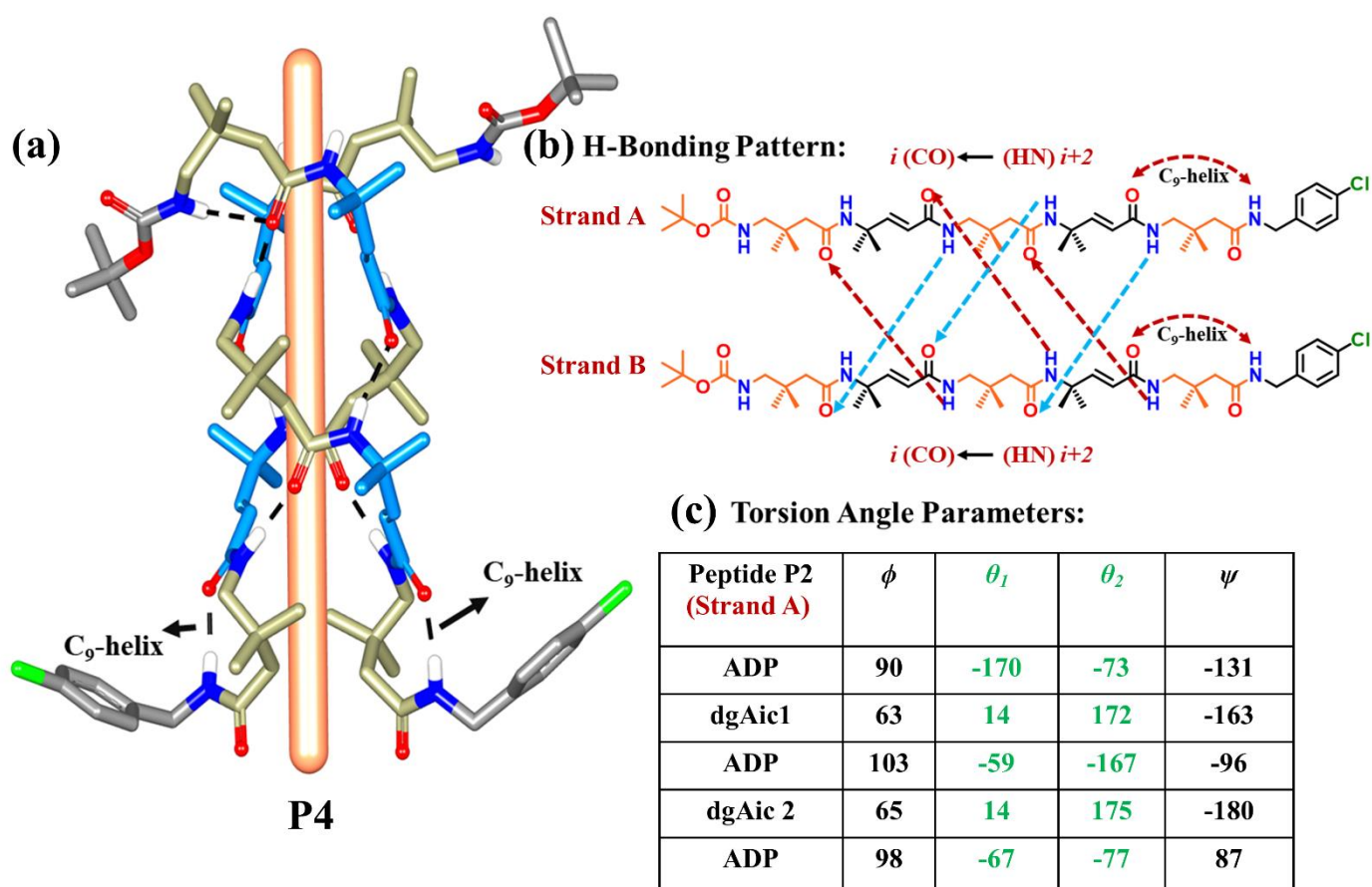


**Figure 7:** (a) Single crystal structure of **P4**. To get a better view of parallel  $\beta$ -double-helices, pictorially rods are created along the central axis. (b) Intermolecular hydrogen bonding patterns between two strand A and strand B and (c) Torsion angle parameters (strand A) are shown.

The X-ray diffracted single crystal structure of peptide **P4** is shown in Figure 7. Interestingly, the hybrid pentapeptide **P4** consisting of alternating Adb and dgAic residues adopted a kind of distorted  $\beta$ -double helix conformation in single crystals. Both the N-terminal and C-terminal Adb residues did not take part in the double-helix conformation. Interestingly, the middle three residues dgAic-Adb-dgAic adopted double-helical conformation. One of the N-terminal Adb residues is involved in the intramolecular 7-membered H-bond. Again, the C-terminal Adb residues are also involved in the intramolecular 9-membered H-bonds. Both peptide strands A and B are intertwined in the middle and adopted double helix conformation. The double helix conformation is stabilized by six inter-strand H-bonds. The donor amide CO group in residue  $i$  of strand B is involved in the H-bonding with the amide NH group of the residue  $i+2$  in strand A ( $i \rightarrow i+2$ ). Similarly, the amide CO group of the residue  $i$  in strand A is involved in the H-bonding with the amide NH group of the residue  $i+2$  in strand B ( $i \rightarrow i+2$ ). The H-bonding pattern observed in **P4** is similar to the pattern observed in **P3**. The schematic representation of the intra and inter-strand H-bonds observed in **P4** is shown in Figure 7b. The H-bond parameters of the **P4** double helix are tabulated in Table 4.

**Table 4:** The H-bond parameters of the **P4** double-helix are tabulated.

<b>Donor (D)</b>	<b>Acceptor (A)</b>	<b>D...A (Å)</b>	<b>DH...A (Å)</b>	<b>NH...O (deg)</b>
<b>N4</b>	<b>O10</b>	<b>2.77</b>	<b>1.91</b>	<b>173</b>
<b>N5</b>	<b>O11</b>	<b>2.98</b>	<b>2.13</b>	<b>166</b>
<b>N6</b>	<b>O12</b>	<b>2.85</b>	<b>1.99</b>	<b>173</b>
<b>N7</b>	<b>O6</b>	<b>2.81</b>	<b>1.96</b>	<b>170</b>
<b>N10</b>	<b>O3</b>	<b>2.85</b>	<b>1.99</b>	<b>176</b>
<b>N11</b>	<b>O4</b>	<b>2.94</b>	<b>2.15</b>	<b>152</b>
<b>N12</b>	<b>O5</b>	<b>2.82</b>	<b>1.96</b>	<b>172</b>
<b>N13</b>	<b>O13</b>	<b>2.80</b>	<b>1.95</b>	<b>170</b>

The crystal structure analysis of **P4** revealed an interesting pattern of torsion angles. The residues involved in the double helix conformation displayed torsion angles similar to the torsion angles observed in the double helix conformation of **P3**. The average torsion angle parameters of the dgAic residues in the **P4** double helix are  $\phi = 65^\circ \pm 3^\circ$ ,  $\theta_1 = 0^\circ \pm 20^\circ$ ,  $\theta_2 = 175^\circ \pm 5^\circ$ , and  $\psi = -171^\circ \pm 9^\circ$ . The Adb residue involved in the double helix structure displayed the torsion angles,  $\phi = 105^\circ \pm 4^\circ$ ,  $\theta_1 = -59^\circ \pm 1^\circ$ ,  $\theta_2 = -170^\circ \pm 3^\circ$ , and  $\psi = -101^\circ \pm 5^\circ$ . Instructively, the torsion angles  $\phi$  and  $\psi$  displayed values  $105^\circ$  and  $-101^\circ$ , respectively. Interestingly, the Adb residues which did not participate in the double helical conformation displayed different torsion angles without a definite pattern. The torsion angles of the peptide **P4** are tabulated and given in Figure 7c. Overall these results suggested that Adb residues can be accommodated into the double helix flanked by the unsaturated dgAic residues. Incorporation of the Adb residues at both *N*- and *C*-terminals of the peptide may not involve in the double-helical conformation.

## 4. Conclusion:

The single crystal analysis of the peptides, **P1-P4**, revealed that the 4,4-dialkyl  $\gamma$ -amino acids (Aic) and 3,3-dialkyl  $\gamma$ -amino acids (Adb) can be accommodated into the  $\beta$ -double helical conformation in the presence of (*E*)- $\alpha,\beta$ -unsaturated 4,4-dimethyl  $\gamma$ -amino acid residues. Further, the structural analysis suggested that Aic can be accommodated into the  $\beta$ -double helix with different torsion angles. Similarly, Adb also displayed a different pattern of torsion angles in the double-helix conformation. More importantly, Adb residues and also Aic residues can be accommodated into the double helix only when the *N*- and *C*-terminus of these residues are coupled with the dgAic residues. The saturated  $\gamma$ -amino acid residues deviate away from the double helix conformation if they are incorporated at the *C*- and *N*- terminus of the peptide sequence. Overall, these results suggested that (*E*)- $\alpha,\beta$ -unsaturated 4,4-dialkyl  $\gamma$ -amino acid residues are essential to induce double-helical conformation in  $\gamma$ -peptide foldamers. Without these unsaturated amino acids, it may be difficult to design  $\beta$ -double helix conformations in  $\gamma$ -peptide foldamers.

## 5. Experimental Section:

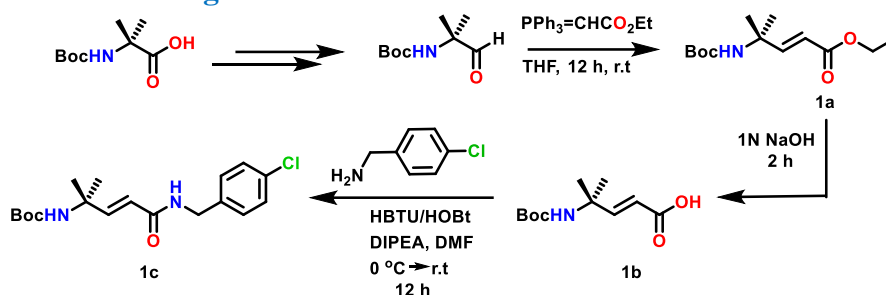
### 5.1. General Method:

All reagents were used without further purification. Column chromatography was performed on neutral alumina (100 -200 mesh).  $^1\text{H-NMR}$  (400 MHz), and  $^{13}\text{C-NMR}$  (101 MHz) were

measured on a Bruker Avance 400 MHz spectrometer. Mass samples were analyzed by High-resolution mass spectrometry using ESI TOF. The X-ray data were collected at 100K temperature on a Bruker APEX(III) DUO CCD diffractometer using Mo K $\alpha$  radiation ( $\lambda = 0.71073 \text{ \AA}$ ).

## 5.2. Procedure for the Synthesis of Peptides:

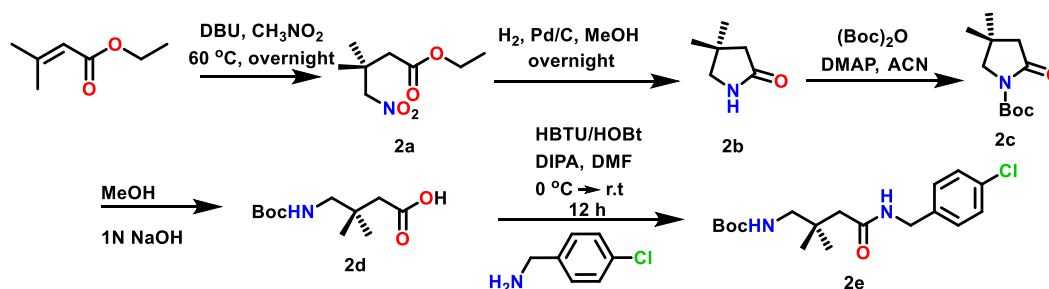
### 5.2.1. Synthesis of Building Unit 1c:



**Scheme 3:** Synthesis of compound 1c.

The  $\alpha,\beta$ -unsaturated  $\gamma^{4,4}$ -amino acid (*trans*- $\alpha,\beta$ -unsaturated 4-aminoisocaproic acid, **1b**) was synthesized starting from the *N*-Boc-Aib acid and then after Wittig reaction, produced **1b** which followed as the previous report.<sup>26</sup> Then **1b** (2.3 g, 10 mmol) was dissolved in 15 mL of DMF and was cooled down to 0 °C under an N<sub>2</sub> atmosphere. To this HBTU (3.79 g, 10 mmol) and HOBt (1.08 g, 8 mmol) were added and the reaction mixture was stirred for 10 minutes. This was followed by the addition of 4-chloro benzylamine (1.8 ml, 15 mmol). The reaction mixture was stirred overnight and the progress was monitored by TLC. Upon completion, the reaction mixture was diluted with 200 mL EtOAc and was washed with 10% HCl (150 mL X 2), 10% Na<sub>2</sub>CO<sub>3</sub> solution (150 mL X 2), and finally brine solution (150 mL X 2). The organic layer was dried over anhydrous Na<sub>2</sub>SO<sub>4</sub> and concentrated under reduced pressure to give a crude powder which was then purified by column chromatography to get a white crystalline product **1c** (yield = 92%).

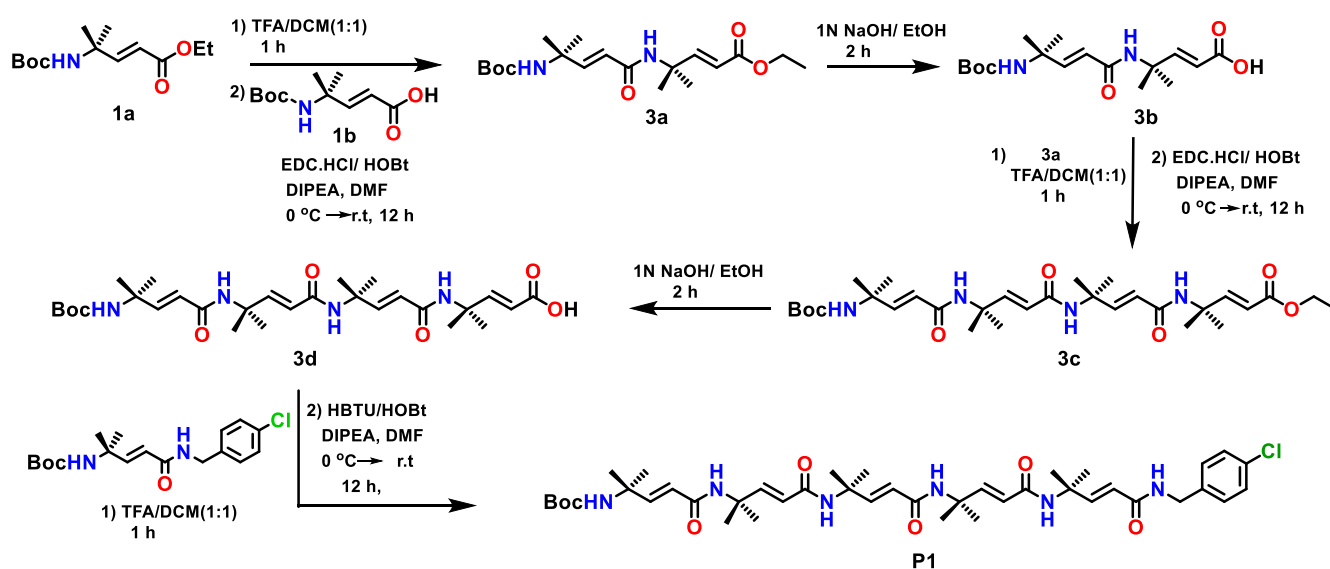
### 5.2.2. Synthesis of Building Unit 2e:



**Scheme 4:** Synthesis of compound 2e.

N-Boc-protected 3,3-dimethyl butanoic acid(2d) was synthesized following the previous report.<sup>24</sup> First, ethyl 3,3-dimethyl acrylate (6.4 g, 50 mmol) was dissolved in nitromethane (13.5 mL, 250 mmol) and DBU (11.2 mL, 75 mmol) was added. The mixture was heated at 65 °C for 12 h. After completion of the reaction 250 ml of EtOAc was added to the reaction mixture and washed with 1M HCl (150 mL X 2). The organic layer was dried over anhydrous Na<sub>2</sub>SO<sub>4</sub> and concentrated under reduced pressure to give a crude colorless oil(2a). After that, 2a was subjected to hydrogenation reaction with H<sub>2</sub>, Pd/C in MeOH (40 mL) and AcOH(5mL) and stirred for 24 h and the reaction was monitored by TLC which leads to the compound 2b. Then amide NH group of compound 2b was protected by the Boc group and then hydrolyzed using 2N NaOH in MeOH to get the final product N-Bocprotected 3,3-dimethyl butanoic acid (2d 78% yield). Then 2d (2.31 g, 10 mmol) was dissolved in 15 mL of DMF and was cooled down to 0 °C under an N<sub>2</sub> atmosphere. To this HBTU (3.79 g, 10 mmol) and HOBt (1.08 g, 8 mmol) were added and the reaction mixture was stirred for 10 minutes. This was followed by the addition of 4-chlorobenzyl amine (1.8 ml, 15 mmol). The reaction mixture was stirred overnight and the progress was monitored by TLC. Upon completion, the reaction mixture was diluted with 200 mL EtOAc and was washed with 10% HCl (150 mL X 2), 10% Na<sub>2</sub>CO<sub>3</sub> solution (150 mL X 2), and finally brine solution (150 mL X 2). The organic layer was dried over anhydrous Na<sub>2</sub>SO<sub>4</sub> and concentrated under reduced pressure to give a crude powder which was then purified by column chromatography to get a white crystalline product **2e** (yield = 88%).

### 5.2.3. Synthesis of Peptide(P1):

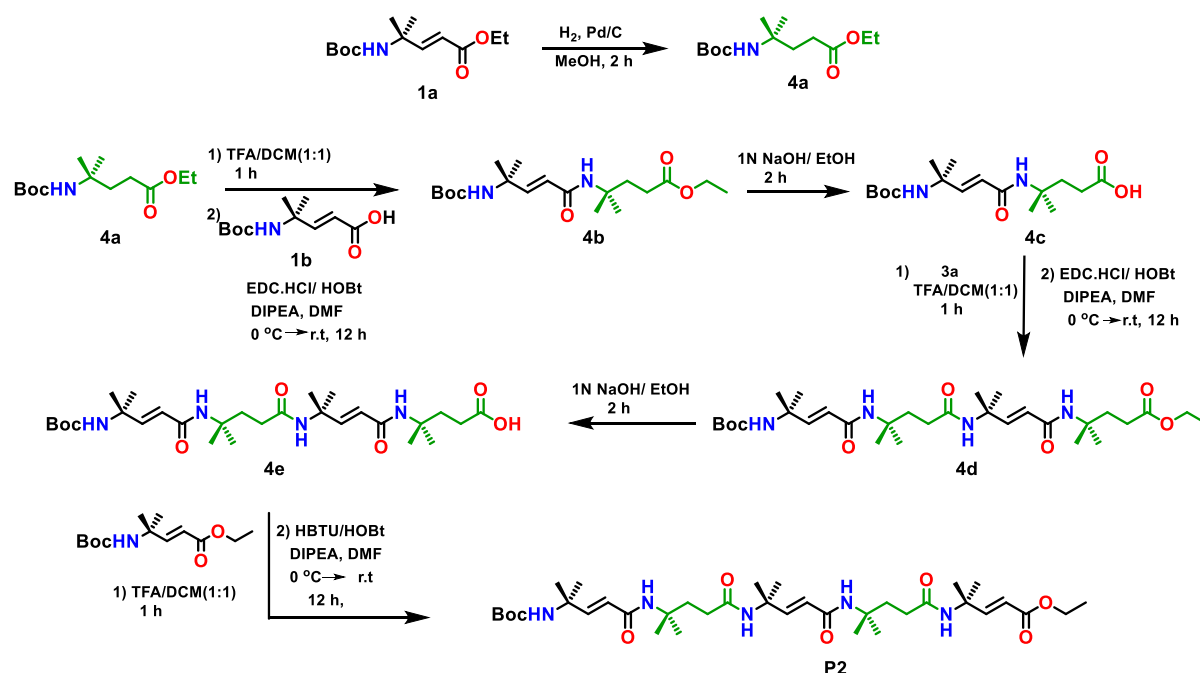


**Scheme 5:** Synthesis of peptide P1.



The compound 3a was synthesized following our previously reported method.<sup>22a</sup> In short, the ethyl ester of compound 1a was deprotected using TFA/DCM (1:1) and then was coupled with compound 1b using EDC.HCl/HOBt as a coupling agent to get compound 3a. Compound 3a was then hydrolyzed with 1N NaOH/EtOH to get the free acid of compound 3b. Then (1+1) coupling of 3a and 3b was carried out using EDC.HCl/HOBt as a coupling agent to get compound 3c. Next, 3c was hydrolyzed with 1N NaOH/EtOH to get free acid of compound 3d. Finally, (4+1) coupling was carried out with 3d and 1c by using HBTU/HOBt, and DIPEA in DMF, and the reaction mixture was stirred for 12 h and the progress was monitored by TLC. Upon completion, the reaction mixture was diluted with 250 mL EtOAc and was washed with 10% HCl (200 mL X 2), 10% Na<sub>2</sub>CO<sub>3</sub> solution (200 mL X 2), and finally brine solution (200mL X 2). The organic layer was dried over anhydrous Na<sub>2</sub>SO<sub>4</sub> and concentrated under reduced pressure to give a crude powder which was then purified by column chromatography to get a white product as peptide **P1** (yield = 71%).

#### 5.2.4. Synthesis of Peptide(P2):

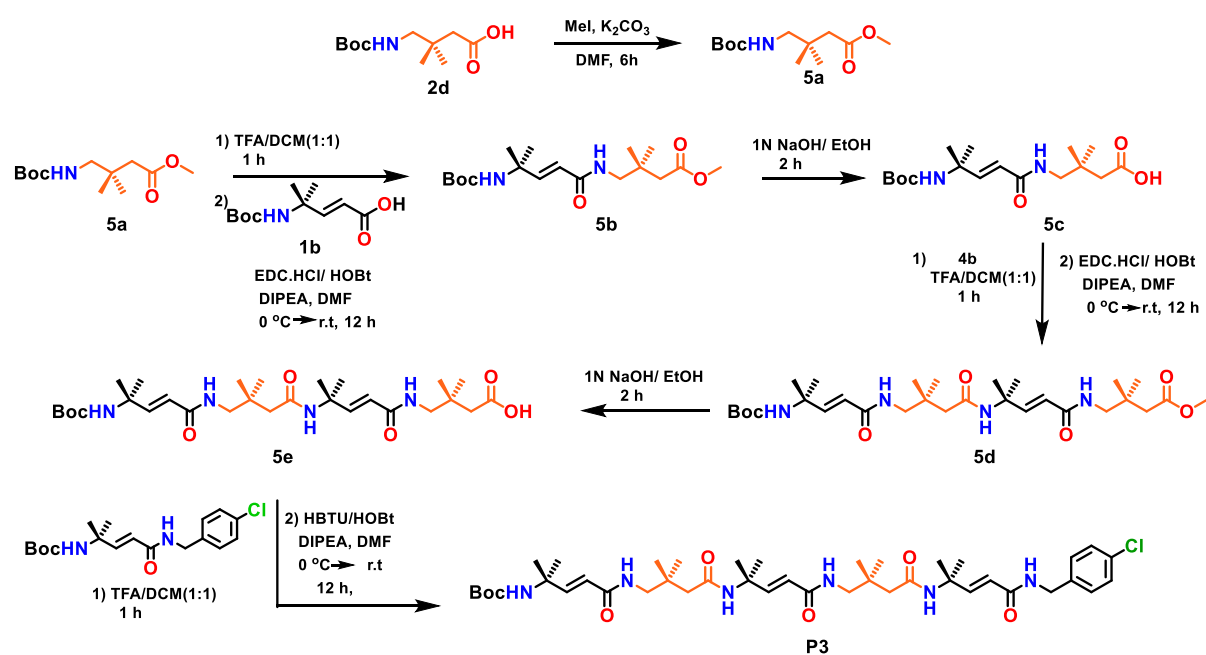


**Scheme 6:** Synthesis of peptide P2.

The ethyl ester of  $\alpha,\beta$ -unsaturated 3,3-dimethyl  $\gamma$ -amino acid(1a) was synthesized as our previous method. Then 1a was subjected to double bond reduction through catalytic transfer hydrogenation to obtain *N*-Boc-ethyl ester of 3,3-dimethyl  $\gamma$ -amino acid(4a). Boc deprotection

of compound 4a (10 mmol, 1.6 g) was carried out by using 5 ml of each TFA and DCM (1:1) for 1 h. After that, TFA and solvent DCM were evaporated and 5-6 times DCM was added and evaporated to remove traces of TFA. The formed crude was TFA-salt of the amine of compound 4a and to this 3 ml of DMF and 4.5 ml, of DIPEA were added to make it free amine of compound 4a. Boc-dgAic-OH(1b)( 10 mmol, 2.3 g) was taken in 10 mL of DMF and the solution was cooled down to 0 °C and kept in an N<sub>2</sub> atmosphere. EDC.HCl(10 mmol, 1.93 g) and HOBt (10 mmol, 1.36 g), and 5 ml DIPEA were added to the solution and the reaction mixture was stirred for 10 mins. After that, the free amine of compound 4a was added to the reaction mixture and stirred for 12 h. Upon completion of the reaction monitored by TLC, the reaction mixture was diluted with 200 ml of ethyl acetate. Then, the mixture was washed with 10% HCl (100 mL X 2), 10% Na<sub>2</sub>CO<sub>3</sub> solution (100 mL X 2), and then NaCl solution (100 mL X 2). The organic layer was collected and dried with anhydrous Na<sub>2</sub>SO<sub>4</sub> and concentrated under reduced pressure. The crude product was purified by column chromatography to get dipeptide 4b as a white solid. Then (2+2) coupling reaction of 4a and 4c was carried out by using EDC.HCl, HOBt, and DIPEA to get tetrapeptide 4d. The tetrapeptide 4d was hydrolyzed in 1N NaOH/EtOH to get free acid of compound 4e and which was then subjected to (4+1) coupling reaction with 1a using HBTU/HOBt, DIPEA in DMF to get pentapeptide P2. The pentapeptide was purified by column chromatography to get a white product as peptide **P2** (yield = 76%).

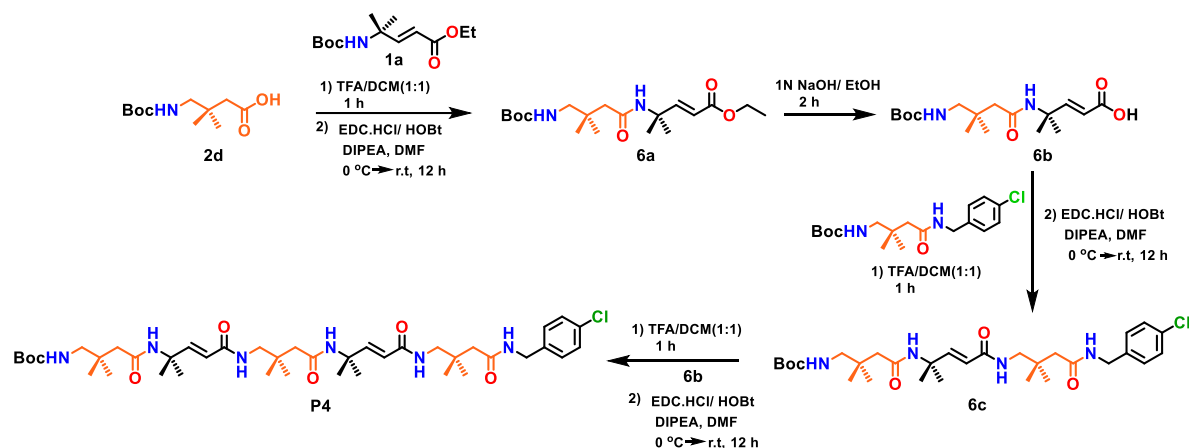
### 5.2.5. Synthesis of Peptide(P3):



**Scheme 7:** Synthesis of peptide **P3**.

The N-Boc-protected 3,3-dimethyl butanoic acid(2d) was synthesized following as previous report<sup>24</sup> and was then subjected to methylation using MeI/K<sub>2</sub>CO<sub>3</sub> in DMF solvent. The reaction mixture was stirred at r.t for 6 h. After completion of the reaction, it was workup by EtOAc and wash with 10% HCl followed by brine. The organic layer was collected and dried over anhydrous Na<sub>2</sub>SO<sub>4</sub> and concentrated under reduced pressure to give a crude semi-solid which was then purified by column chromatography to get product 5a. Boc deprotection of compound 5a (10 mmol, 2.45 g) was carried out by using 5 ml of each TFA and DCM (1:1) for 1 h. After that, TFA and solvent DCM were evaporated and 5-6 times DCM was added and evaporated to remove traces of TFA. The formed crude was TFA-salt of the amine of compound 5a and to this 3 ml of DMF and 4.5 ml, of DIPEA were added to make it free amine of compound 5a. Boc-dgAic-OH(1b)( 10 mmol, 2.3 g) was taken in 10 mL of DMF and the solution was cooled down to 0 °C and kept in an N<sub>2</sub> atmosphere. EDC.HCl(10 mmol, 1.93 g) and HOBt (10 mmol, 1.36 g), and 5 ml DIPEA were added to the solution and the reaction mixture was stirred for 10 mins. After that, the free amine of compound 5a was added to the reaction mixture and stirred for 12 h. Upon completion of the reaction monitored by TLC, the reaction mixture was diluted with 200 ml of ethyl acetate. Then, the mixture was washed with 10% HCl (100 mL X 2), 10% Na<sub>2</sub>CO<sub>3</sub> solution (100 mL X 2), and then NaCl solution (100 mL X 2). The organic layer was collected and dried with anhydrous Na<sub>2</sub>SO<sub>4</sub> and concentrated under reduced pressure. The crude product was purified by column chromatography to get dipeptide 5b as a white solid. Then (2+2) coupling reaction of 5b and 5c was carried out by using EDC.HCl, HOBt, and DIPEA to get tetrapeptide 5d. The tetrapeptide 5d was hydrolyzed in 1N NaOH/EtOH to get free acid of compound 5e and which was then subjected to (4+1) coupling reaction with 1c using HBTU/HOBt, DIPEA in DMF to get pentapeptide **P3**. The pentapeptide was purified by column chromatography to get a white product as peptide **P3** (yield = 68%).

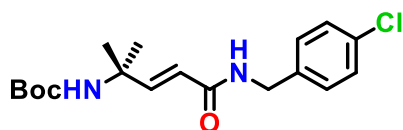
### 5.2.6. Synthesis of Peptide(P4):



**Scheme 8:** Synthesis of peptide **P4**.

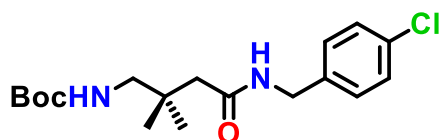
Ethyl ester of compound 1a (10 mmol, 2.57 g) was deprotected using TFA/DCM(1:1) and 3 ml DIPEA was added to get free amine of 1a. N-Boc-protected 3,3-dimethyl butanoic acid (2d) (10 mmol, 2.3 g) was taken in 10 mL of DMF and the solution was cooled down to 0 °C and kept in an N<sub>2</sub> atmosphere. EDC.HCl (10 mmol, 1.93 g) and HOBt (10 mmol, 1.36 g), and 5 ml DIPEA were added to the solution and the reaction mixture was stirred for 10 mins. After that, the free amine of compound 1a was added to the reaction mixture and stirred for 12 h. Upon completion of the reaction monitored by TLC, the reaction mixture was diluted with 200 ml of ethyl acetate. Then, the mixture was washed with 10% HCl (100 mL X 2), 10% Na<sub>2</sub>CO<sub>3</sub> solution (100 mL X 2), and then NaCl solution (100 mL X 2). The organic layer was collected and dried with anhydrous Na<sub>2</sub>SO<sub>4</sub> and concentrated under reduced pressure. The crude product was purified by column chromatography to get dipeptide 6a as a white solid. The dipeptide 6a was hydrolyzed in 1N NaOH/EtOH to get free acid of dipeptide 6a and which was then subjected to (2+1) coupling reaction with 2e using EDC.HCl, HOBt, and DIPEA to get tripeptide 6c. The Boc-deprotection of tripeptide 6c was carried out by using 5 ml of each TFA and DCM (1:1) for 1 h. After that, TFA and solvent DCM were evaporated and 5-6 times DCM was added and evaporated to remove traces of TFA. The formed crude was TFA-salt of the amine of compound 6c and to this 3 ml of DMF and 3 ml, of DIPEA were added to make it free amine of compound 6c. Then (3+2) coupling reaction of 6c and 6b was carried out by using EDC.HCl, HOBt, and DIPEA to get pentapeptide P4. The pentapeptide was purified by column chromatography to get a white product as peptide **P4** (yield = 73%).

### 5.3. Characterization of Building Units and Peptides(P1-P4):



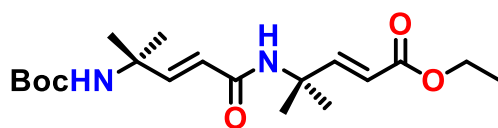
**compound 1c**

**$^1\text{H NMR}$**  (400 MHz,  $\text{CDCl}_3$ )  $\delta$  7.28 (d,  $J = 8.5$  Hz, 2H), 7.21 (d,  $J = 8.5$  Hz, 2H), 6.86 (d,  $J = 15.5$  Hz, 1H), 6.02 (s, 1H), 5.83 (d,  $J = 15.5$  Hz, 1H), 4.66 (s, 1H), 4.45 (d,  $J = 5.9$  Hz, 2H), 1.40 (s, 9H), 1.39 (s, 6H).  **$^{13}\text{C NMR}$**  (101 MHz,  $\text{CDCl}_3$ )  $\delta$  165.97, 136.94, 133.39, 129.37, 128.91, 120.65, 79.60, 52.92, 43.10, 28.52.



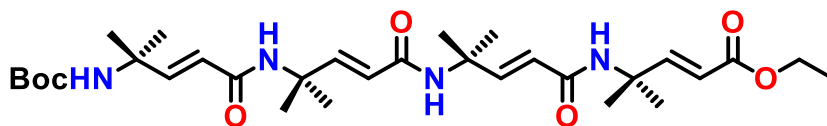
**compound 2e**

**$^1\text{H NMR}$**  (400 MHz,  $\text{CDCl}_3$ )  $\delta$  7.57 (s, 1H), 7.27 (d,  $J = 8.6$  Hz, 2H), 7.24 (d,  $J = 8.8$  Hz, 2H), 5.07 (t,  $J = 7.0$  Hz, 1H), 4.39 (d,  $J = 5.8$  Hz, 2H), 3.00 (d,  $J = 7.0$  Hz, 2H), 2.09 (s, 2H), 1.42 (s, 9H), 0.94 (s, 6H).  **$^{13}\text{C NMR}$**  (101 MHz,  $\text{CDCl}_3$ )  $\delta$  171.32, 157.33, 137.48, 133.05, 129.31, 128.76, 79.87, 49.63, 45.51, 42.93, 34.98, 28.47, 26.27.



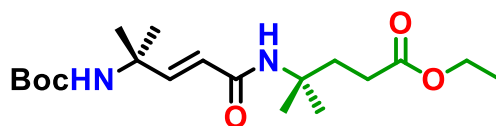
**compound 3a**

**$^1\text{H NMR}$**  (400 MHz,  $\text{CDCl}_3$ )  $\delta$  7.03 (d,  $J = 15.9$  Hz, 1H), 6.77 (d,  $J = 15.5$  Hz, 1H), 5.84 (d,  $J = 15.9$  Hz, 1H), 5.77 (d,  $J = 15.5$  Hz, 1H), 5.60 (d,  $J = 7.5$  Hz, 1H), 4.64 (s, 1H), 4.17 (q,  $J = 7.1$  Hz, 2H), 1.48 (s, 6H), 1.41 (s, 9H), 1.39 (s, 6H), 1.27 (t,  $J = 7.1$  Hz, 3H).  **$^{13}\text{C NMR}$**  (101 MHz,  $\text{CDCl}_3$ )  $\delta$  166.83, 165.08, 152.74, 121.25, 118.91, 77.59, 60.55, 53.90, 52.88, 28.54, 27.51, 27.26, 14.36. MALDI/TOF-TOF  $m/z$  calculated for  $\text{C}_{19}\text{H}_{32}\text{N}_2\text{O}_5$  [ $\text{M}+\text{Na}^+$ ] is 407.230 and the observed peak is 407.408.



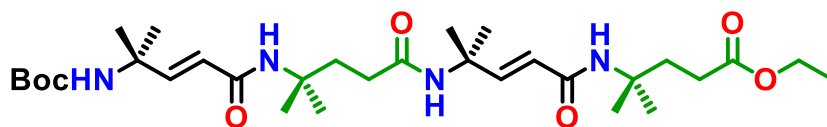
**compound 3c**

**$^1\text{H NMR}$**  (400 MHz,  $\text{CDCl}_3$ )  $\delta$  8.26 (s, 1H), 7.65 (s, 1H), 7.57 (s, 1H), 7.15 (d,  $J = 15.9$  Hz, 1H), 6.75 – 6.69 (m, 3H), 5.97 (d,  $J = 15.2$  Hz, 1H), 5.84 (d,  $J = 15.9$  Hz, 1H), 5.73 (d,  $J = 15.3$  Hz, 1H), 5.65 (d,  $J = 15.3$  Hz, 1H), 4.75 (s, 1H), 4.15 (d,  $J = 7.1$  Hz, 2H), 1.49 (s, 9H), 1.46 (t,  $J = 3.2$  Hz, 18H), 1.39 (s, 6H), 1.26 (s, 4H).  **$^{13}\text{C NMR}$**  (101 MHz,  $\text{CDCl}_3$ )  $\delta$  167.44, 165.40, 165.13, 164.96, 155.08, 154.93, 148.54, 148.04, 147.34, 121.71, 121.60, 120.92, 117.91, 80.25, 60.23, 54.51, 54.10, 53.97, 53.59, 28.79, 14.43. MALDI/TOF-TOF  $m/z$  calculated for  $\text{C}_{31}\text{H}_{50}\text{N}_4\text{O}_7$  [ $\text{M}+\text{Na}^+$ ] is 613.367, and the observed peak is 613.740.



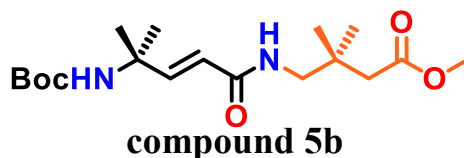
**compound 4b**

**$^1\text{H NMR}$**  (400 MHz,  $\text{CDCl}_3$ )  $\delta$  6.74 (d,  $J = 15.5$  Hz, 1H), 5.71 (d,  $J = 15.4$  Hz, 1H), 5.64 (s, 1H), 4.62 (s, 1H), 4.10 (t,  $J = 7.1$  Hz, 2H), 2.33 (dd,  $J = 8.3, 7.1$  Hz, 2H), 2.05 (dd,  $J = 8.4, 7.0$  Hz, 2H), 1.41 (s, 9H), 1.38 (s, 6H), 1.35 (s, 6H), 1.24 (t,  $J = 7.1$  Hz, 3H).  **$^{13}\text{C NMR}$**  (101 MHz,  $\text{CDCl}_3$ )  $\delta$  174.24, 165.37, 121.87, 77.56, 60.73, 53.47, 52.89, 35.24, 29.69, 28.53, 26.87, 14.32. MALDI/TOF-TOF  $m/z$  calculated for  $\text{C}_{19}\text{H}_{34}\text{N}_2\text{O}_5$  [ $\text{M}+\text{H}^+$ ] is 371.248, and the observed peak is 371.440.

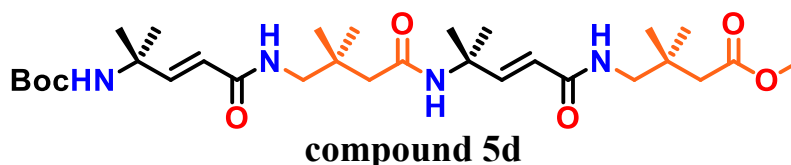


**compound 4d**

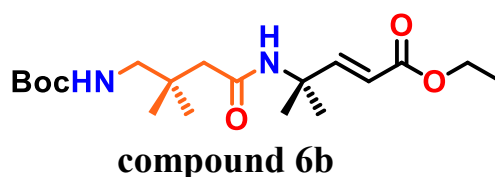
**$^1\text{H NMR}$**  (400 MHz,  $\text{CDCl}_3$ )  $\delta$  6.90 (s, 1H), 6.74 – 6.73 (m, 1H), 6.70 – 6.69 (m, 1H), 6.48 (d,  $J = 3.2$  Hz, 1H), 6.41 (s, 1H), 5.80 (d,  $J = 15.4$  Hz, 1H), 5.68 (d,  $J = 15.4$  Hz, 1H), 4.76 (s, 1H), 2.35 – 2.31 (m, 2H), 2.14 (d,  $J = 7.9$  Hz, 2H), 2.10 – 2.07 (m, 2H), 2.06 – 2.03 (m, 2H), 2.01 (t,  $J = 5.3$  Hz, 2H), 1.44 (s, 6H), 1.42 (s, 9H), 1.38 (s, 6H), 1.33 (d,  $J = 1.4$  Hz, 12H), 1.25 – 1.21 (m, 3H).  **$^{13}\text{C NMR}$**  (101 MHz,  $\text{CDCl}_3$ )  $\delta$  174.33, 172.73, 165.52, 148.29, 147.43, 121.88, 77.79, 60.55, 35.01, 31.89, 29.89, 28.62, 27.88, 27.61, 27.30, 26.86, 14.33. MALDI/TOF-TOF  $m/z$  calculated for  $\text{C}_{31}\text{H}_{54}\text{N}_4\text{O}_7$  [ $\text{M}+\text{H}^+$ ] is 617.339, and the observed peak is 617.700.



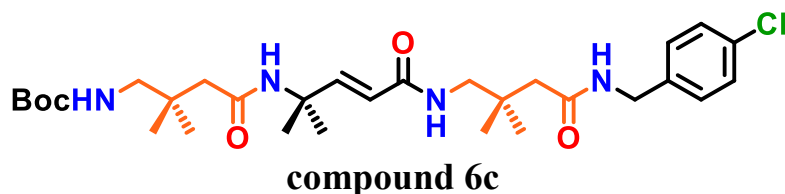
**<sup>1</sup>H NMR** (400 MHz, CDCl<sub>3</sub>) δ 6.83 (s, 1H), 6.19 (d, *J* = 6.6 Hz, 1H), 5.81 (d, *J* = 15.5 Hz, 1H), 4.65 (s, 1H), 3.66 (s, 3H), 3.23 (d, *J* = 6.6 Hz, 2H), 2.25 (s, 2H), 1.41 (s, 9H), 1.40 (s, 6H), 1.00 (s, 6H). **<sup>13</sup>C NMR** (101 MHz, CDCl<sub>3</sub>) δ 173.11, 166.19, 121.03, 79.63, 52.96, 51.68, 48.86, 44.41, 35.24, 28.50, 27.52, 25.96. MALDI/TOF-TOF *m/z* calculated for C<sub>18</sub>H<sub>32</sub>N<sub>2</sub>O<sub>5</sub> [M+H<sup>+</sup>] is 357.231, and the observed peak is 357.402.



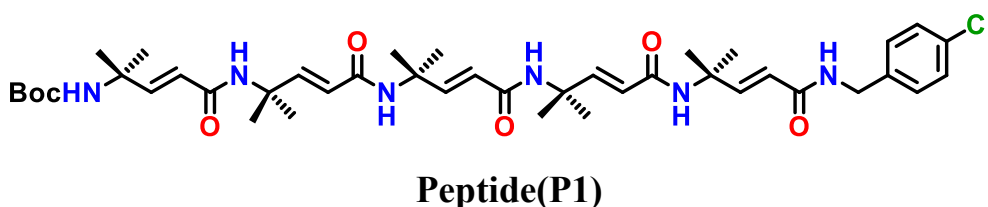
**<sup>1</sup>H NMR** (400 MHz, CDCl<sub>3</sub>) δ 6.79 (d, *J* = 15.5 Hz, 1H), 6.72 (d, *J* = 15.4 Hz, 2H), 6.19 (s, 1H), 5.82 (d, *J* = 15.5 Hz, 3H), 4.72 (s, 1H), 3.65 (s, 4H), 3.22 (d, *J* = 6.5 Hz, 3H), 2.26 (s, 3H), 1.97 – 1.92 (m, 2H), 1.47 (s, 6H), 1.42 (s, 15H), 1.38 (s, 6H), 1.00 (s, 6H). **<sup>13</sup>C NMR** (101 MHz, CDCl<sub>3</sub>) δ 173.06, 166.37, 165.12, 147.79, 121.43, 121.34, 79.67, 54.14, 53.10, 51.54, 49.18, 44.23, 35.21, 28.58, 27.73, 27.53, 25.65.



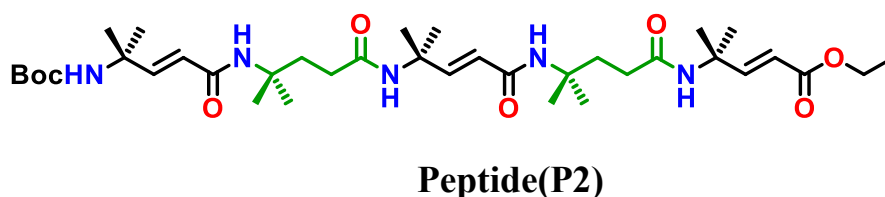
**<sup>1</sup>H NMR** (400 MHz, CDCl<sub>3</sub>) δ 6.73 (dd, *J* = 15.5, 1.1 Hz, 1H), 5.71 (d, *J* = 15.5 Hz, 1H), 5.65 (s, 1H), 4.62 (s, 1H), 4.10 (dd, *J* = 7.2, 1.3 Hz, 3H), 2.34 – 2.30 (m, 2H), 2.07 – 2.03 (m, 2H), 1.41 (d, *J* = 1.4 Hz, 9H), 1.38 (d, *J* = 1.3 Hz, 6H), 1.35 (d, *J* = 1.4 Hz, 6H), 1.23 (dd, *J* = 7.1, 1.3 Hz, 3H). **<sup>13</sup>C NMR** (101 MHz, CDCl<sub>3</sub>) δ 174.22, 165.36, 121.85, 79.51, 60.71, 53.45, 52.88, 35.22, 29.68, 28.52, 26.86, 14.31. MALDI/TOF-TOF *m/z* calculated for C<sub>19</sub>H<sub>34</sub>N<sub>2</sub>O<sub>5</sub> [M+H<sup>+</sup>] is 371.247, and the observed peak is 371.434.



**<sup>1</sup>H NMR** (400 MHz, CDCl<sub>3</sub>) δ 8.07 – 8.02 (m, 1H), 7.26 (s, 4H), 7.15 (s, 1H), 6.85 (d, *J* = 15.6 Hz, 1H), 6.72 (t, *J* = 6.7 Hz, 1H), 5.89 (d, *J* = 15.6 Hz, 1H), 4.99 (t, *J* = 6.8 Hz, 1H), 4.39 (d, *J* = 5.9 Hz, 2H), 3.16 (d, *J* = 6.7 Hz, 2H), 3.02 (d, *J* = 6.9 Hz, 2H), 2.10 (s, 2H), 1.98 (s, 2H), 1.45 (s, 7H), 1.43 (s, 9H), 0.96 (s, 6H), 0.94 (s, 6H). **<sup>13</sup>C NMR** (101 MHz, CDCl<sub>3</sub>) δ 171.61, 170.72, 167.50, 157.25, 149.29, 137.73, 129.32, 128.74, 120.89, 79.91, 53.70, 49.50, 48.97, 46.14, 45.73, 42.85, 35.04, 34.90, 28.50, 27.25, 26.60, 26.31. MALDI/TOF-TOF *m/z* calculated for C<sub>30</sub>H<sub>47</sub>ClN<sub>4</sub>O<sub>5</sub> [M+H<sup>+</sup>] is 601.324, and the observed peak is 601.707.

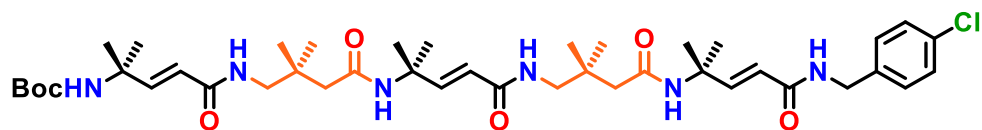


**<sup>1</sup>H NMR** (400 MHz, CDCl<sub>3</sub>) δ 8.56 (s, 2H), 8.50 (s, 1H), 8.29 (s, 1H), 7.86 (s, 1H), 7.30 (s, 2H), 7.26 (s, 2H), 6.71 (dd, *J* = 20.9, 15.4 Hz, 6H), 5.99 (d, *J* = 15.2 Hz, 1H), 5.78 – 5.70 (m, 4H), 4.71 (s, 1H), 4.48 (s, 1H), 4.33 (s, 1H), 1.73 – 1.62 (m, 6H), 1.59 (s, 6H), 1.50 (s, 9H), 1.39 – 1.33 (m, 13H), 1.28 (s, 6H). MALDI/TOF-TOF *m/z* calculated for C<sub>42</sub>H<sub>61</sub>ClN<sub>6</sub>O<sub>7</sub> [M+Na<sup>+</sup>] is 819.429, and the observed peak is 819.995.



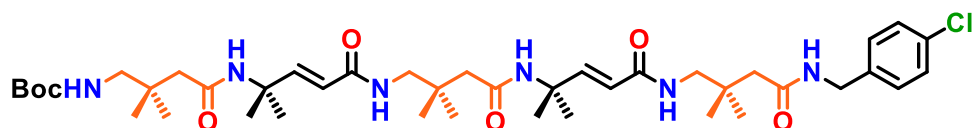
**<sup>1</sup>H NMR** (400 MHz, CDCl<sub>3</sub>) δ 8.06 (s, 1H), 7.89 (s, 1H), 7.60 (s, 1H), 7.12 (d, *J* = 15.9 Hz, 1H), 6.69 (d, *J* = 2.5 Hz, 1H), 6.65 (d, *J* = 2.6 Hz, 1H), 5.85 (d, *J* = 1.7 Hz, 1H), 5.81 (d, *J* = 2.4 Hz, 1H), 5.59 (d, *J* = 15.2 Hz, 1H), 4.69 (s, 1H), 4.18 – 4.14 (m, 2H), 4.11 (q, *J* = 7.0 Hz, 2H), 2.04 (s, 4H), 1.75 – 1.69 (m, 4H), 1.50 (s, 4H), 1.48 (s, 6H), 1.46 (s, 9H), 1.40 (s, 6H), 1.33 (s, 8H), 1.29 – 1.25 (m, 5H), 1.26 – 1.23 (m, 3H).





**Peptide(P3)**

**<sup>1</sup>H NMR** (400 MHz, CDCl<sub>3</sub>) δ 8.21 (s, 1H), 8.13 (s, 1H), 7.52 (s, 1H), 7.28 (d, *J* = 8.4 Hz, 2H), 7.25 (d, *J* = 8.4 Hz, 2H), 6.78 – 6.63 (m, 4H), 5.95 (d, *J* = 15.1 Hz, 1H), 5.70 (dd, *J* = 15.4, 10.6 Hz, 2H), 4.76 (s, 1H), 4.39 (d, *J* = 5.6 Hz, 2H), 1.75 – 1.62 (m, 4H), 1.47 (s, 14H), 1.40 (s, 8H), 1.38 (s, 9H), 1.35 (s, 9H), 1.27 (d, *J* = 15.1 Hz, 3H).



**Peptide(P4)**

**<sup>1</sup>H NMR** (400 MHz, CDCl<sub>3</sub>) δ 8.42 (d, *J* = 8.0 Hz, 1H), 8.00 (s, 1H), 7.80 (d, *J* = 32.1 Hz, 2H), 7.54 (d, *J* = 14.4 Hz, 1H), 7.28 (dd, *J* = 8.5, 1.9 Hz, 2H), 7.26 – 7.22 (m, 2H), 6.76 (dd, *J* = 15.7, 2.9 Hz, 1H), 6.62 (d, *J* = 15.2 Hz, 1H), 5.99 (d, *J* = 15.8 Hz, 1H), 5.72 (d, *J* = 15.4 Hz, 1H), 4.97 (s, 1H), 4.37 (d, *J* = 5.7 Hz, 2H), 3.07 (d, *J* = 31.2 Hz, 5H), 2.06 (d, *J* = 10.7 Hz, 4H), 1.83 (d, *J* = 51.8 Hz, 4H), 1.47 (s, 6H), 1.44 (d, *J* = 1.3 Hz, 9H), 1.38 (d, *J* = 3.1 Hz, 6H), 0.96 (d, *J* = 5.7 Hz, 12H), 0.91 (d, *J* = 2.7 Hz, 6H). MALDI/TOF-TOF *m/z* calculated for C<sub>42</sub>H<sub>67</sub>ClN<sub>6</sub>O<sub>7</sub> [M+Na<sup>+</sup>] is 825.476, and the observed peak is 8256.060.

## 6. Appendix:

### 6.1. ORTEP Diagrams:

#### A) ORTEP Diagram of Peptide(P1):

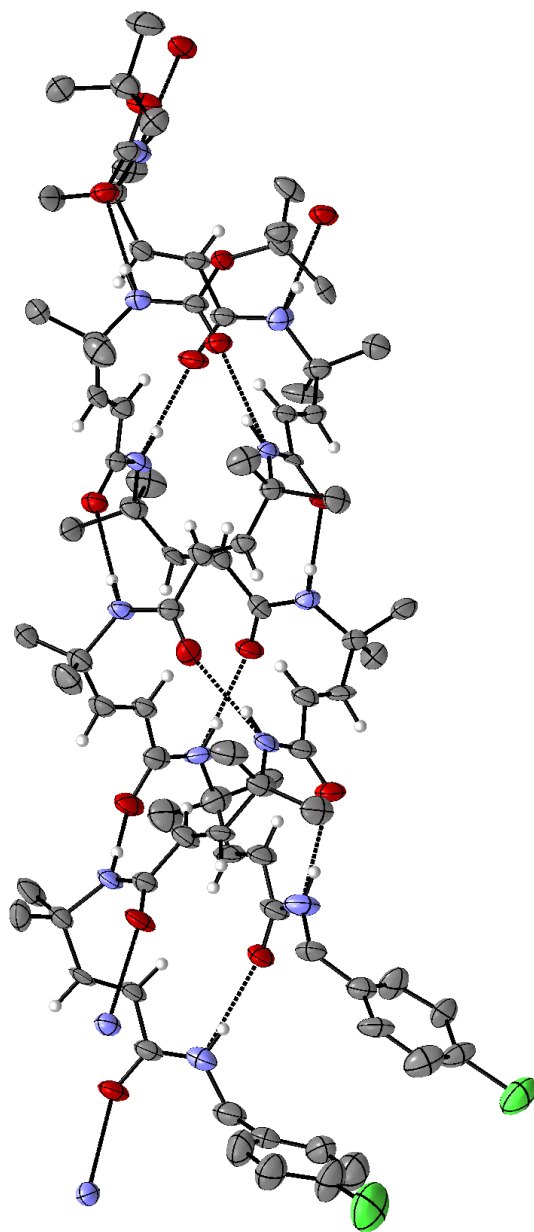


**Figure 8:** ORTEP diagram of **P1**. H-bonds are shown in dotted lines. H-atoms are omitted for clarity. Ellipsoids are drawn at 50% probability.

## B) ORTEP Diagram of Peptide(P2):

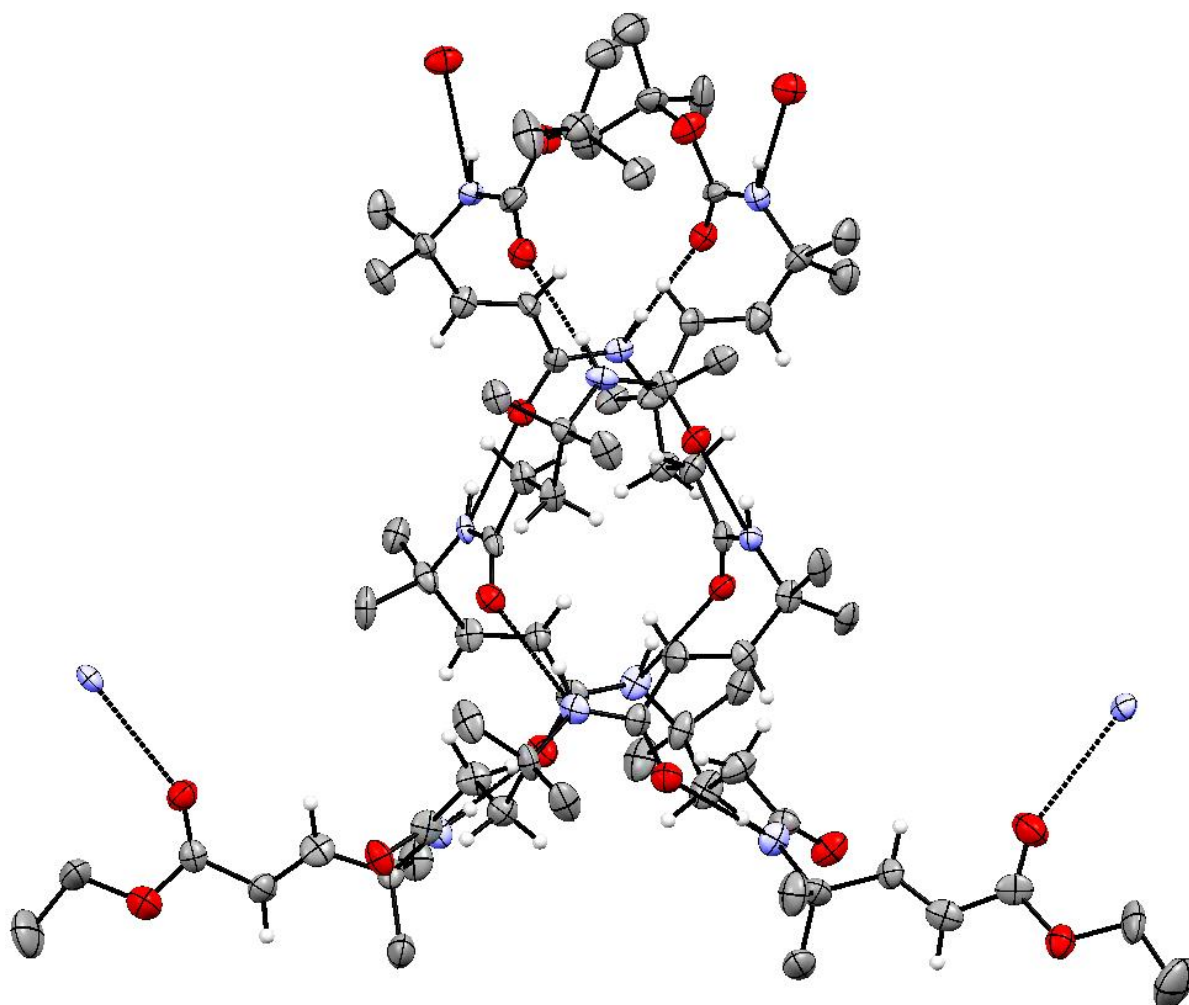


**Figure 9:** ORTEP diagram of **P2**. H-bonds are shown in dotted lines. H-atoms are omitted for clarity. Ellipsoids are drawn at 50% probability.

C) ORTEP Diagram of Peptide(P3):

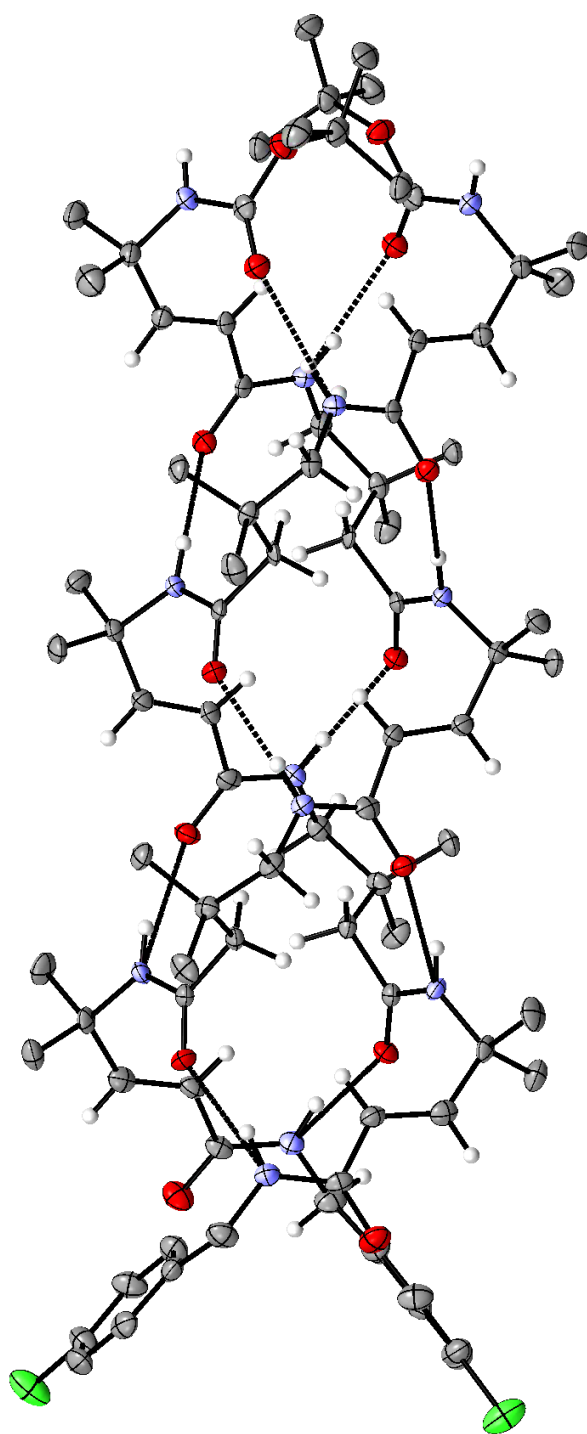


**Figure 10:** ORTEP diagram of **P3**. H-bonds are shown in dotted lines. H-atoms are omitted for clarity. Ellipsoids are drawn at 50% probability.

D) ORTEP Diagram of Peptide(P4):

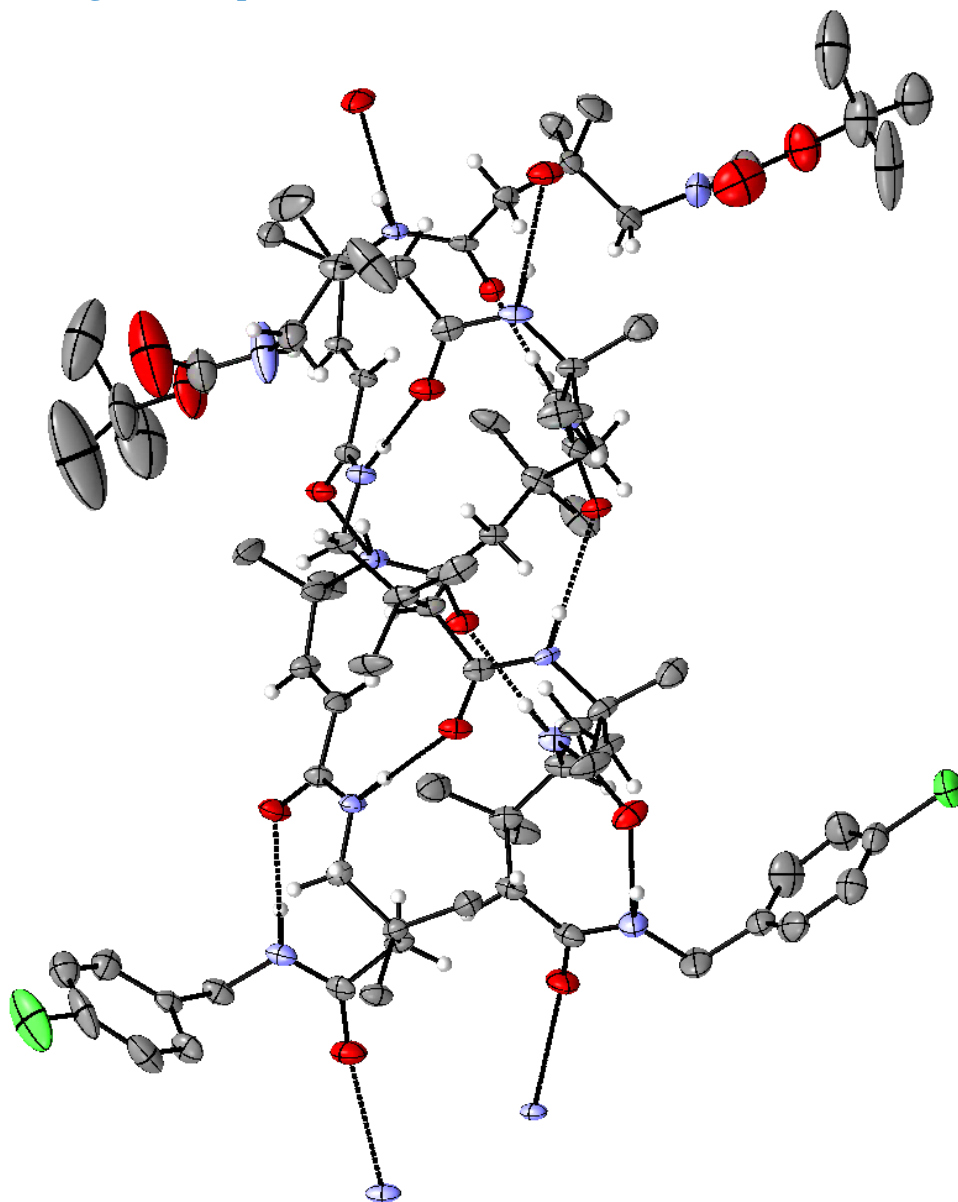


**Figure 11:** ORTEP diagram of **P4**. H-bonds are shown in dotted lines. H-atoms are omitted for clarity. Ellipsoids are drawn at 50% probability.

## 6.2. Crystal Structure Information:

Parameters	Peptide(P1)	Peptide(P2)	Peptide(P3)	Peptide(P4)
Solvent for crystallization	CHCl <sub>3</sub> /n-heptane	DCM/Xylene	EtOAc/n-hexane	EtOAc/n-hexane
Chemical formula	C <sub>85</sub> H <sub>123</sub> Cl <sub>2</sub> N <sub>11</sub> O <sub>14</sub>	C <sub>169</sub> H <sub>252</sub> N <sub>23</sub> O <sub>34</sub>	C <sub>42</sub> H <sub>65</sub> Cl <sub>1</sub> N <sub>6</sub> O <sub>7</sub>	C <sub>84</sub> H <sub>136</sub> Cl <sub>2</sub> N <sub>12</sub> O <sub>14</sub>
Molecular weight	1593.84	3149.94	801.45	1608.95
Crystal size (nm)	(0.14 × 0.10 × 0.12) mm	(0.18 × 0.14 × 0.14) mm	(0.18 × 0.16 × 0.18) mm	(0.12 × 0.16 × 0.10) mm
Radiation source	Mo K $\alpha$ ( $\lambda = 0.71073\text{\AA}$ )	Mo K $\alpha$ ( $\lambda = 0.71073\text{\AA}$ )	Mo K $\alpha$ ( $\lambda = 0.71073\text{\AA}$ )	Mo K $\alpha$ ( $\lambda = 0.71073\text{\AA}$ )
Space group	P2 <sub>1</sub> /c (monoclinic)	Cc (monoclinic)	P2 <sub>1</sub> 2 <sub>1</sub> 2 (orthorhombic)	P2 <sub>1</sub> /c (monoclinic)
a (Å)	22.868(8)	20.21(1)	12.771(3)	17.991(5)
b (Å)	19.843(7)	20.215(12)	14.245(2)	26.363(8)
c (Å)	25.101(9)	46.72(3)	25.046(5)	22.005(6)
$\alpha$ (°)	90	90	90	90
$\beta$ (°)	113.596(9)	91.845(13)	90	105.917(7)
$\gamma$ (°)	90	90	90	90
h <sub>max</sub>	30	24	18	24
k <sub>max</sub>	26	26	19	35
l <sub>max</sub>	33	62	33	25
Volume (Å <sup>3</sup> )	10438(6)	19077(19)	4556.4(15)	10037(5)
Z	4	4	4	4

Density (g/cm <sup>3</sup> )(cal)	1.014	1.097	1.168	1.065
Molecules in the asymmetric unit	1	4	1	2
F (000)	3424.0	6796.0	1728.0	3480.0
2 $\theta$ Max. (°)	57.128	59.26	64.502	56.886
$\mu$ mm <sup>-1</sup>	0.118	0.077	0.136	0.123
Reflections (cal)	25300	43807	12392	24765
Variables	475	2092	519	1037
R (reflections)	6257	20989	7615	12774
R <sub>factor</sub>	0.2780	0.1235	0.1547	0.1960
wR2 (Reflections)	0.6043	0.3374	0.2611	0.5241
Goodness-of- fit (S)	2.279	1.038	1.181	1.802
Software used	Bruker APEX(III)	Bruker APEX(III)	Bruker APEX(III)	Bruker APEX(III)
Method used	SHELXS-97 <sup>31</sup>	SHELXS-97 <sup>31</sup>	SHELXS-97 <sup>31</sup>	SHELXS-97 <sup>31</sup>

### 6.3. Torsion Angle Parameters:

Peptide P1 (Stand B)	$\phi$	$\theta_1$	$\theta_2$	$\psi$
dgAic 1	73	36	169	-164
dgAic 2	70	3	173	-173
dgAic 3	68	26	173	-166
dgAic 4	69	17	173	-179
dgAic 5	55	46	180	171

Peptide P2 (Stand B)	$\phi$	$\theta_1$	$\theta_2$	$\psi$
dgAic 1	-73	-10	-170	167
Aic	-63	-46	-162	178
dgAic 2	-71	-14	-175	160
Aic	-73	-48	-158	-134
dgAic 3	58	-145	-175	175

Peptide P3 (Stand B)	$\phi$	$\theta_1$	$\theta_2$	$\psi$
dgAic 1	-68	-14	-171	166
ADP	-99	61	176	99
dgAic 2	-64	-21	-172	164
ADP	-104	59	167	102
dgAic 3	-70	-10	-178	175

Peptide P2 (Stand B)	$\phi$	$\theta_1$	$\theta_2$	$\psi$
ADP	-134	-55	-54	-122
dgAic 1	60	22	174	-163
ADP	109	-58	-173	-107
dgAic 2	68	5	178	-176
ADP	104	63	-77	85

## 7. References:

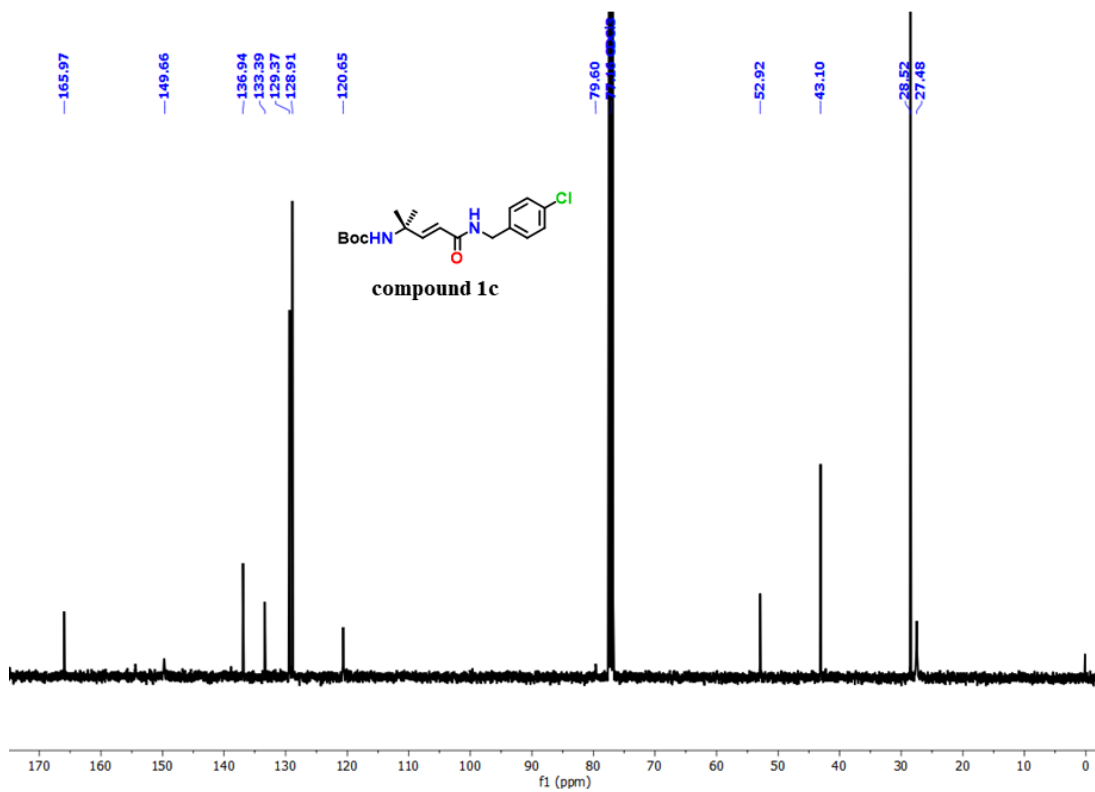
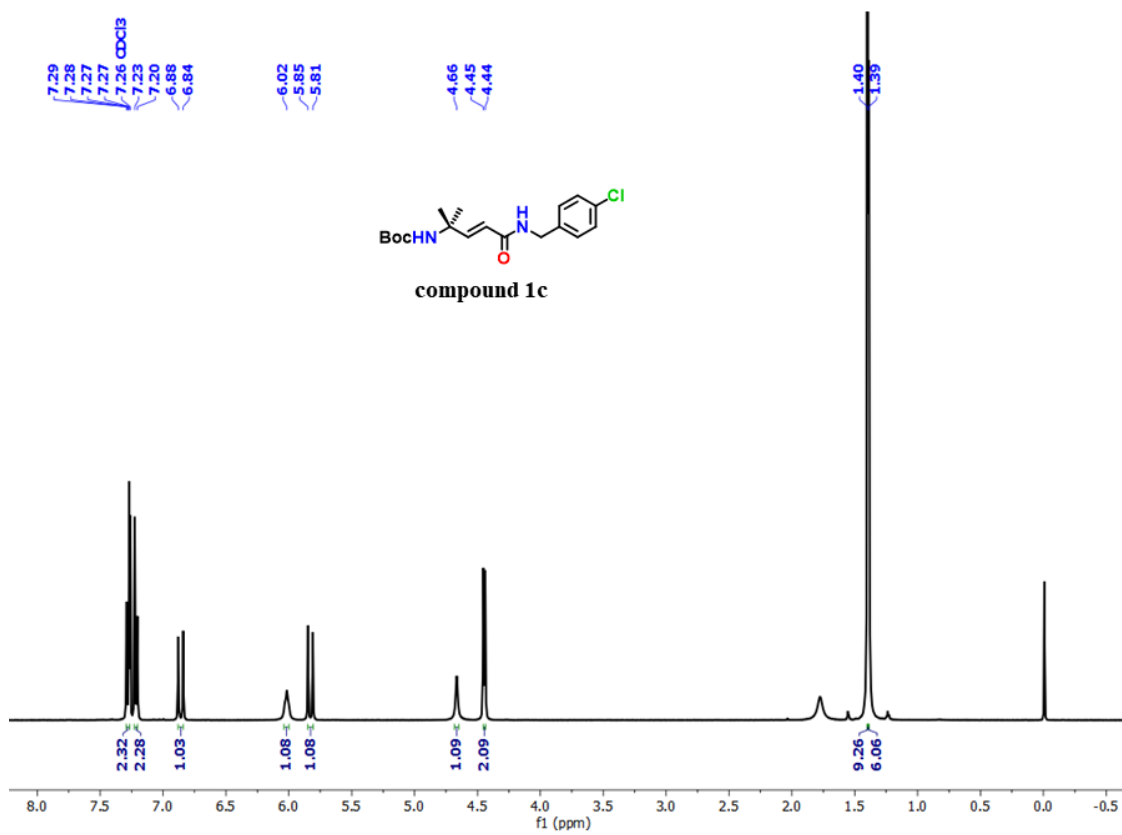
1. (a) Watson, J. D.; Crick, F. C. H. *Nature*, **1953**, *171*, 737. (b) Alberts, B.; Johnson, A.; Lewis, J.; Morgan, D.; Raff, M.; Roberts, K.; Walter, P. *Mol. Biol. Cell*, 6th ed.; Garland Science: New York,
2. Saenger, W. Principles of Nucleic Acid Structure; *Springer-Verlag*: New York, 1984.
3. (a) Langes, D. A. *Science* **1988**, *241*, 188. (b) Urry, D. W.; Glickson, J. D.; Mayers, D. F.; Haider, J. *Biochemistry* **1972**, *11*, 487. (c) Wallace, B. A.; Ravikumar, K. *Science* **1988**; *241*, 182. (d) Sychev, S. V.; Barsukov, L. I.; Ivanov, V. T. *J. Pept. Sci.* **2013**, *19*, 452. (e) Kelkar, D. A.; Chattopadhyay, A. *Biochim. Biophys. Acta.* **2007**, *1768*, 2011. (f) Sychev, S. V.; Barsukov, L. I.; Ivanov, V. T. *Eur. Biophys. J.* **1993**, *22*, 279.
4. Zhang, Z.; Pascal, S. M.; Cross, T. A. *Biochemistry* **1992**, *31*, 8822
5. Arsemev, A. S.; Barsukov, I. L.; Bystrov, V. F. *FEBS. Lett.* **1984**, *180*, 33.
6. Roux, B.; Bruschiweiler, R.; Ernst, R. R. *Eur. J. Biochem.* **1990**, *194*, 57.
7. Pascal, S. M.; Cross, T. A. *J. Biomol. NMR*, **1993**, *3*, 495.
8. Langes, D. A. *Biopolymers*, **1989**, *28*, 259.
9. Woolley, G. A.; Wallace, B. A. *J. Membr. Biol.* **1992**, *129*, 109.
10. Ketchum, R. R.; Hu, W.; Cross, T. A. *Science*, **1993**, *261*, 1457.

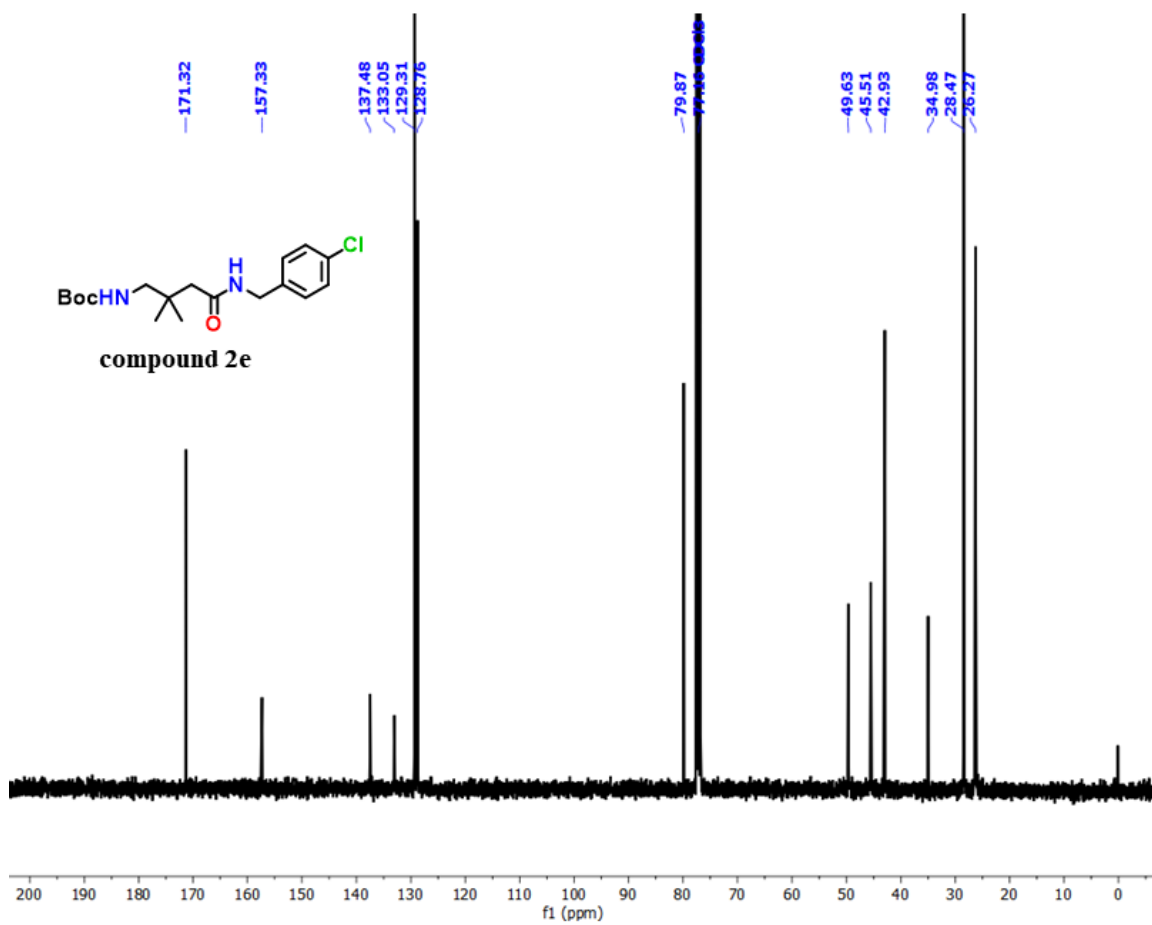
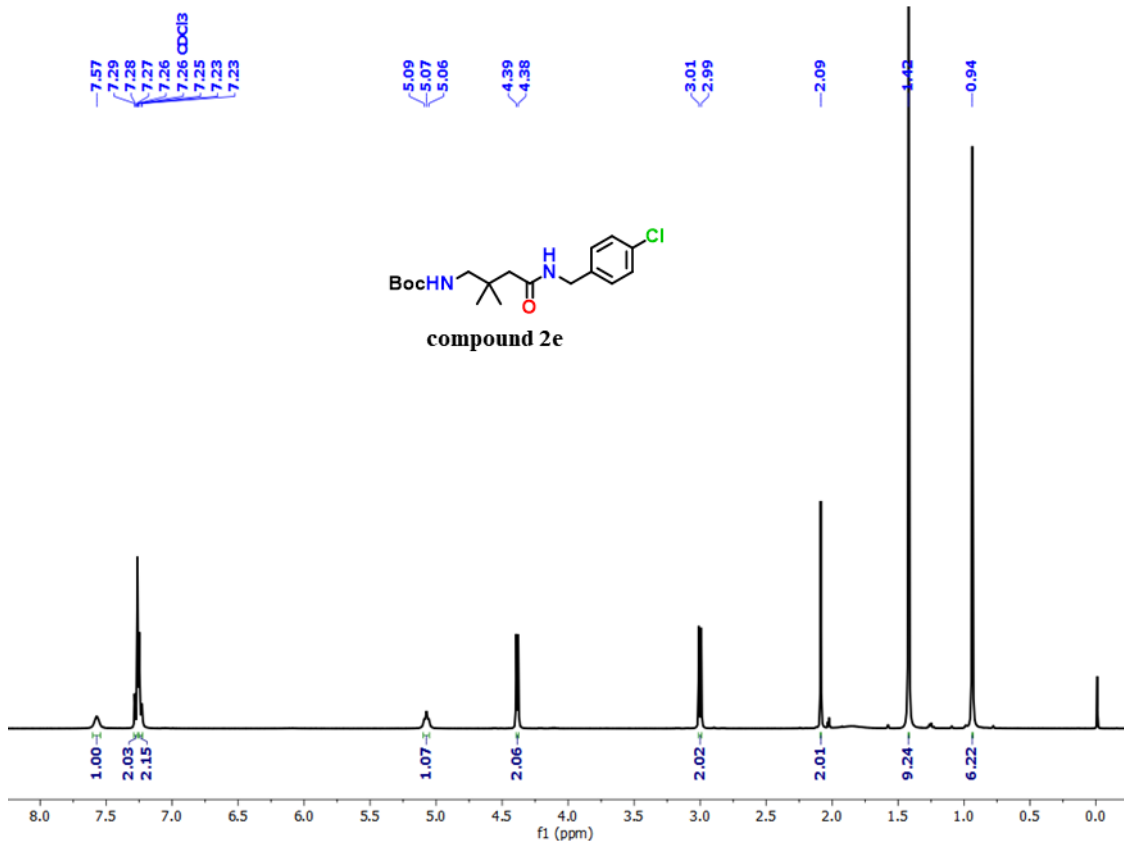


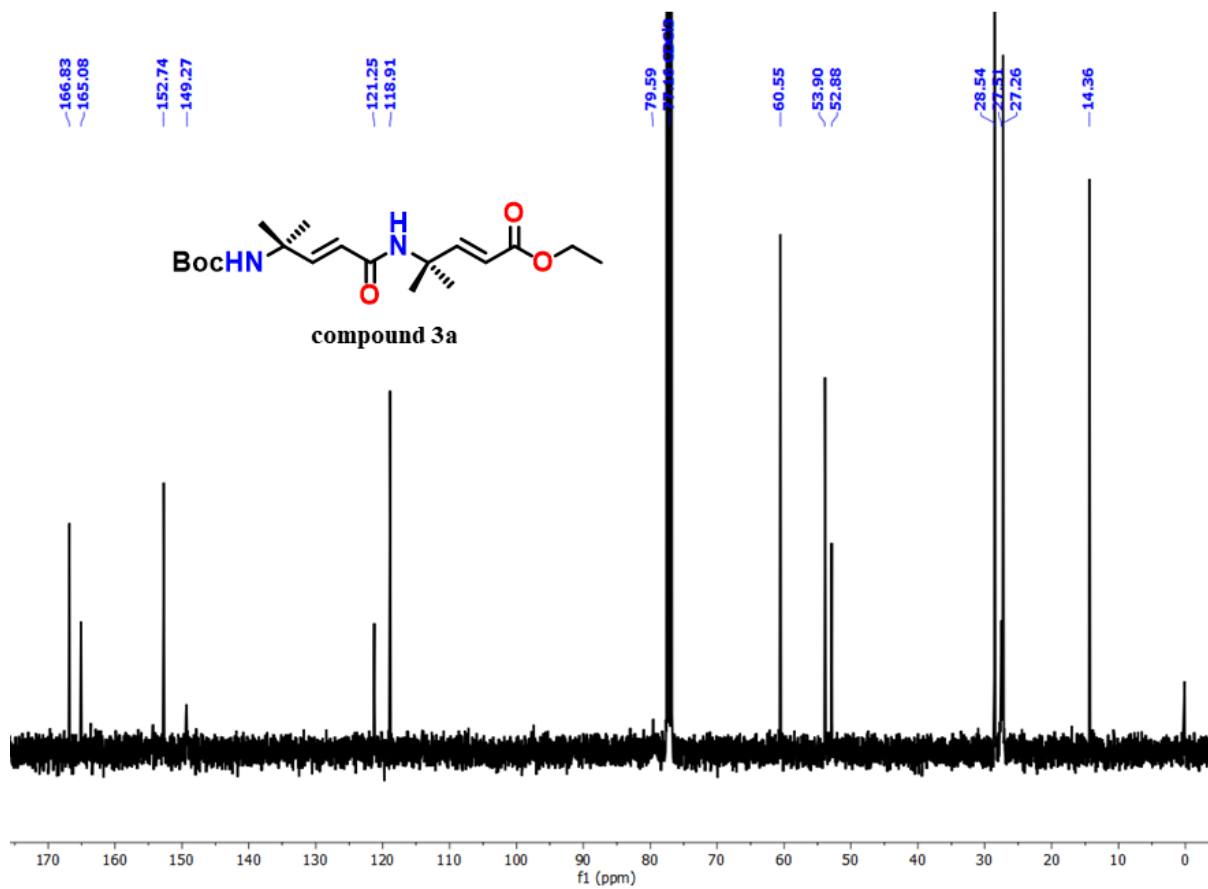
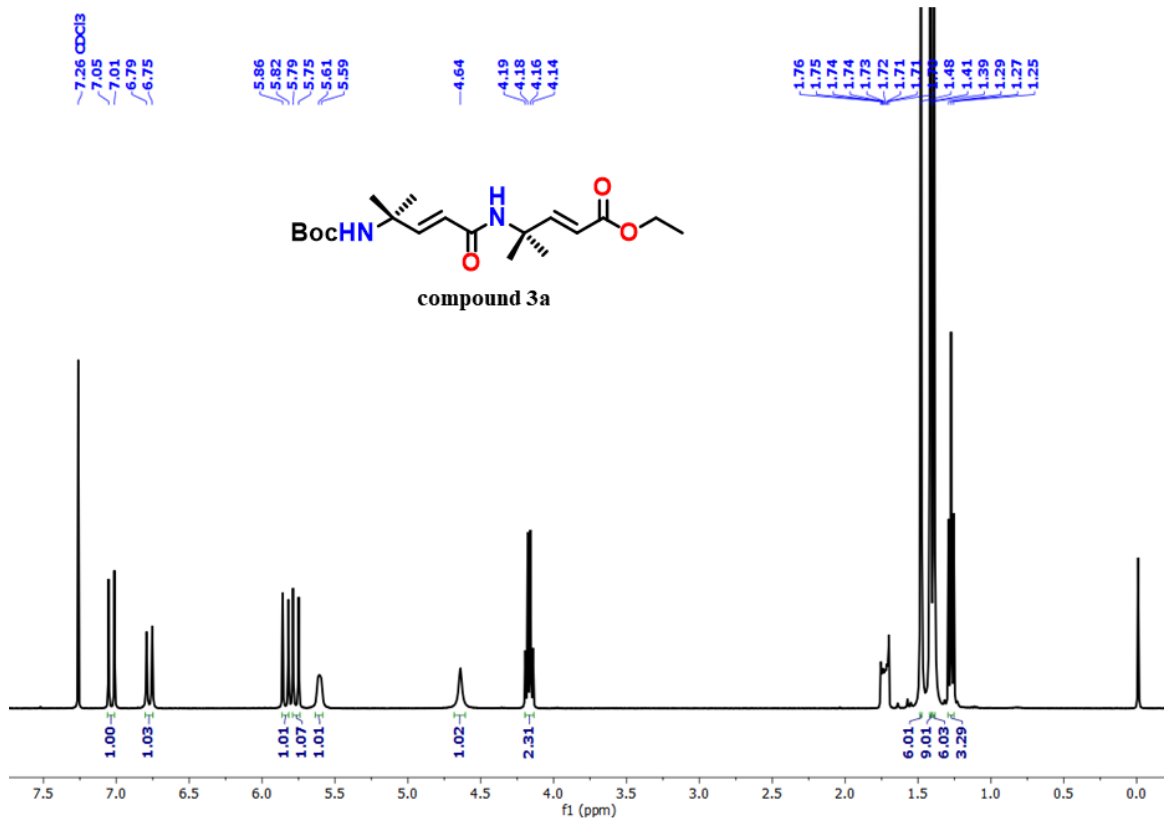
11. Kovacs, F.; Quine, J.; Cross, T. A. *Proc. Natl. Acad. Sci. USA*. **1999**, *96*, 7910.
12. Vertesy, L.; Aretz, W.; Knauf, M.; Markus, A.; Vogel, M.; Wink, J. *J. Antibiot.* **1999**, *52*, 374.
13. Férir, G.; Hänchen, A.; François, K. O.; Hoorelbeke, B.; Huskens, D.; Dettner, F.; Süßmuth, R. D.; Schols, D. *Virology*, **2012**, *433*, 308.
14. Dettner, F.; Hnchen, A.; Schols, D.; Toti, L.; Nusser, A.; Sussmuth, R. D. *Angew. Chem. Int. Ed.* **2009**, *48*, 1856.
15. (a) Benedetti, E.; Di Blasio, B.; Pedone, C.; Lorenzi, G. P.; Tomasic, L.; Gramlich, V. *Nature*, **1979**, *282*, 630. (b) Di Blasio, B.; Benedetti, E.; Pavone, V.; Pedone, C.; Gerber, C.; Lorenzi, G. P. *Biopolymers* **1989**, *28*, 203.
16. (a) Kulp, J. L.; Clark, T. D. *Chem. Eur. J.* **2009**, *15*, 11867. (b) Navarro, E.; Fenude, E.; Celda, B. *Biopolymers* **2004**, *73*, 229. (c) Sastry, M.; Brown, C.; Wagner, G.; Clark, T. D. *J. Am. Chem. Soc.* **2006**, *128*, 10650. (d) Schramm, P.; Hofmann, H. -J. *J. Pept. Sci.* **2010**, *16*, 276. (e) Jadhav, K. B.; Lichtenecker, R. J.; Bullach, A.; Mandal, B.; Arndt, H. -D. *Chem. Eur. J.* **2015**, *21*, 5898.
17. (a) Berl, V.; Huc, I.; Khoury, R. G.; Krische, M. J.; Lehn, J. -M. *Nature* **2000**, *407*, 720. (b) Gan, Q.; Wang, X.; Kauffmann, B.; Rosu, F.; Ferrand, Y.; Huc, I. *Nature Nanotech.* **2017**, *12*, 447. (c) Wang, X.; Wicher, B.; Ferrand, Y.; Huc, I. *J. Am. Chem. Soc.* **2017**, *139*, 9350. (d) Li, X.; Markandeya, N.; Jonusauskas, G.; McClenaghan, N. D.; Maurizot, V.; Denisov, S. A.; Huc, I. *J. Am. Chem. Soc.* **2016**, *138*, 13568. (e) Denisov, S. A.; Gan, Q.; Wang, X.; Scarpantonio, L.; Ferrand, Y.; Kauffmann, B.; Jonusauskas, G.; Huc, I.; McClenaghan, N. D. *Angew. Chem. Int. Ed.* **2016**, *55*, 1328. (f) Shang, J.; Gan, Q.; Dawson, S. J.; Rosu, F.; Jiang, H.; Ferrand, Y.; Huc, I. *Org. Lett.* **2014**, *16*, 4992. (g) Denisov, S. A.; Gan, Q.; Wang, X.; Scarpantonio, L.; Ferrand, Y.; Kauffmann, B.; Jonusauskas, G.; Huc, I.; McClenaghan, N. D. *Angew. Chem. Int. Ed.* **2016**, *55*, 1328. (h) Denisov, S. A.; Gan, Q.; Wang, X.; Scarpantonio, L.; Ferrand, Y.; Kauffmann, B.; Jonusauskas, G.; Huc, I.; McClenaghan, N. D. *Angew. Chem. Int. Ed.* **2016**, *55*, 1328. (i) Maurizot, V.; J. Léger, M.; Guionneau, P.; Huc, I. *Russ. Chem. Bull. Int. Ed.*, **2004**, *53*, 1572. (j) Zhan, C.; Léger, J.-M.; Huc, I. *Angew. Chem. Int. Ed.* **2006**, *45*, 4625. (k) Haldar, D.; Jiang, H.; Léger, J.-M.; Huc, I. *Angew. Chem. Int. Ed.* **2006**, *45*, 5483.

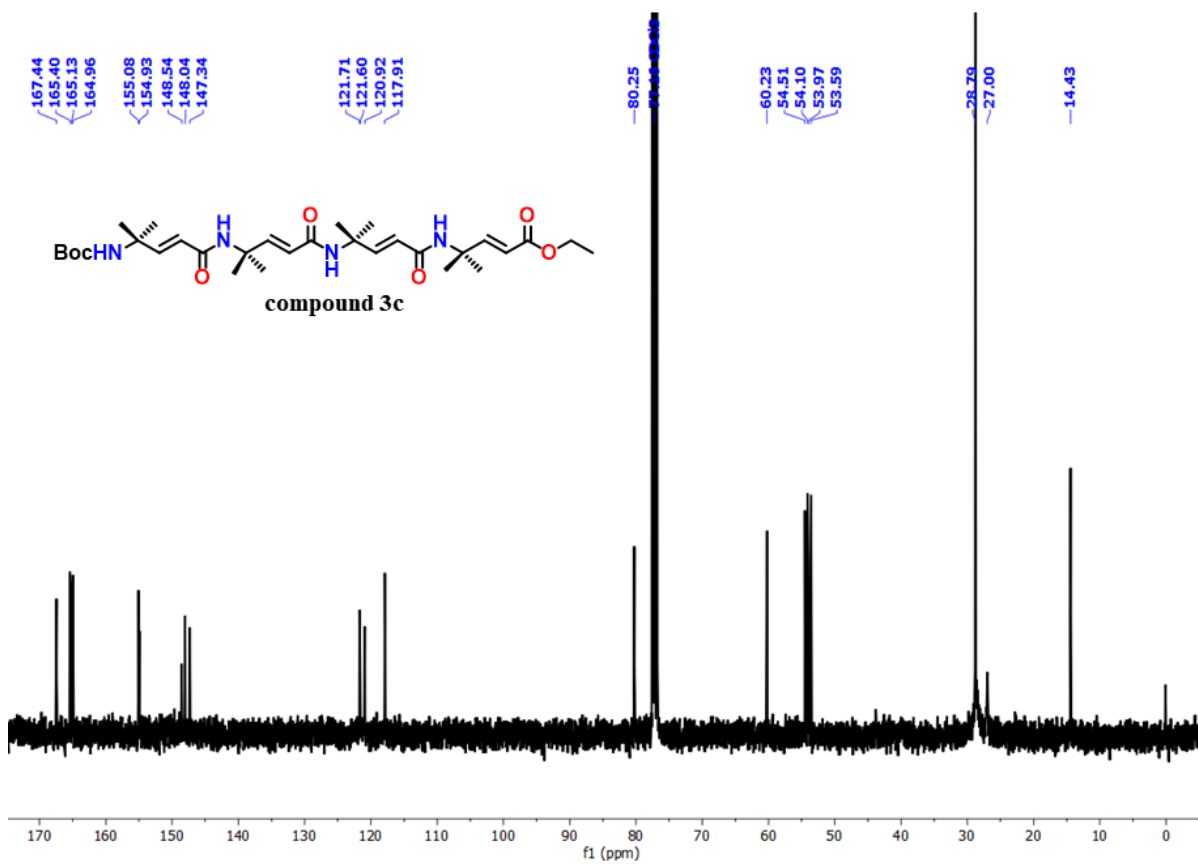
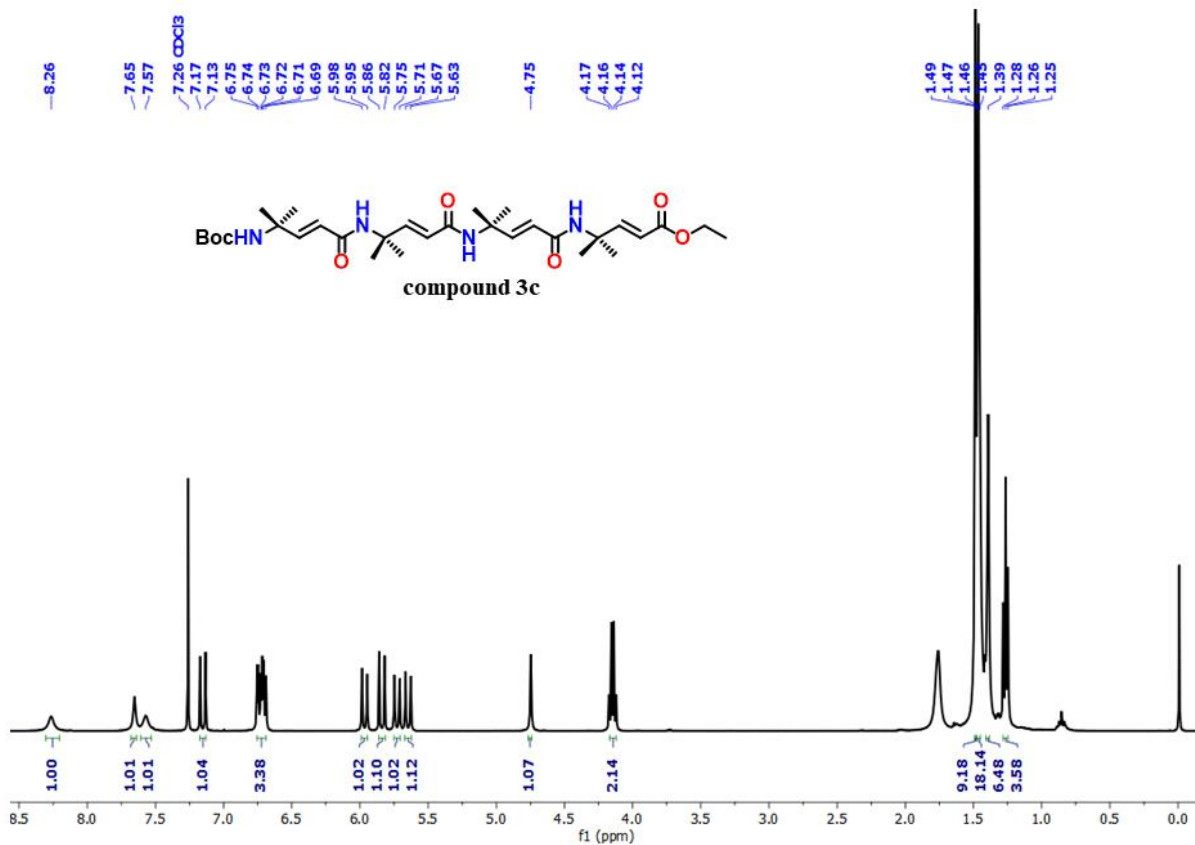
18. Yashima, E.; Maeda, K.; Furusho, Y. *Acc. Chem. Res.* **2008**, *41*, 1166.
19. Koert, U.; Harding, M.M.; Lehn, J.-M. *Nature*, **1990**, 346, 339.
20. (a) Gabriel, G. J.; Iverson, B. L.; *J. Am. Chem. Soc.*, **2002**, *124*, 15174. (b) Lokey, R.S.; Iverson, B.L. *Nature*, **1995**, 375, 303. (c) Ikkanda, B. A.; Iverson, B. L. *Chem. Commun.*, **2016**, *52*, 7752.
21. (a) Tanaka, Y.; Katagiri, H.; Furusho, Y. Yashima, E. *Angew. Chem., Int. Ed.*, **2005**, *44*, 3867. (b) E. Yashima, N. Ousaka, D. Taura, K. Shimomura, T. Ikai, K. Maeda, *Chem. Rev.* **2016**, *116*, 13752. (c) Wang, J.; Meersman, F.; Esnouf, R.; Froeyen, M.; Busson, R. Heremans, K.; Herdewijn, P.; *Helv. Chim. Acta*, **2001**, *84*, 2398. (d) Liu, Z.; Li, X.; Lu, Y.; Zhang, C.; Zhang, Y.; Huang, T.; Zhang, D.; Duan, L. *Nat. Commun.* **2022**, *13*, 1215.
22. (a) Misra, R.; Dey, S.; Reja, R. M.; Gopi, H. N. *Angew. Chem. Int. Ed.* **2018**, *57*, 1057. (b) Veeresh, K.; Singh, M.; Gopi, H. N. *Org. Biomol. Chem.* **2019**, *17*, 9226.
23. Jadhav, S. V.; Gopi, H. N. *Chem. Commun.*, **2013**, *49*, 9179
24. Misra, R.; George, G.; Saseendran, A.; Raghothama, S.; Hosahudya N. Gopi, H. N. *Chem. Asian J.* **2019**, *14*, 4408.
25. (a) Jeffrey, G. A. *An Introduction to Hydrogen Bonding*; Oxford University Press: New York, **1997**. (b) Desiraju, G. R.; Steiner, T. *The Weak Hydrogen Bond in Structural Chemistry and Biology*; Oxford Science Publications: Oxford, **1999**. (c) Hobza, P.; Havlas, Z. *Chem. Rev.* **2000**, *100*, 4253. (d) Desiraju, G. R. *Angew. Chem., Int. Ed.* **2007**, *46*, 8342. (e) Gu, Y.; Kar, T.; Scheiner, S. *J. Am. Chem. Soc.* **1999**, *121*, 9411.
26. (a) Mali, S. M.; Bandyopadhyay, A.; Jadhav, S. V.; Ganesh Kumar, M.; Gopi, H. N. *Org. Biomol. Chem.* **2011**, *9*, 6566. (b) Bandyopadhyay, A.; Gopi, H. N. *Org. Lett.* **2012**, *14*, 2770.

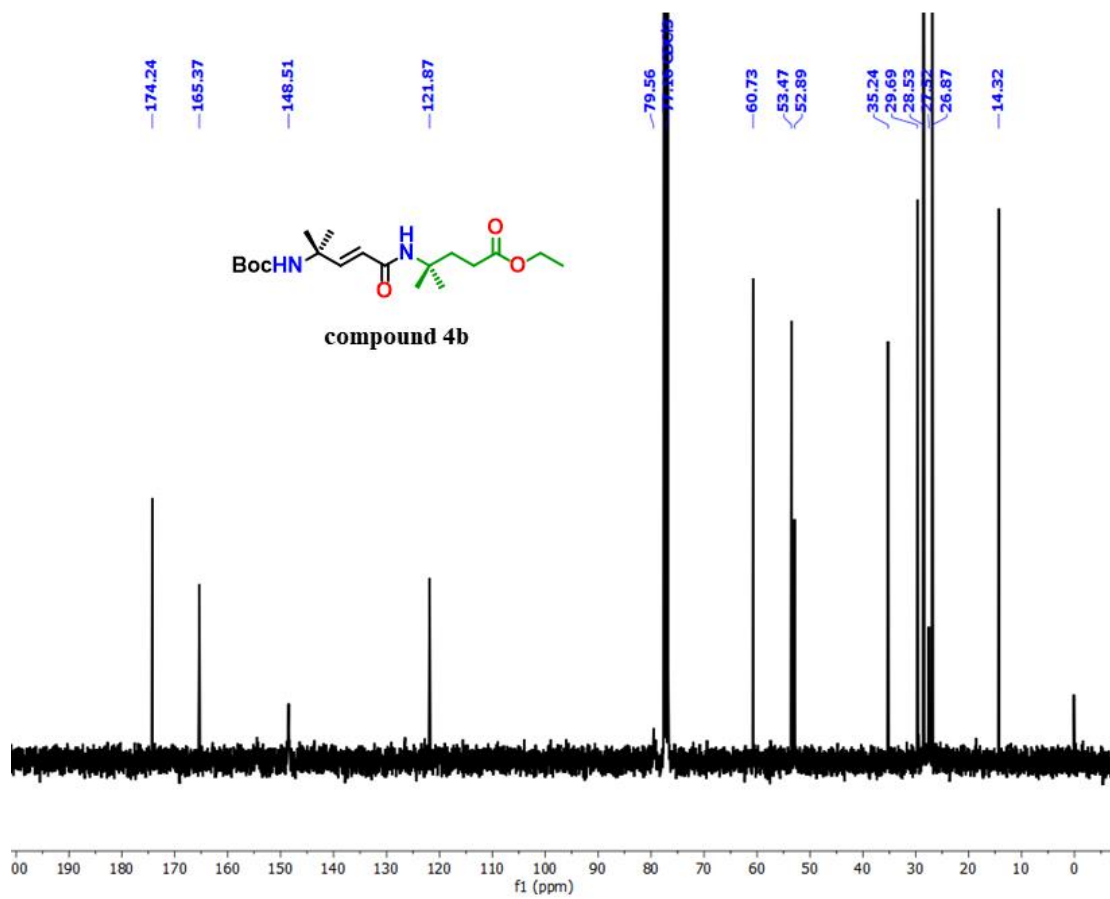
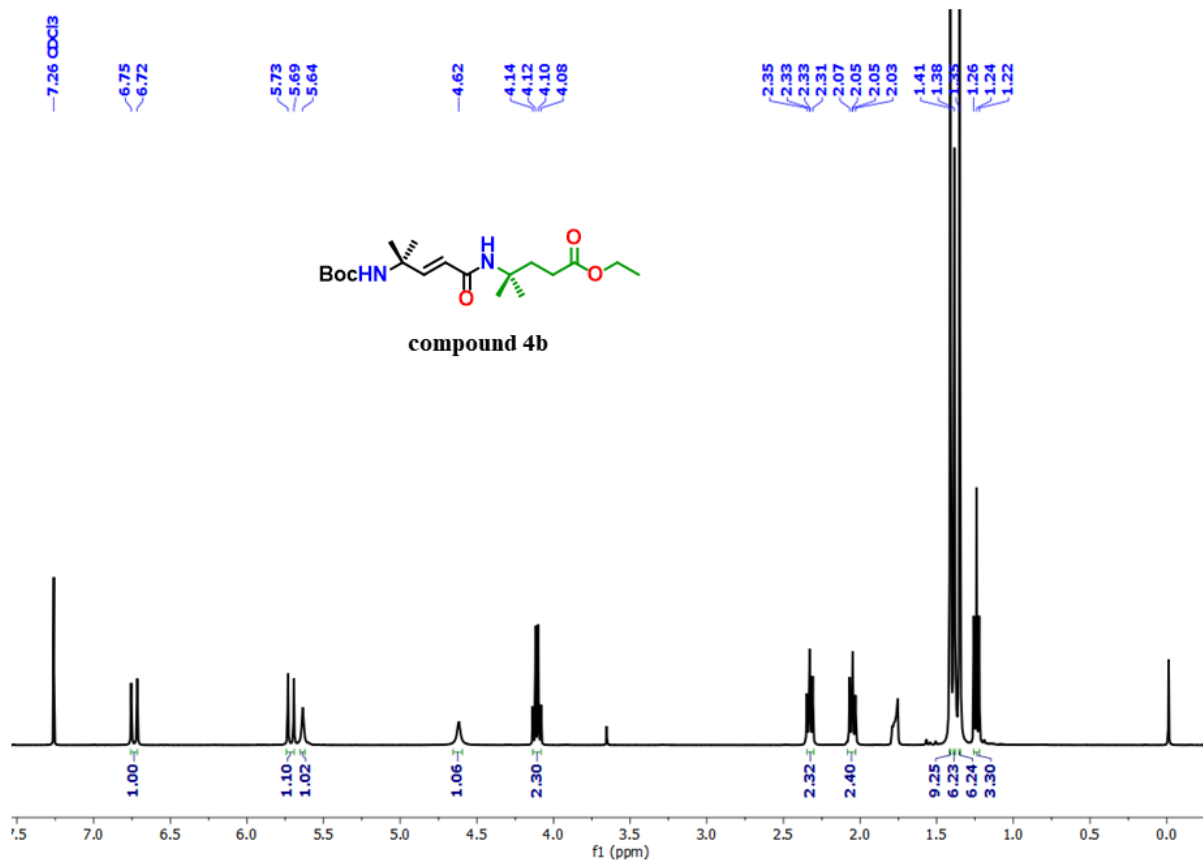
## 8. $^1\text{H}$ , $^{13}\text{C}$ NMR and Mass Spectra of Peptides P1-P4:

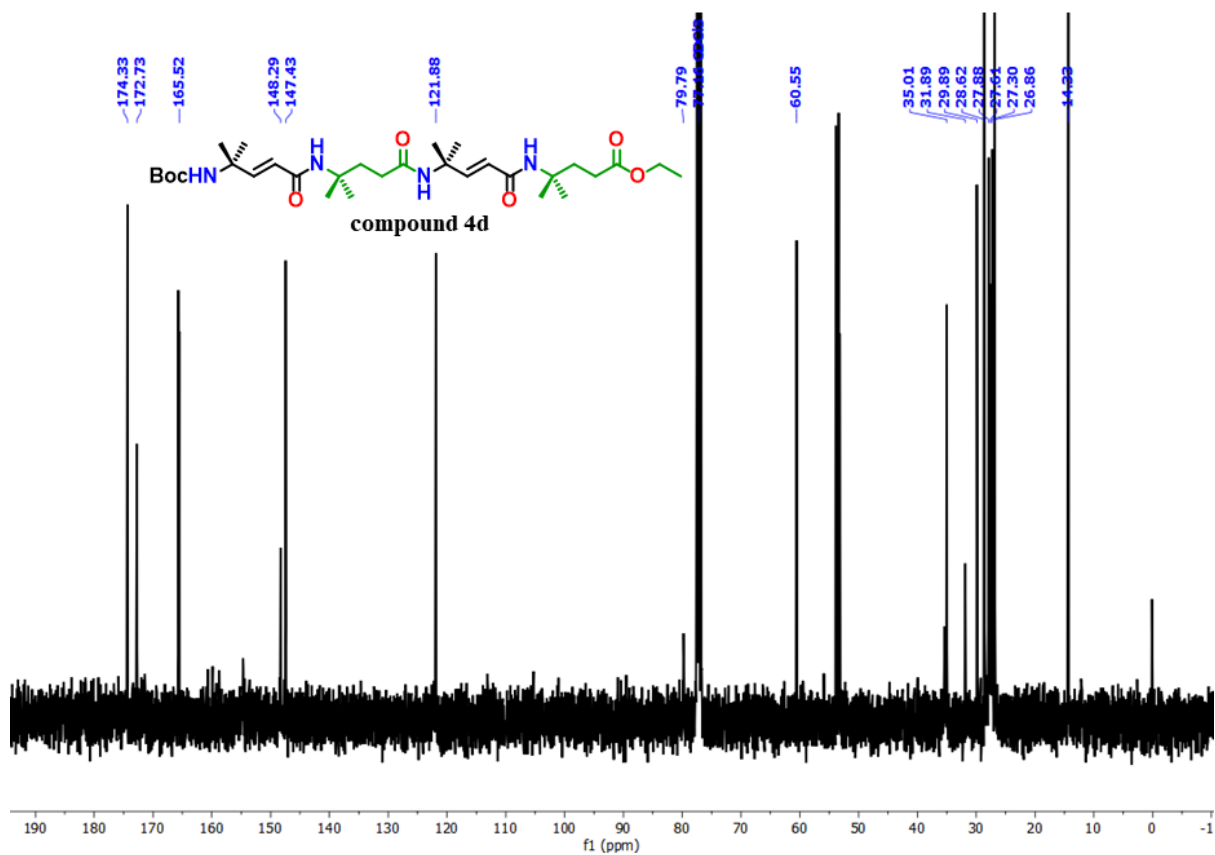
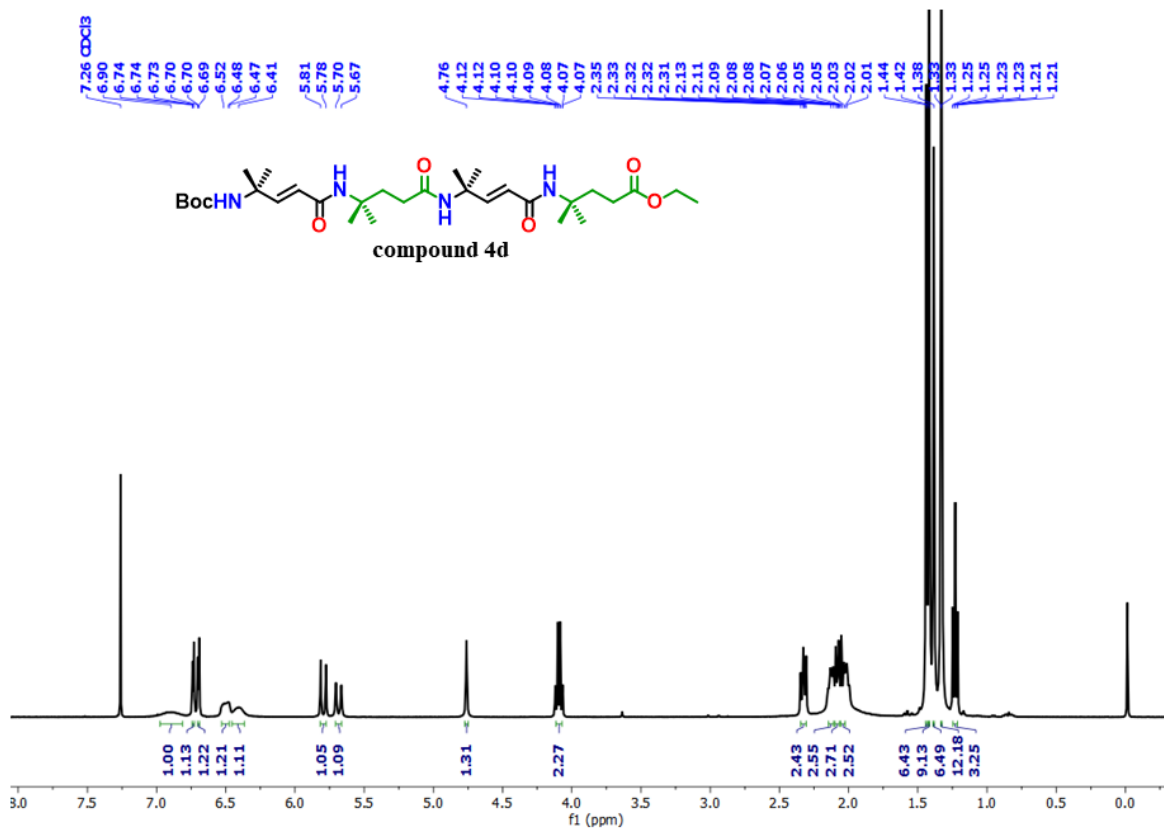




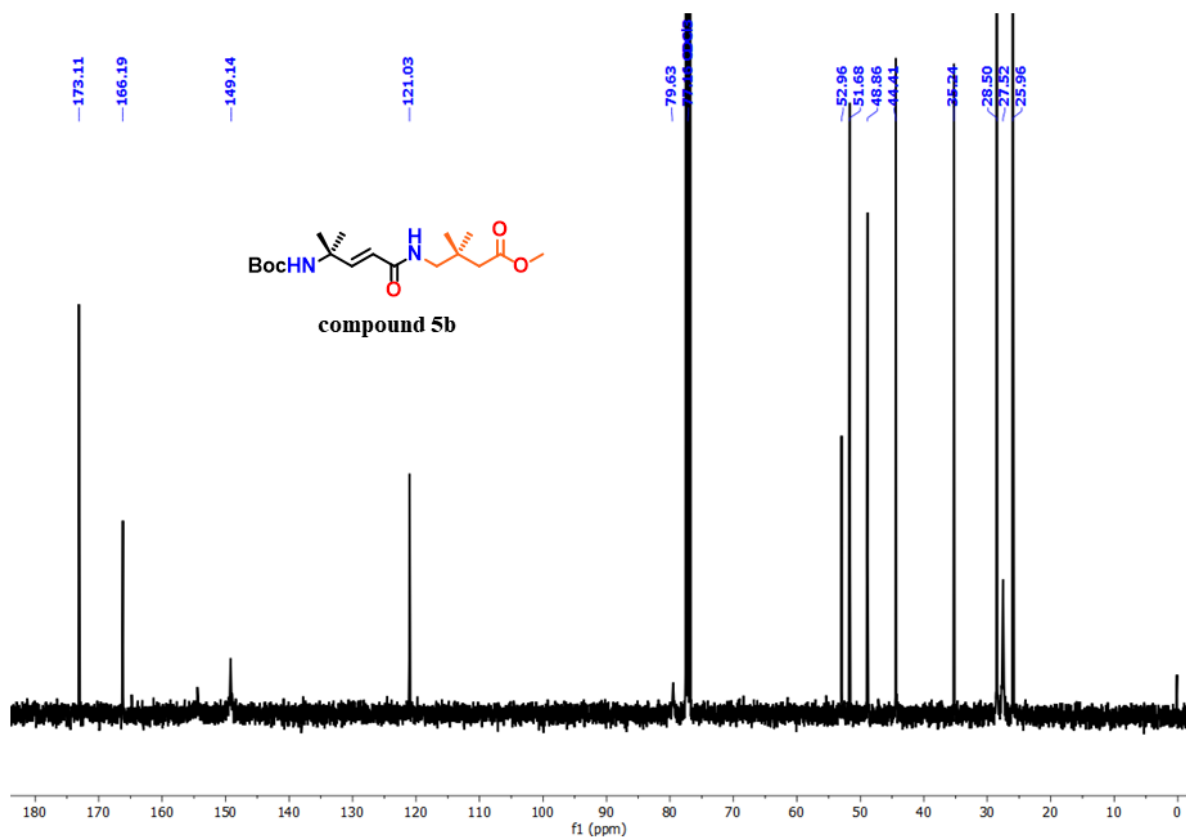
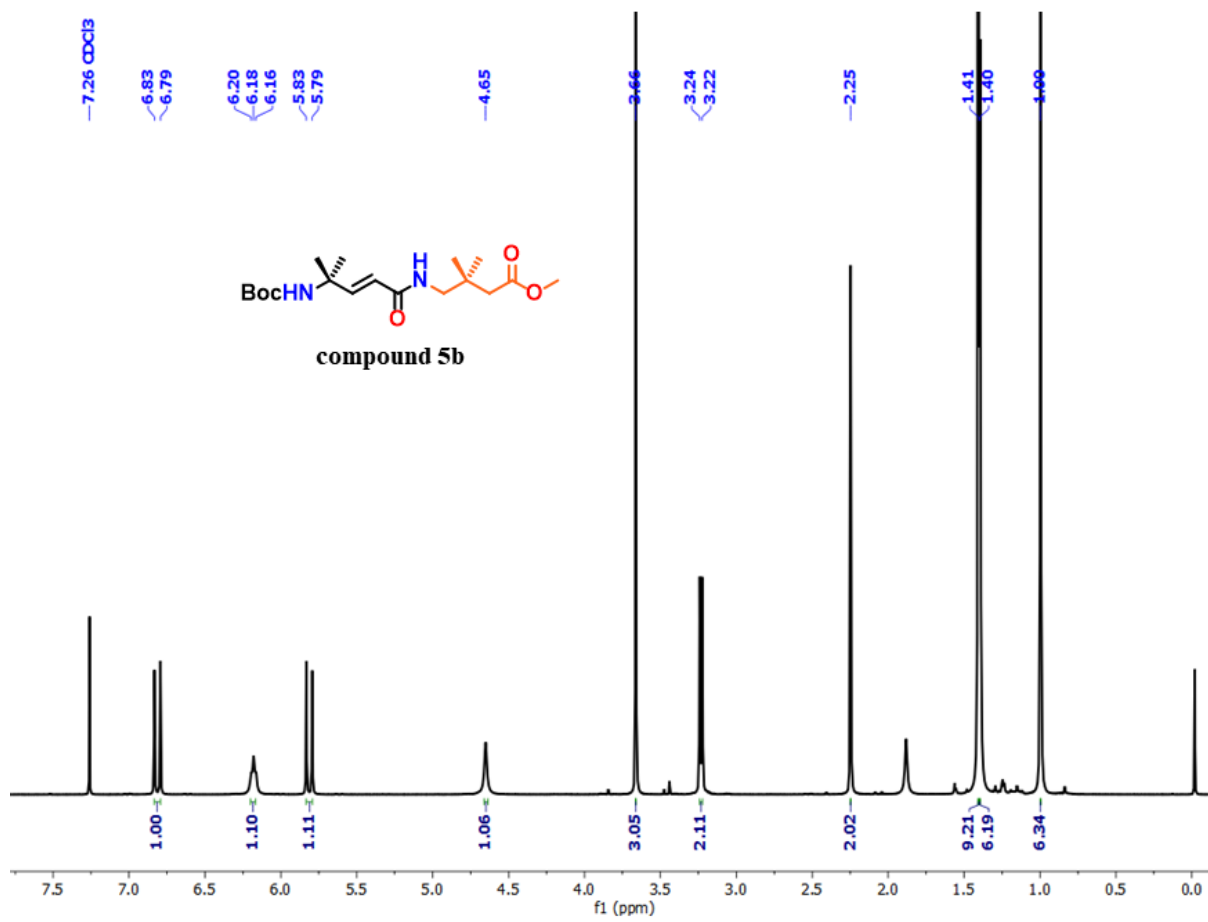


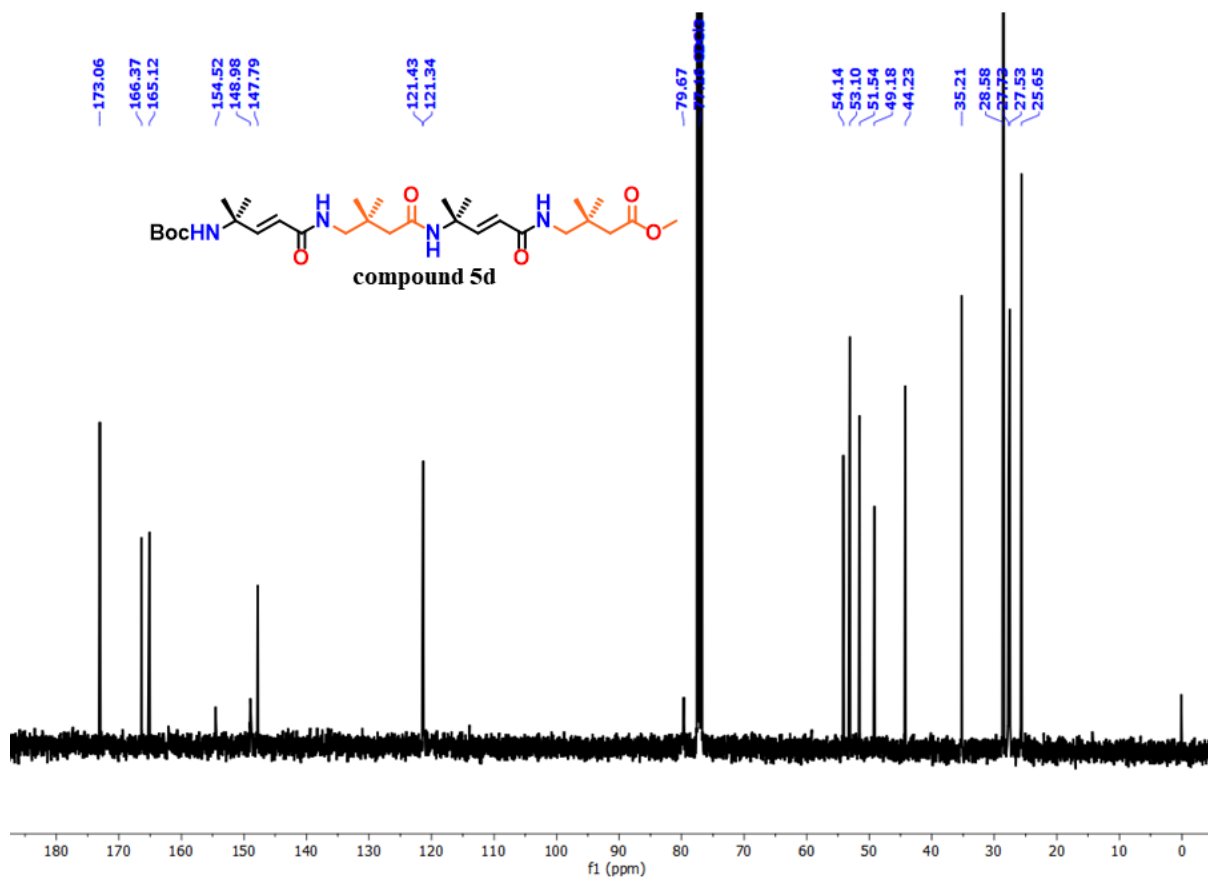
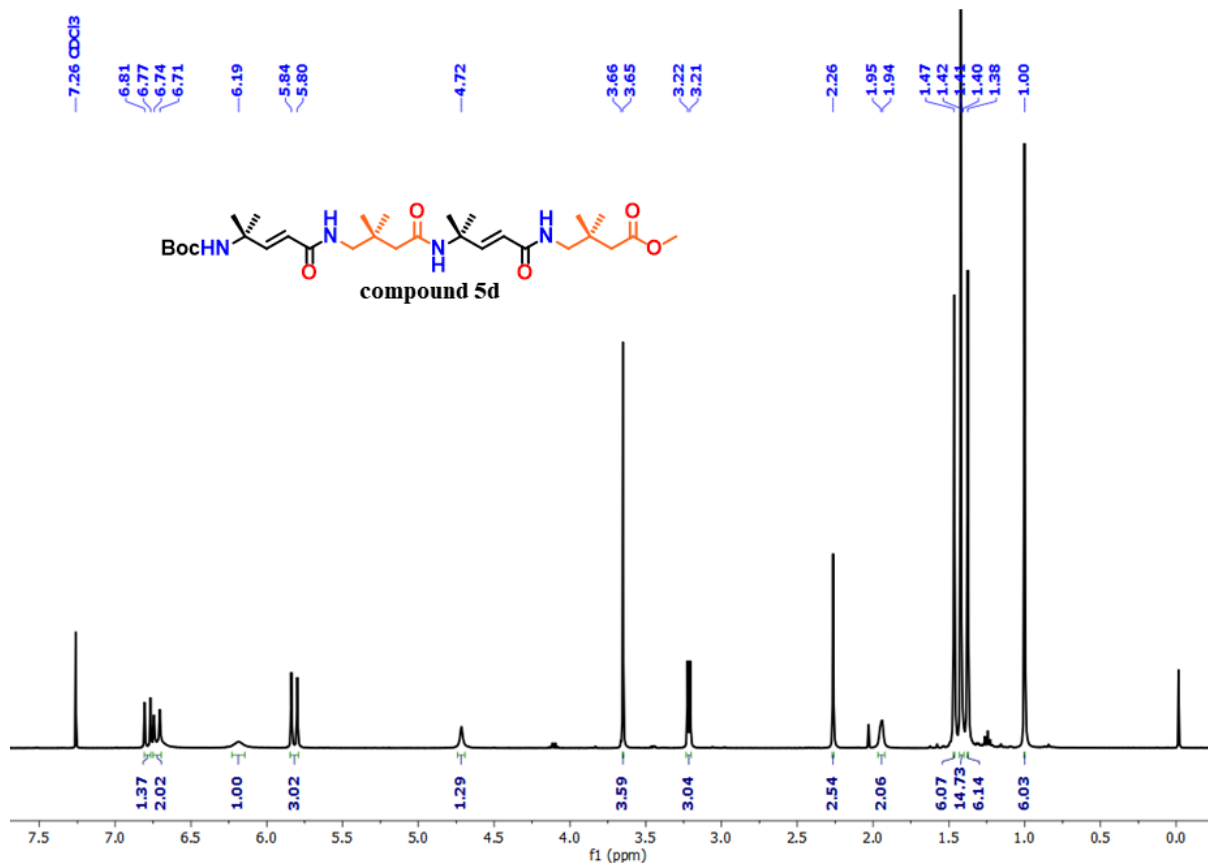


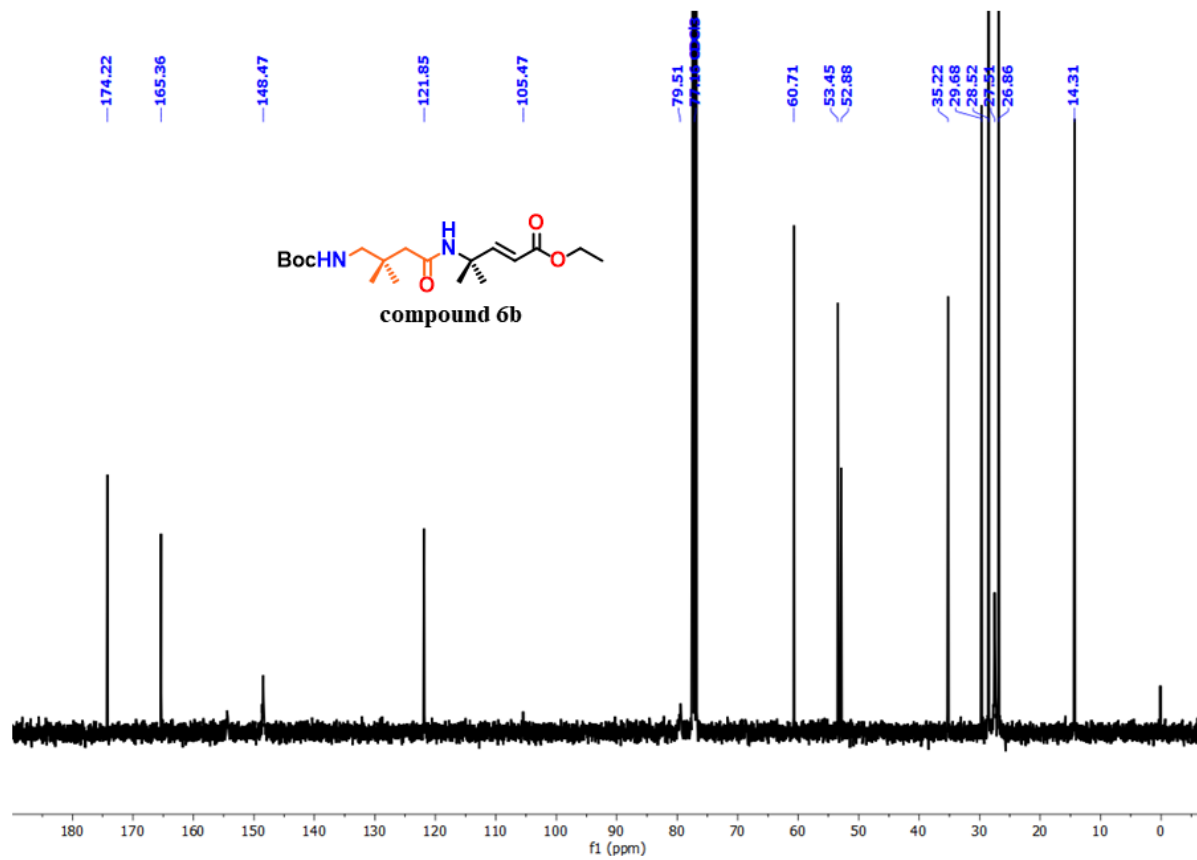
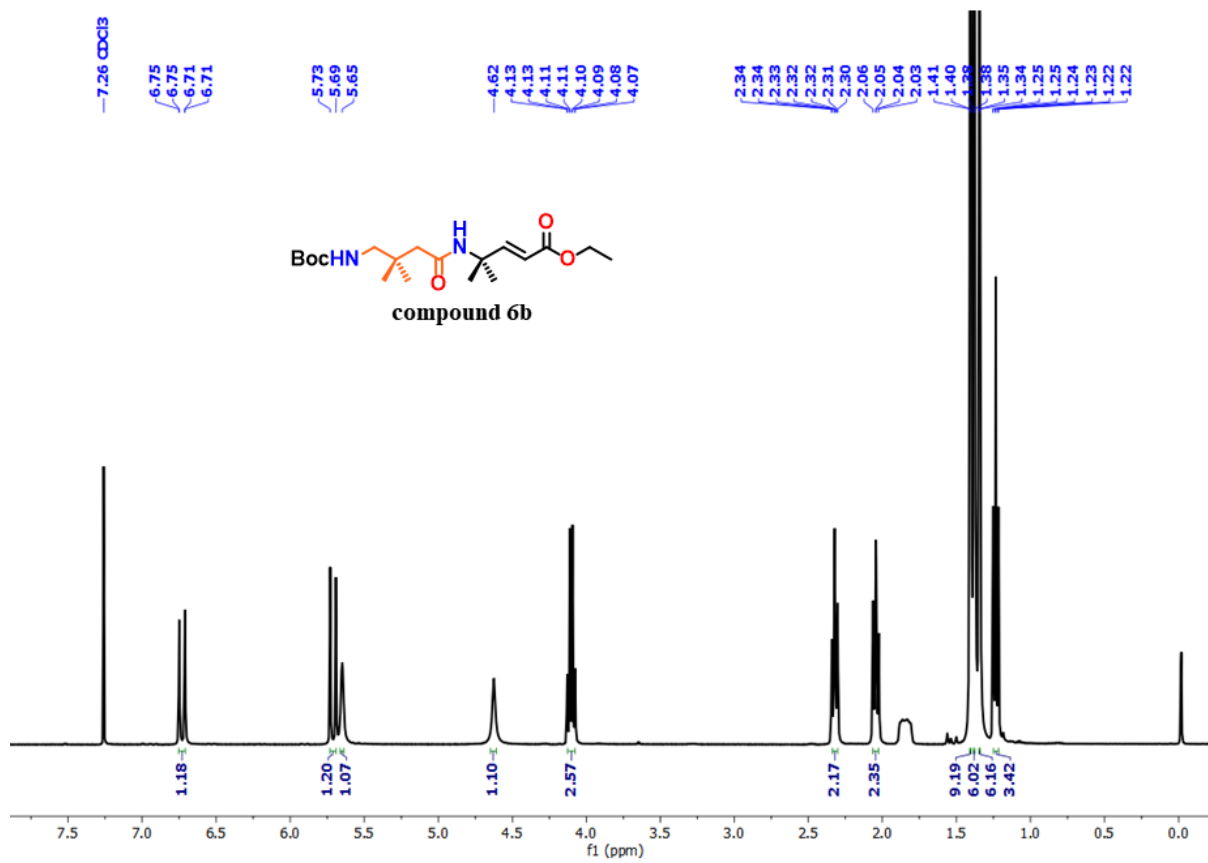


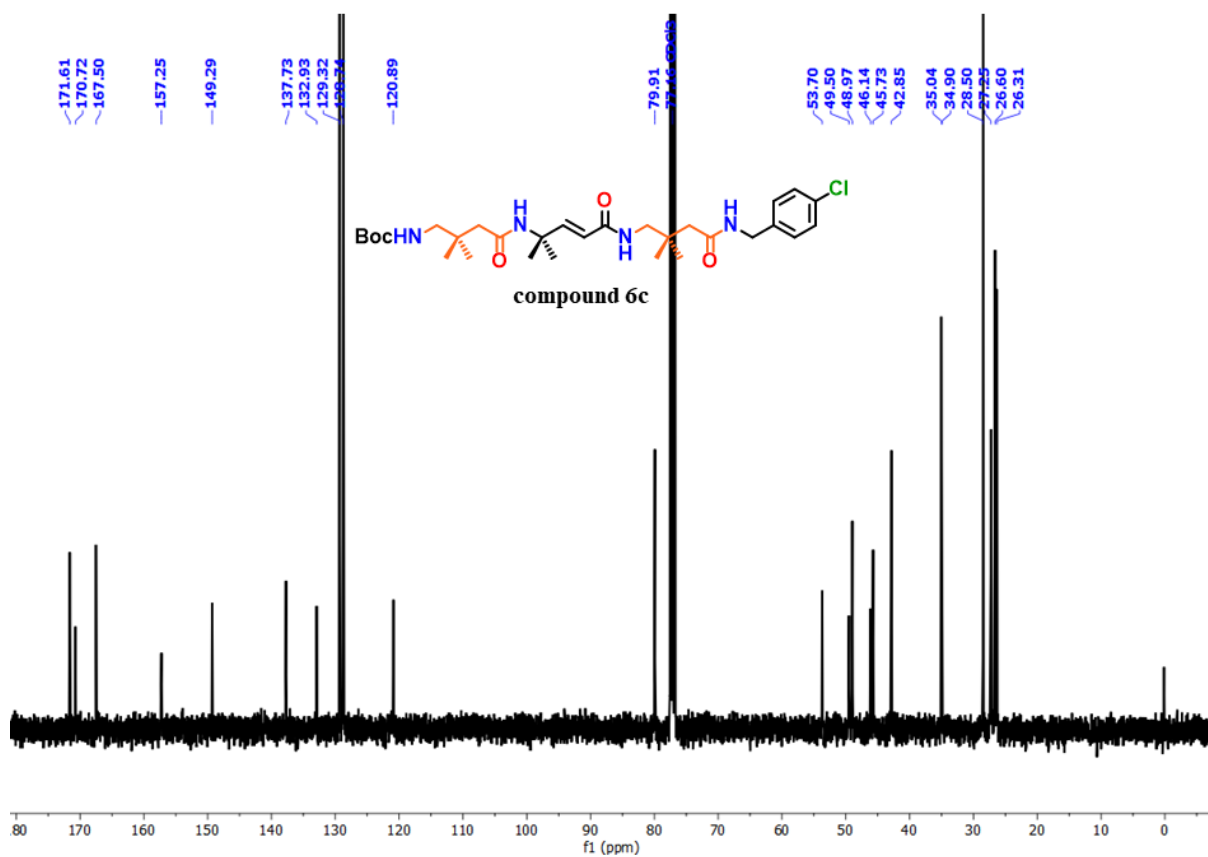
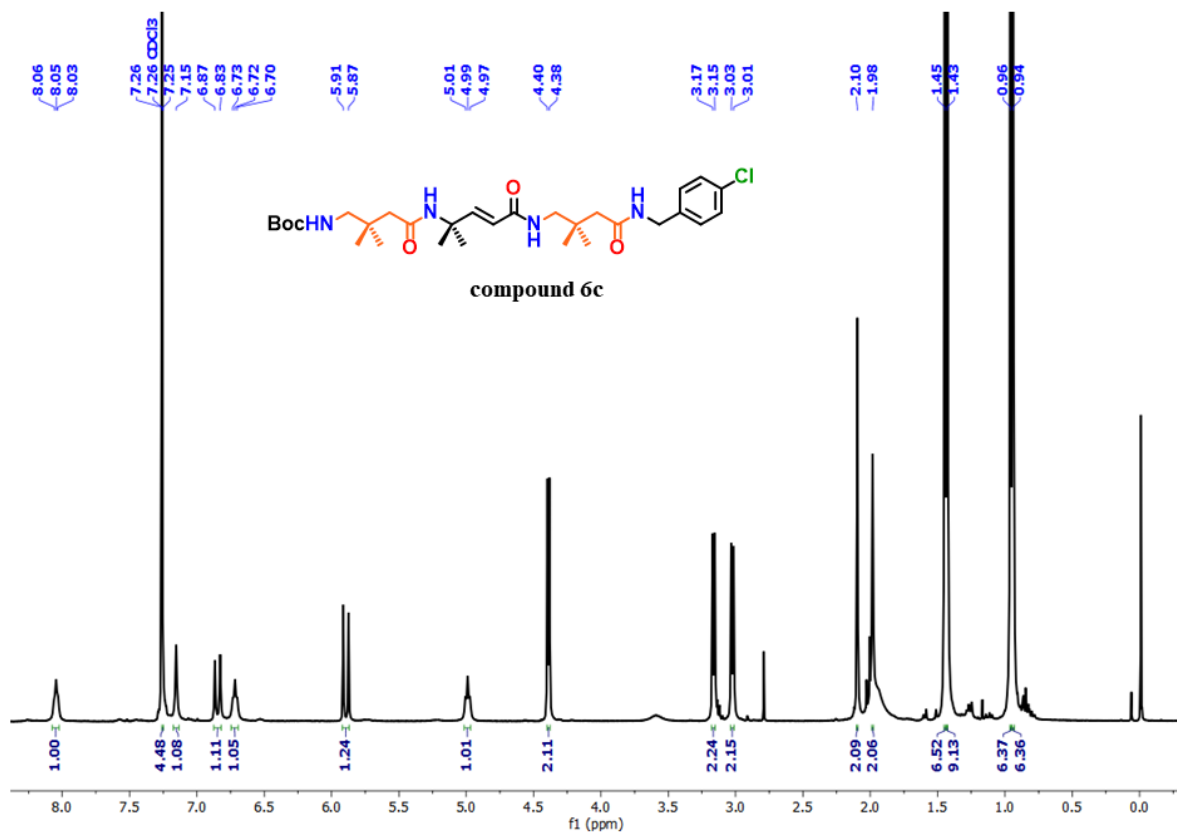


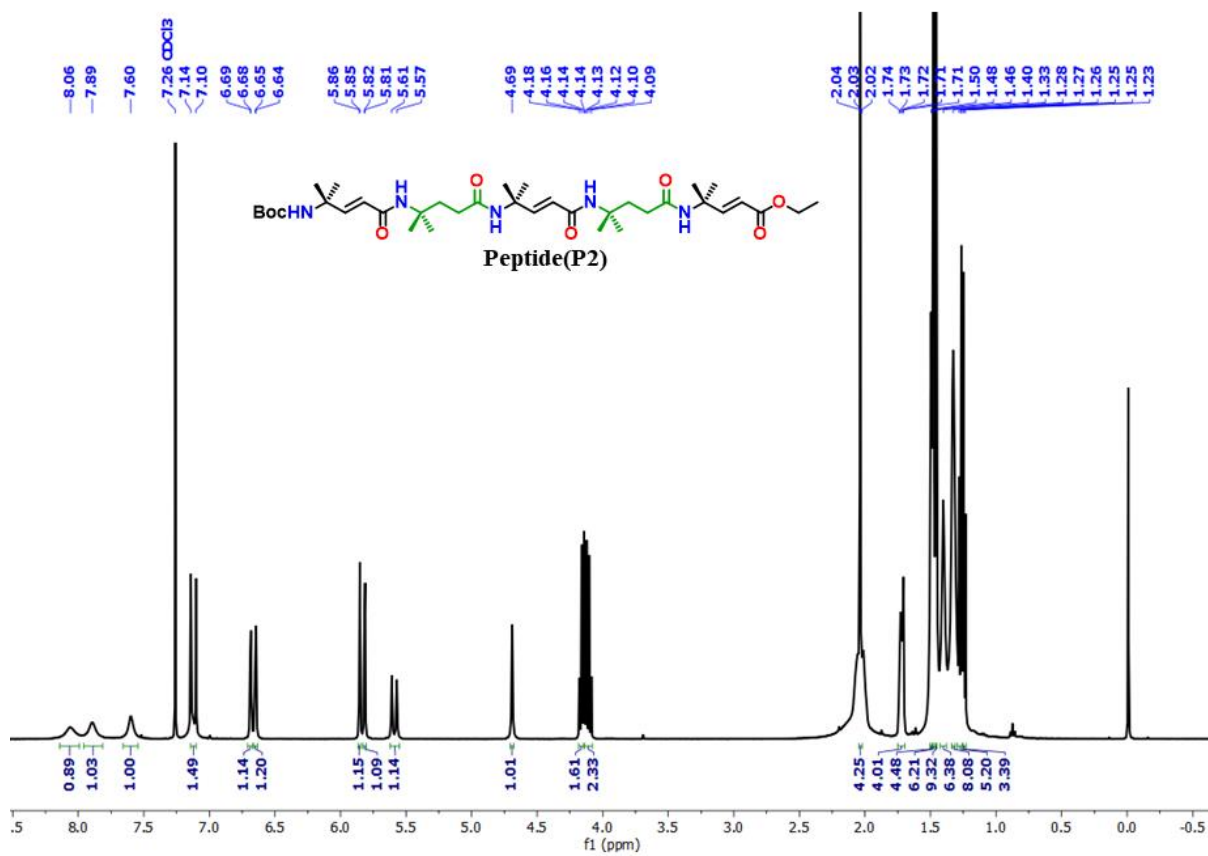
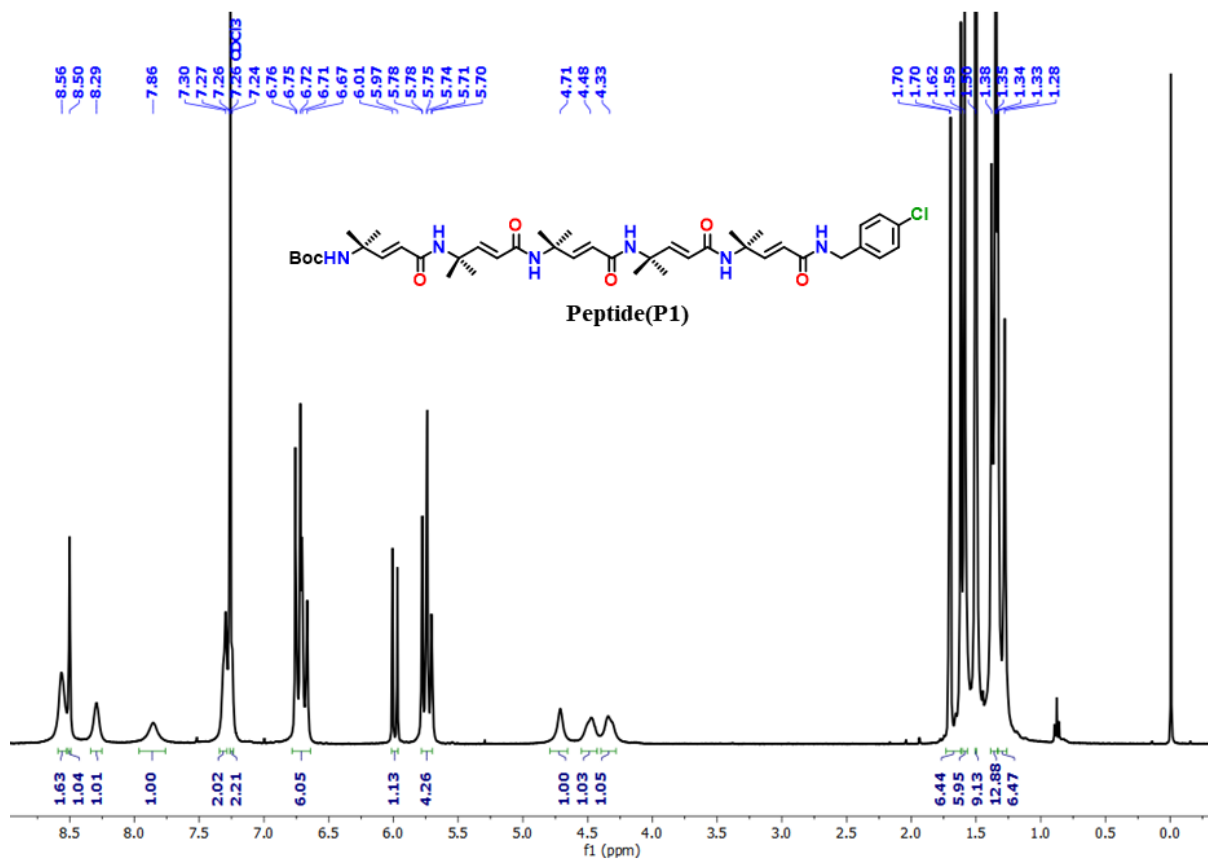


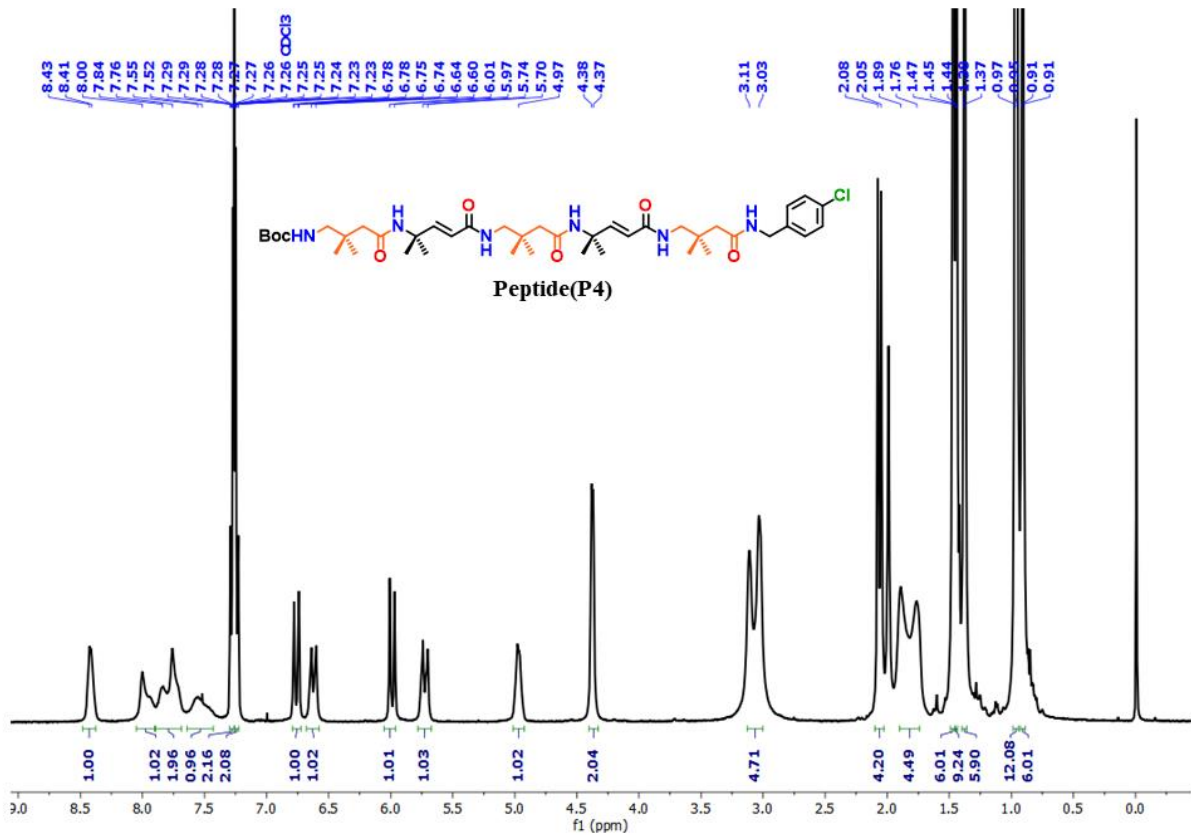
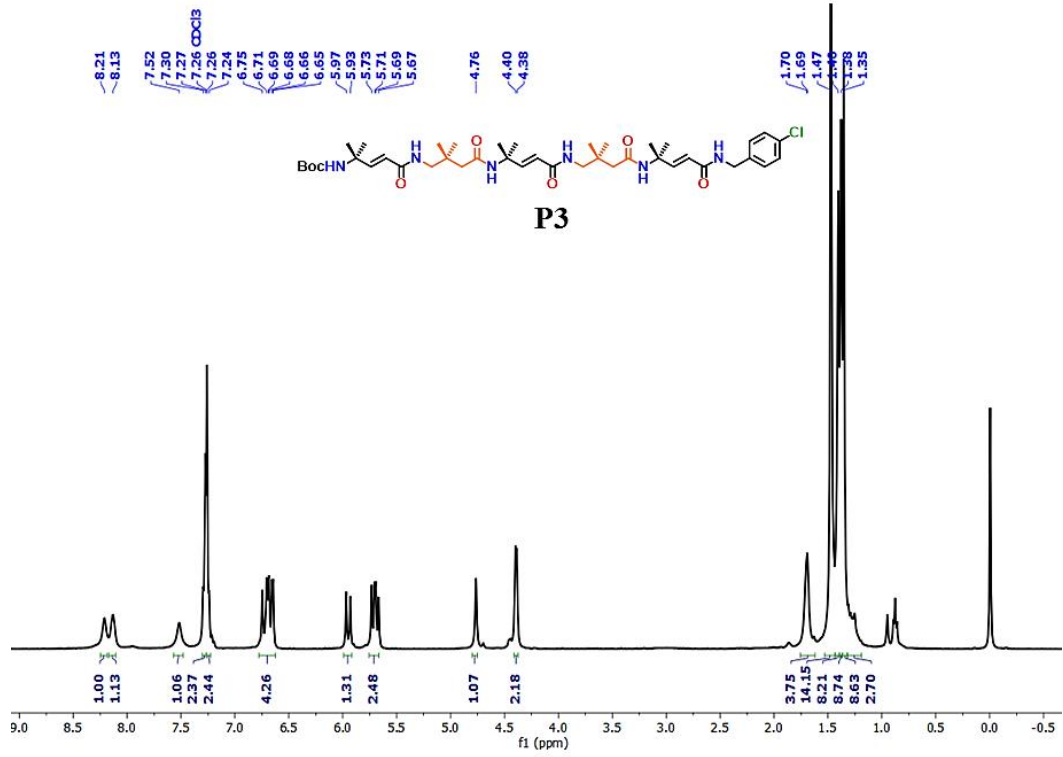






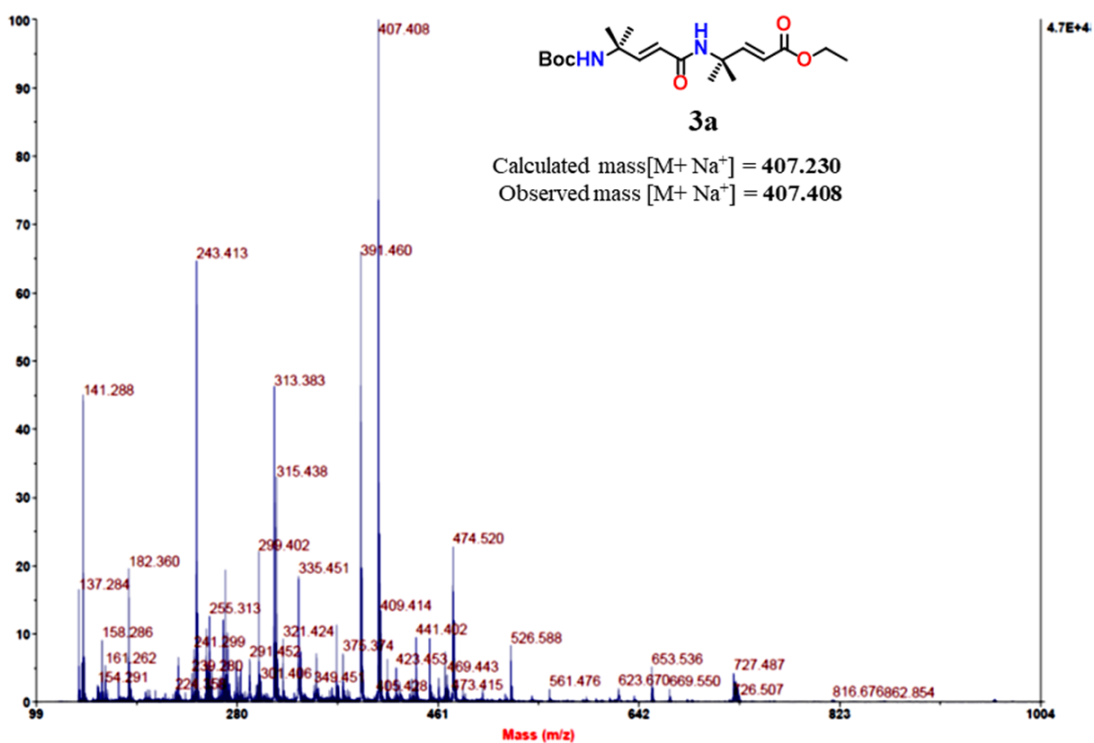






### Spectrum Report

Final - Shots 400 - IISER-96-2-2018: Label E9



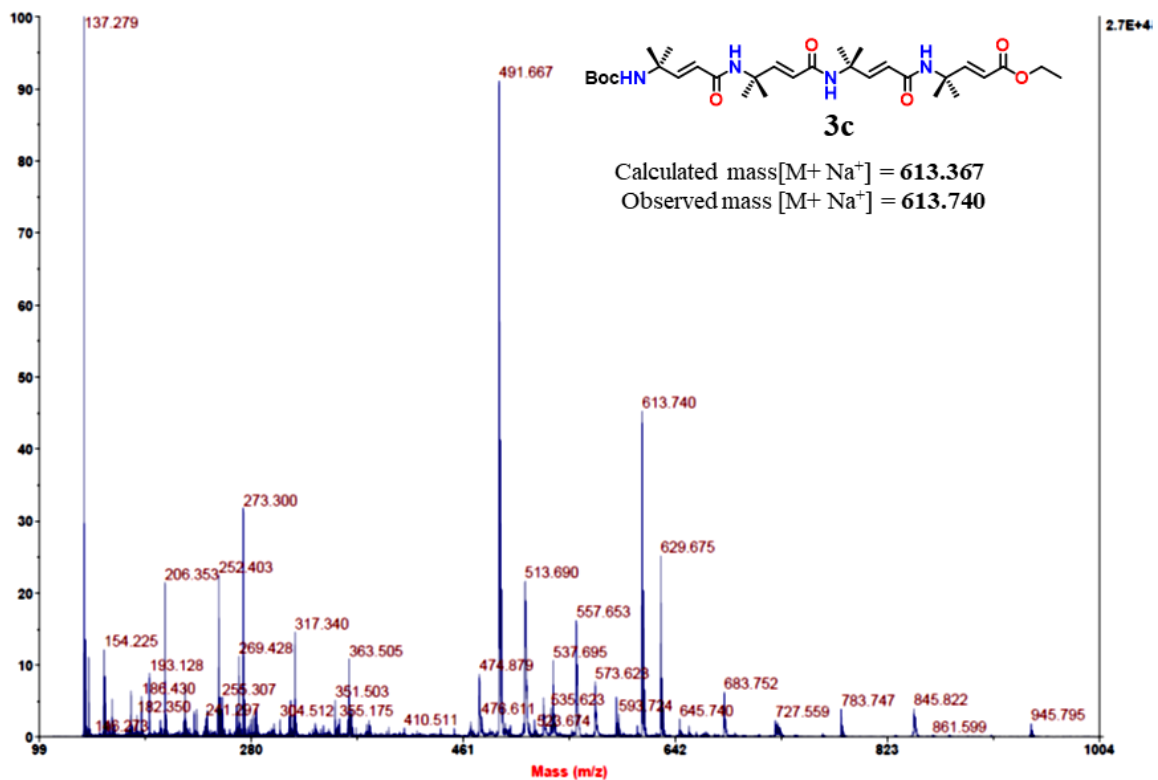
2018IISER-96-2-2018 Label E9 Run # 500

Page 1

10/18/2022 10:33:53 AM

### Spectrum Report

Final - Shots 400 - IISER-96-2-2018: Label E10



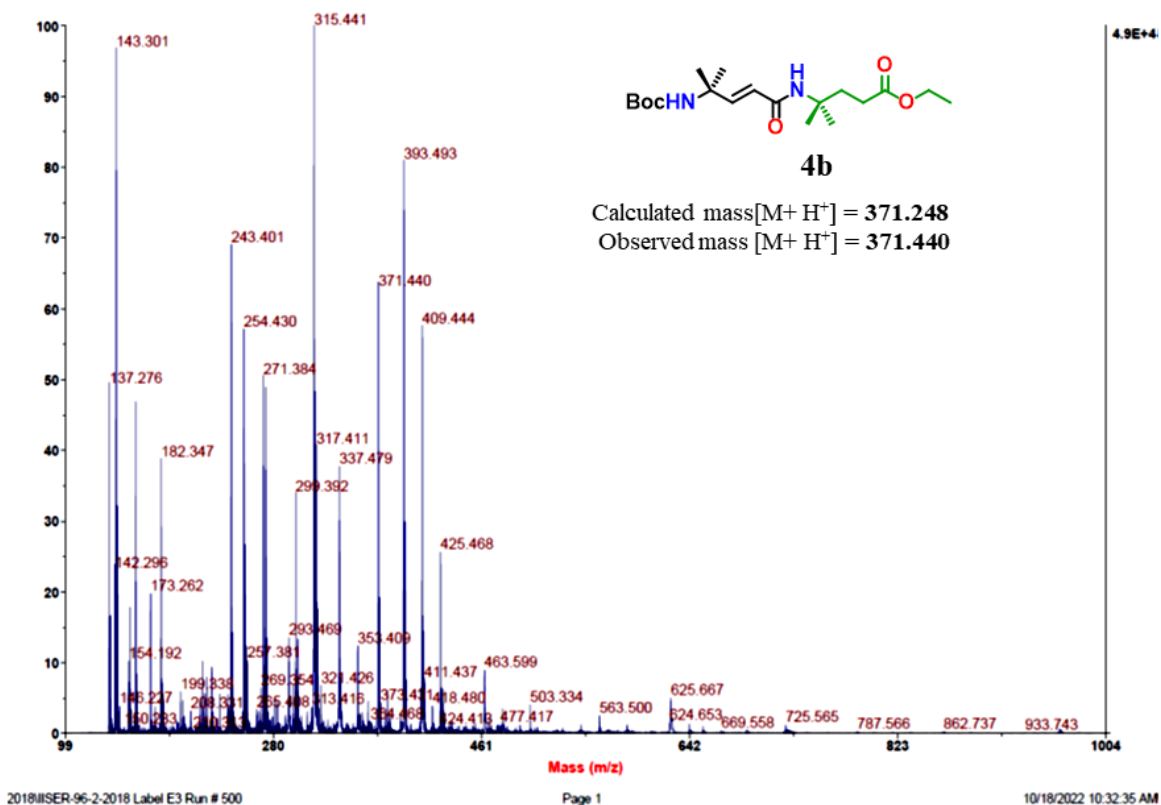
2018IISER-96-2-2018 Label E10 Run # 500

Page 1

10/18/2022 10:34:07 AM

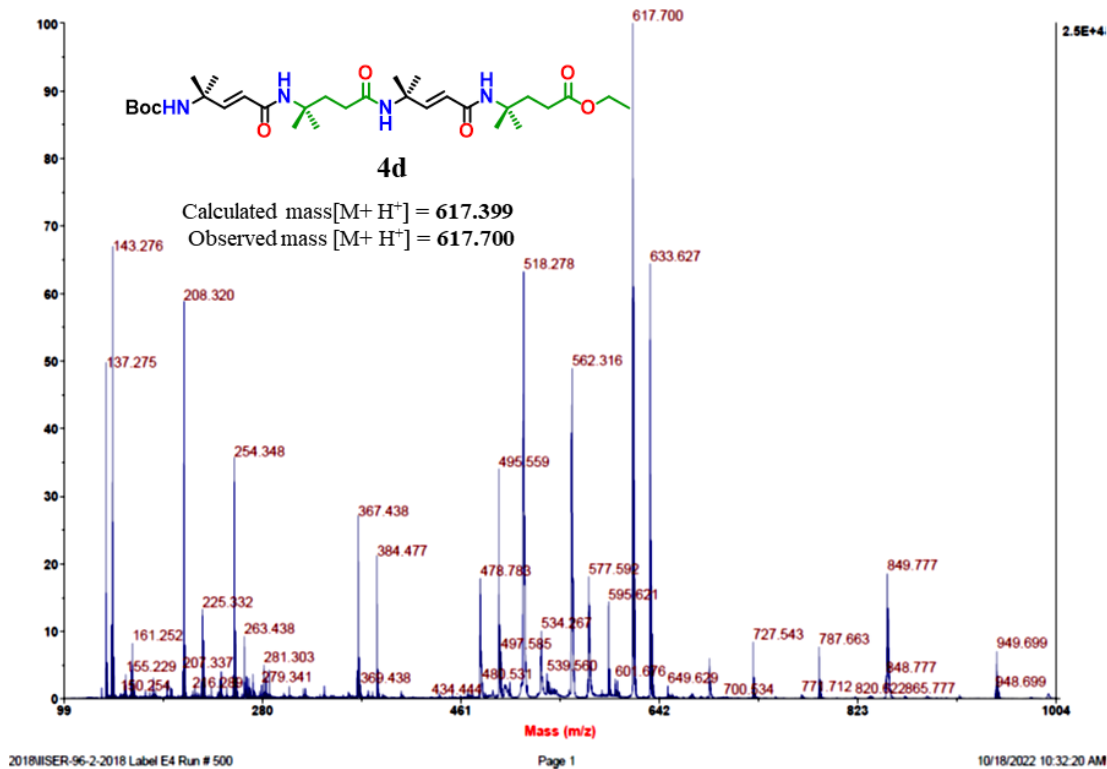
### Spectrum Report

Final - Shots 400 - IISER-96-2-2018; Run #500; Label E3



### Spectrum Report

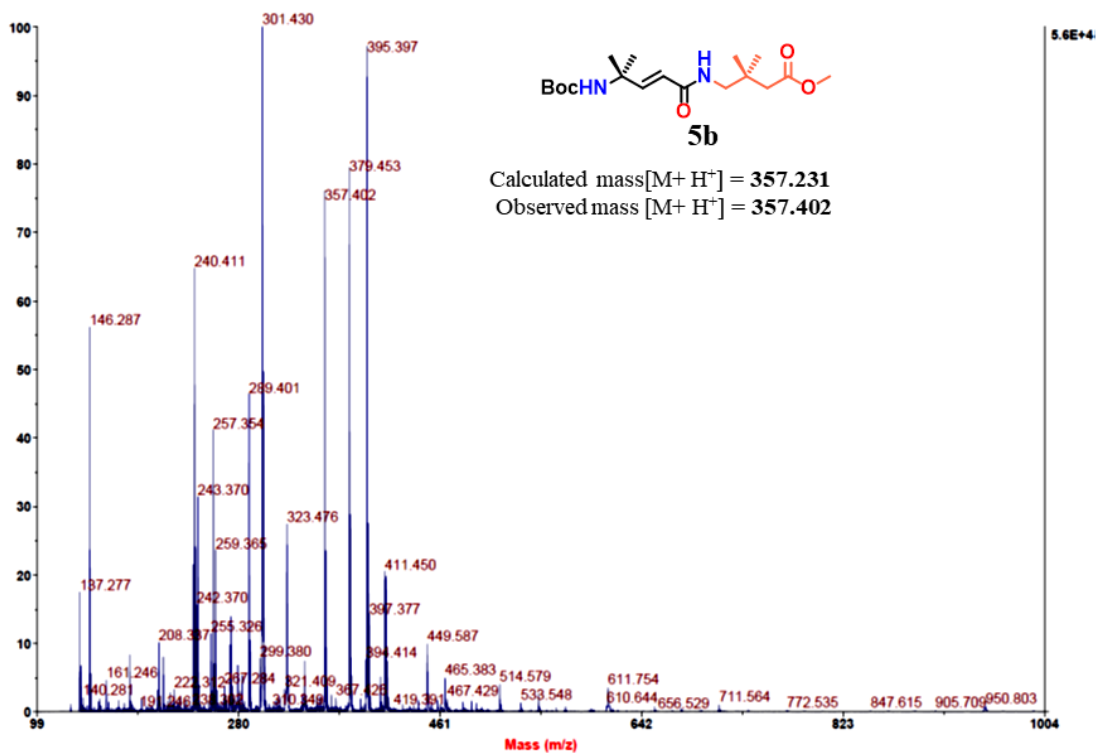
Final - Shots 400 - IISER-96-2-2018; Label E4





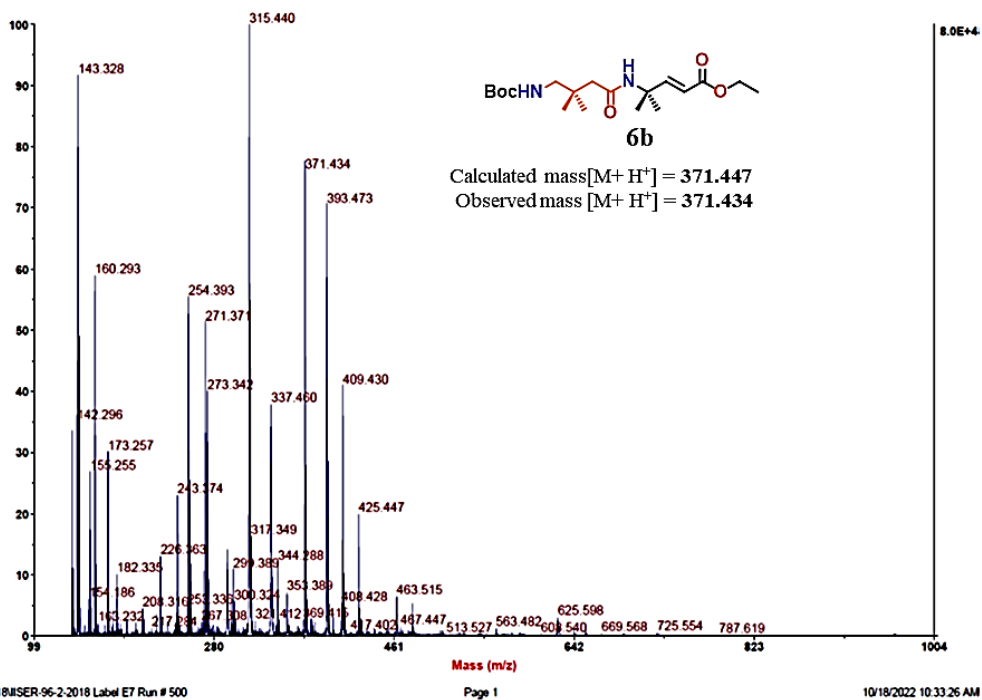
### Spectrum Report

Final - Shots 400 - IISER-96-2-2018; Label E5



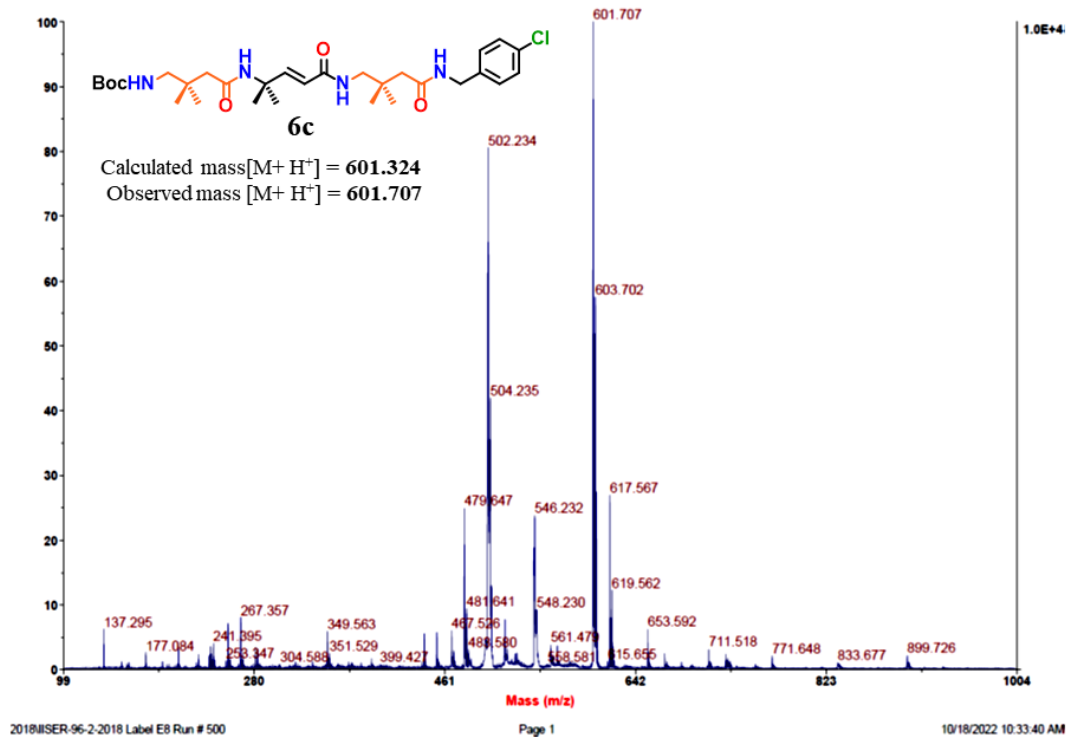
### Spectrum Report

Final - Shots 400 - IISER-96-2-2018; Label E7



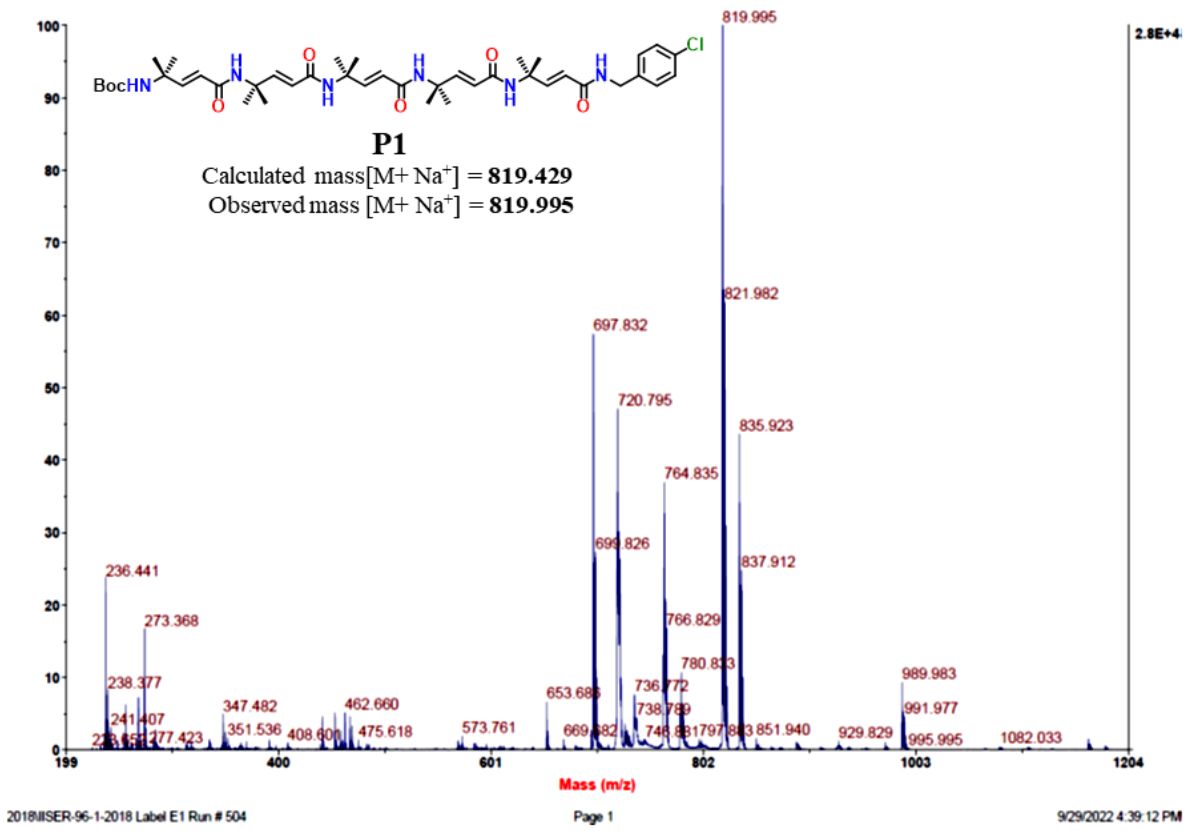
### Spectrum Report

Final - Shots 400 - IISER-96-2-2018; Label E8



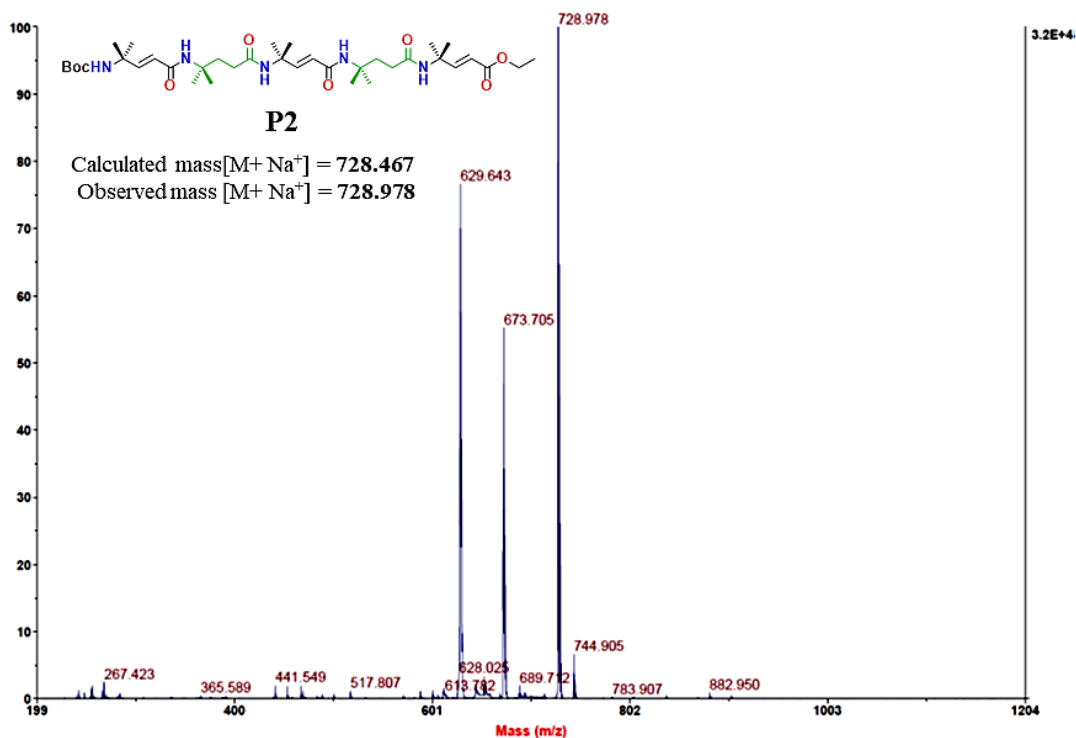
### Spectrum Report

Final - Shots 400 - IISER-96-1-2018; Label E1



### Spectrum Report

Final - Shots 400 - IISER-96-1-2018; Label E3



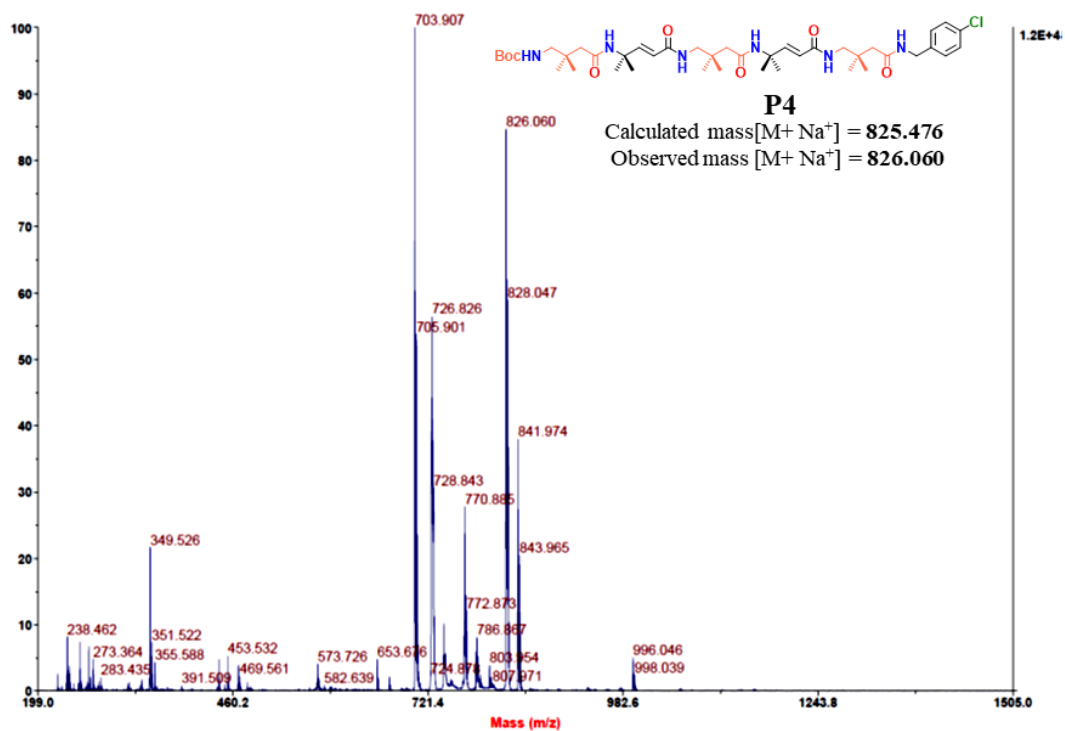
2018IISER-96-1-2018 Label E3 Run # 504

Page 1

9/29/2022 4:39:59 PM

### Spectrum Report

Final - Shots 400 - IISER-96-1-2018; Label E4



2018IISER-96-1-2018 Label E4 Run # 504

Page 1

9/29/2022 4:47:31 PM

## *Chapter 2B*

### *Chirality Induction on Achiral Double Helices*

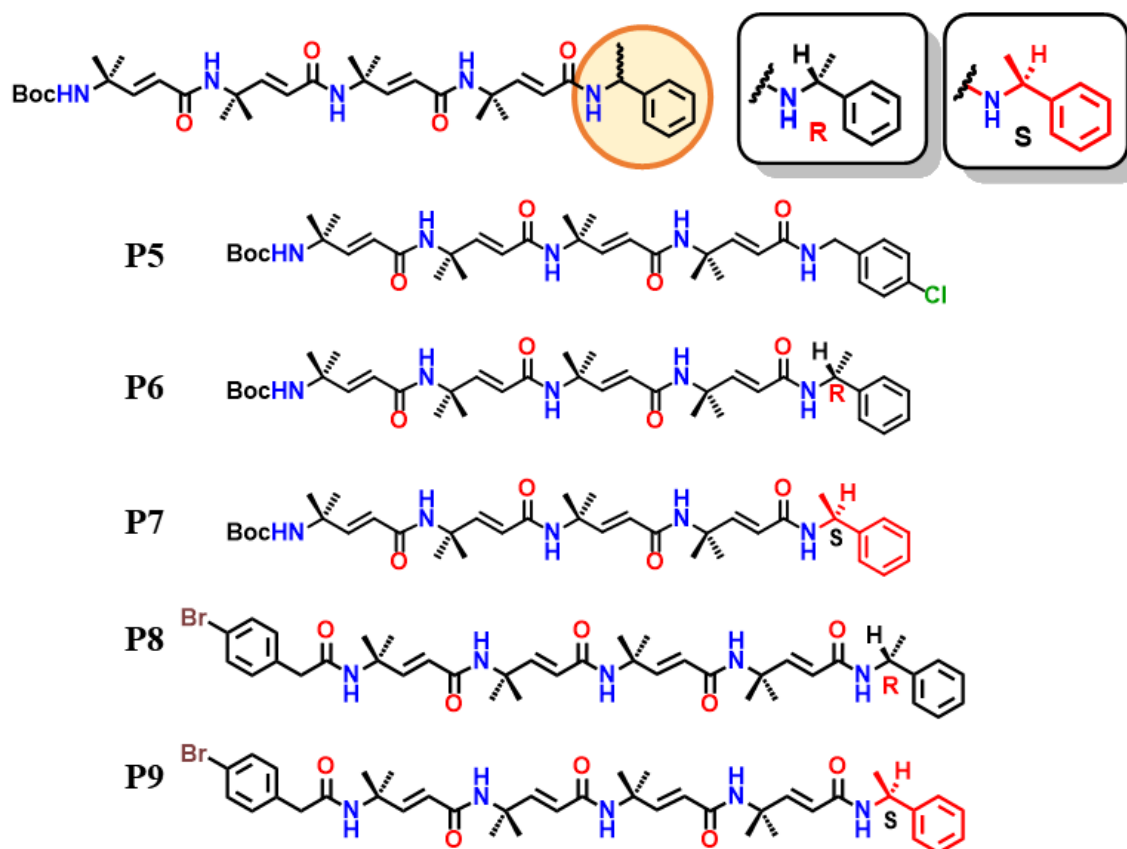
## 1. Introduction:

In previous section 2A, we demonstrated the  $\beta$ -double helix conformations from the  $\gamma$ -peptides consisting of achiral (*E*)- $\alpha,\beta$ -unsaturated 4,4-dialkyl  $\gamma$ -amino acids.<sup>1</sup> In addition, we have shown accommodation of 4,4-dimethyl and 3,3-dimethyl  $\gamma$ -amino acids into the double helical structures without deviating from the overall double helix fold. So far, the double-helical structure reported from the  $\gamma$ -peptide foldamers are achiral in nature.<sup>1,2</sup> For that matter, many synthetic  $\beta$ -double helices are achiral.<sup>3-12</sup> In this context, we sought to investigate the possibilities of designing the chiral  $\beta$ -double helical structures. As the  $\gamma$ -peptide double helices consist of achiral amino acids, we hypothesized that it may be possible to construct chiral double-helices by coupling chiral amines at the C-terminal of the achiral peptides.

## 2. Results and Discussion:

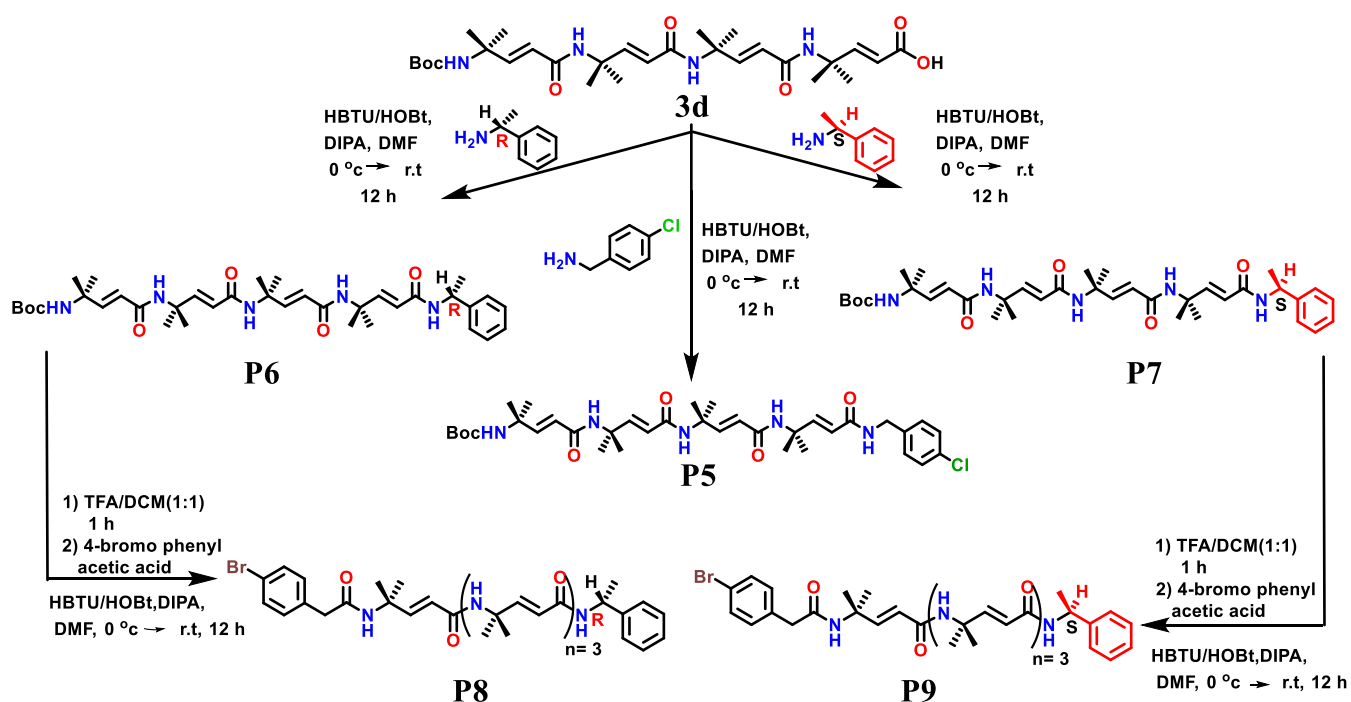
### 2.1 Design and Synthesis of Peptides (P5-P9):

In order to understand the conformational properties of chiral double helices, we designed the tetrapeptides, **P5-P9**. The sequences of these peptides are shown in Scheme 1.



**Scheme 1:** Sequences of design peptides **P5-P9** for chirality induction on the achiral double-helix.

The peptide **P5** is a control achiral peptide. Peptides **P6** and **P7** consist of chiral (*R*) and (*S*) methyl benzylamine at C-terminus, respectively. Peptides **P8** and **P9** consist of the same sequences of **P6** and **P7** respectively except the N-terminal Boc- group was replaced by the *p*-bromo benzoyl group. The (*E*)- $\alpha,\beta$ -unsaturated 4,4-dialkyl  $\gamma$ -amino acid and all peptides were synthesized as reported earlier.<sup>13,14</sup> The schematic representation of the synthesis of the peptides is shown in Scheme 2.



**Scheme 2:** Synthesis of peptides **P5-P9**.

All other peptides were synthesized using the deprotection and coupling methods. All peptides were isolated in good yield and subjected to crystallization for structural analysis.

## 2.2 Crystal Structure Analysis of Peptide **P5**:

In order to understand the unambiguous conformation of peptides, we subjected all peptides to crystallization in various solvent combinations. The single crystals of peptide **P5** were obtained from the slow evaporation of the peptide solution in ethyl acetate/*n*-hexane. The single crystal structure of peptide **P5** is shown in Figure 1. Similar to the tetrapeptides reported earlier<sup>1</sup> and also in the previous section, the peptide **P5** adopted double-helical conformation in single crystals. Being an achiral peptide, the asymmetric unit consists of two molecules with opposite

chirality. In the double helix structure, the two peptide strands are held together by eight intermolecular H-bonds between strand A and strand B. The donor amide CO group in residue  $i$  of strand B is involved in the H-bonding with the amide NH group of residue  $i+2$  in strand A ( $i \rightarrow i+2$ ).

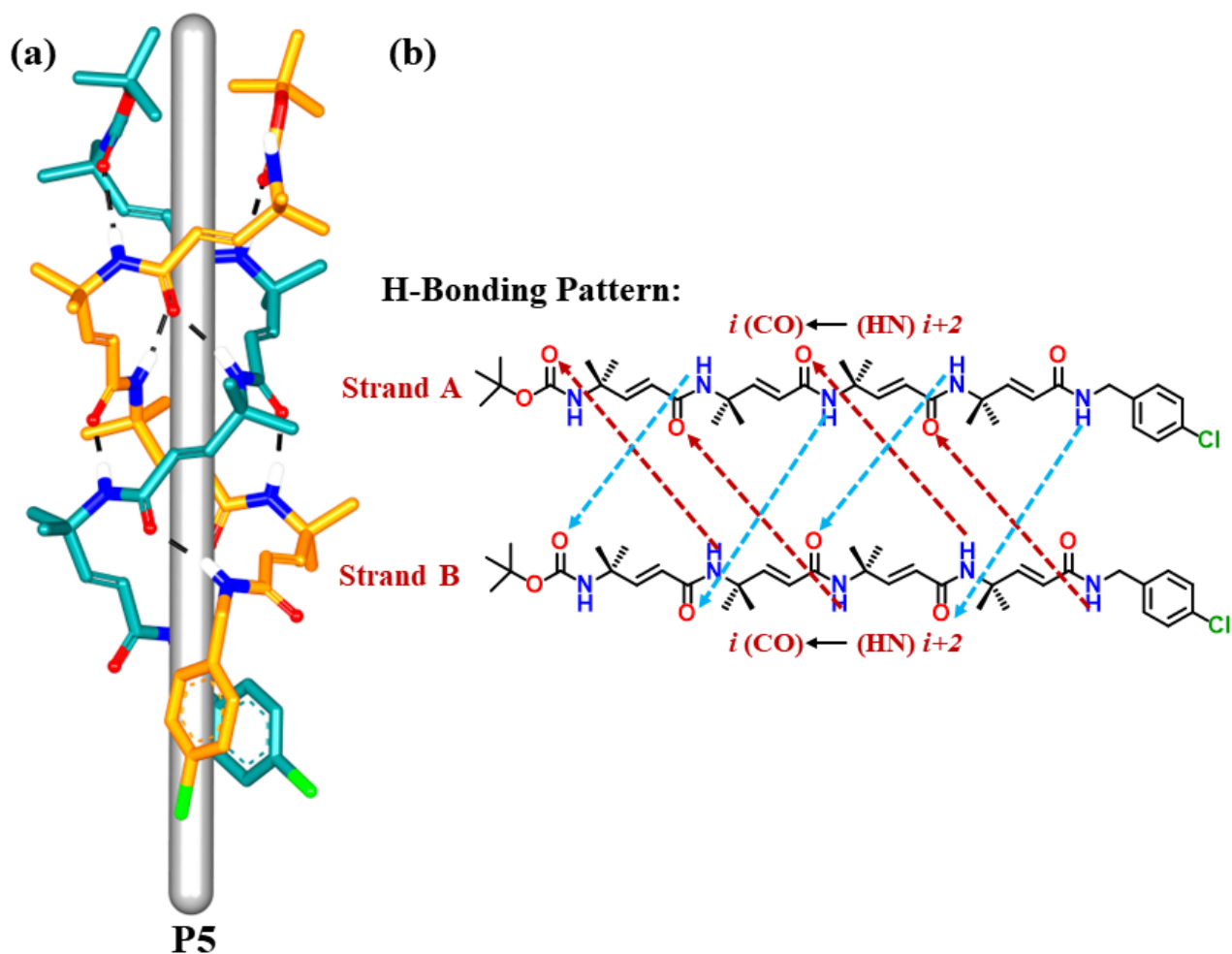


**Figure 1:** (a) Single crystal structure of **P5**. To get a better view of parallel  $\beta$ -double helices, pictorially rods are created along the central axis. (b) Intermolecular hydrogen bonding patterns between two strand A and strand B are shown.

Additionally, the amide CO group of the residue  $i$  in strand A is involved in the H-bonding with the amide NH group of the residue  $i+2$  in strand B. More importantly, no amide NH or CO groups along the strands are exposed for the H-bonds with other strands, except the N-terminal amide NH of strand B and the C-terminal amide CO of strand A. The intermolecular H-bonds between strand A and strand B are depicted in Figure **1b**. The H-bond parameters of the **P5** double-helix are tabulated in Table **1**. The parameters of the observed H-bonds are within the limits of standard H-bonds parameters.<sup>15,16</sup>

**Table 1:** The H-bond parameters of the **P5** double-helix are tabulated.

<b>Donor (D)</b>	<b>Acceptor (A)</b>	<b>D...A (Å)</b>	<b>DH...A (Å)</b>	<b>NH...O (deg)</b>
N2	O8	2.87	2.02	170
N3	O9	2.76	1.92	167
N4	O10	2.83	1.97	174
N5	O11	2.90	2.06	169
N7	O2	2.90	2.06	166
N8	O3	2.90	2.06	168
N9	O4	2.81	2.00	158
N10	O5	2.80	1.96	167

The torsion angles of peptide **P5** are given in Table 2. The observed torsion angle parameters of **P5** are similar to the torsion angles observed in the peptide **P1**. The peptide adopted an achiral  $\beta$ -double-helical conformation in single crystals.

**Table 2:** Torsion angle parameters for strand A and strand B of the **P5** double-helix are tabulated.

<b>Peptide P5 (Strand A)</b>	$\phi$	$\theta_1$	$\theta_2$	$\psi$
<b>d<math>\gamma</math>Aic 1</b>	<b>-72</b>	<b>-18</b>	<b>-167</b>	<b>169</b>
<b>d<math>\gamma</math>Aic 2</b>	<b>-77</b>	<b>-11</b>	<b>-173</b>	<b>171</b>
<b>d<math>\gamma</math>Aic 3</b>	<b>-83</b>	<b>-12</b>	<b>-175</b>	<b>173</b>
<b>d<math>\gamma</math>Aic 4</b>	<b>-60</b>	<b>-27</b>	<b>-175</b>	<b>175</b>



Peptide P5 (Strand B)	$\phi$	$\theta_1$	$\theta_2$	$\psi$
d $\gamma$ Aic 1	-67	-10	-178	174
d $\gamma$ Aic 2	-64	-26	-174	173
d $\gamma$ Aic 3	-65	-40	-169	164
d $\gamma$ Aic 4	-78	1	179	-175

### 2.3 Solution State Conformational Analysis of Peptides P6 and P7:

Even after extensive efforts, both **P6** and **P7** did not give single crystals in various solvent combinations. In order to understand their conformation solution, we subjected both peptides to the solution NMR analysis. The  $^1\text{H}$ -NMR analyses revealed that **P6** and **P7** in  $\text{C}_2\text{D}_2\text{Cl}_4$  gave well-resolved spectra conforming to one set of protons. To investigate the double helix structure in **P6** and **P7** in solution, temperature-dependent  $^1\text{H}$ -NMR and DMSO- $d_6$  NMR titration experiments were carried out.

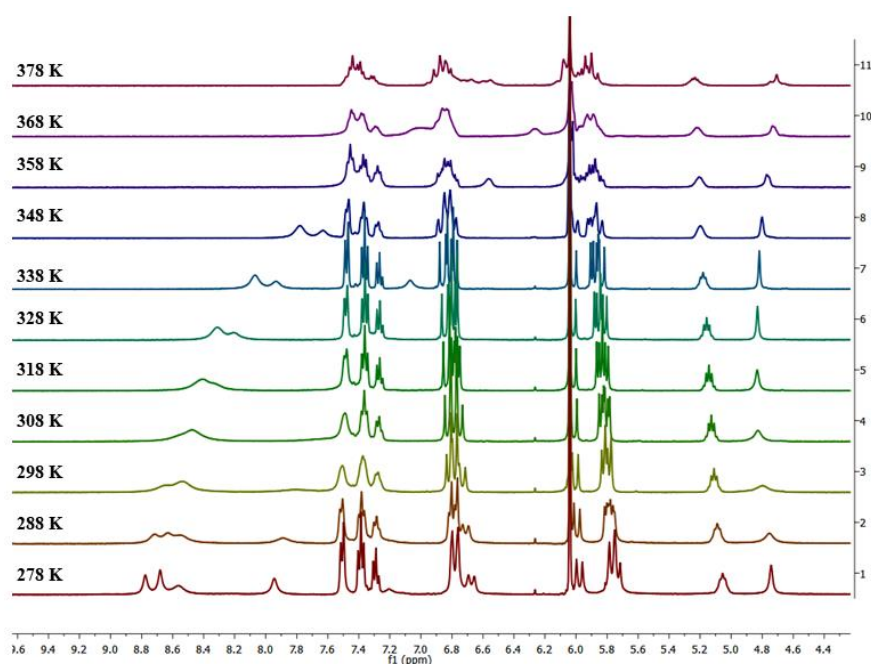


**Figure 2:** Temperature-dependent  $^1\text{H}$ -NMR of **P6** in  $\text{C}_2\text{D}_2\text{Cl}_4$ .

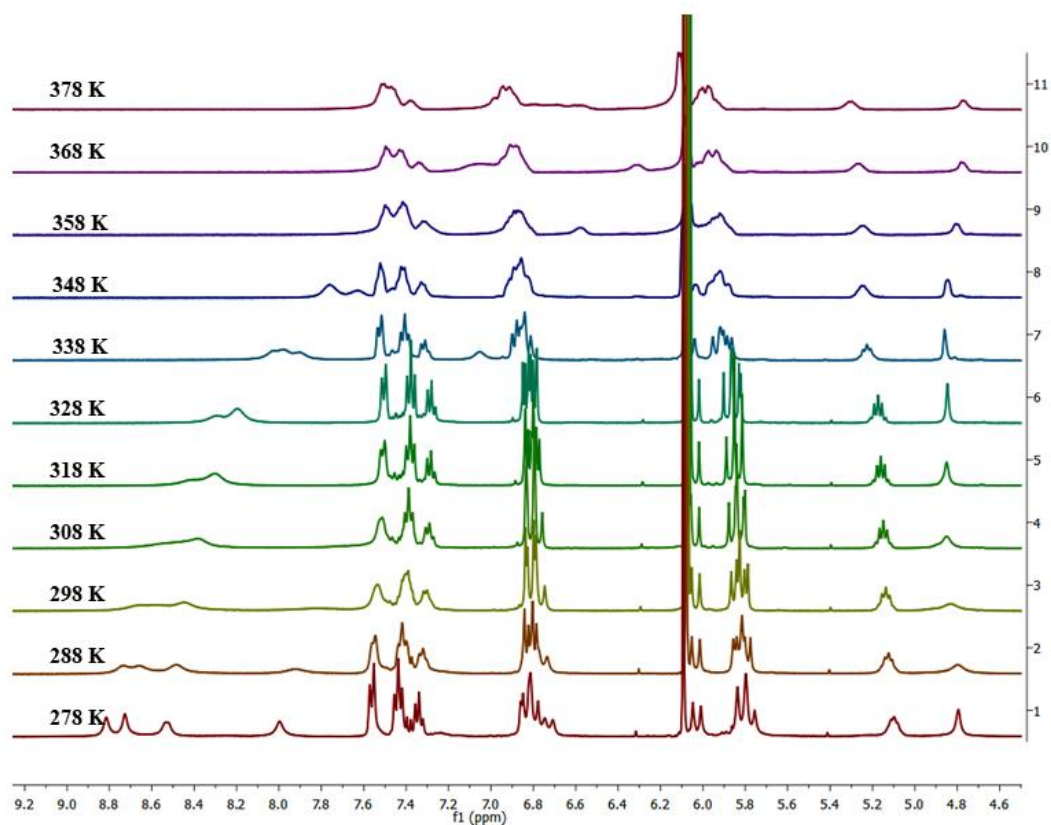


**Figure 3:** Temperature-dependent  $^1\text{H}$ -NMR of **P7** in  $\text{C}_2\text{D}_2\text{Cl}_4$ .

The temperature-dependent  $^1\text{H}$  NMR experiments of **P6** and **P7** in  $\text{C}_2\text{D}_2\text{Cl}_4$  displayed gradual up-field amide NH chemical shifts upon increasing temperature. The amide NH region of  $^1\text{H}$ -NMR spectra depicting the up-field chemical shifts of the peptide **P6** and **P7** are shown in Figures 2 and 3, respectively. Results are suggesting that the possible breaking of H-bonds upon increasing temperature leads to the dissociation of double helix conformation into individual strands in the solution.

Further, the  $\text{DMSO-d}_6$  titration experiments suggested that except the N-terminal Boc amide NH, all other amide NH protons in the peptides **P6** and **P7** showed a very small change in their chemical shift position upon increasing the concentration of  $\text{DMSO-d}_6$ . The results of  $\text{DMSO-d}_6$  titration are shown in Figures 4 and 5, respectively. These results suggested the involvement of backbone amide NH and CO groups in the intermolecular H-bonds between the peptide strands in the double helix. In addition, Boc-NH protons revealed a downfield shift upon increasing the concentration of  $\text{DMSO-d}_6$ , suggesting the exposure of N-terminal NH protons in both **P6** and **P7** to the solvent for H-bonding. These results indirectly suggest that both peptides adopted double helical conformations in solution.

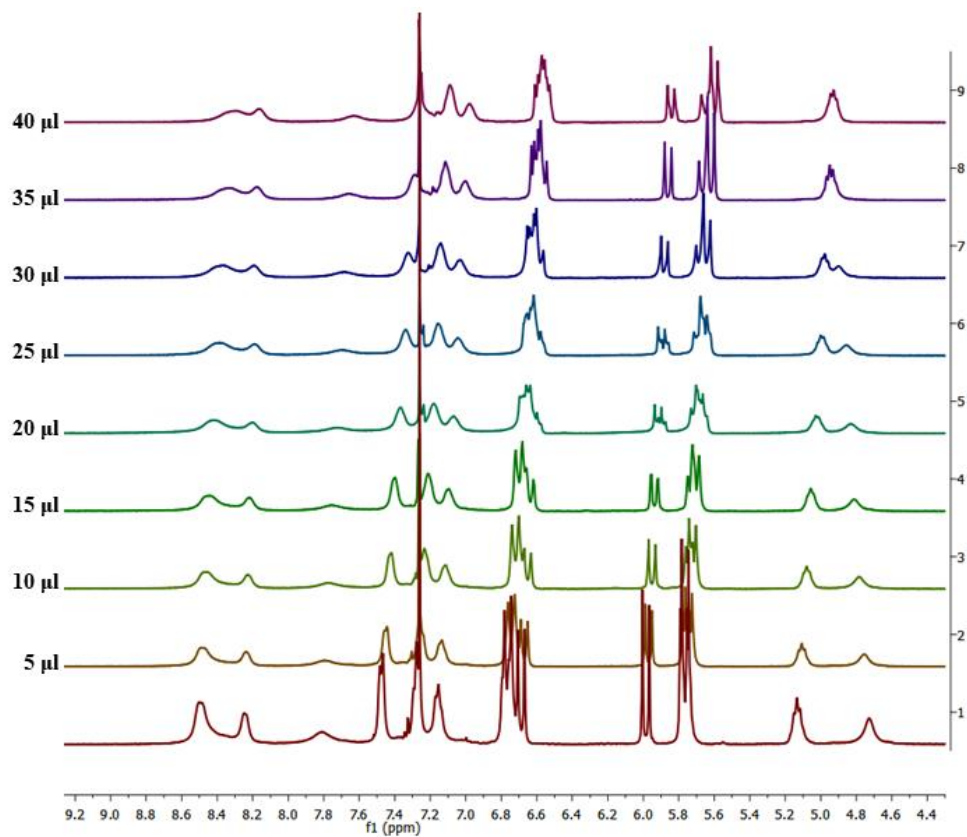


**Figure 4:**  $\text{DMSO-d}_6$   $^1\text{H-NMR}$  titration **P6** in  $\text{CHCl}_3$

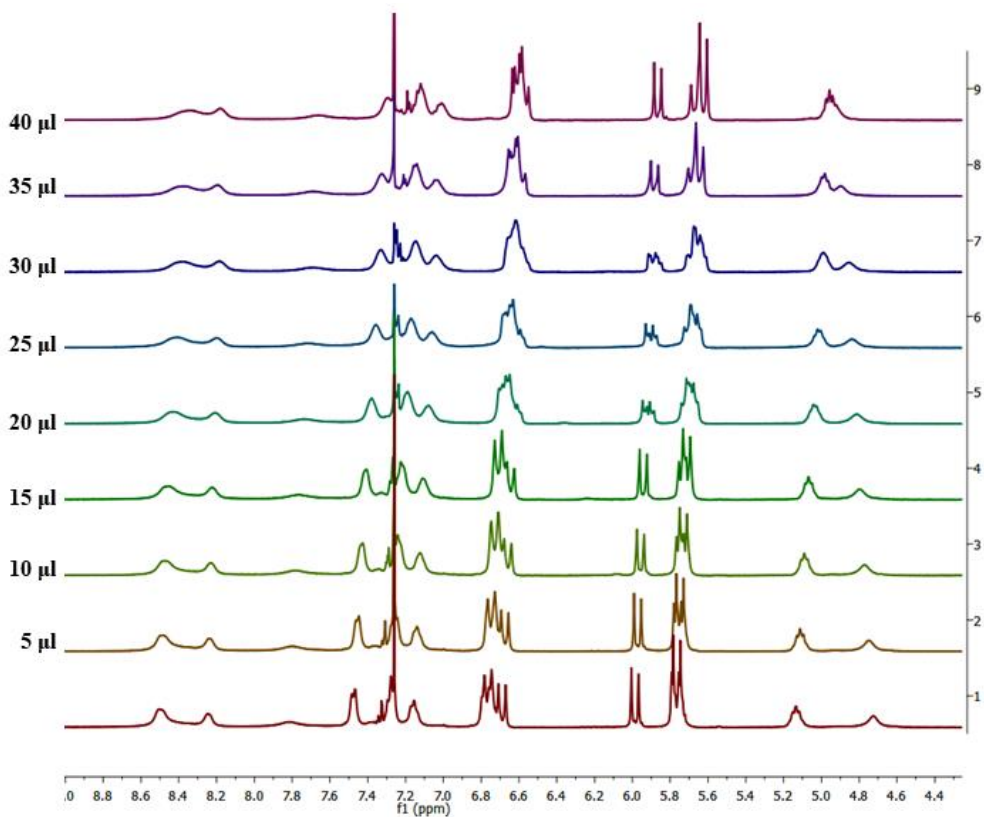


**Figure 5:**  $\text{DMSO-d}_6$   $^1\text{H-NMR}$  titration **P6** in  $\text{CHCl}_3$ .

## 2.4 Circular Dichroism (CD) Spectroscopy of Peptides P6 and P7:

Further, we subjected both peptides **P6** and **P7** along with the achiral peptide **P5** for the circular dichroism (CD) analysis in  $C_2D_2Cl_4$  solvent. The CD spectral analysis revealed remarkable results on the chirality of the peptides. The CD spectra of all three peptides are shown in Figure 6. The peptide **P6** displayed CD maxima at around 245 nm and **P7** displayed exactly the opposite spectrum with CD minima at 245 nm. The achiral **P5** displayed no characteristic CD signature.

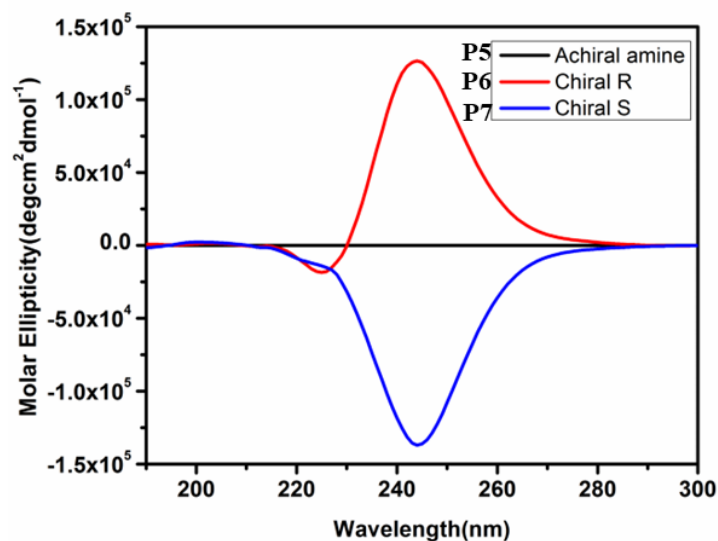


**Figure 6:** Circular dichroism (CD) spectra of peptides **P5-P7** showing the effect of chirality induction on the achiral double-helix.

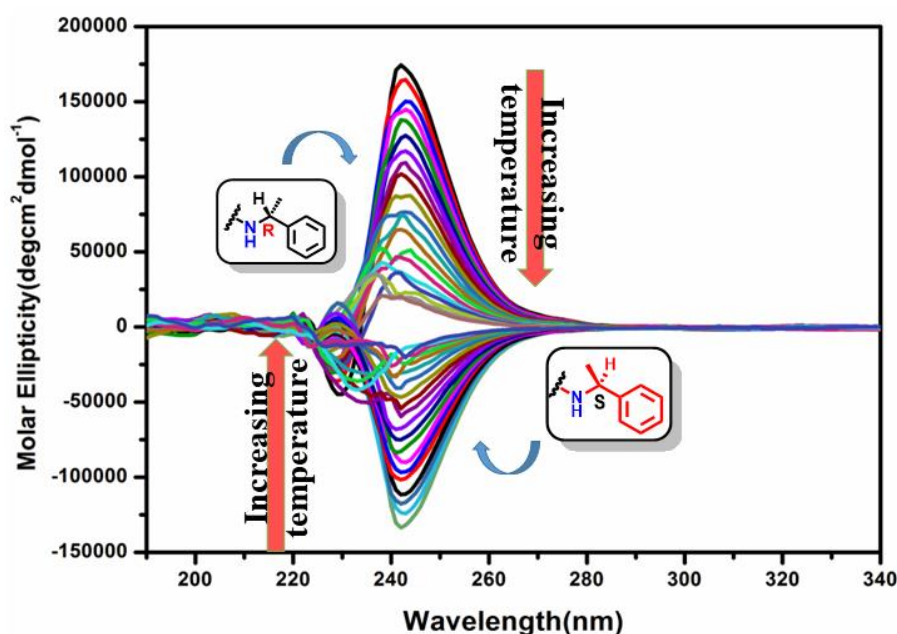


**Figure 7:** Temperature-dependent circular dichroism (CD) spectra of peptides **P6** and **P7**.

We further subjected both **P6** and **P7** to the temperature-dependent CD analysis. The CD maxima in **P6** decrease upon increasing temperature. Similarly, the CD minima observed in **P7** decrease with increasing temperature. These results infer that even at the higher temperature, they partly retain the double-helical conformation. These results are depicted in Figure 7. Fascinatingly, the single chiral atom can induce chirality across the double helix. These results suggested the chiral double helices can be designed by just introducing one chiral atom at the C-terminus of the achiral peptides.

### 2.5. Crystal Structure Analysis of Chiral Double helix of Peptide **P8**:

As we did not get the single crystals for the chiral peptides **P6** and **P7**, we further designed two more peptides **P8** and **P9** with an *N*-terminal *p*-Br phenylacetyl group. Both peptides were synthesized and subjected to crystallization to understand the conformations of chiral  $\beta$ -double helices in single crystals. Out of these two peptides, peptide **P8** gave single crystals after the slow evaporation of the peptide solution in the  $\text{CHCl}_3$  and toluene solvent mixture. The X-ray diffracted single crystal structure of peptide **P8** is shown in Figure 8. Remarkably, the hybrid pentapeptide **P8** adopted a right-handed double helix conformation in single crystals.

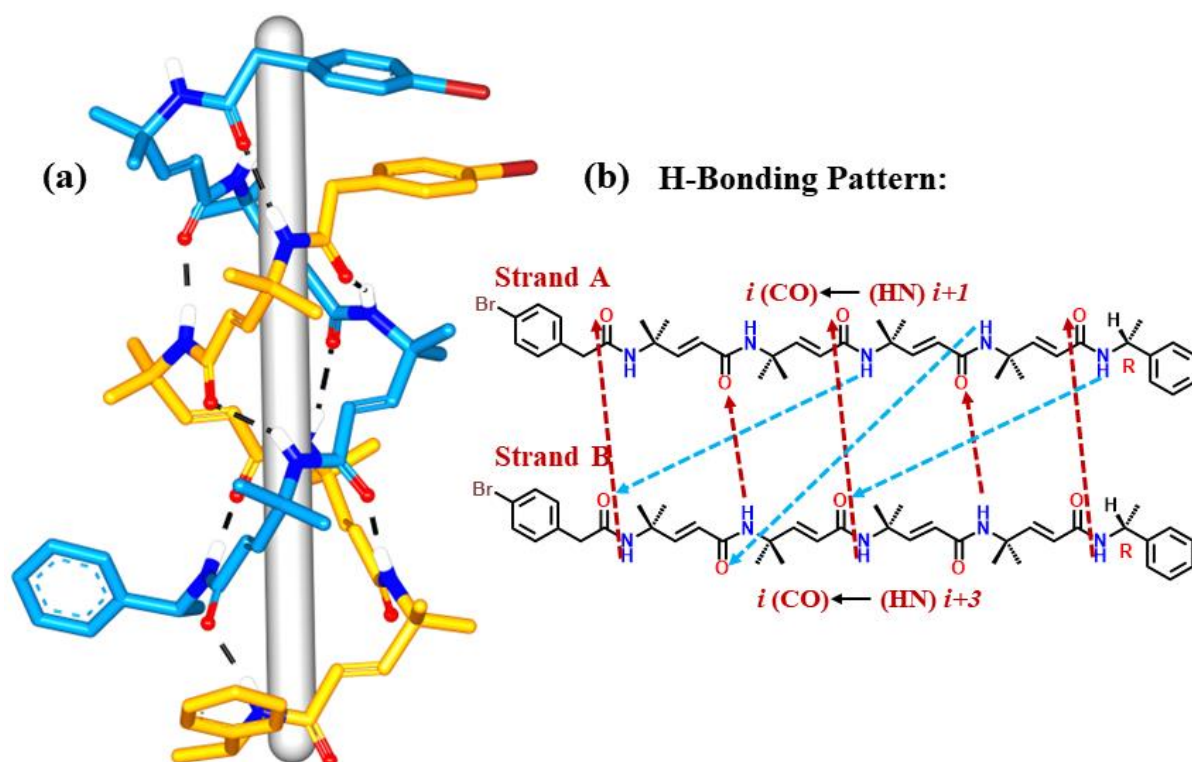


**Figure 8:** (a) Single crystal structure of **P5**. To get a better view of parallel  $\beta$ -double-helices, pictorially rods are created along the central axis. (b) Intermolecular hydrogen bonding patterns between two strand A and strand B are shown.

The H-bonding pattern observed in the **P8** is different from that of other double-helices. The peptide strands A and B are intertwined along the helix axis and they are held together by eight inter-strand H-bonds. The donor amide CO group in residue  $i$  of strand A is involved in the H-bonding with the amide NH group of residue  $i+1$  in strand B ( $i \rightarrow i+1$ ). Interestingly, the amide CO group of residue  $i$  in strand B is involved in the H-bonding with the amide NH group of residue  $i+3$  in strand A ( $i \rightarrow i+3$ ). The two N-terminal NH groups in strand A and the two C-terminal amide CO groups in strand B are not involved in the inter-strand H-bonds. The inter-strand H-bonds observed in the **P8** are shown in Figure **8b**. The H-bond parameters of the **P8** double helix are tabulated in Table 3. The parameters of the observed H-bonds are within the limits of standard H-bonds parameters.<sup>15,16</sup>

**Table 3:** The H-bond parameters of the **P8** double-helix are tabulated.

<b>Donor (D)</b>	<b>Acceptor (A)</b>	<b>D....A (Å)</b>	<b>DH....A (Å)</b>	<b>NH....O (deg)</b>
<b>N6</b>	<b>O1</b>	<b>2.89</b>	<b>2.04</b>	<b>171</b>
<b>N7</b>	<b>O2</b>	<b>2.83</b>	<b>1.98</b>	<b>168</b>
<b>N8</b>	<b>O3</b>	<b>2.90</b>	<b>2.06</b>	<b>164</b>
<b>N9</b>	<b>O4</b>	<b>2.85</b>	<b>2.00</b>	<b>172</b>
<b>N10</b>	<b>O5</b>	<b>2.76</b>	<b>1.93</b>	<b>159</b>
<b>N3</b>	<b>O6</b>	<b>2.83</b>	<b>2.07</b>	<b>148</b>
<b>N4</b>	<b>O7</b>	<b>2.83</b>	<b>2.07</b>	<b>147</b>
<b>N5</b>	<b>O8</b>	<b>2.76</b>	<b>1.93</b>	<b>164</b>

The crystal structure analysis of **P8** revealed an interesting pattern of torsion angle parameters. The dgAic residues displayed similar torsion angle parameters as that of the residues observed in the structure of **P5**. The average torsion angle parameters of the dgAic residues in the double helix **P8** are  $\phi = -70^\circ \pm 8^\circ$ ,  $\theta_1 = -21^\circ \pm 14^\circ$ ,  $\theta_2 = -169^\circ \pm 9^\circ$ , and  $\psi = +169^\circ \pm 10^\circ$ . The torsion angles of the peptide **P8** are given in Table 4.

**Table 4:** Torsion angle parameters for strand A and strand B of the **P8** double helix are tabulated.

Peptide P8 ( Strand A)	$\phi$	$\theta_1$	$\theta_2$	$\psi$	Peptide P8 ( Strand B)	$\phi$	$\theta_1$	$\theta_2$	$\psi$
d $\gamma$ Aib 1	-65	-25	-168	177	d $\gamma$ Aib 1	-63	-21	-176	170
d $\gamma$ Aib 2	-71	-17	-169	160	d $\gamma$ Aib 2	-62	-35	-168	167
d $\gamma$ Aib 3	-79	-15	-173	170	d $\gamma$ Aib 3	-71	-22	-171	175
d $\gamma$ Aib 4	-78	-7	-174	178	d $\gamma$ Aib 4	-65	-28	-162	157

### 2.6. Circular Dichroism (CD) Spectroscopy of Peptides P8 and P9:

Further, we subjected both peptides **P8** and **P9** to the circular dichroism (CD) analysis in  $C_2D_2Cl_4$  solvent. The CD spectral analysis revealed remarkable results on the chirality of the peptides. The CD spectra of peptides **P8** and **P9** are shown in Figure 9. The peptide **P8** displayed CD maxima at around 245 nm and **P9** displayed exactly the opposite spectrum with CD minima at 245 nm similar to that of peptides **P6** and **P7**. These results suggested chiral double-helices can be designed by introducing on chiral atom at the C-terminus of the achiral peptide.

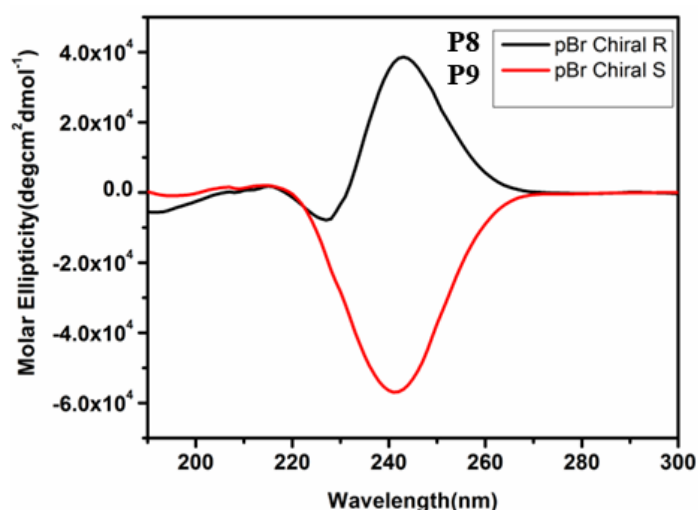


**Figure 9:** Circular dichroism (CD) spectra of peptides **P8-P9** showing the effect of chirality induction on the achiral double-helix.

### 3. Conclusion:

In summary, the short  $\gamma$ -peptides constructed from the achiral (*E*)-  $\alpha,\beta$ -unsaturated 4,4-gem-dimethyl  $\gamma$ -amino acids containing chiral amine at the C-terminus fold into chiral  $\beta$ -double

helix structures. The chiral peptides consisting of *R* and *S* chiral amines displayed opposite CD signatures. So far, the synthetic double helices reported in the literature are mostly achiral in nature, however, these achiral amino acids can be converted into chiral double helices by coupling chiral amines at the C-terminus of the peptides. The results reported here suggest that a single chiral atom can induce chirality across the double helix. These results advocated that the chiral double-helices can be designed by just introducing one chiral atom at the C-terminus of the achiral peptides.

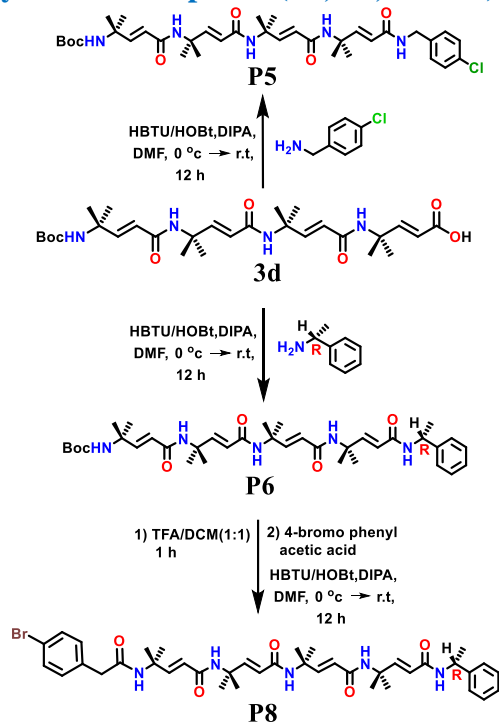
## 4. Experimental Section:

### 4.1. General Method:

All reagents were used without further purification. Column chromatography was performed on neutral alumina (100-200 mesh). <sup>1</sup>H-NMR (400 MHz), and <sup>13</sup>C-NMR (101 MHz) were measured on a Bruker Avance 400 MHz spectrometer. Mass samples were analyzed by High-resolution mass spectrometry using ESI TOF. The X-ray data were collected at 100K temperature on a Bruker APEX(III) DUO CCD diffractometer using Mo K<sub>α</sub> radiation ( $\lambda = 0.71073 \text{ \AA}$ ).

### 4.2. Procedure for the Synthesis of Peptides:

#### 4.2.1. Procedure for the Synthesis of Peptides (P5, P6, and P8):



**Scheme 3:** Synthesis of peptides **P5**, **P6**, and **P8**.

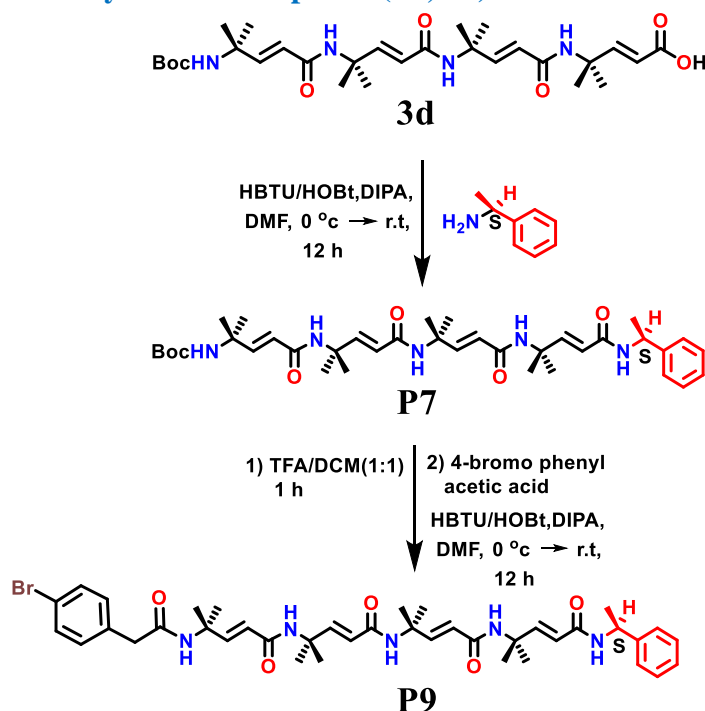


The compound 3d was synthesized following previous chapter 2A and which was reported in our previous method.<sup>22a</sup> The tetrapeptide acid 3d (1.4 g, 2.5 mmol) was dissolved in 5 mL of DMF and was cooled down to 0 °C under an N<sub>2</sub> atmosphere. To this HBTU (1.0 g, 2.5 mmol) and HOBt (0.34 g, 2.5 mmol) were added and the reaction mixture was stirred for 10 minutes. This was followed by the addition of 4-chloro benzylamine (0.45 ml, 3.75 mmol). The reaction mixture was stirred overnight and the progress was monitored by TLC. Upon completion, the reaction mixture was diluted with 125 mL EtOAc and was washed with 10% HCl (75 mL X 2), 10% Na<sub>2</sub>CO<sub>3</sub> solution (75 mL X 2), and finally brine solution (75mL X 2). The organic layer was dried over anhydrous Na<sub>2</sub>SO<sub>4</sub> and concentrated under reduced pressure to give a crude powder which was then purified by column chromatography to get a white crystalline product **P5** (yield = 82%). Similarly, the tetrapeptide acid 3d (1.4 g, 2.5 mmol) was dissolved in 5 mL of DMF and was cooled down to 0 °C under an N<sub>2</sub> atmosphere. To this HBTU (1.0 g, 2.5 mmol) and HOBt (0.34 g, 2.5 mmol) were added and the reaction mixture was stirred for 10 minutes. This was followed by the addition of (R)-1-phenylethan-1-amine (0.48 ml, 3.75 mmol). The reaction mixture was stirred overnight and the progress was monitored by TLC. Upon completion, the reaction mixture was diluted with 125 mL EtOAc and was washed with 10% HCl (75 mL X 2), 10% Na<sub>2</sub>CO<sub>3</sub> solution (75 mL X 2), and finally brine solution (75mL X 2). The organic layer was dried over anhydrous Na<sub>2</sub>SO<sub>4</sub> and concentrated under reduced pressure to give a crude powder which was then purified by column chromatography to get a white crystalline product **P6** (yield = 78%).

Boc-deprotection of peptide P6 (0.3 mmol 0.2 g) was carried out by using 1 ml of each TFA and DCM (1:1) for 1 h. After that, TFA and solvent DCM were evaporated and 5-6 times DCM was added and evaporated to remove traces of TFA. The formed crude was TFA-salt of the amine of peptide P6 and to this 0.5 ml of DMF and 0.5 ml, of DIPEA were added to make it free amine of compound P6. The 4-bromophenylacetic acid (0.39 mmol, 0.083 g) was dissolved in 1 mL of DMF and was cooled down to 0 °C under an N<sub>2</sub> atmosphere. To this HBTU (0.39 mmol, 0.15 g) and HOBt (0.39 mmol, 0.053 g) were added and the reaction mixture was stirred for 10 minutes. This was followed by the addition of free amine of tetrapeptide P6. The reaction mixture was stirred overnight and the progress was monitored by TLC. Upon completion, the reaction mixture was diluted with 50 mL EtOAc and was washed with 10% HCl (50 mL X 2), 10% Na<sub>2</sub>CO<sub>3</sub> solution (50 mL X 2) and finally brine solution (50 mL X 2). The organic layer was dried over anhydrous Na<sub>2</sub>SO<sub>4</sub> and concentrated under reduced pressure to give a crude

powder which was then purified by column chromatography to get a white crystalline product **P8** (yield = 65%).

#### 4.2.2. Procedure for the Synthesis of Peptides (**P7**, **P9**):



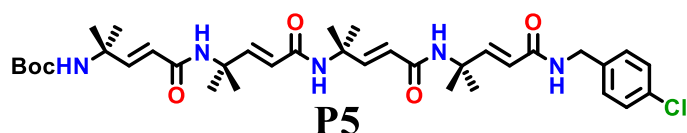
**Scheme 4:** Synthesis of peptides **P7**, **P9**.

The tetrapeptide acid **3d** (1.4 g, 2.5 mmol) was dissolved in 5 mL of DMF and was cooled down to  $0\text{ }^\circ\text{C}$  under an  $\text{N}_2$  atmosphere. To this HBTU (1.0 g, 2.5 mmol) and HOBt (0.34 g, 2.5 mmol) were added and the reaction mixture was stirred for 10 minutes. This was followed by the addition of (S)-1-phenylethylamine (0.48 mL, 3.75 mmol). The reaction mixture was stirred overnight and the progress was monitored by TLC. Upon completion, the reaction mixture was diluted with 125 mL EtOAc and was washed with 10% HCl (75 mL X 2), 10%  $\text{Na}_2\text{CO}_3$  solution (75 mL X 2), and finally brine solution (75 mL X 2). The organic layer was dried over anhydrous  $\text{Na}_2\text{SO}_4$  and concentrated under reduced pressure to give a crude powder which was then purified by column chromatography to get a white crystalline product **P7** (yield = 75%).

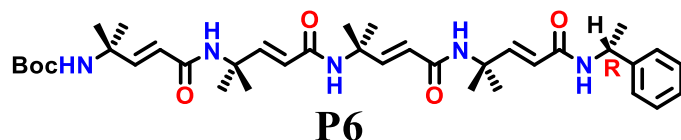
Boc-deprotection of peptide **P7** (0.3 mmol, 0.2 g) was carried out by using 1 mL of each TFA and DCM (1:1) for 1 h. After that, TFA and solvent DCM were evaporated and 5-6 times DCM was added and evaporated to remove traces of TFA. The formed crude was TFA-salt of the amine of peptide **P7** and to this 0.5 mL of DMF and 0.5 mL of DIPEA were added to make it free amine of peptide **P7**. The 4-bromophenyl acetic acid (0.39 mmol, 0.083 g) was dissolved

in 1 mL of DMF and was cooled down to 0 °C under an N<sub>2</sub> atmosphere. To this HBTU (0.39 mmol, 0.15 g) and HOBt (0.39 mmol, 0.053 g) were added and the reaction mixture was stirred for 10 minutes. This was followed by the addition of free amine of tetrapeptide P7. The reaction mixture was stirred overnight and the progress was monitored by TLC. Upon completion, the reaction mixture was diluted with 50 mL EtOAc and was washed with 10% HCl (50 mL X 2), 10% Na<sub>2</sub>CO<sub>3</sub> solution (50 mL X 2) and finally brine solution (50 mL X 2). The organic layer was dried over anhydrous Na<sub>2</sub>SO<sub>4</sub> and concentrated under reduced pressure to give a crude powder which was then purified by column chromatography to get a white crystalline product **P9** (yield = 61%).

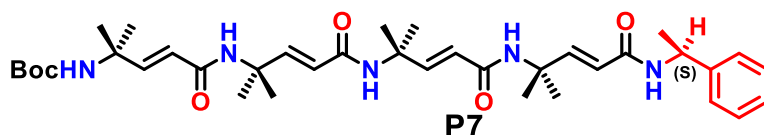
### 4.3. Characterization of Peptides(P5-P7):



<sup>1</sup>H NMR (400 MHz, CDCl<sub>3</sub>) δ 8.43 (s, 1H), 8.29 (dd, *J* = 12.7, 6.9 Hz, 1H), 7.30 – 7.28 (m, 2H), 7.24 (d, *J* = 7.9 Hz, 2H), 7.21 – 7.19 (m, 3H), 6.75 – 6.64 (m, 3H), 5.97 (d, *J* = 15.2 Hz, 1H), 5.93 (s, 1H), 5.78 – 5.71 (m, 1H), 5.68 (d, *J* = 15.6 Hz, 1H), 4.44 (d, *J* = 6.1 Hz, 1H), 4.38 (d, *J* = 5.9 Hz, 3H), 1.76 (s, 4H), 1.57 (s, 4H), 1.49 (s, 10H), 1.31 (d, *J* = 26.9 Hz, 14H).



<sup>1</sup>H NMR (400 MHz, CDCl<sub>3</sub>) δ 8.49 (s, 2H), 8.24 (s, 1H), 7.81 (s, 1H), 7.48 (d, *J* = 7.5 Hz, 2H), 7.29 (d, *J* = 8.2 Hz, 2H), 7.16 (d, *J* = 7.1 Hz, 2H), 6.78 – 6.66 (m, 4H), 5.99 (d, *J* = 15.2 Hz, 1H), 5.78 (t, *J* = 3.6 Hz, 2H), 5.75 (t, *J* = 3.6 Hz, 2H), 5.13 (d, *J* = 8.1 Hz, 1H), 4.73 (s, 1H), 1.68 (s, 4H), 1.61 (s, 4H), 1.52 (s, 3H), 1.51 (s, 9H), 1.41 – 1.33 (m, 11H), 1.28 (s, 4H)



<sup>1</sup>H NMR (400 MHz, CDCl<sub>3</sub>) δ 8.50 (s, 2H), 8.24 (s, 1H), 7.81 (s, 1H), 7.48 (d, *J* = 7.5 Hz, 2H), 7.33 – 7.27 (m, 2H), 7.20 – 7.11 (m, 2H), 6.79 – 6.67 (m, 5H), 5.99 (d, *J* = 15.2 Hz, 1H), 5.78 (t, *J* = 3.4 Hz, 2H), 5.75 (q, *J* = 3.2, 2.7 Hz, 2H), 5.13 (dd, *J* = 10.7, 4.4 Hz, 1H), 4.73 (s, 1H),

1.66 (s, 4H), 1.61 (s, 4H), 1.52 (s, 3H), 1.50 (d,  $J = 1.1$  Hz, 9H), 1.48 (s, 2H), 1.42 – 1.32 (m, 13H), 1.28 (s, 4H).

## 5. Appendix:

### 5.1 ORTEP Diagrams:

#### A) ORTEP Diagram of Peptide(P5):

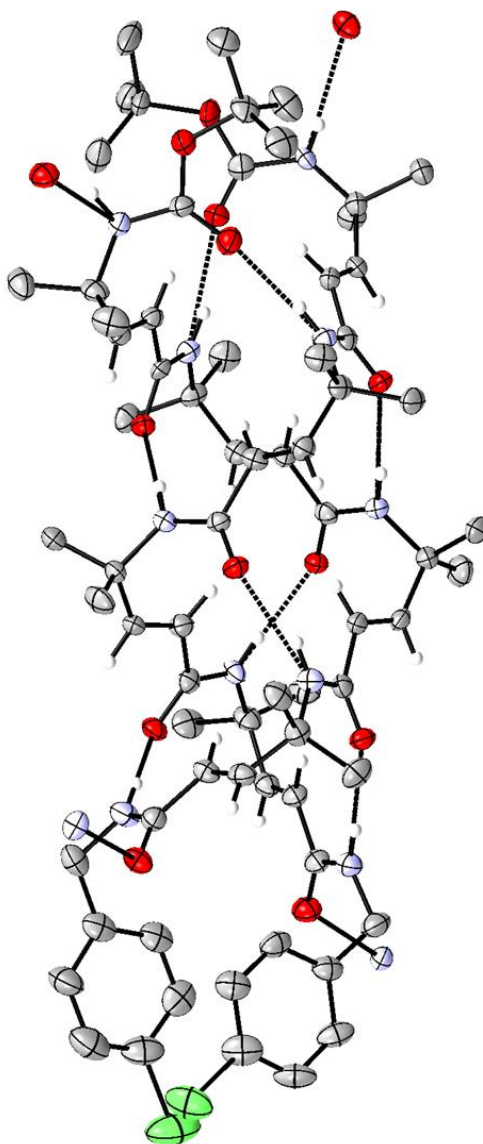


**Figure 10:** ORTEP diagram of **P5**. H-bonds are shown in dotted lines. H-atoms are omitted for clarity. Ellipsoids are drawn at 50% probability.

**B) ORTEP Diagram of Peptide(P8):**

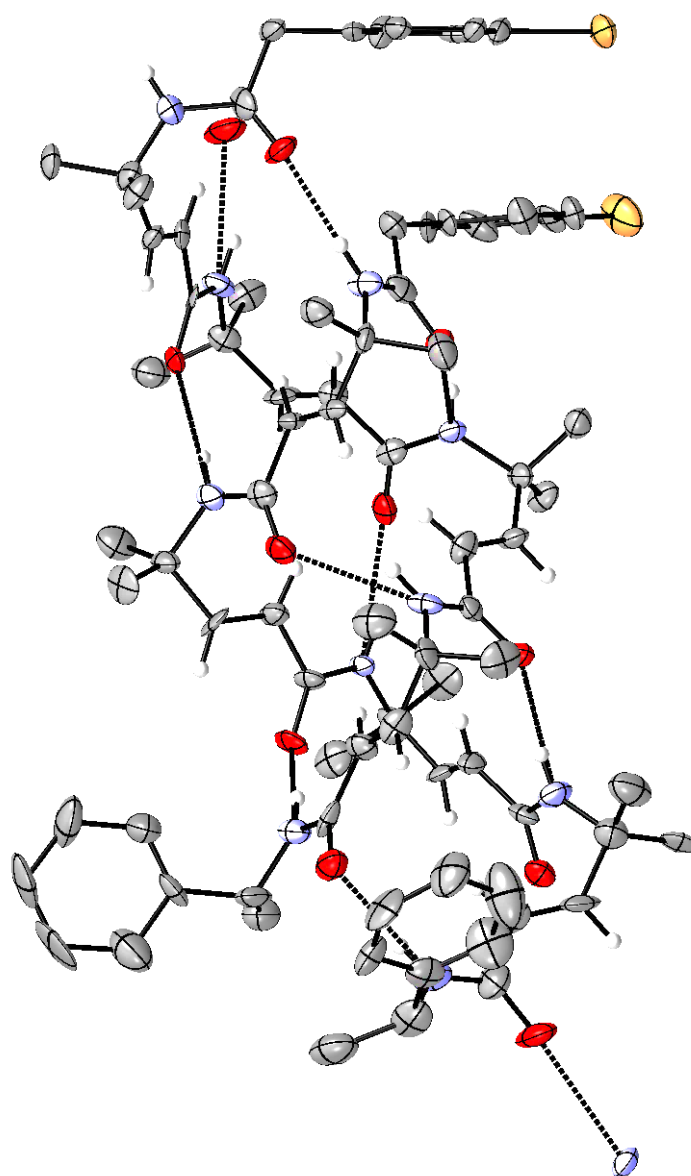


**Figure 11:** ORTEP diagram of **P8**. H-bonds are shown in dotted lines. H-atoms are omitted for clarity. Ellipsoids are drawn at 50% probability.

## 5.2. Crystal Structures Information:

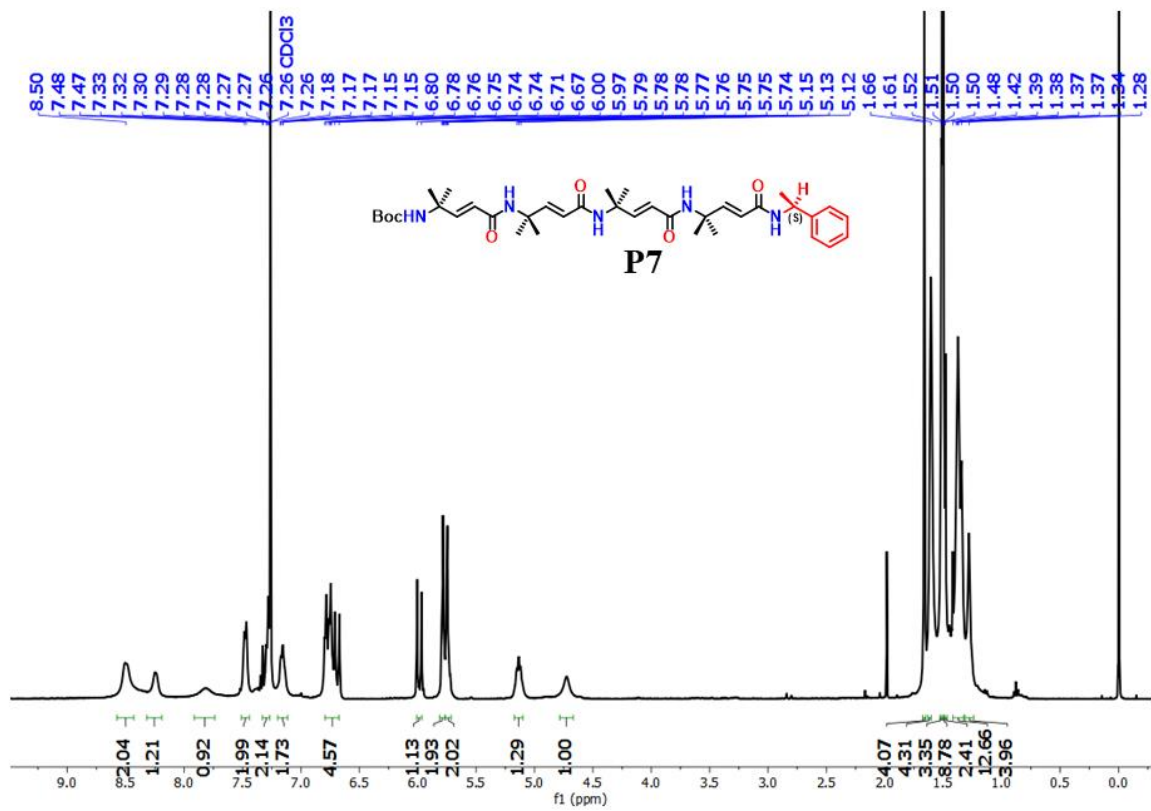
Parameters	Peptide(P1)	Peptide(P3)
Solvent for crystallization	EtOAc/n-hexane	CHCl <sub>3</sub> / Toluene
Chemical formula	C <sub>74</sub> H <sub>110</sub> Cl <sub>2</sub> N <sub>11</sub> O <sub>12</sub>	C <sub>87</sub> H <sub>112</sub> Br <sub>2</sub> N <sub>10</sub> O <sub>10</sub>
Molecular weight	1416.63	1617.67
Crystal size (nm)	(0.18 × 0.12 × 0.18) nm	(0.12 × 0.10 × 0.10) nm
Radiation source	Mo K $\alpha$ ( $\lambda = 0.71073 \text{ \AA}$ )	Mo K $\alpha$ ( $\lambda = 0.71073 \text{ \AA}$ )
Space group	P2 <sub>1</sub> 2 <sub>1</sub> 2 <sub>1</sub> (orthorhombic)	P2 <sub>1</sub> 2 <sub>1</sub> 2 <sub>1</sub> (orthorhombic)
a (Å)	17.57(3)	12.772(2)
b (Å)	18.14(3)	19.045(4)
c (Å)	27.91(5)	36.205(7)
$\alpha$ (°)	90	90
$\beta$ (°)	90	90
$\gamma$ (°)	90	90
Volume (Å <sup>3</sup> )	8896(26)	8807(3)
Z	4	4
h <sub>max</sub>	23	17
k <sub>max</sub>	24	23
l <sub>max</sub>	37	46
Density (g/cm <sup>3</sup> )(cal)	1.058	1.220
Molecules in the asymmetric unit	1	1
F (000)	3044.0	3146.0
2 $\theta$ Max. (°)	56.678	56.78
$\mu$ mm <sup>-1</sup>	0.130	0.981
Reflections (cal)	21982	21733
Variables	917	1002
R (reflections)	11155	10012
R <sub>factor</sub>	0.1069	0.1687
wR2 (Reflections)	0.3328	0.3144
Goodness-of- fit (S)	1.013	1.153
Software used	Bruker APEX(III)	Bruker APEX(III)
Method used	SHELXS-97 <sup>31</sup>	SHELXS-97 <sup>31</sup>

## 6. References:

1. Misra, R.; Dey, S.; Reja, R. M.; Gopi, H. N. *Angew. Chem. Int. Ed.* **2018**, *57*, 1057.
2. Veeresh, K.; Singh, M.; Gopi, H. N. *Org. Biomol. Chem.* **2019**, *17*, 9226.
3. Benedetti, E.; Di Blasio, B.; Pedone, C.; Lorenzi, G. P.; Tomasic, L.; Gramlich, V. *Nature*, **1979**, 282, 630.
4. Di Blasio, B.; Benedetti, E.; Pavone, V.; Pedone, C.; Gerber, C.; Lorenzi, G. P. *Biopolymers* **1989**, *28*, 203.
5. Kulp, J. L.; Clark, T. D. *Chem. Eur. J.* **2009**, *15*, 11867.
6. Navarro, E.; Fenude, E.; Celda, B. *Biopolymers* **2004**, *73*, 229.
7. Schramm, P.; Hofmann, H. -J. *J. Pept. Sci.* **2010**, *16*, 276.
8. Jadhav, K. B.; Lichtenecker, R. J.; Bullach, A.; Mandal, B.; Arndt, H. -D. *Chem. Eur. J.* **2015**, *21*, 5898.
9. Berl, V.; Huc, I.; Khoury, R. G.; Krische, M. J.; Lehn, J. -M. *Nature* **2000**, *407*, 720.
10. Gan, Q.; Wang, X.; Kauffmann, B.; Rosu, F.; Ferrand, Y.; Huc, I. *Nature Nanotech.* **2017**, *12*, 447.
11. Wang, X.; Wicher, B.; Ferrand, Y.; Huc, I. *J. Am. Chem. Soc.* **2017**, *139*, 9350.
12. Yashima, E.; Ousaka, N.; Taura, D.; Shimomura, K.; Ikai, T.; Maeda, K. *Chem. Rev.* **2016**, *116*, 13752.
13. Jadhav, S. V.; Gopi, H. N. *Chem. Commun.*, **2013**, *49*, 9179.
14. Mali, S. M.; Bandyopadhyay, A.; Jadhav, S. V.; Ganesh Kumar, M.; Gopi, H. N. *Org. Biomol. Chem.* **2011**, *9*, 6566.
15. Desiraju, G. R. *Angew. Chem., Int. Ed.* **2007**, *46*, 8342.
16. Gu, Y.; Kar, T.; Scheiner, S. *J. Am. Chem. Soc.* **1999**, *121*, 9411.

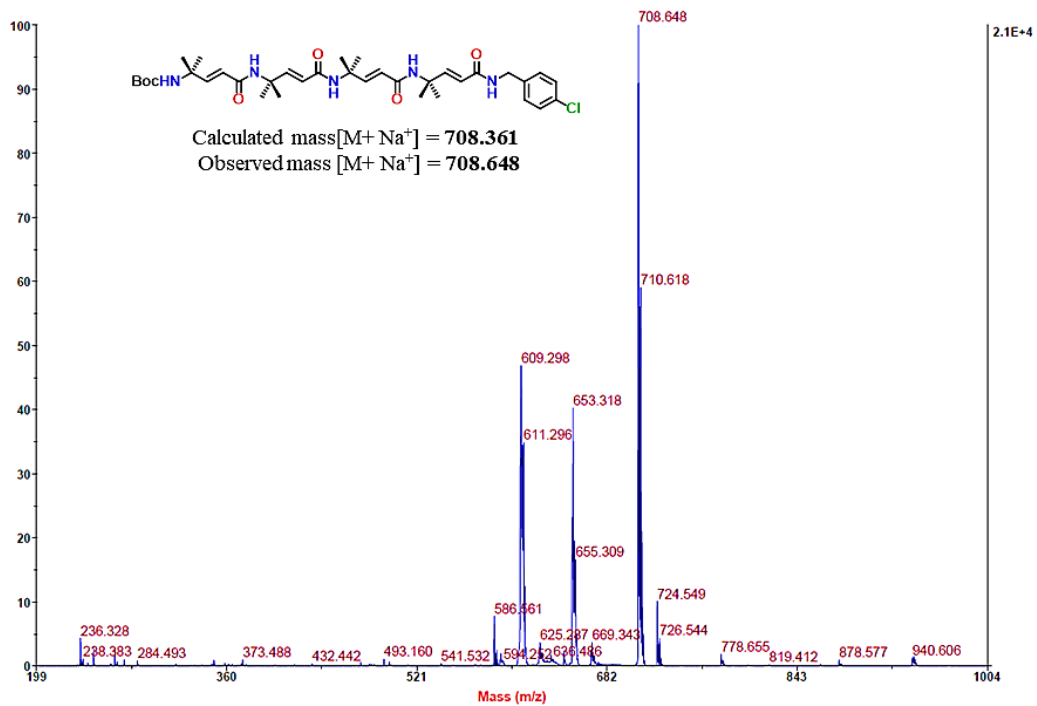






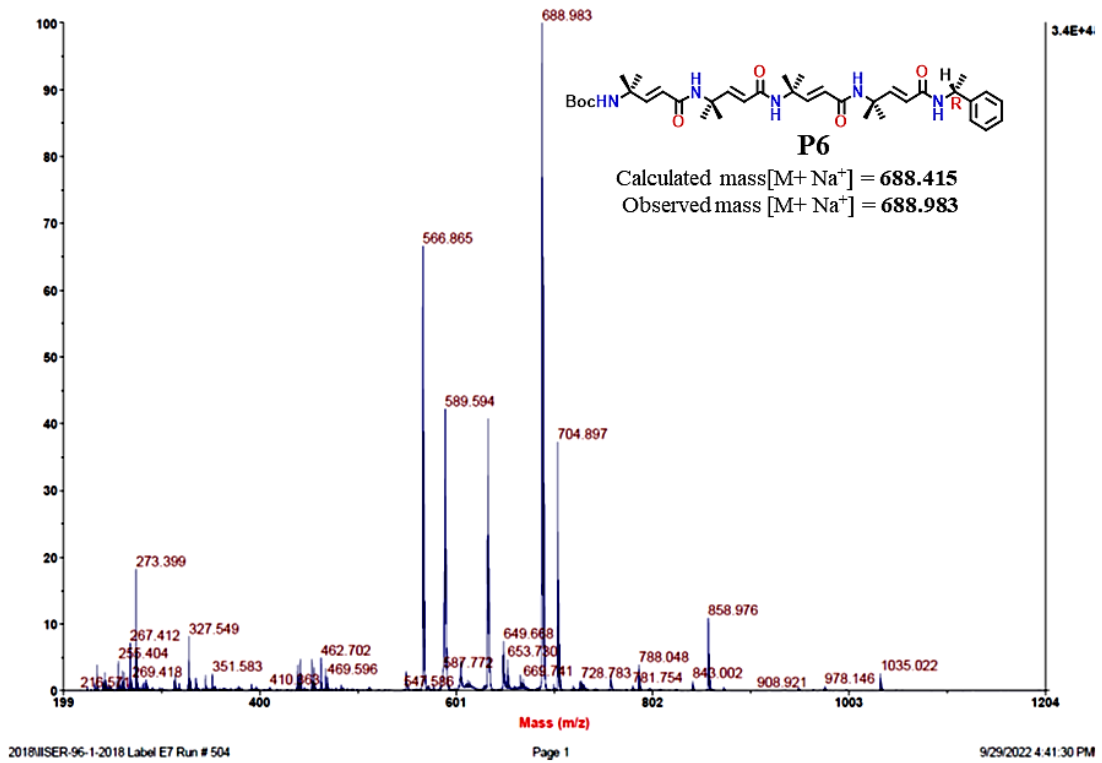
Spectrum Report

Final - Shots 400 - IISER-96-1-2018; Label D3



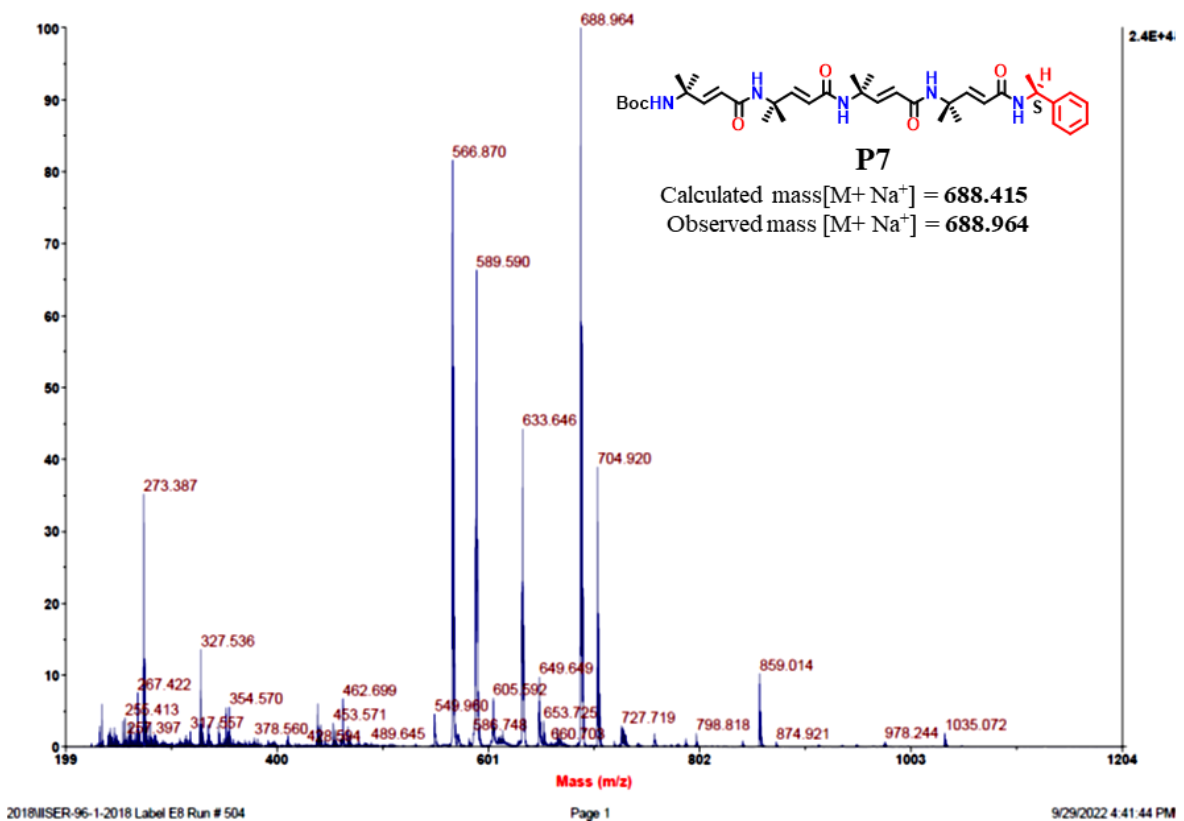
### Spectrum Report

Final - Shots 400 - IISER-96-1-2018; Label E7



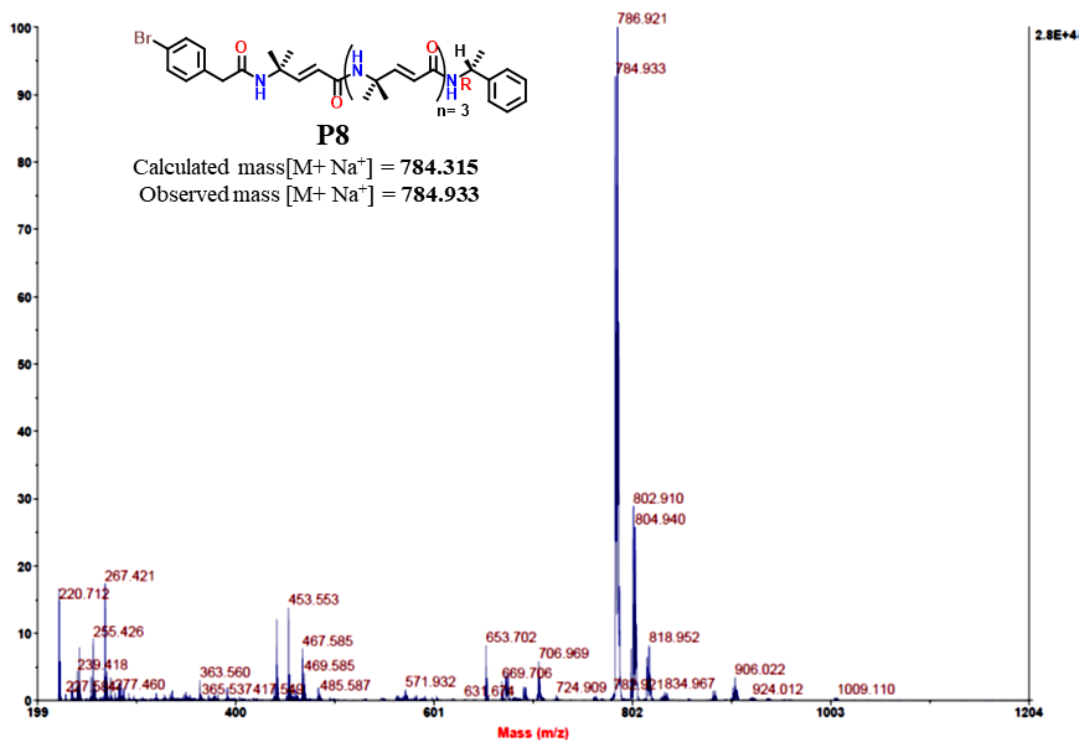
### Spectrum Report

Final - Shots 400 - IISER-96-1-2018; Label E8



### Spectrum Report

Final - Shots 400 - IISER-96-1-2018; Label E9



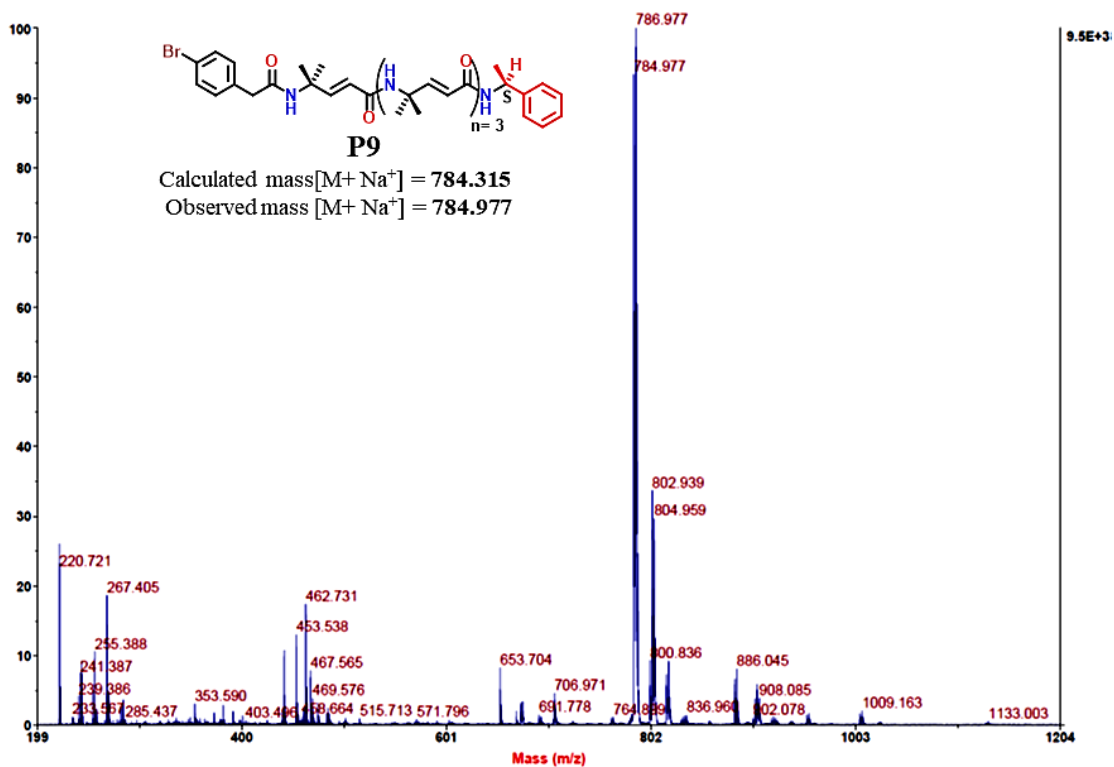
2018IISER-96-1-2018 Label E9 Run # 504

Page 1

9/29/2022 4:41:59 PM

### Spectrum Report

Final - Shots 400 - IISER-96-1-2018; Label E10



2018IISER-96-1-2018 Label E10 Run # 504

Page 1

9/29/2022 4:42:13 PM

## *Chapter 3*

### *Metal-Ions Tuned Structural Modulation of Metal-Helical Peptide Coordination Assemblies: Architectures from Porous Framework to Hierarchical Superhelix*

## 1. Introduction:

The combination of stable protein secondary structures and metal ions can provide a unique opportunity to construct advanced self-assembled structures. Recently, metal-coordinated peptide architectures are gaining momentum due to their close resemblance to native biological systems. Metal-coordinated supramolecular assembly of various organic and biomolecules represents a powerful approach for constructing discrete and well-defined three-dimensional architectures.<sup>1</sup> Along with the non-covalent interactions, metal ions also play an important role in stimulating ordered supramolecular architectures from proteins. Besides their involvement in the structural organizations of various types of proteins, the redox properties of metal ions enabled proteins to perform a variety of biochemical functions.<sup>2</sup> Synthetic peptides represent an alternative and attractive class of ligands that can encompass the properties of both small molecules and proteins. In addition to the attractive features of peptides such as diverse functional groups, lipophilicity, polarity, and charge, various metal coordinating sites have been introduced and studied the ordered self-assembling properties of peptides.<sup>3</sup> Metal coordination is an important force to direct the ordered association of peptide molecules. The advantage of this strategy is that the functional properties of peptides and metal ions can be explored to design novel self-assembled peptide-based materials and also metalloprotein mimetics. Recently, Fujita and colleagues showed the metal-dictated knotted networks from the short peptides.<sup>4</sup> In their pioneering work, the groups of Chmielewski<sup>5</sup> and Conticello<sup>6</sup> have studied the protein-like architectures from metal-mediated supramolecular assemblies of collagen and coiled-coil peptides. In addition, Horne and colleagues have shown the metal-mediated assembly of peptide coiled-coils into well-defined supramolecular nets and frameworks.<sup>7</sup> Schneider and colleagues<sup>8</sup> and others<sup>9</sup> have demonstrated metal-triggered ordered  $\beta$ -hairpin conformations. Further, Rosseinsky and colleagues have extensively studied the short peptide-based metal-peptide frameworks with the tunability of porosity of the framework and enantioselective chiral drug separation.<sup>10</sup> Additionally, the groups of Shionoya<sup>11</sup> and Miyake<sup>12</sup> have reported metal-mediated macrocycles from the short peptides. In continuation, Lee and colleagues<sup>13</sup> reported  $\beta$ -peptide foldamer-based frameworks. Further, a significant effort was done by Maayan and colleagues<sup>14</sup> to understand the metal-peptoids coordination assembly for the application of electrocatalysis and biology.

The diverse nature of supramolecular interactions and assembly of proteins and peptides are modulated by physical and chemical stimuli (e.g., temperature,<sup>15</sup> pH,<sup>16</sup> metal ions,<sup>17</sup> and chemical accompaniments<sup>18</sup>). The key aspects that should be considered when metal-coordinated self-assembly is used to develop nanostructures include metal coordination chemistry, design rules of metal-binding ligands, selecting rational combinations of various functional components, and control of self-assembled structures. The advantage of peptide-based ligands in self-assembly is that they can provide additional intermolecular H-bonds through amide –NH or –CO along with other non-covalent interactions. It is expected that the metal-peptide complex underlies more structural diversity as compared to non-peptide-based ligands. Therefore, the design of peptide sequences plays a key factor to construct metal-peptide coordinated structural architectures.

## 2. Object of the Present Work:

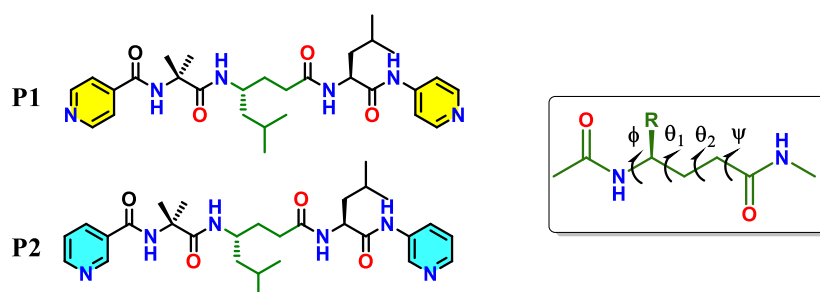
The formation of structure-based supramolecular architectures mainly with biomolecules has drawn great attention. In particular peptides with the advantages of biocompatibility, functional diversity, flexibility, hydrophobicity, structural adaptability, and chirality are promising templates for such structural diversity.<sup>19</sup> The peptide backbone motif shows conformational adaptation (helix or sheet) via H-bond formation and indeed, peptides can show self-assembly properties that open the window of various applications. Inspired by the role and functions of metal ions in the biological system, attempts are made to mimic many metalloproteins and metalloenzymes. Therefore, the combination of metal ions and peptide-building units as linkers has been extensively explored to construct various metal-peptide coordination assemblies networks in particular porous architectures that have significant attention with a wide range of applications.<sup>20</sup> Although metal-mediated supramolecular assembly of structured peptides provided an attractive opportunity to design a variety of assemblies and nano-architectures. However, structured peptides have scarcely been utilized to design porous metal-peptide frameworks. The major obstacle here is the requirement of longer  $\alpha$ -peptide sequences to obtain stable secondary structures. We<sup>21</sup> and others<sup>22</sup> demonstrated the stable 12-helical secondary structures from  $\alpha,\gamma$ -hybrid peptides even in short sequences. Recently, we reported the metal-helix frameworks using short  $\alpha,\gamma$ -tripeptide 12-helices consisting of terminal pyridines and helix-promoting Aib residues in the sequence.<sup>23a</sup> The previous report shows after coordinating with the metal  $\text{Ag}^+$  ion, it forms structural diversity of  $\alpha,\gamma$ -tripeptide 12-helix from macrocycle and porous networks depending on the bonding site of peptides. Motivated by the previous result, we thought to examine the effect of  $\alpha,\gamma$ -tripeptide 12-helices with higher coordinating

metal ions and their coordination assemblies. As metal coordinated architectures not only depend on the position of binding of the ligands but also the nature of metal ions.<sup>24</sup>

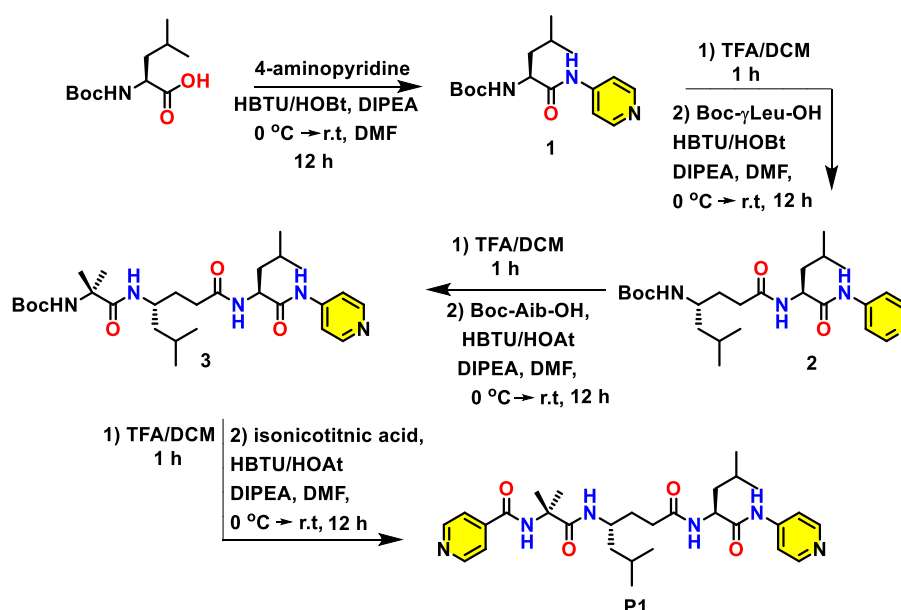
### 3. Results and Discussion:

#### 3.1. Design and Synthesis of Peptides (P1-P7):

As these  $\alpha,\gamma$ -hybrid peptides fold into stable 12-helices even in short peptide sequences,<sup>21,22</sup> we hypothesized that these short helices with suitable metal coordinating ligands at the N- and C-termini can be explored to construct metal foldamer structural architectures. The sequences of the designed short  $\alpha,\gamma$ -hybrid peptides **P1** and **P2** with terminal pyridyl moieties are shown in Scheme 1. Both 3-pyridyl and 4-pyridyl metal binding ligands were used to understand the impact of coordinating sites on the metal-coordinated foldamer assemblies.



**Scheme 1:** Sequences of short  $\alpha,\gamma$ -hybrid tripeptides **P1** and **P2**. Local torsion variables of  $\gamma$ -residue are also shown.



**Scheme 2:** Synthesis of short  $\alpha,\gamma$ -hybrid tripeptide **P1**.

All tripeptides consist of  $\alpha\gamma\alpha$  sequence patterns. All tripeptides were synthesized through a standard solution-phase strategy following the Boc- deprotection and coupling method and the synthetic procedure has shown in Scheme 2. All peptides **P1** and **P2** were synthesized by solution phase and purified by column chromatography following Scheme 2 with 68% to 71% yield.

### 3.2. Crystal Structures Analysis of Peptide P1, and P2:

As single crystal X-ray diffraction studies provide unambiguous structural information of peptides, we subjected these short hybrid peptides for crystallization in various solvent combinations. Both **P1** and **P2** gave X-ray diffraction quality single crystals from the solution of peptides in aqueous methanol and their structures are shown in Figure 1. The structural analysis revealed that both **P1** and **P2** adopted 12-helix structures in single crystals. The 12-helix structures are stabilized by two successive intramolecular 12-membered hydrogen bonds between the residues  $i$  and  $i+3$ .

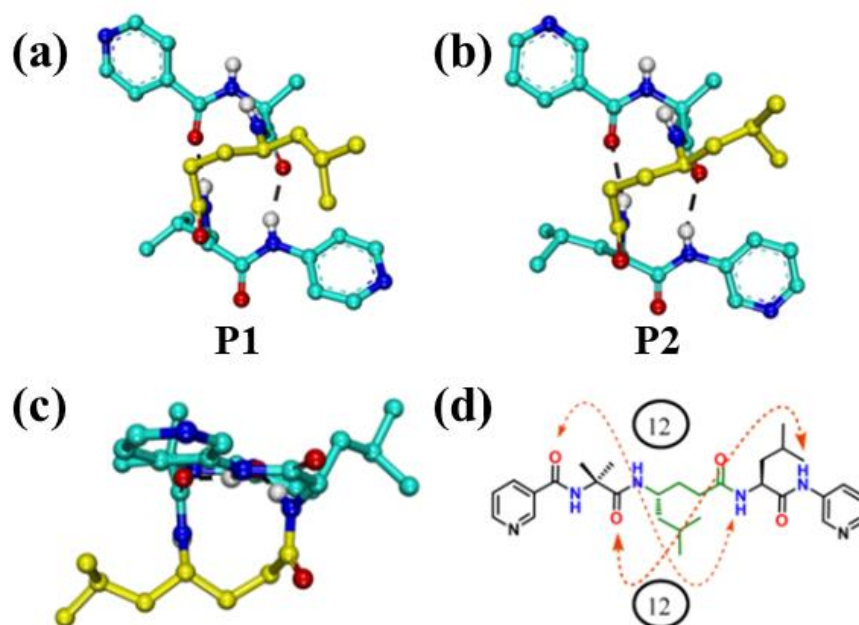


**Figure 1:** X-ray structures of (a) **P1** (b) **P2**. (c) The top views of P2 and (d) H-bonding pattern of **P2** 12-helix are also shown.

The two amide NH protons at the N-terminus and two carbonyl groups at the C-terminus are involved in the head-to-tail intermolecular H-bonding with other helices in the crystal packing. The backbone conformation of  $\gamma$ -residues can be recognized through the torsion angles  $\phi$ ,  $\theta_1$ ,  $\theta_2$ , and  $\psi$  as shown in Scheme 1. The  $\gamma$ -residues adopted helix favoring *gauche*<sup>+</sup> ( $g^+$ ), and *gauche*<sup>+</sup> ( $g^+$ ) conformation along  $C^\gamma$ - $C^\beta$  ( $\theta_1$ ) and  $C^\beta$ - $C^\alpha$  ( $\theta_2$ ) bonds. The top view of the **P2** 12-



helix is shown in Figure 1c. The cartoon representation depicting the H-bonding in 12-helices is shown in Figure 1d. Overall, both **P1** and **P2** peptides adopted the shortest 12-helix structures in single crystals. The torsion angles and H-bond parameters of **P1** and **P2** are given in Table S1-S2.

**Table S1:** Torsion angle parameters of **P1**, and **P2**.

Peptide		Residue	$\phi$	$\theta_1$	$\theta_2$	$\Psi$
<b>P1</b>	<b>Molecule 1</b>	Aib	-55	-	-	-43
		$\gamma$ Leu	-130	53	62	-116
		Leu	-52	-	-	-50
	<b>Molecule 2</b>	Aib	-57	-	-	-45
		$\gamma$ Leu	-134	48	65	-109
		Leu	-71	-	-	-31
	<b>Molecule 3</b>	Aib	-53	-	-	-48
		$\gamma$ Leu	-134	56	62	-110
		Leu	-71	-	-	-34
	<b>Molecule 4</b>	Aib	-56	-	-	-39
		$\gamma$ Leu	-133	55	60	-112
		Leu	-61	-	-	-41
<b>P2</b>	Aib	-57	-	-	-44	
	$\gamma$ Leu	-122	48	69	-117	
	Leu	-88	-	-	-20	

**Table S2: H-bond Parameters of P1 and P2.**

Peptide	Hydrogen Bond (intramolecular)	C=O...H-N	C=O...N-H	∠O...H-N	
		in angstroms		in degrees	
<b>P2</b>	Py CO ← Leu NH	2.23	3.06	161	
	Aib CO ← NH Py	2.12	2.93	157	
<b>P1</b>	<b>Molecule 1</b>	Py CO ← Leu NH	2.04	2.90	175
		Aib CO ← NH Py	2.15	2.99	166
	<b>Molecule 2</b>	Py CO ← Leu NH	2.00	2.84	166
		Aib CO ← NH Py	2.07	2.88	156
	<b>Molecule 3</b>	Py CO ← Leu NH	2.01	2.85	168
		Aib CO ← NH Py	2.11	2.92	157
	<b>Molecule 4</b>	Py CO ← Leu NH	2.06	2.91	168
		Aib CO ← NH Py	2.01	2.84	160

Peptide	Hydrogen bond (intermolecular)	C=O...H-N	C=O...N-H	∠O...H-N
		in Angstroms		in Degrees
<b>P2</b>	Leu CO ← NH γLeu	2.10	2.90	154
<b>P1</b>	Leu CO ← NH Aib (1)	2.19	3.04	169
	Leu CO ← NH Aib (2)	2.08	2.94	173

### 3.3. Metal-Peptide Coordinated Supramolecular Assembly of Peptide **P1**:

Two positional isomeric short peptide ligands **P1** and **P2** with 4- or 3-pyridyl groups are systematically investigated as building linker units toward metal coordination. As pyridyl groups have a high affinity for  $\text{Zn}^{2+}$  and  $\text{Cd}^{2+}$  similar to  $\text{Ag}^+$ , we subjected these peptides to the coordination with  $\text{ZnCl}_2$  and  $\text{CdI}_2$  to comprehend their metal-coordination properties. The peptide **P1** gave single crystals at the interface of methanol/water upon treatment of  $\text{ZnCl}_2$  and  $\text{CdI}_2$  separately at ambient temperature. We observed polyhedral crystals in the case **P1-ZnCl<sub>2</sub>** complex and square-shaped crystals in the case of the **P1-CdI<sub>2</sub>** complex and their X-ray diffracted single-crystal structural analysis is shown in Figure 2.

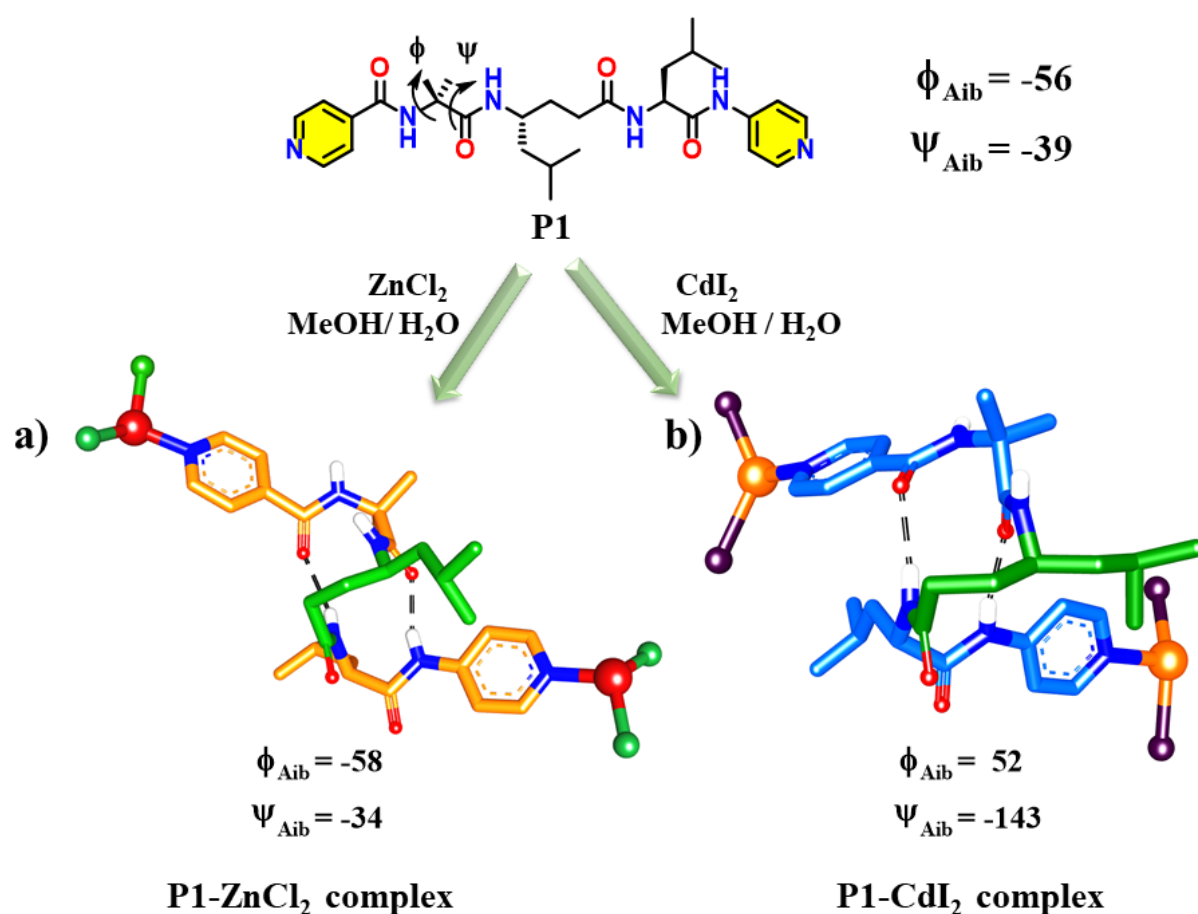


**Figure 2:** Metal-peptide complexation of **P1** with different metal salts. The change in the torsion angle parameters ( $\phi$  and  $\psi$ ) of **Aib residue** before and after complexation has been shown.

The X-ray diffracted single-crystal structural analysis revealed that  $\text{ZnCl}_2$  coordinated both C- and N-terminal 4-pyridyl groups of the peptide **P1** in a “head-to-tail” fashion with an angle of  $\angle_{\text{pyN-Zn-Npy}} = 100.7^\circ$ ,  $\angle_{\text{pyN-Zn-Cl}} = 109.6^\circ$  and  $\angle_{\text{pyN-Zn-Cl}} = 106.3^\circ$  of two helices,

respectively (Figure 3a). The peptide **P1** adopted 12-helix conformation. The helical structure is stabilized by the two consecutive intramolecular 12-membered H-bonds between the CO ( $i$ )  $\leftarrow$  NH ( $i+3$ ). We observed a remarkable framework of helical polymerization through various non-covalent interactions of the  $[(\text{ZnCl}_2)_n\text{P1}_n]$  unit.

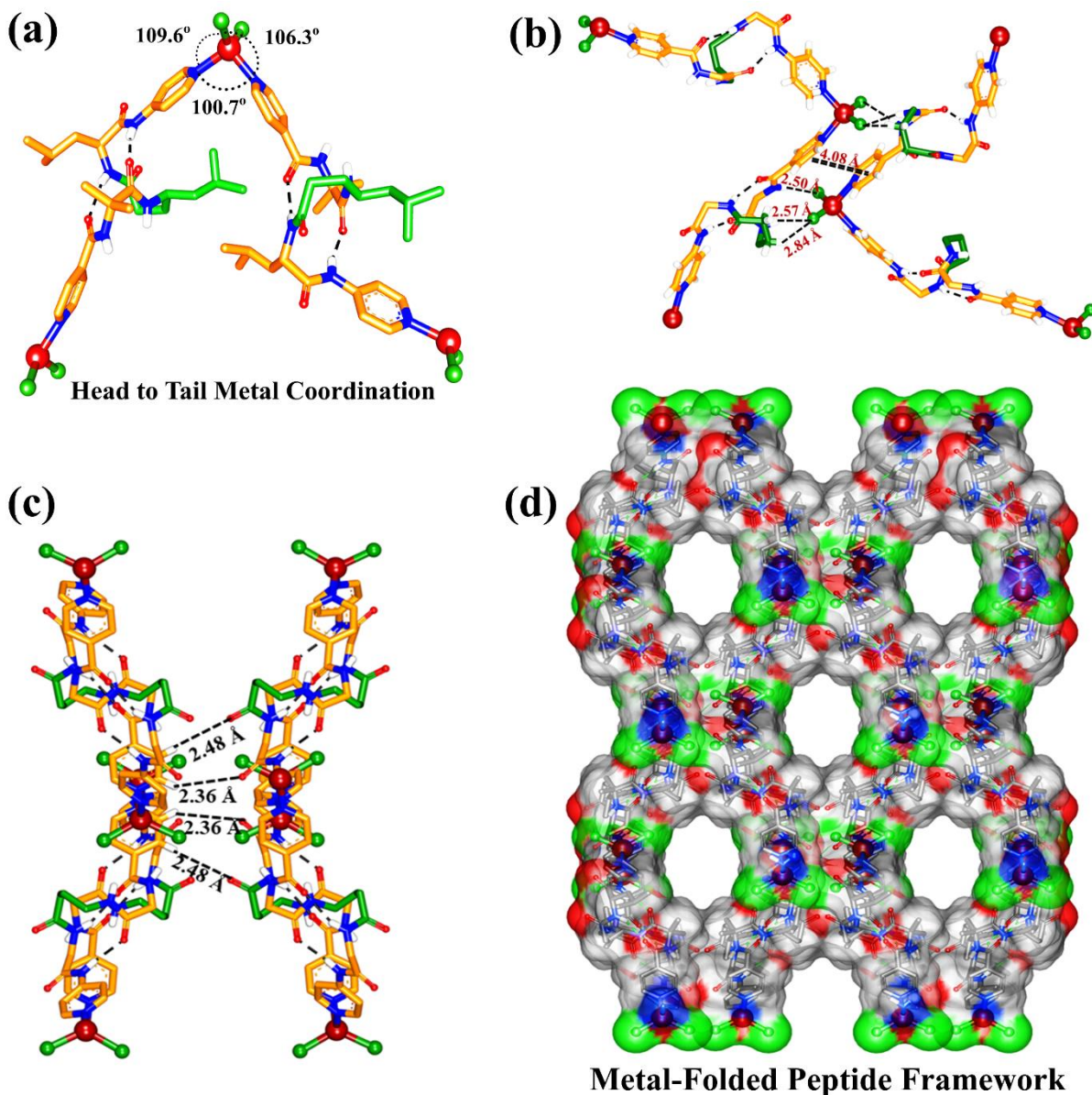


**Figure 3:** The X-ray diffracted single-crystal structure of the **P1-ZnCl<sub>2</sub>** complex. (a)  $\text{Zn}^{2+}$  ion coordination between the two helices in a “Head-to-Tail” fashion. (b) Cl---HN H-bonds between the exposed amide NH groups in the helix and  $\text{ZnCl}_2$  along the a-axis and (c) The interactions of aromatic C-H and C-terminal exposed carbonyl groups of the helix along the c-axis. (d) The metal-helix 3D supramolecular framework along the c-axis.

The  $\gamma$ -Leu residue in **P1** adopted *gauche*<sup>+</sup>, *gauche*<sup>+</sup> ( $\theta_1, \theta_2 \approx 60^\circ$ ) conformation and nicely accommodated into the helix. The  $\phi$  and  $\psi$  values of  $\gamma$ -residues were found to be  $-132^\circ$  and  $-109^\circ$ , respectively. Both  $\alpha$ -residues displayed average torsion angles  $\phi$  ( $-59 \pm 1^\circ$ ) and  $\psi$  ( $-42 \pm 8^\circ$ ) similar to  $\alpha$  peptide helices.<sup>25</sup> In helical structures, the N-terminal exposed amide NH groups are generally involved in the intermolecular H-bonding with the C-terminal exposed carbonyl groups of the other helices. However, in this structure, the Cl atoms from ZnCl<sub>2</sub> are involved in the intermolecular H-bonds with the N-terminal amide NH groups through Cl---H-N interactions with bond distances 2.50 Å and 2.57 Å, respectively, and the C-terminal exposed carbonyl groups of  $\gamma$ -Leu2 and Leu3 are stabilized by the 4-pyridyl C-H groups of another helix through CO---H-C-bond distances 2.48 Å and 2.36 Å, respectively. In addition, we observed the  $\pi$ - $\pi$  stacking interactions between two 4-pyridyl groups of two helices with a mean distance of 4.03 Å between the centroids (Figures 3b and 3c). The H-bonds and  $\pi$ - $\pi$  stacking interactions of [(ZnCl<sub>2</sub>)<sub>n</sub>P1<sub>n</sub>] complex dictate the supramolecular polymerization to form a metal-coordinated helix porous framework. We observed the porous architectures along the c-axis with a wider pore window of 10-12 Å (Figure 3d and Figure 4).

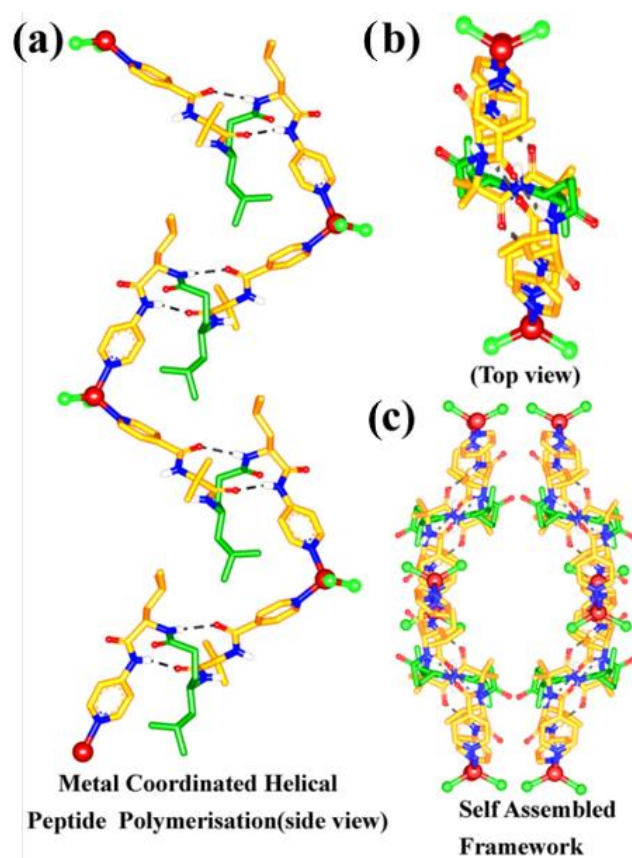


**Figure 4:** Peptide-zinc supramolecular assembled polymerization.

The porous framework observed in the  $\text{ZnCl}_2$  coordinated peptide is different from that of the framework observed in the  $\text{Ag}^+$  coordinated helical assembly of the same peptide **P1**.<sup>23a</sup>

As porous metal-organic frameworks have been explored in the separation, storage, and catalysis of various gases and organic solvents,<sup>26</sup> extensive synthetic efforts have been made over the years to design metal-mediated self-assembled frameworks with permanent porosity. Inspired by the porous framework displayed by the  $\text{Zn}^{2+}$  ion coordinated **P1**, we sought to examine whether or not this porous framework can act as a host to encapsulate small organic molecules. To understand the bulk phase purity and porous framework stability of the **P1-ZnCl<sub>2</sub>** complex, we have carried out PXRD and TGA analysis. The PXRD studies confirm that there is no change in the metal-helix framework bulk phase and also thermogravimetric analysis revealed that crystals of the **P1-ZnCl<sub>2</sub>** complex are stable up to 250 °C as shown in Figure 5.

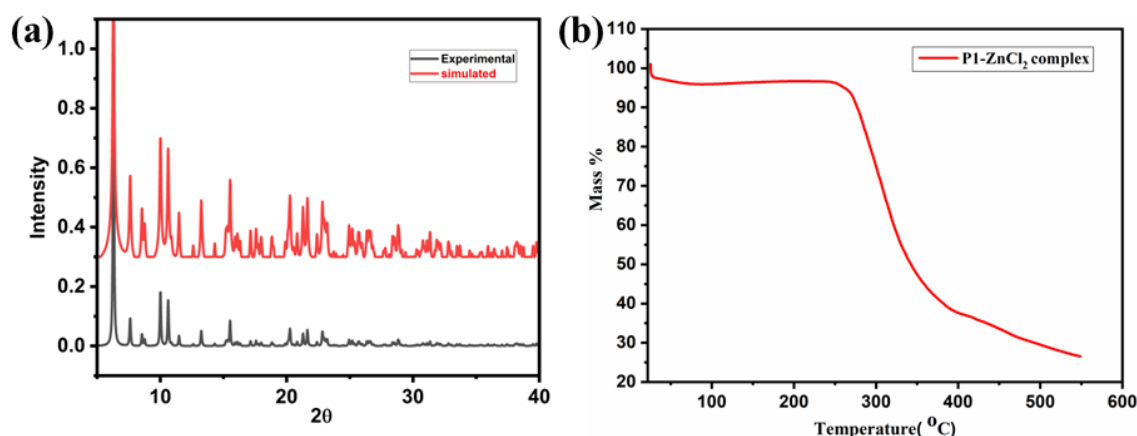


**Figure 5:** (a) PXRD and (b) TGA profile of P1-ZnCl<sub>2</sub> complex.

Further, these crystals were screened against various organic guest small molecules by soaking them in various solvents and a mixture of solvents. After incubating the crystals in various solvents and solvent combinations, we examined all crystal structures using SC-XRD. Out of many crystals tested, we were able to get the solvent-encapsulated structures from the crystal soaked in the solvents nitromethane and 1,2-dichloroethane. The solvents encapsulated in  $\text{Zn}^{2+}$  ion coordinated helical framework structures are shown in Figure 6. The guest molecules encapsulated in the  $\text{Zn}^{2+}$  ion coordinated peptide framework retained their original framework in both cases. In the case of crystals soaked in nitromethane, the pores are filled with nitromethane guest molecules. The structure elucidation suggested that there is no change in

the structure of the peptide, conformation of the amino acid residues, H-bonding pattern, and the crystallographic symmetry of the assembled architecture after the

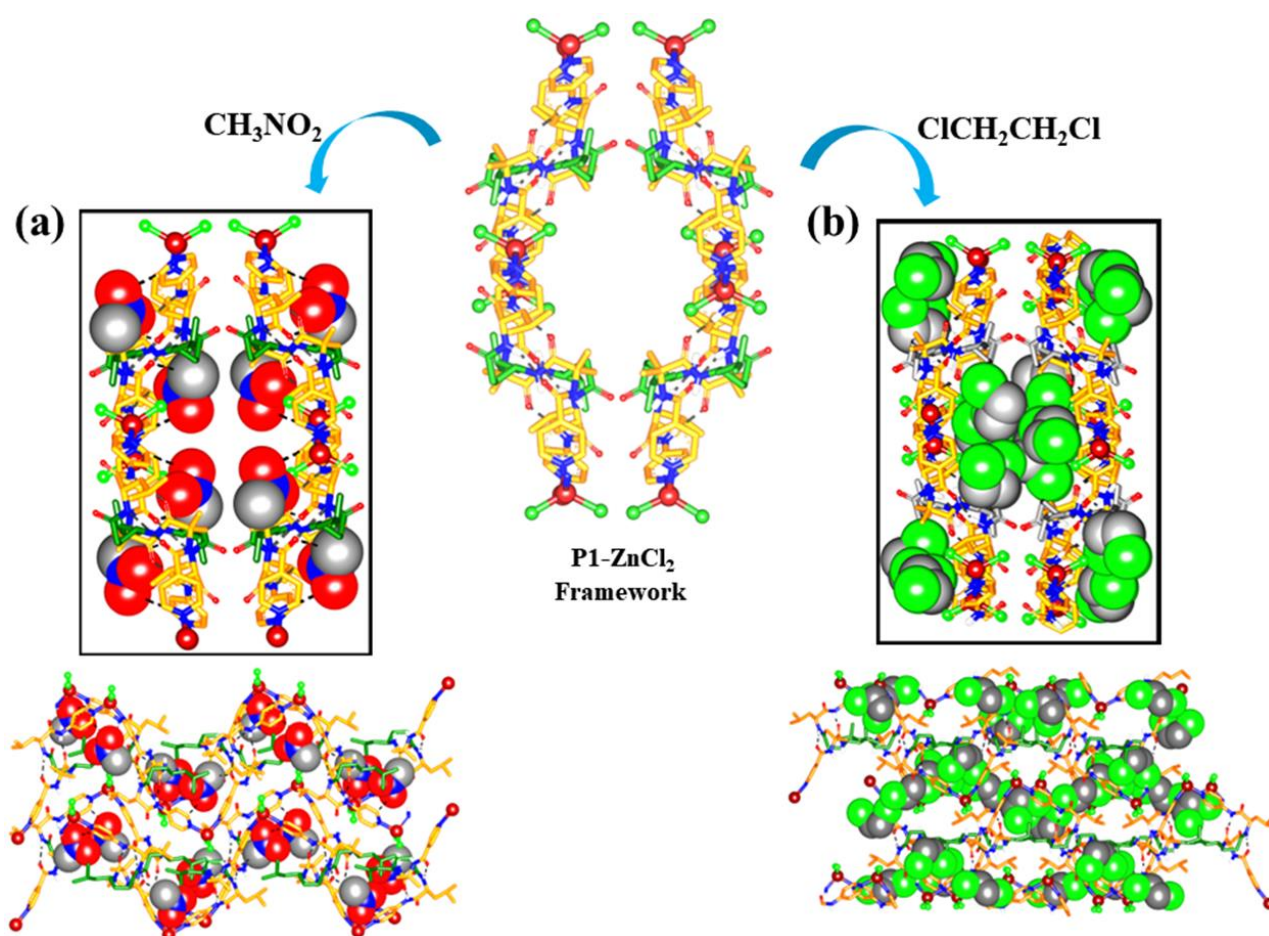


**Figure 6:** The X-ray diffracted single-crystal structures of (a) Nitromethane (along the c-axis) and (b) 1,2-Dichloroethane (along b-axis) encapsulated in the metal-helix framework (**P1-ZnCl<sub>2</sub>**).

accommodation of nitromethane guest molecules. Similarly, in the case of crystals obtained after soaking in the solvent 1,2-dichloroethane, the cavity is filled with 1,2-dichloroethane. To accommodate into the cavity, one of the 1,2-dichloroethane molecules adopted *gauche* conformation, and the other adopted *staggered* conformation. No interaction of the porous surface with staggered 1,2-dichloroethane is observed. In contrast, two Cl atoms interacted with the aromatic C-H groups in the *gauche* 1,2-dichloroethane. The analysis revealed that except for the crystallographic symmetry, no change in the structure, assembly, and H-bonding pattern has been observed. These preliminary studies demonstrate the permanent porosity of the Zn<sup>2+</sup> ion coordinated short helix framework, which can be used to selectively house the nitromethane and 1,2-dichloroethane guest molecules.

On the other hand, the X-ray diffracted single-crystal structure of  $\text{CdI}_2$ -coordinated helix **P1** is shown in Figure 7. The peptide adopted a 12-helix conformation stabilized by two independent intramolecular H-bonds (space group  $P4_12_12$ ). The X-ray diffracted single-crystal structure analysis showed that  $\text{CdI}_2$  coordinated both C- and N-terminal pyridine moieties of two helices in a “head-to-tail” fashion with an angle of  $\angle\text{pyN-Cd-Npy} = 91.4^\circ$ ,  $\angle\text{pyN-Cd-I} = 120.6^\circ$  and  $\angle\text{pyN-Cd-I} = 99.1^\circ$  of two helices, respectively (Figure 7a).

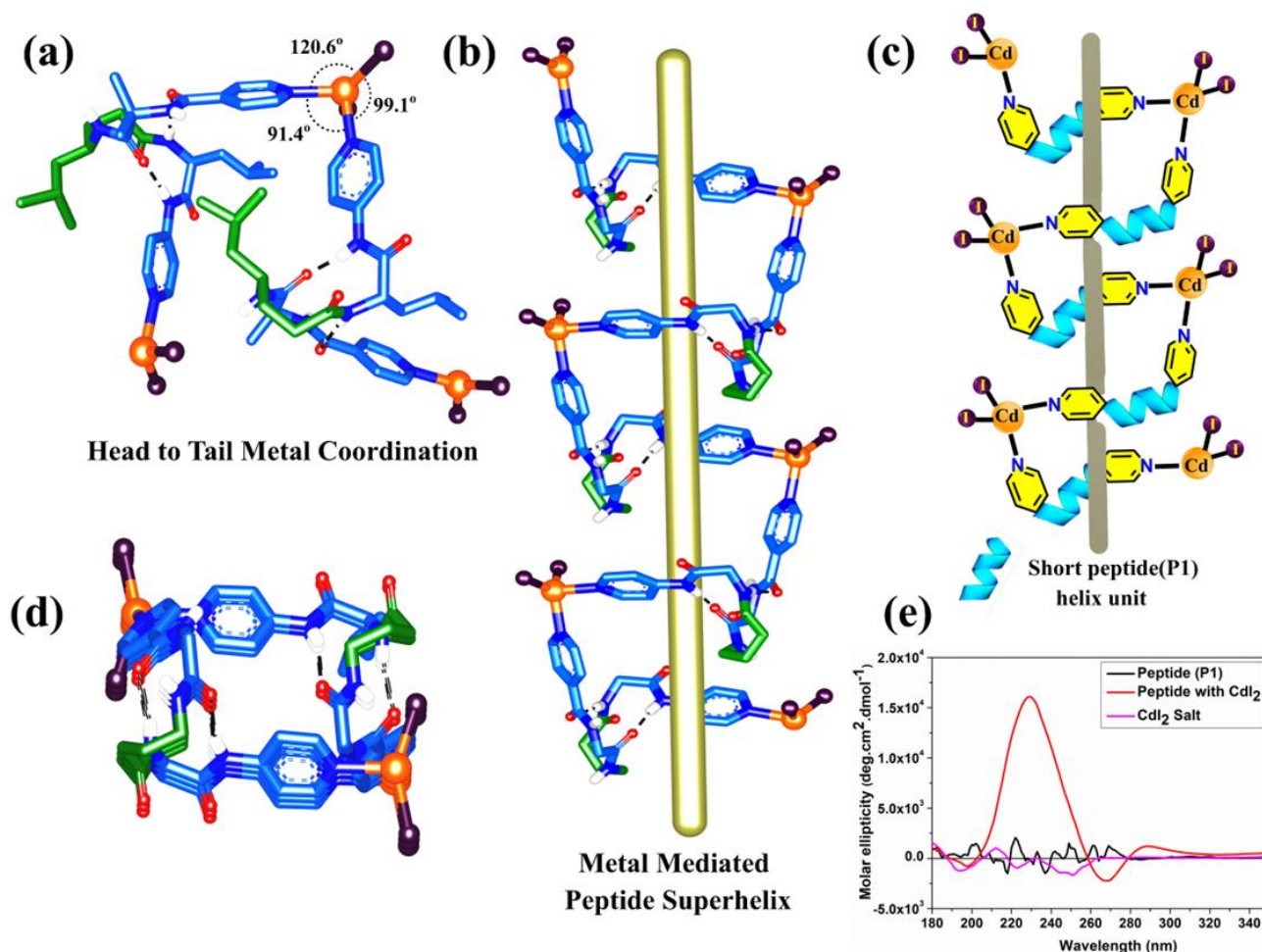


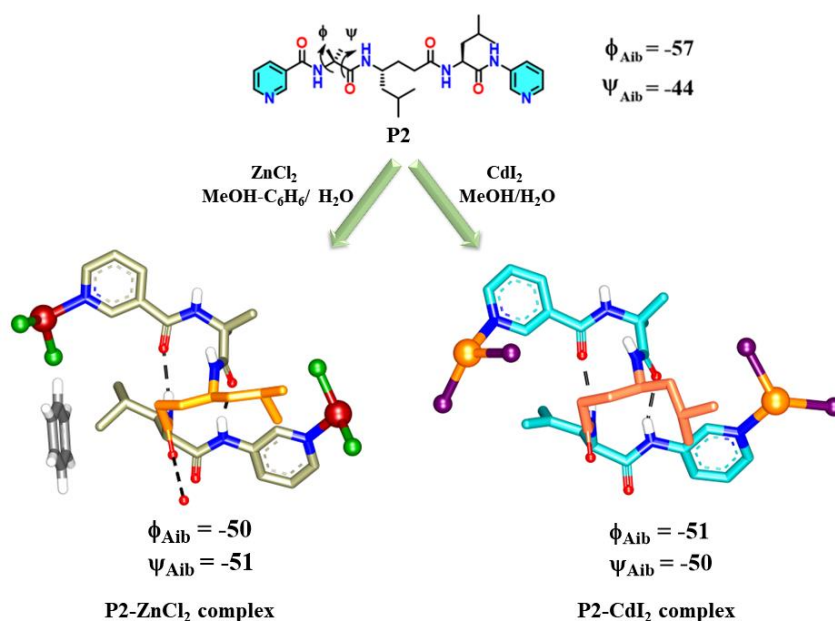
**Figure 7:** The X-ray diffracted single-crystal structure of the **P1**- $\text{CdI}_2$  complex. (a) Coordination of  $\text{CdI}_2$  with **P1** in a “Head-to-Tail” fashion. (b)  $\text{Cd}^{2+}$  ion coordinated the right-handed superhelix of **P1** along the c-axis. (c) A cartoon representation of  $\text{CdI}_2$  coordinated superhelix. (d) The top view of the superhelix along the b-axis (side arm of amino acid residues are removed for clarity). (e) CD spectra of **P1**,  $\text{CdI}_2$ , and **P1**- $\text{CdI}_2$  complex in solution.

The detailed no change in the conformations of the other two residues in the P1 helix has been on ( $\phi = 52$  and  $\psi = -143$ ).<sup>27</sup> However, there is no change in the conformations of the other two



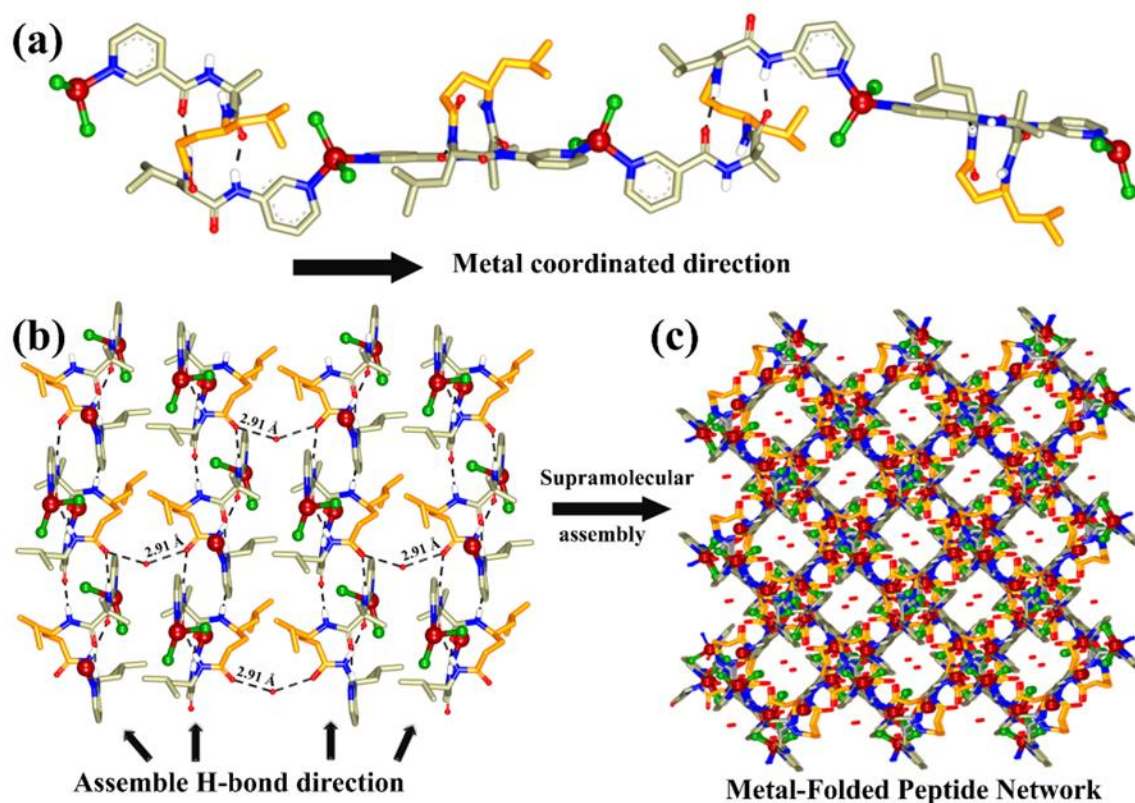
residues in the **P1** helix has been observed. In **P1-CdI<sub>2</sub>** complex involves a “head-to-tail” coordination between two helices as observed in Zn<sup>2+</sup> ion-coordinated helix polyhedral-shaped crystals. In comparison to the **P1-ZnCl<sub>2</sub>** framework, the “head-to-tail” CdI<sub>2</sub>-coordination of helices leads to a remarkable right-handed superhelix structure as shown in (Figure 7b-7d). To understand the superhelical signature of the **P1-CdI<sub>2</sub>** in solution, we subjected the **P1-CdI<sub>2</sub>** complex to circular dichroism (CD) spectroscopy along with **P1** and CdI<sub>2</sub>. The CD spectra are shown in Figure 7e. The analysis revealed that the **P1-CdI<sub>2</sub>** complex displayed CD maximum at 230 nm. In contrast, no characteristic CD signature was observed for **P1** and CdI<sub>2</sub>. These results indicate the chiral nature of the **P1-CdI<sub>2</sub>** coordinated complex and support the chiral superhelical signature of the **P1-CdI<sub>2</sub>** complex in solution. The superhelical structures are commonly observed in proteins and supramolecular assembled polymers.<sup>28</sup> These structures are primarily stabilized by the various non-covalent interactions. In addition, metal-mediated double and triple helices and helical bundles have been reported.<sup>29</sup> In contrast, the formation of the superhelix through “head-to-tail” metal coordination of helical structures is rarely observed. These findings reveal a notable metal-coordinated right-handed superhelix from a short 12-helix.

### 3.4. Metal-Peptide Coordinated Supramolecular Assembly of Peptide P2:



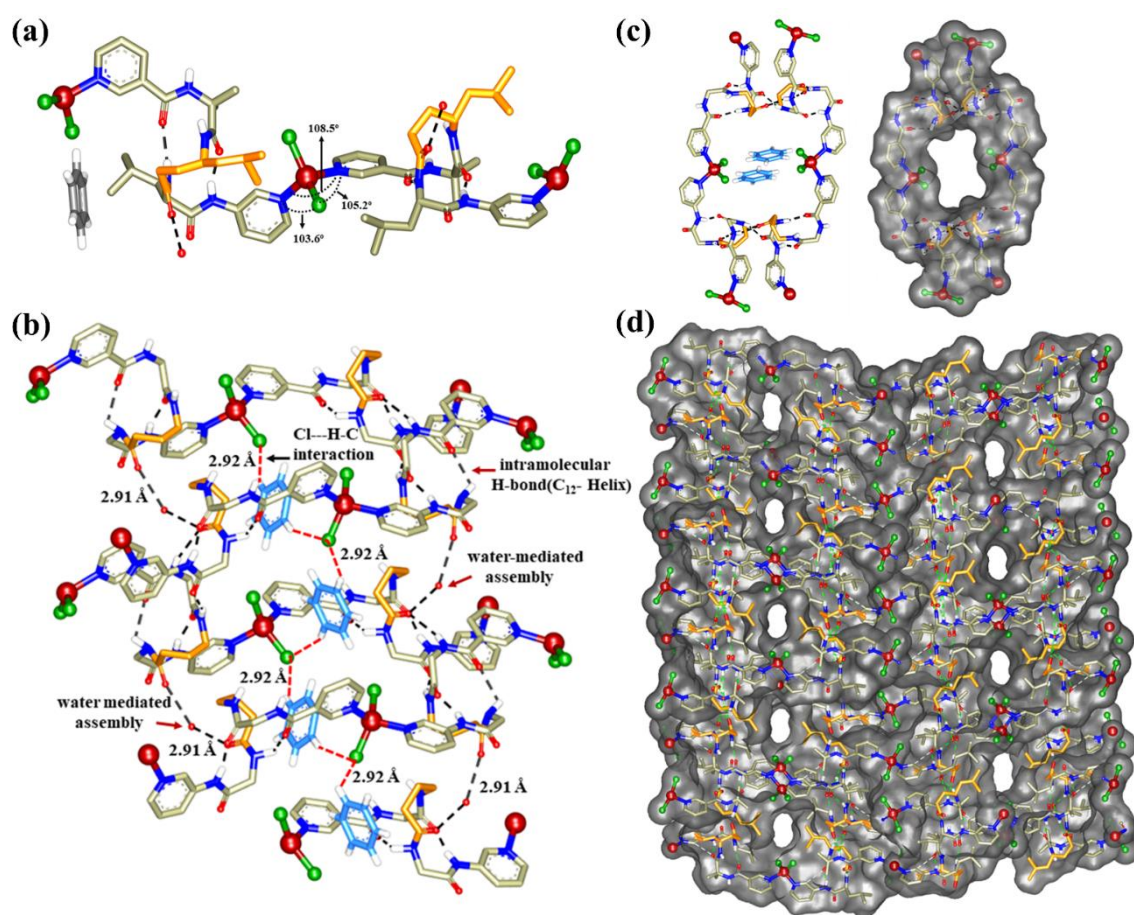
**Figure 8:** Metal-peptide complexation of **P2** with different metal salts. The change in the torsion angle parameters ( $\phi$  and  $\Psi$ ) of **Aib residue** before and after complexation has been shown.

As the extended coordination, the assembled network with desired structural architectures not only depends on the nature of metal ions but also the position of binding of the ligands.<sup>24</sup> In this context, we have designed isomeric peptide **P2** containing terminal 3-pyridyl groups. We subjected the helical tripeptide **P2** for metal coordination with ZnCl<sub>2</sub> and CdI<sub>2</sub> to gain further insight into the metal-coordinated self-assembled architectures. Upon treatment of ZnCl<sub>2</sub> with **P2** at ambient temperature, we observed rod-shaped crystals at the methanol-benzene/water interface. Whereas, on treatment with CdI<sub>2</sub> with **P2**, forms plate-shaped crystals in the methanol solvent. The X-ray diffracted single-crystal structural analysis of **P2**-metal complexes is shown in Figure 8. Similar to **P1**, the X-ray diffraction single-crystal analysis suggested that ZnCl<sub>2</sub>-coordinated with both C- and N-terminal 3-pyridyl groups of two helices in a “head-to-tail” fashion with an angle of  $\angle\text{pyN-Zn-Npy} = 108.5^\circ$ ,  $\angle\text{pyN-Zn-Cl} = 103.6^\circ$  and  $\angle\text{pyN-Zn-Cl} = 105.2^\circ$  shown in Figure 9a.



**Figure 9:** The X-ray diffracted single-crystal structure of the **P2**-ZnCl<sub>2</sub> complex. (a) Zn<sup>2+</sup> ion coordination between the two helices in a “Head-to-Tail” fashion was observed in the crystal packing. (b) The non-covalent interactions and supramolecular assembly along the b-axis (solvent benzene has been removed for clarity). (c) The metal-helix supramolecular network along the c-axis (a side arm of residue has been removed for clarity).

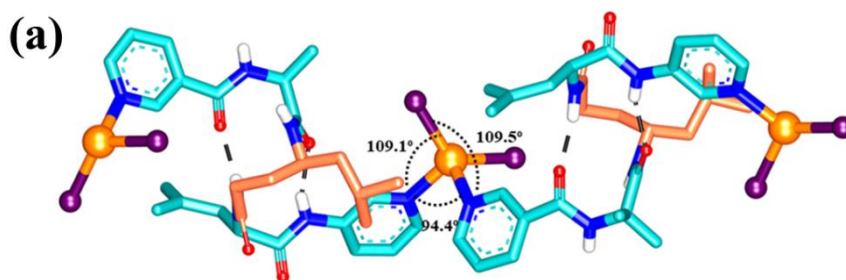
The two helical units are perpendicular to each other along the coordination polymers. The helical structure is stabilized by two consecutive intramolecular 12-membered H-bonds between the CO ( $i$ )  $\leftarrow$  NH ( $i+3$ ). Similar to **P1**, the  $\gamma$ -Leu adopted *gauche*<sup>+</sup>, *gauche*<sup>+</sup> ( $\theta_1, \theta_2 \approx 60^\circ$ ) conformation and accommodated into the helix. The  $\phi$  and  $\psi$  values of  $\gamma$ -residues were found to be  $-121^\circ$  and  $-122^\circ$ , respectively. Both  $\alpha$ -residues displayed average torsion angles  $\phi$  ( $-65 \pm 9^\circ$ ) and  $\psi$  ( $-38 \pm 8^\circ$ ). Similar to the **P1-ZnCl<sub>2</sub>** complex, H-bonds have driven helical polymerization of  $[(\text{ZnCl}_2)_n\text{P}2_n]$  is observed. The structural analysis suggested water bridges the helical peptides through an intermolecular H-bond between the CO groups of  $\gamma$ -Leu residues of two helices. A compact 3D porous network of **P2-ZnCl<sub>2</sub>** coordination polymer has been observed along the C-axis and the associated supramolecular interaction have shown in Figure 9c and Figure 10.



**Figure 10:** The X-ray diffracted structure of the P2-ZnCl<sub>2</sub> complex. (a) Zn<sup>2+</sup> ion coordination between the two helices (b,c) formation of supramolecular assembly and porosity with benzene and water molecules. (d) Coordination assembles a network with porosity along the b-axis (benzene and sidearm of amino acid residue has been removed for clarity).

However, the porous network observed in the  $\text{ZnCl}_2$  coordinated peptide **P2** is different from that of the network observed in the **P1-ZnCl<sub>2</sub>**. In **P2-ZnCl<sub>2</sub>** supramolecular assembly solely involves the intermolecular H-bonds between two helices and through water molecules. In addition, solvent benzene is also involved in Zn-Cl---H-C interaction.

Further, we have studied the X-ray diffracted single-crystal structure of  $\text{CdI}_2$ -coordinated helix **P2**. Like **P1**,  $\text{CdI}_2$ -coordinate both C- and N-terminal 3-pyridyl groups of two helices in a “head-to-tail” of **P2** with an angle of  $\angle_{\text{pyN-Cd-Npy}} = 94.4^\circ$ ,  $\angle_{\text{pyN-Cd-I}} = 109.1^\circ$  and  $\angle_{\text{pyN-Cd-I}} = 109.5^\circ$  of two helices respectively (Figure 11a). The structural analysis suggested that the peptide adopted a regular 12-helix conformation. The Aib residue in the **P2-CdI<sub>2</sub>** complex adopted regular right-handed conformation ( $\phi = -51$  and  $\psi = -50$ ) which is in sharp contrast with the torsion angles of the Aib residue observed in the **P1-CdI<sub>2</sub>** complex. The polymeric  $\text{CdI}_2$ -coordination of helices leads to a remarkable right-handed superhelix structure as shown in Figure 11b. In addition, both iodine atoms of  $\text{CdI}_2$  are in close proximity with the H atoms of the aromatic pyridine moieties with a distance of 3.10 Å. Instructively, each **P2-CdI<sub>2</sub>** coordinated superhelix is interconnected with intermolecular “head-to-tail” H-bonds of the **P2** helices that indulge hierarchical superhelical  $\beta$ -sheet structure (Figure 11c, 11d). This type of remarkably ordered self-assembled superhelices is rarely observed in the proteins and synthetic peptides or their self-assembled structures<sup>30</sup>. To understand the hierarchical superhelical signature in solution, we subjected the **P2**,  $\text{CdI}_2$ , and **P2-CdI<sub>2</sub>** coordination complex in methanol for circular dichroism (CD) analysis. The CD spectra are shown in Figure 11e. The analysis revealed that the **P2-CdI<sub>2</sub>** complex gave two intense peaks, one maximum at 234 nm and another minimum at 207 nm respectively. Similar to **P1**, **P2** is also CD inactive. These results indicate the chiral nature of the **P2-CdI<sub>2</sub>** coordinated superhelix in solution. In addition, the CD signature of the **P2-CdI<sub>2</sub>** complex is different from the **P1-CdI<sub>2</sub>** complex. This is probably because of the H-bond-mediated hierarchical assembly of superhelices in the **P2-CdI<sub>2</sub>** complex, which is missing in the **P1-CdI<sub>2</sub>** complex.



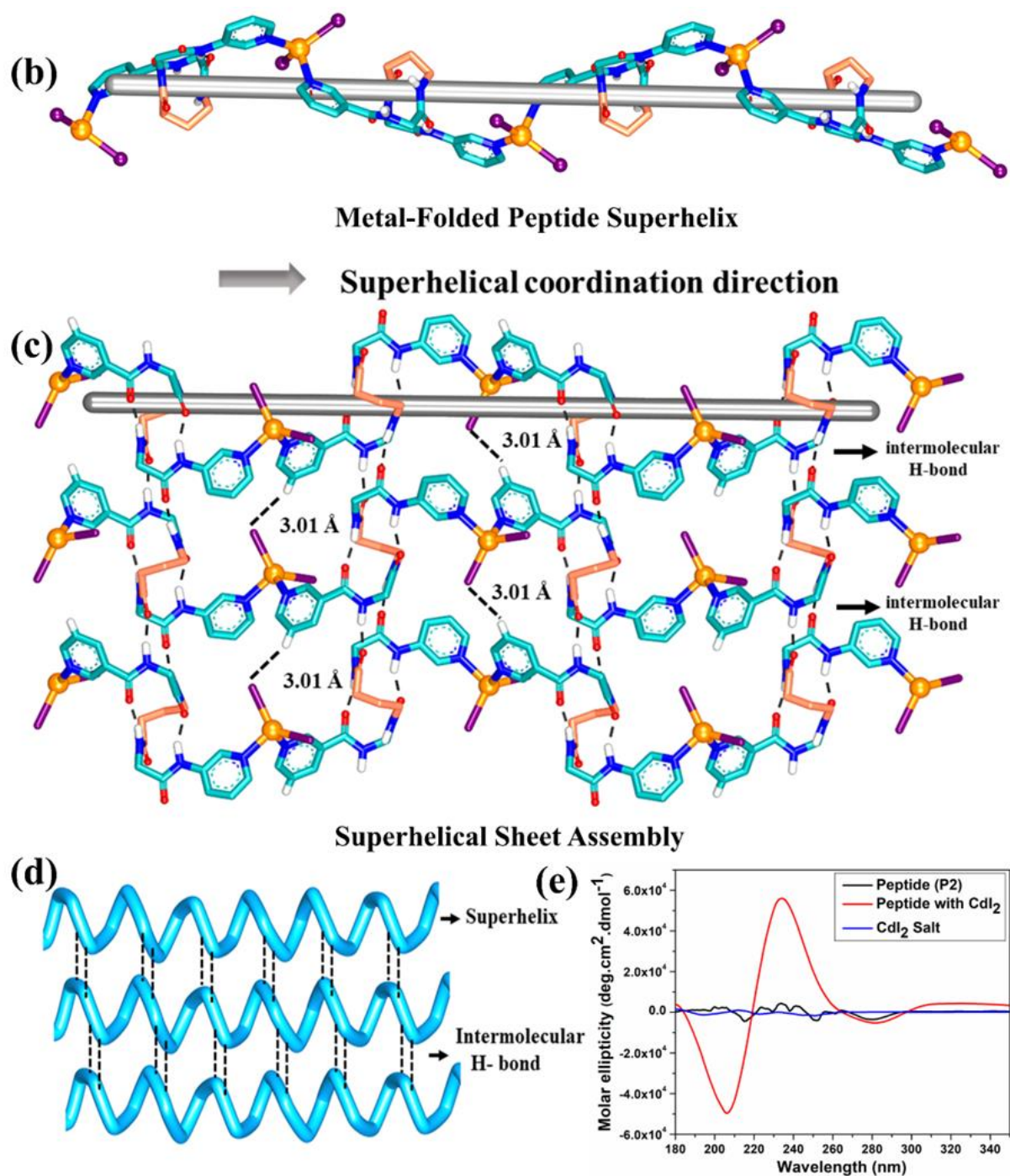


**Figure 11:** The X-ray diffracted single-crystal structure of the **P2-CdI<sub>2</sub>** complex. (a,b) Cd<sup>2+</sup> ion coordination between the two helices in a “Head-to-Tail” fashion observed in the crystal packing and the metal-peptide coordinated right-handed superhelical polymer along the b-axis (side arm of amino acid residues is removed for clarity). (c) Supramolecular assembly of the superhelical polymer by intermolecular H-bonds. (d) A cartoon representation of a hierarchical assembly of superhelices. (e) CD spectra of chiral superhelical signature of the **P2-CdI<sub>2</sub>** complex, **P2** and **CdI<sub>2</sub>** in solution.

### 3.5. Crystal Structures Analysis of Metal-Peptide Complexes:

The short helix **P1** and **P2** displayed remarkable self-assembling properties depending on the coordination capability of the metal ions. Both the peptides **P1** and **P2** maintained the overall 12-helix conformation in all crystal structures, demonstrating the power of helical structure. These results suggested the structural plasticity of the hybrid peptide helix **P1**.

**Table S3:** Torsion angle parameters of peptides and metal-peptide complexes

Complex	Residue	$\phi$	$\theta_1$	$\theta_2$	$\Psi$
<b>Ligand Peptide P1</b>	Aib	-56	-	-	-46
	$\gamma$ Leu	-134	49	64	-110
	Leu	-70	-	-	-31
<b>P1-ZnCl<sub>2</sub> complex</b>	Aib	-58	-	-	-34
	$\gamma$ Leu	-132	54	62	-109
	Leu	-60	-	-	-50
<b>P1-CdI<sub>2</sub> complex</b>	Aib	52	-	-	-143
	$\gamma$ Leu	-123	61	64	-115
	Leu	-76	-	-	-38
<b>Ligand Peptide P2</b>	Aib	-57	-	-	-44
	$\gamma$ Leu	-142	48	69	-116
	Leu	-88	-	-	-20
<b>P2-ZnCl<sub>2</sub> complex</b>	Aib	-56	-	-	-46
	$\gamma$ Leu	-121	58	57	-122
	Leu	-74	-	-	-30
<b>P2-CdI<sub>2</sub> complex</b>	Aib	-52	-	-	-49
	$\gamma$ Leu	-129	60	63	-114
	Leu	-79	-	-	-37

**Table S4:** H-bond Parameters of peptides and metal-peptide complexes.

Peptide	Hydrogen Bond	C=O...H-N	C=O...N-H	$\angle$ O...H-N
		in angstroms		in degrees
<b>P1-ZnCl<sub>2</sub> complex</b>	Py CO $\leftrightarrow$ Leu NH	2.23	3.05	158
	Aib CO $\leftrightarrow$ NH Py	2.00	2.84	163
<b>P1-CdI<sub>2</sub> complex</b>	Py CO $\leftrightarrow$ Leu NH	2.17	3.03	170
	Aib CO $\leftrightarrow$ NH Py	2.03	2.86	160
<b>P2-ZnCl<sub>2</sub> complex</b>	Py CO $\leftrightarrow$ Leu NH	2.06	2.91	169
	Aib CO $\leftrightarrow$ NH Py	1.92	2.75	161
<b>P2-CdI<sub>2</sub> complex</b>	Py CO $\leftrightarrow$ Leu NH	2.0	2.02	167
	Aib CO $\leftrightarrow$ NH Py	2.84	2.83	157

Besides the unusual conformation at the N-terminal Aib residue, we also observed a slight difference in the  $\angle$ pyN-M-Npy bond angles of all the structures. The analysis suggests the relative steric-free interactions of **P1** with the ZnCl<sub>2</sub> lead to the formation of ordered porous structures as compared to the **P2-ZnCl<sub>2</sub>** complex. The dimethyl residues of Aib have projected away from the metal coordination site in the **P1-ZnCl<sub>2</sub>** complex, but in the case of the **P2-ZnCl<sub>2</sub>** complex, Aib residues are in very close proximity with the coordination site. The Aib residue in the **P1-CdI<sub>2</sub>** complex adopted an unusual polyproline-type conformation at the N-terminus without deviating from the overall helical fold. Interestingly, the Cl atoms in ZnCl<sub>2</sub> are involved in unique NH---Cl H-bonds in the P1-ZnCl<sub>2</sub> complex, however, the type of NH---Cl H-bonds is missing in the **P2-ZnCl<sub>2</sub>** complex. Further, the N-terminal amide bond in P1-CdI<sub>2</sub> is almost perpendicular to the rest of the amide bonds in the helical structure. In sharp contrast, all amide bonds are unidirectional in the **P2-CdI<sub>2</sub>** complex. The distinction between

the **P1-CdI<sub>2</sub>** and **P2-CdI<sub>2</sub>** structures is that in the case of the **P2-CdI<sub>2</sub>** complex, the terminal exposed amide NH groups and C-terminal carbonyl groups with  $\angle\text{C=O}\cdots\text{H-N} = 152^\circ$  are participating in the regular “head-to-tail” intermolecular H-bonds, whereas in the case **P1-CdI<sub>2</sub>** exposed NH and carbonyl groups with  $\angle\text{C=O}\cdots\text{H-N} = 122^\circ$  are not involved regular “head-to-tail” H-bonds. The continuous helix “head-to-tail” intermolecular H-bonds lead to the ordered arrangement of superhelical structures in **P2-CdI<sub>2</sub>**-like  $\beta$ -sheet structures in proteins. Overall, these studies show a subtle change in the coordination site of the same ligands leads to a large change in the self-assembled structures are shown in Figures 12-14.

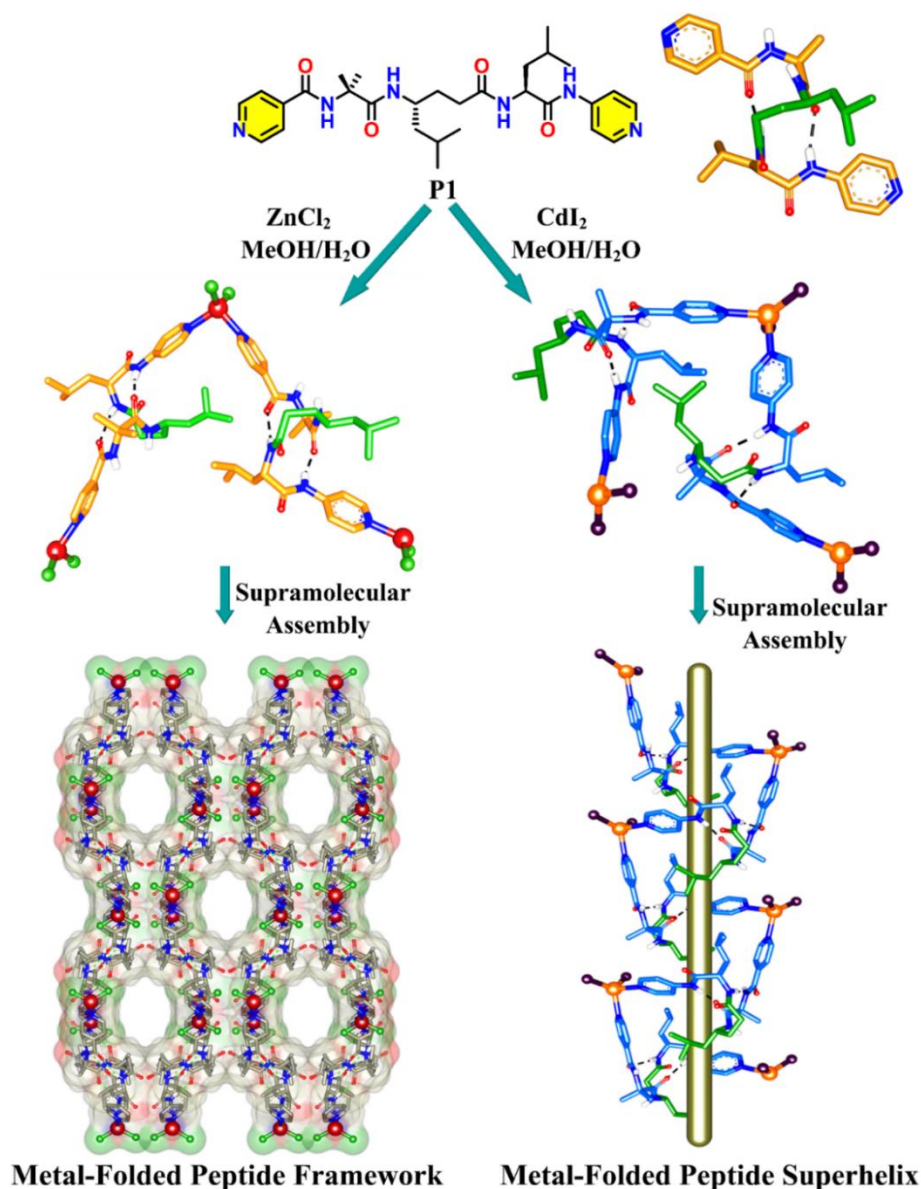


**Figure 12:** Metal Ion Tuned Structural Modulation of Metal-Peptide (**P1**) Coordinated Assembly.



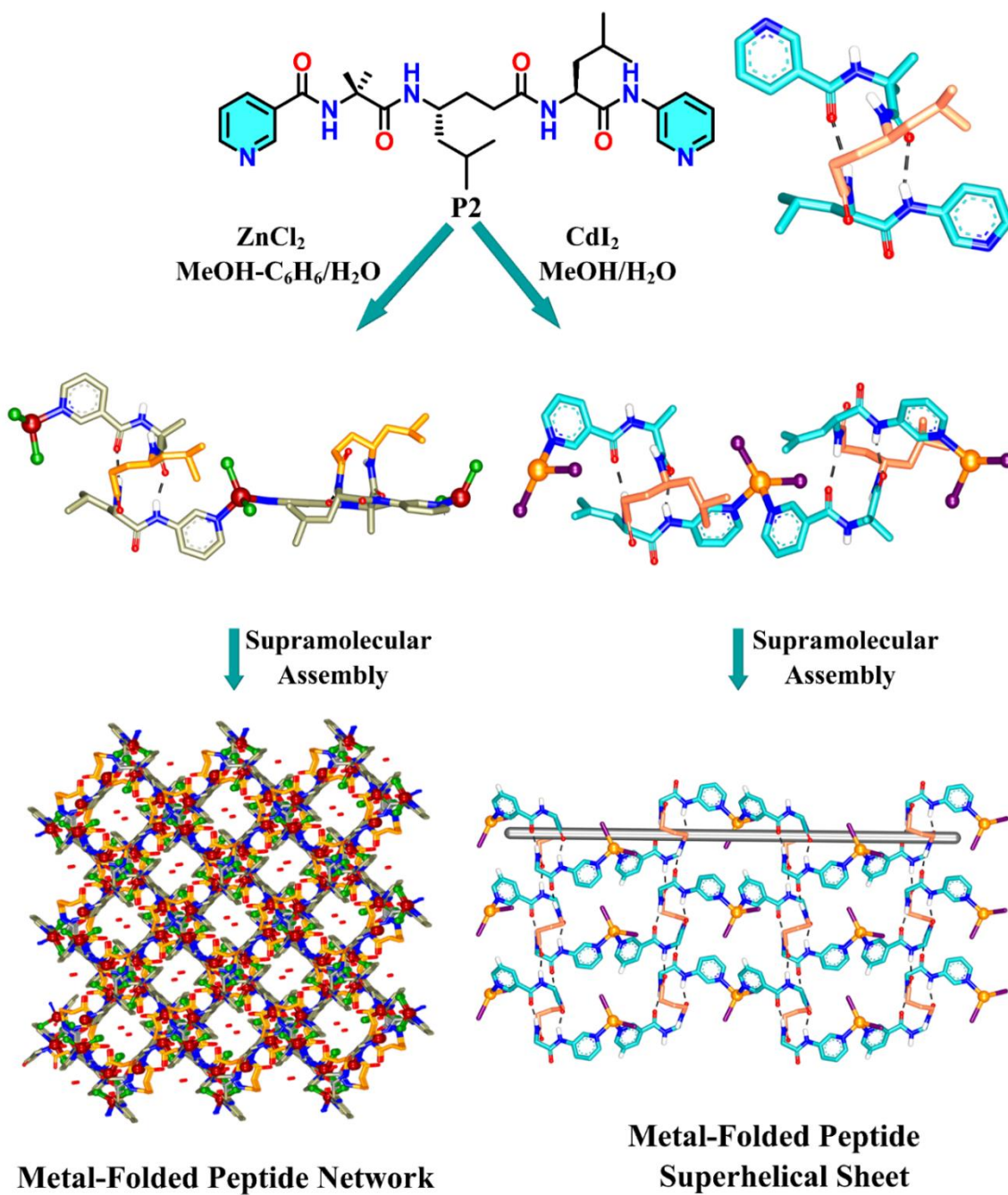


**Figure 13:** Metal Ion Tuned Structural Modulation of Metal-Peptide (P2) Coordinated Assembly.

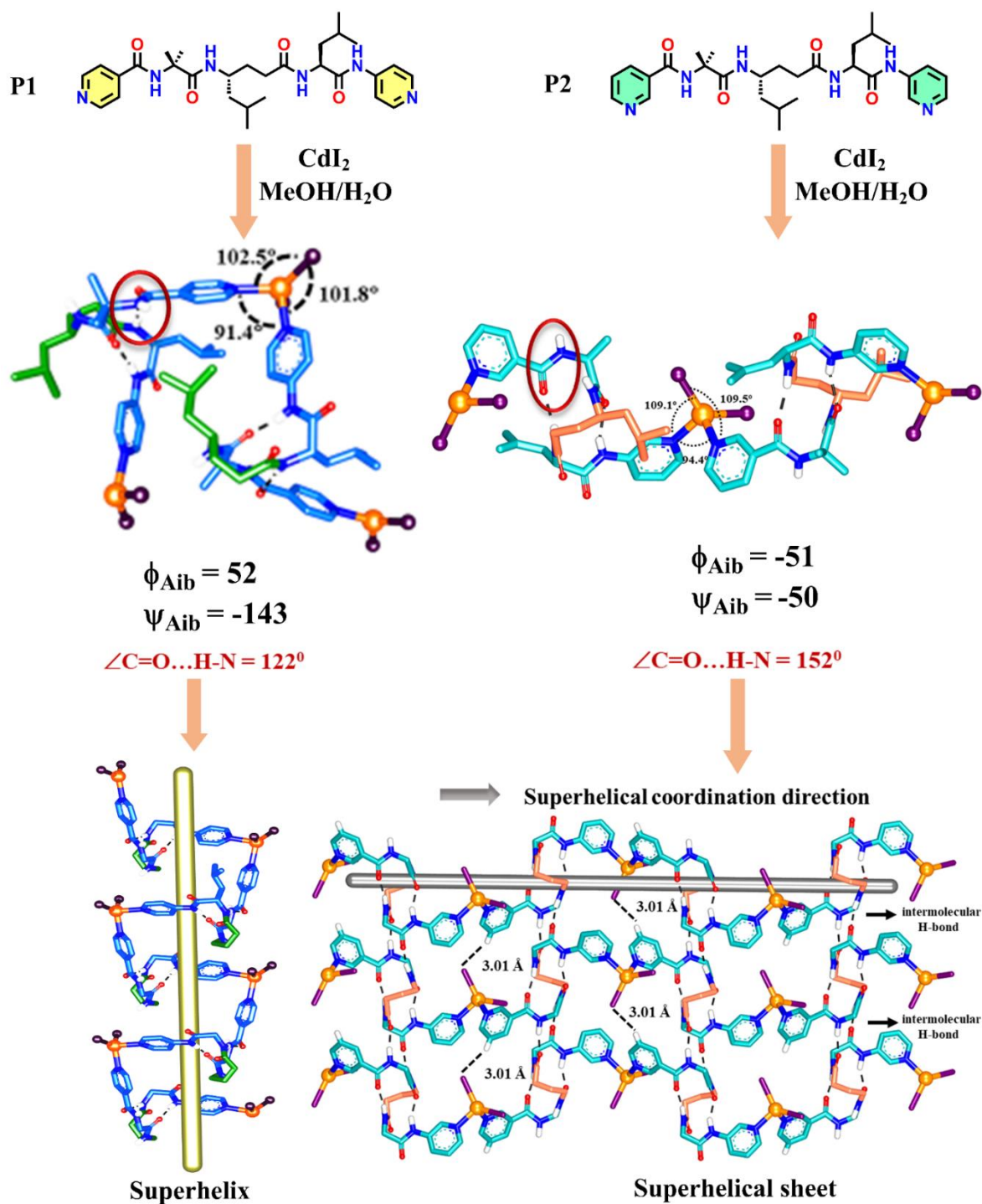


**Figure 14:** Effect of Aib Residue and Comparison of Superhelix and Superhelical Sheet.

In all complexes, the hybrid tripeptides are nicely accommodated into metal-coordinated structures without much deviation in their overall helical signature.

## 4. Conclusion:

In conclusion, we have shown the multifaceted supramolecular assembly from the metal coordinated short isomorphous  $\alpha,\gamma$ -hybrid peptide foldamers coupled with the terminal metal-binding sites. The short helical peptide ligands can serve as rigid linkers to design ordered metal-coordinated self-assembled architectures. The porosity of the metal-peptide complex is depending on the coordination site. The coordination of **P1** with  $\text{ZnCl}_2$  leads to a porous framework, which can uptake guest molecules. The size of the porosity decreases in the **P2-ZnCl<sub>2</sub>** complex. Along with the steric factors and NH---Cl interactions are responsible for the creation porous framework in the **P1-ZnCl<sub>2</sub>** complex. The same helical peptide **P1** displayed right-handed superhelical structures upon coordination with  $\text{CdI}_2$ . The “head-to-tail” intermolecular H-bond interactions of helical peptides in the superhelical structures in the **P2-CdI<sub>2</sub>** complex lead to a distinctive assembly of superhelices like  $\beta$ -sheets in protein structures. Irrespective of the molecular assembly, the short hybrid peptides adopted an overall 12-helix fold. It is evident from these studies that the short peptide foldamers can be used as stable ligands to derive new metal-coordinated assemblies with different functions. The functional and structural group diversity of hybrid peptide foldamers is yet to be explored in the design of metal-coordinated assemblies. The metal-folded peptide assemblies may provide an opportunity to build artificial enzymes, catalysts, delivery agents, and storage materials.

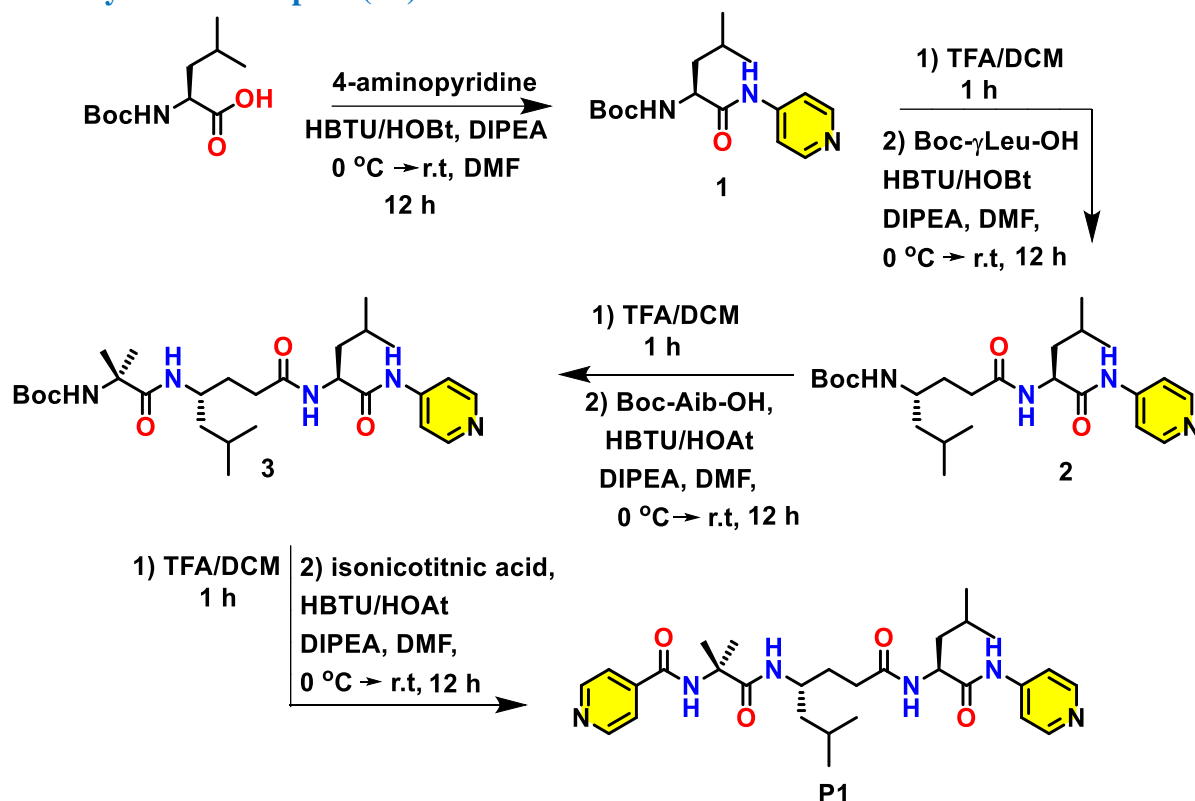
## 5. Experimental Section:

### 5.1. General Method:

All reagents were used without further purification. Column chromatography was performed on neutral alumina (100 -200 mesh).  $^1\text{H}$  NMR (400 MHz), and  $^{13}\text{C}$  NMR (100 MHz) were measured on a Bruker Avance 400 MHz spectrometer. Mass samples were analyzed by High-resolution mass spectrometry using ESI TOF. The X-ray data were collected at 100K temperature on a Bruker APEX(III) DUO CCD diffractometer using  $\text{Mo K}_\alpha$  radiation ( $\lambda = 0.71073 \text{ \AA}$ ) and  $\text{Cu K}_\alpha$  radiation ( $\lambda = 1.5406 \text{ \AA}$ ).

## 5.2. Procedure for the Synthesis of Peptides:

### 5.2.1. Synthesis of Peptide(P1):



**Scheme 2:** Synthesis of short  $\alpha,\gamma$ -hybrid tripeptide **P1**.

Boc-Leucine-OH (10 mmol, 2.31 g) was taken in 20 mL of DMF and the solution was cooled down to 0 °C and kept in an N<sub>2</sub> atmosphere. Then HBTU (10 mmol, 3.8 g) and HOBt (10 mmol, 1.36 g) were added to the solution and left stirring for 5 mins. After that 4-aminopyridine (12 mmol, 1.13 g) was added to the reaction mixture and it was stirred for 12 h. Upon completion of the reaction monitored by TLC, the reaction mixture was diluted with 250 ml of ethyl acetate. Then, it was washed with (100 mL X 2), 10% Na<sub>2</sub>CO<sub>3</sub> solution (100 mL X 2), and then NaCl solution (100 mL X 2). The organic layer was collected and dried with anhydrous Na<sub>2</sub>SO<sub>4</sub> and concentrated under reduced pressure. The crude product was purified by column chromatography to get 1 as a white solid (Yield- 2.5 g, 82%).

Boc deprotection of compound 1(5.2 mmol, 1.6 g) was carried out by using 5 ml of each TFA and DCM (1:1) for 1 h. After that, TFA and solvent DCM were evaporated and 5-6 times DCM was added and evaporated to remove traces of TFA. The formed crude was TFA-salt of the amine of compound C1 and to this 3 ml of DMF and 4.5 ml, of DIPEA were added to make it free amine of compound 1.

Boc- $\gamma$ leucine -OH (5 mmol, 1.3 g) was taken in 10 mL of DMF and the solution was cooled down to 0 °C and kept in an N<sub>2</sub> atmosphere. HBTU (5 mmol, 1.96 g) and HOBT (5 mmol, 0.68 g), and 2.5 ml DIPEA were added to the solution and the reaction mixture was stirred for 10 mins. After that, the free amine of compound 1 was added to the reaction mixture and stirred for 12 h. Upon completion of the reaction monitored by TLC, the reaction mixture was diluted with 200 ml of ethyl acetate. Then, the mixture was washed with (100 mL X 2), 10% Na<sub>2</sub>CO<sub>3</sub> solution (100 mL X 2), and then NaCl solution (100 mL X 2). The organic layer was collected and dried with anhydrous Na<sub>2</sub>SO<sub>4</sub> and concentrated under reduced pressure. The crude product was purified by column chromatography to get dipeptide 2 as a white solid (Yield- 1.7 g, 73%).

Boc deprotection of dipeptide 2 (3.8 mmol, 1.7 g) was carried out by using 4 ml of each TFA and DCM (1:1) for 1 h. After that, TFA and solvent DCM were evaporated and 5-6 times DCM was added and evaporated to remove traces of TFA. The formed crude was TFA-salt of the amine of compound 2 and to this 2 ml of DMF and 3 ml, of DIPEA were added to make it free amine of dipeptide 2.

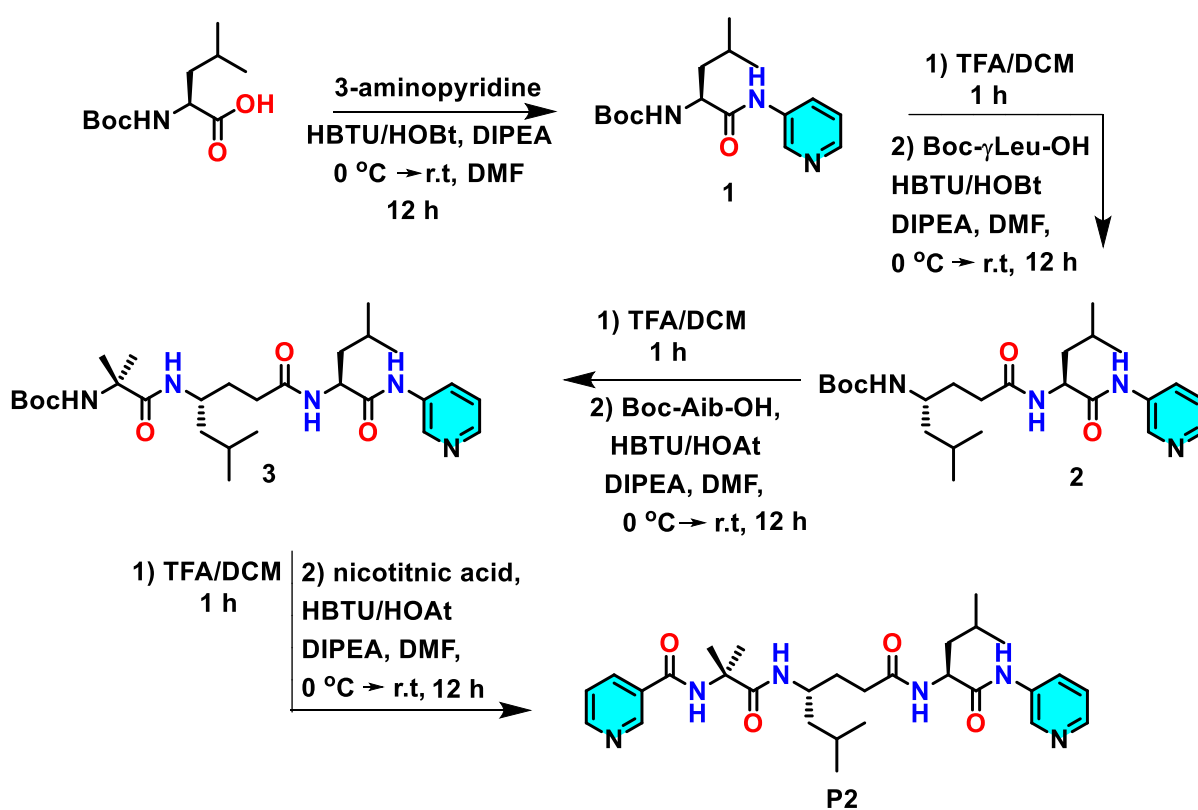
Boc-Aib-OH (3.7 mmol, 0.75 g) was taken in 6 mL of DMF and the solution was cooled down to 0 °C and kept in an N<sub>2</sub> atmosphere. HBTU (3.7 mmol, 1.41 g) and HOAt (3.7 mmol, 1.41 g) were added to the solution and the reaction mixture was stirred for 10 mins. After that, the free amine of dipeptide 2 was added to the reaction mixture and stirred for 12 h. Upon completion of the reaction monitored by TLC, the reaction mixture was diluted with 120 ml of ethyl acetate. Then, the mixture was washed with (100 mL X 2), 10% Na<sub>2</sub>CO<sub>3</sub> solution (100 mL X 2), and then NaCl solution (100 mL X 2). The organic layer was collected and dried with anhydrous Na<sub>2</sub>SO<sub>4</sub> and concentrated under reduced pressure. The crude product was purified by column chromatography to get tripeptide 3 as a white solid (Yield- 1.3 g, 66%).

Boc deprotection of tripeptide 3 (2.4 mmol, 1.3 g) was carried out by using 3 ml of each TFA and DCM (1:1) for 1 h. After that, TFA and solvent DCM were evaporated and 5-6 times DCM was added and evaporated to remove traces of TFA. The formed crude was TFA-salt of the amine of tripeptide C3 and to this 4 ml of DMF and 4 ml, of DIPEA were added to make it free amine of tripeptide 3.

Finally, isonicotinic acid (2.3 mmol, 0.283 g) dissolved in a mixture of 5 mL of DMF and 2 ml of DIPEA was added and the solution was cooled down to 0 °C and kept in an N<sub>2</sub> atmosphere. HBTU (2.3 mmol, 0.87 g) and HOAt (2.3 mmol, 0.32 g) were added to the solution and the reaction mixture was stirred for 10 mins. After that, the free amine of tripeptide 3 was added

to the reaction mixture and stirred for 12 h. Upon completion of the reaction monitored by TLC, the reaction mixture was diluted with 100 ml of ethyl acetate. Then, the mixture was washed with (100 mL X 2), 10% Na<sub>2</sub>CO<sub>3</sub> solution (100 mL X 2), and then NaCl solution (100 mL X 2). The organic layer was collected and dried with anhydrous Na<sub>2</sub>SO<sub>4</sub> and concentrated under reduced pressure. The crude product was purified by column chromatography to get peptide P1 as a white solid (Yield- 0.88 g, 71%).

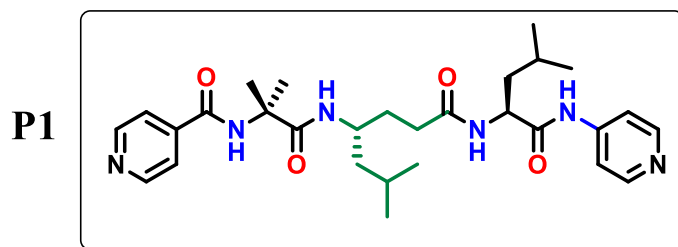
### 5.2.2. Synthesis of Peptide(P2):



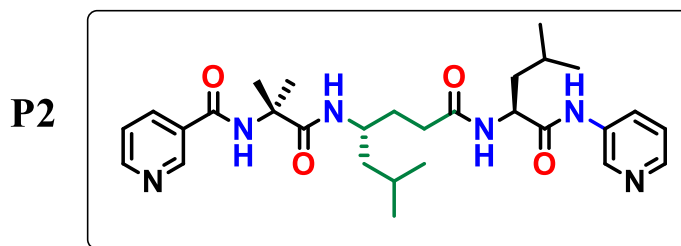
**Scheme 3:** Synthesis of short  $\alpha,\gamma$ -hybrid tripeptide **P2**.

The synthesis of **P2** was carried out as described in the above scheme, following similar protocols as of **P1** (Yield- 0.62 g, 68%).

### 5.3. Characterization of Peptides(P1-P2):



**Peptide P1:** White solid; yield 71%;  $^1\text{H}$  NMR (400 MHz, DMSO- $d_6$ )  $\delta$  10.32 (s, 1H), 8.54 (d,  $J = 5.4$  Hz, 2H), 8.30 (s, 2H), 8.25 (s, 1H), 7.89 – 7.83 (m, 1H), 7.69 (d,  $J = 5.8$  Hz, 2H), 7.63 – 7.53 (m, 2H), 7.18 (d,  $J = 12$  Hz, 1H), 4.19 (m, 1H), 4.02 (m, 1H), 2.56 (t,  $J = 12.7$  Hz, 1H), 2.30 – 2.12 (m, 2H), 1.94 – 1.88 (m, 1H), 1.84 (s, 3H), 1.72 (s, 3H), 1.69 (s, 3H), 1.58 (s, 3H), 0.89 (m, 6H), 0.85 – 0.79 (m, 6H).  $^{13}\text{C}$  NMR (100 MHz,  $\text{CDCl}_3$ )  $\delta$  174.97, 174.26, 173.86, 166.06, 150.21, 140.27, 121.20, 57.85, 46.03, 40.86, 27.03, 25.27, 24.74, 23.68, 23.16, 23.01, 22.66, 21.61. MALDI/TOF-TOF  $m/z$  calculated for  $\text{C}_{29}\text{H}_{42}\text{N}_6\text{O}_4$  [ $\text{M}+\text{K}^+$ ] is 577.29 and the observed peak is 577.44.



**Peptide P1:** White solid; yield 68%;  $^1\text{H}$  NMR (400 MHz,  $\text{CDCl}_3$ )  $\delta$  10.36 (s, 1H), 9.12 (d,  $J = 2.2$  Hz, 1H), 8.80 (d,  $J = 2.4$  Hz, 1H), 8.49 (s, 1H), 8.43 (dd,  $J = 4.7, 1.6$  Hz, 1H), 8.20 (dd,  $J = 4.7, 1.5$  Hz, 1H), 8.16 (dt,  $J = 8.1, 2.0$  Hz, 1H), 8.05 (s, 1H), 7.93 (dt,  $J = 8.3, 2.0$  Hz, 1H), 7.44 (d,  $J = 9.7$  Hz, 1H), 7.07 (dd,  $J = 8.0, 4.7$  Hz, 1H), 7.00 (dd,  $J = 8.4, 4.7$  Hz, 1H), 4.23 (dt,  $J = 10.0, 4.7$  Hz, 1H), 4.07 (d,  $J = 13.1$  Hz, 1H), 2.61 (t,  $J = 12.2$  Hz, 1H), 2.32 – 2.17 (m, 2H), 1.94 (dd,  $J = 13.4, 6.8$  Hz, 1H), 1.84 (s, 3H), 1.71 (s, 3H), 1.66 – 1.56 (m, 3H), 1.52 – 1.35 (m, 3H), 0.90 (dd,  $J = 13.4, 6.4$  Hz, 6H), 0.80 (dd,  $J = 8.9, 6.5$  Hz, 6H).  $^{13}\text{C}$  NMR (101 MHz,  $\text{CDCl}_3$ )  $\delta$  175.22, 174.55, 173.46, 166.21, 152.40, 149.12, 144.51, 142.10, 135.77, 135.18, 129.02, 127.02, 122.99, 57.87, 56.36, 46.40, 41.19, 32.33, 32.03, 27.22, 25.37, 24.91, 23.97, 23.44, 23.21, 22.67, 21.73. MALDI/TOF-TOF  $m/z$  calculated value for  $\text{C}_{29}\text{H}_{42}\text{N}_6\text{O}_4$  [ $\text{M}+\text{K}^+$ ] is 577.29 and the observed peak is 577.43.

## 6. Appendix:

### 6.1. Crystallographic Information:

Parameters	Peptide(P1)	Peptide(P2)	P1-ZnCl <sub>2</sub> complex	Nitromethane in P1-ZnCl <sub>2</sub> complex
Solvent for crystallization	aqueous methanol	aqueous methanol	H <sub>2</sub> O/MeOH (layering method)	CH <sub>3</sub> NO <sub>2</sub> addition in P1-ZnCl <sub>2</sub> complex
Chemical formula	C <sub>29</sub> H <sub>42</sub> N <sub>6</sub> O <sub>4</sub>	C <sub>29</sub> H <sub>42</sub> N <sub>6</sub> O <sub>4</sub>	C <sub>29</sub> H <sub>42</sub> Cl <sub>2</sub> N <sub>6</sub> O <sub>4</sub> Zn <sub>1</sub>	C <sub>30</sub> H <sub>45</sub> Cl <sub>2</sub> N <sub>7</sub> O <sub>6</sub> Zn <sub>1</sub>
Molecular weight	577.29	577.29	713.576	774.616
Crystal size (nm)	(0.18 × 0.11 × 0.16) mm	(0.14 × 0.12 × 0.18) mm	(0.18 × 0.12 × 0.14) mm	(0.16 × 0.11 × 0.12) mm
Radiation source	Cu Kα (λ = 1.54178 Å)	Mo Kα (λ = 0.71073 Å)	Cu Kα (λ = 1.54178 Å)	Mo Kα (λ = 0.71073 Å)
Space group	P 2 <sub>1</sub> (monoclinic)	P4 <sub>1</sub> 2 <sub>1</sub> 2 (tetragonal)	C222 <sub>1</sub> (orthorhombic)	C222 <sub>1</sub> (orthorhombic)
a (Å)	19.2036(5)	12.0364(19)	17.6578(5)	18.078(11)
b (Å)	17.0535(5)	12.0364(19)	23.1005(7)	23.500(14)
c (Å)	20.3429(5)	40.500(9)	20.6680(6)	20.411(12)
α (°)	90	90	90	90
β (°)	106.52	90	90	90
γ (°)	90	90	90	90
h <sub>max</sub>	22	16	21	25
k <sub>max</sub>	20	16	26	32
l <sub>max</sub>	24	54	24	23



Volume (Å <sup>3</sup> )	6387(3)	5867(2)	8430.6(4)	8671(9)
Z	2	8	8	8
Density (g/cm <sup>3</sup> )(cal)	1.170	1.220	1.064	1.128
Molecules in the asymmetric unit	4	1	1	2
F (000)	2414	2574	2832	3088
2θ Max. (°)	133.944	57.20	137.394	60.348
μ mm <sup>-1</sup>	0.669	0.083	2.245	0.731
Reflections (cal)	22763	7471	7798	12841
Variables	1484	358	387	423
R (reflections)	19873	4245	7151	9017
R <sub>factor</sub>	0.0795	0.0743	0.0261	0.0983
wR2 (Reflections)	0.2134	0.1900	0.0623	0.2158
Goodness-of- fit (S)	0.895	1.014	1.022	1.093
Software used	Bruker APEX(III)	Bruker APEX(III)	Bruker APEX(III)	Bruker APEX(III)
Method used	SHELXS-97 <sup>31</sup>	SHELXS-97 <sup>31</sup>	SHELXS-97 <sup>31</sup>	SHELXS-97 <sup>31</sup>
Special method used	SQUEEZE of program PLATON <sup>32</sup>	-	SQUEEZE of program PLATON <sup>32</sup>	SQUEEZE of program PLATON <sup>32</sup>

<b>Parameters</b>	<b>1,2-Dichloroethane in P1-ZnCl<sub>2</sub> complex</b>	<b>P1-CdI<sub>2</sub> Complex</b>	<b>P2-ZnCl<sub>2</sub> complex</b>	<b>P2-CdI<sub>2</sub> Complex</b>
Solvent for crystallization	1,2-Dichloroethane in P1-ZnCl <sub>2</sub> complex	H <sub>2</sub> O/MeOH (layering method)	H <sub>2</sub> O/MeOH/C <sub>6</sub> H <sub>6</sub> (layering method)	MeOH (complexation)
Chemical formula	C <sub>64</sub> H <sub>90</sub> Cl <sub>10</sub> N <sub>12</sub> O <sub>8</sub> Zn <sub>2</sub>	C <sub>29</sub> H <sub>42</sub> Cd <sub>1</sub> I <sub>2</sub> N <sub>6</sub> O <sub>4</sub>	C <sub>70</sub> H <sub>96</sub> Cl <sub>4</sub> N <sub>12</sub> O <sub>9</sub> Zn <sub>2</sub>	C <sub>29</sub> H <sub>41</sub> I <sub>2</sub> N <sub>6</sub> O <sub>4</sub> Cd <sub>1</sub>
Molecular weight	812.536	943.51	713.576	943.51
Crystal size (nm)	(0.14 × 0.10 × 0.12) mm	(0.20 × 0.14 × 0.16) mm	(0.16 × 0.10 × 0.12) mm	(0.12 × 0.10 × 0.10) mm
Radiation source	Mo K $\alpha$ ( $\lambda = 0.71073\text{\AA}$ )	Mo K $\alpha$ ( $\lambda = 0.71073\text{\AA}$ )	Mo K $\alpha$ ( $\lambda = 0.71073\text{\AA}$ )	Mo K $\alpha$ ( $\lambda = 0.71073\text{\AA}$ )
Space group	P2 <sub>1</sub> 2 <sub>1</sub> 2 <sub>1</sub> (orthorhombic)	P4 <sub>1</sub> 2 <sub>1</sub> 2 (tetragonal)	P4 <sub>1</sub> 2 <sub>1</sub> 2 (tetragonal)	Pca2 <sub>1</sub> (tetragonal)
a (Å)	18.1717(15)	13.8103(8)	12.1626(4)	17.103(2)
b (Å)	20.3789(17)	13.8103(8)	12.1626(4)	8.5730(1)
c (Å)	22.8754(18)	37.582(3)	52.103(3)	24.367(3)
$\alpha$ (°)	90	90	90	90
$\beta$ (°)	90	90	90	90
$\gamma$ (°)	90	90	90	90
h <sub>max</sub>	24	18	16	22
k <sub>max</sub>	27	18	16	11
l <sub>max</sub>	30	50	69	32
Volume (Å <sup>3</sup> )	8471.2(12)	7167.8(10)	7707.5(7)	3572.8(6)
Z	4	8	4	4
Density (g/cm <sup>3</sup> )(cal)	1.286	1.677	1.312	1.680
Molecules in asymmetric unit	1	1	1	1

F (000)	3408	3552	3200	1772
2 $\theta$ Max. (°)	56.816	56.816	56.782	56.816
$\mu$ mm <sup>-1</sup>	0.934	2.371	0.821	2.379
Reflections (cal)	21298	9028	9675	8997
Variables	860	386	444	385
R (reflections)	14797	8883	7958	7269
R <sub>factor</sub>	0.1210	0.0237	0.1266	0.0488
wR2 (Reflections)	0.2609	0.0544	1.074	0.1069
Goodness-of- fit (S)	1.119	0.485	1.074	1.029
Software used	Bruker APEX(III)	Bruker APEX(III)	Bruker APEX(III)	Bruker APEX(III)
Method used	SHELXS-97 <sup>31</sup>	SHELXS-97 <sup>31</sup>	SHELXS-97 <sup>31</sup>	SHELXS-97 <sup>31</sup>
Special method used	SQUEEZE of program PLATON <sup>32</sup>	-	-	-

## 7. References:

- (a) Zhou, H.-C.; Long, J. R.; Yaghi, O. M. *Chem. Rev.* **2012**, *112*, 673. (b) Furukawa, H.; Cordova, K. E.; Keffe, M. O.; Yaghi, O. M. *Science*, **2013**, *341*, 1230444; (c) Zhou, H. -C.; Kitagawa, S. *Chem. Soc. Rev.* **2014**, *43*, 5415. (d) Bloch, E. D.; Queen, W. L.; Krishna, R.; Zadrozny, J. M.; Brown, C. M.; Long, J. R. *Science*, **2012**, *335*, 1606. (e) Bailey, J. B.; Tezcan, A. F. *J. Am. Chem. Soc.* **2020**, *142*, 17265. (f) Churchfield, L. A.; Tezcan, A. F. *Acc. Chem. Res.* **2019**, *52*, 345. (g) McConnell, A. J.; Wood, C. S.; Neelakandan, P. P.; Nitschke, J. R. *Chem. Rev.* **2015**, *115*, 7729. (h) Zhang, D.; Ronson, T. K.; Nitschke, J. R. *Acc. Chem. Res.* **2018**, *51*, 2423. (i) Pullen, S.; Clever, G. H. *Acc. Chem. Res.* **2018**, *51*, 3052.
- (a) Lu, Y.; Yeung, N.; Sieracki, N.; Marshall, N. M. *Nature*, **2009**, *460*, 855. (b) Valdez, C. E.; Smith, Q. A.; Nechay, M. R.; Alexandrova, A. N. *Acc. Chem. Res.* **2014**, *47*, 3110. (c) Waldron, K. L.; Rutherford, J. C.; Ford, D.; Robinson, N. J. *Nature*, **2009**, *460*, 823. (d) Andreini, C.; Bertini, I.; Cavallaro, G.; Holliday, G. L.; Thornton, J. M. *J. Biol. Inorg. Chem.* **2008**, *13*, 1205.

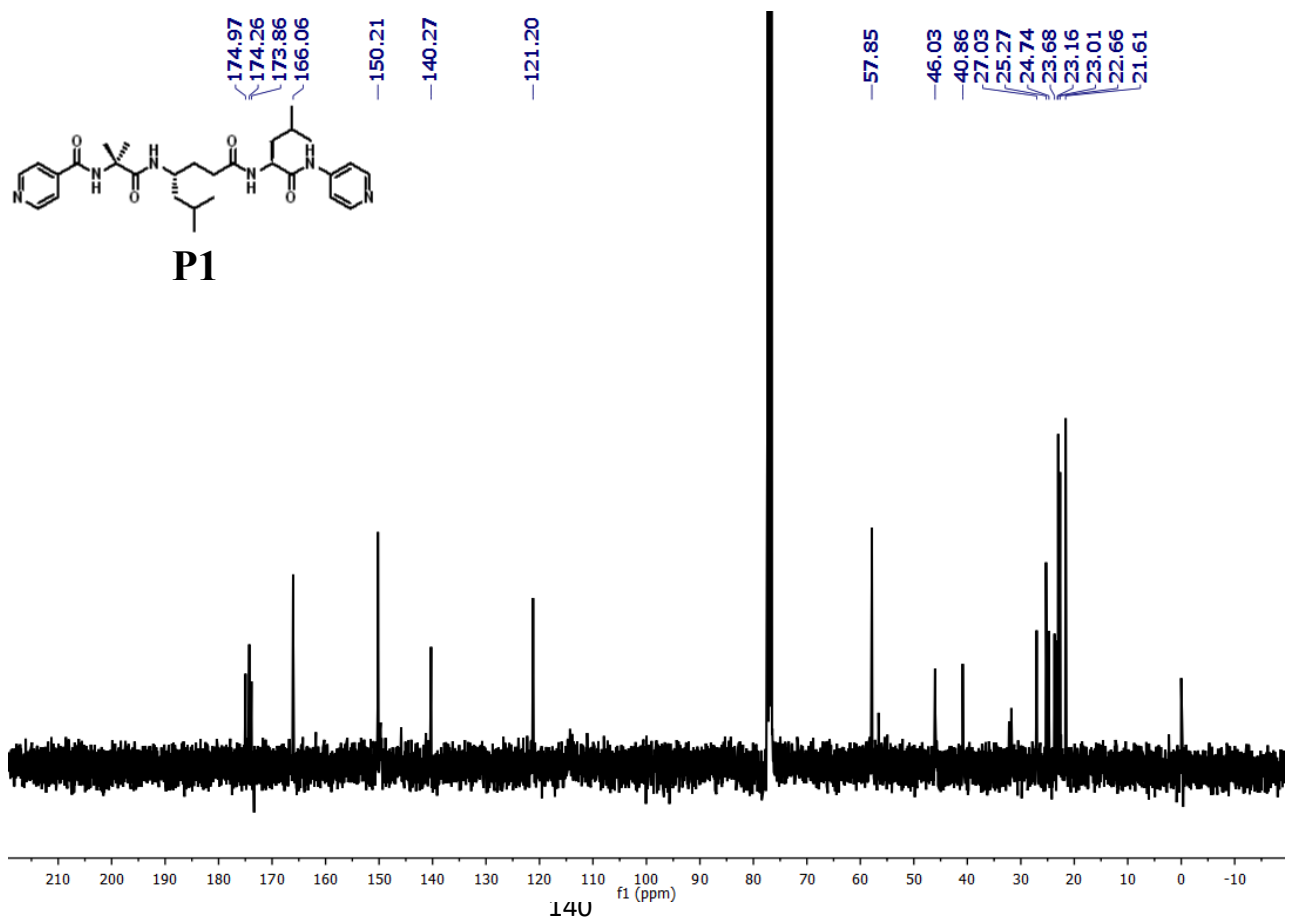
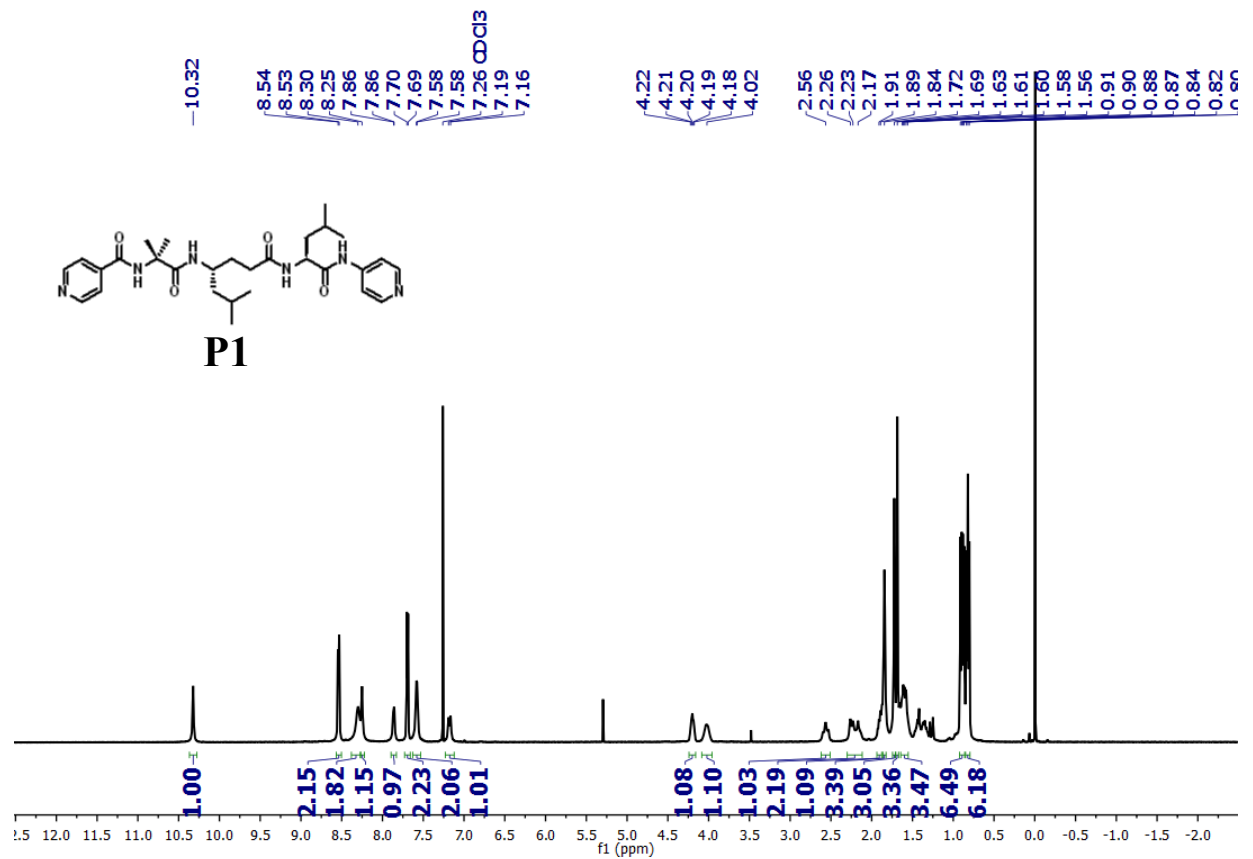
3. (a) Ghosh, T.; Fridman, N.; Kosa, M.; Maayan, G. *Angew. Chem. Int. Ed.* **2018**, *57*, 7703. (b) Zou, R.; Wang, Q.; Wu, J.; Wu, J.; Schmuck, C.; Tian, H. *Chem. Soc. Rev.* **2015**, *44*, 5200. (c) Tashiro, S.; Shionoya, M. *Chem. Lett.* **2013**, *42*, 456. (d) Ousaka, N.; Takeyama, Y.; Iida, H.; Yashima, E. *Nat. Chem.* **2011**, *3*, 856. (e) Albrecht, M.; Stortz, P.; Engeser, M.; Schalley, C. A. *Synlett*, **2004**, 2821. (f) Solà, J.; Bolte, M.; Alfonso, I. *CrystEngComm*, **2016**, *18*, 3793.
4. (a) Sawada, T.; Matsumoto, A.; Fujita, M. *Angew. Chem. Int. Ed.* **2014**, *53*, 7228. (b) Sawada, T.; Yamagami, M.; Akinaga, S.; Miyaji, T.; Fujita, M. *Chem. Asian J.* **2017**, *12*, 1715. (c) Inomata, Y.; Sawada, T.; Fujita, M. *Chem* **2020**, *6*, 294. (d) Sawada, T.; Fujita, M. *Chem* **2020**, *6*, 1861. (e) Sawada, T.; Iwasaki, W.; Yamagami, M.; Fujita, M. *Nat. Sci.* **2021**, *1*.
5. (a) Przybyla, D. E.; Chmielewski, J. *J. Am. Chem. Soc.* **2008**, *130*, 12610. (b) Nepal, M.; Sheedlo, M. J.; Das, C.; Chmielewski, J. *J. Am. Chem. Soc.* **2016**, *138*, 11051. (c) Pires, M. M.; Chmielewski, J. *J. Am. Chem. Soc.* **2009**, *131*, 2706. (d) Przybyla, D.; Chmielewski, J. *J. Am. Chem. Soc.* **2010**, *132*, 7866.
6. (a) Dublin, S. N.; Conticello, V. P. *J. Am. Chem. Soc.* **2008**, *130*, 49. (b) Anzini, P.; Xu, C.; Hughes, S.; Magnotti, E.; Jiang, T.; Hemmingsen, L.; Demeler, B.; Conticello, V. *J. Am. Chem. Soc.* **2013**, *135*, 10278.
7. (a) Tavenor, N. A.; Murnin, M. J.; Horne, W. S. *J. Am. Chem. Soc.* **2017**, *139*, 2212. (b) Scheib, K. A.; Tavenor, N. A.; Lawless, M. J.; Saxena, S.; Horne, W. S. *Chem Commun.* **2019**, *55*, 7752. (c) Rao, S. R.; Schettler, S. L.; Horne, W. S. *ChemPlusChem* **2021**, *86*, 137.
8. Micklitsch, C. M.; Knerr, P. J.; Branco, M. C.; Nagarkar, R.; Pochan, D. J.; Schneider, J. P. *Angew. Chem. Int. Ed.* **2011**, *50*, 1577.
9. (a) De Leon-Rodriguez, L. M.; Hemar, Y.; Mitra, A. K.; Brimble, M. A. *Biomater. Sci.* **2017**, *5*, 1993. (b) Wang, J.; Zhang, L.; Yang, J.; Yan, H.; Li, X.; Wang, C.; Wang, D.; Sun, Y.; Xu, H. *Langmuir* **2019**, *35*, 5617. (c) Wang, J.; Wang, C.; Ge, Y.; Sun, Y.; Wang, D.; Xu, H. *Peptide Science.* **2021**, *113*, e24208.
10. (a) Rabone, J.; Yue, Y.-F.; Chong, S. Y.; Stylianou, K. C.; Bacsá, J.; Bradshaw, D.; Darling, G. R.; Berry, N. G.; Khimyak, Y. Z.; Ganin, A. Y.; Wiper, P.; Claridge, J. B.; Rosseinsky, M. J. *Science*, **2010**, *329*, 1053. (b) Martí-Gastaldo, C.; Antypov, D.; Warren, J. E.; Briggs, M. E.; Chater, P. A.; Wiper, P. V.; Miller, G. J.; Khimyak, Y. Z.; Darling, G. R.; Berry, N. G.; Rosseinsky, M. J. *Nat. Chem.* **2014**, *6*, 343. (c) Navarro-Sánchez, J.; Argente-García, A. I.; Moliner-Martínez, Y.; Roca-Sanjuán, D.; Antypov,

- D.; Campíns-Falcó, P.; Rosseinsky, M. J.; Martí-Gastaldo, C. *J. Am. Chem. Soc.* **2017**, *139*, 4294. (d) Katsoulidis, A. P.; Antypov, D.; Whitehead, G. F. S.; Carrington, E. J.; Adams, D. J.; Berry, N. G.; Darling, G. R.; Dyer, M. S.; Rosseinsky, M. J. *Nature*, **2019**, *565*, 213.
11. (a) Miyake, R.; Tashiro, S.; Shiro, M.; Tanaka, K.; Shionoya, M. *J. Am. Chem. Soc.* **2008**, *130*, 5646. (b) Miyake, R.; Shionoya, M. *Inorg. Chem.* **2014**, *53*, 5717. (c) Miyake, R.; Shionoya, M. *Chem. Commun.* **2012**, *48*, 7553.
12. Miyake, R.; Ando, A.; Ueno, M.; Muraoka, T. *J. Am. Chem. Soc.* **2019**, *141*, 8675.
13. Jeong, S.; Zhang, L.; Kim, J.; Gong, J.; Choi, J.; Ok, K. M.; Lee, Y.; Kwon, S.; Lee, H.-S. *Angew. Chem. Int. Ed.* **2022**, *61*, e202108364.
14. (a) Ghosh, P.; Maayan, G. *Chem. Sci.*, **2020**, *11*, 10127. (b) Ghosh, P.; Fridman, N.; Maayan, G. *Chem. Eur. J.* **2021**, *27*, 634. (c) Ghosh, P.; Maayan, G. *Chem. Eur. J.* **2021**, *27*, 138. (d) Baskin, M.; Zhu, H.; Qu, Z.-W.; Chill, J. H.; Grimme, S.; Maayan, G. *Chem. Sci.*, **2019**, *10*, 620. (e) Ruan, G.; Ghosh, P.; Fridman, N.; Maayan, G. *J. Am. Chem. Soc.* **2021**, *143*, 10614.
15. (a) Kusumoto, Y.; Lomakin, A.; Teplow, D. B.; Benedek, G. B. *Proc. Natl. Acad. Sci. U. S. A.* **1998**, *95*, 12277. (b) Verel, R.; Tomka, I. T.; Bertozzi, C.; Cadalbert, R.; Kammerer, R. A.; Steinmetz, M. O.; Meier, B. H. *Angew. Chem. Int. Ed.* **2008**, *47*, 5842.
16. (a) Zimenkov, Y.; Dublin, S. N.; Ni, R.; Tu, R. S.; Breedveld, V.; Apkarian, R. P.; Conticello, V. P. *J. Am. Chem. Soc.* **2006**, *128*, 6770. (b) Ozbas, B.; Kretsinger, J.; Rajagopal, K.; Schneider, J. P.; Pochan, D. J. *Macromolecules* **2004**, *37*, 7331.
17. (a) Wang, F.; Feng, C. L. *Angew. Chem. Int. Ed.* **2018**, *57*, 5655. (b) Ramadan, D.; Cline, D. J.; Bai, S.; Thorpe, C.; Schneider, J. P. *J. Am. Chem. Soc.* **2007**, *129*, 2981. (c) Ji, W.; Yuan, C.; Tal, S. Z.; Xing, R.; Chakraborty, P.; Tao, K.; Gilead, S.; Yan, X.; Gazit, E. *ACS Nano*. **2019**, *13*, 7300.
18. (a) Li, J.; Du, X. W.; Hashim, S.; Shy, A.; Xu, B. *J. Am. Chem. Soc.* **2017**, *139*, 71. (b) Li, J.; Zhan, Z.; Du, X.; Wang, J.; Hong, B.; Xu, B. *Angew. Chem. Int. Ed.* **2018**, *57*, 11716.
19. (a) Levin, A.; Hakala, T. A.; Schnaider, L.; Bernardes, G. J. L.; Gazit, E.; Knowles, T. P. J. *Nat. Chem. Rev.* **2020**, *4*, 615. (b) Cui, H.; Webber, M. J.; Stupp, S. I. *Pept. Sci.* **2010**, *94*, 1.
20. (a) Li, G.; Yu, W.; Cui, Y. *J. Am. Chem. Soc.* **2008**, *130*, 458. (b) Das, M. C.; Guo, Q.; He, Y.; Kim, J.; Zhao, C.-G.; Hong, K.; Xiang, S.; Zhang, Z.; Thomas, K. M.; Krishna,

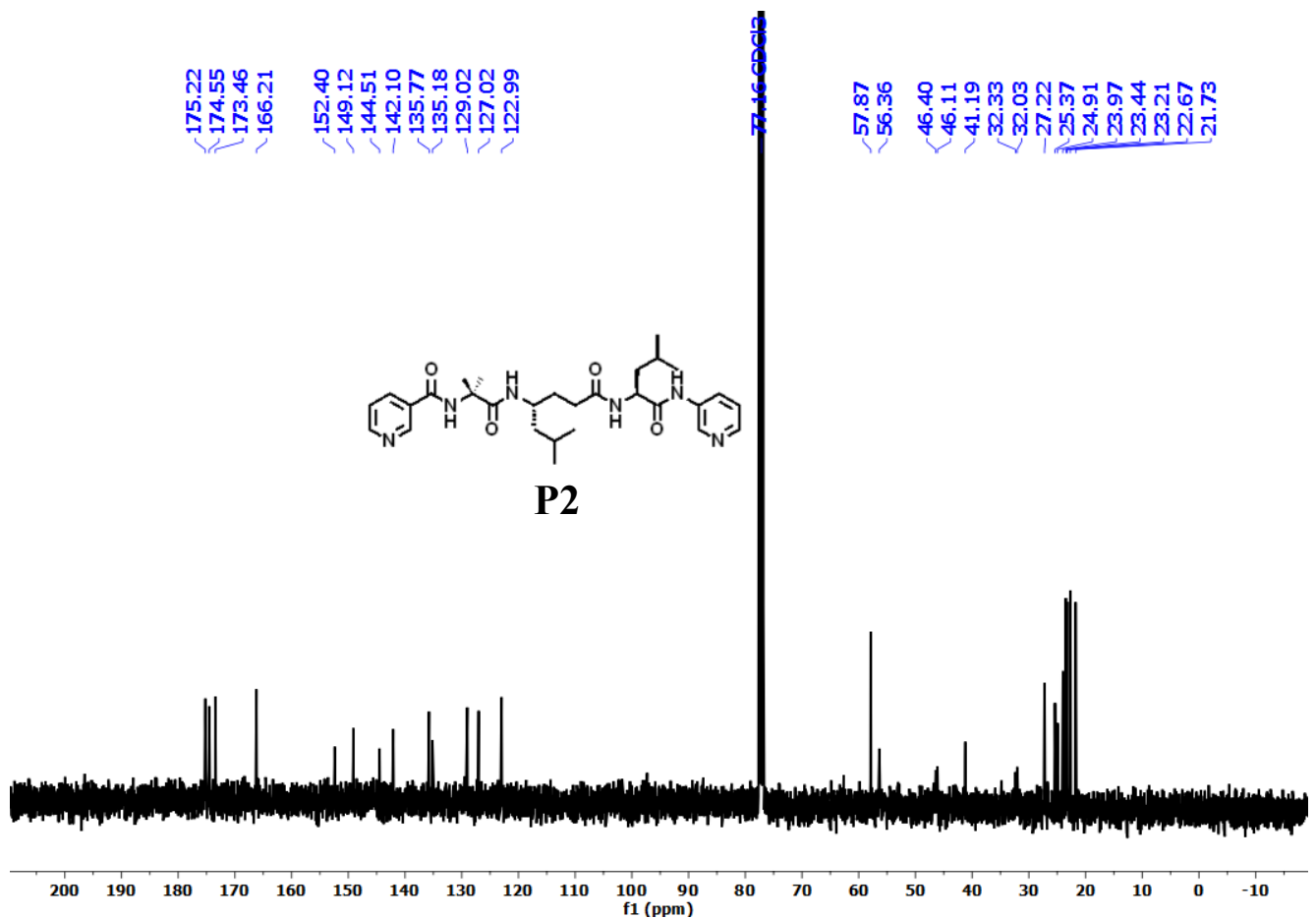
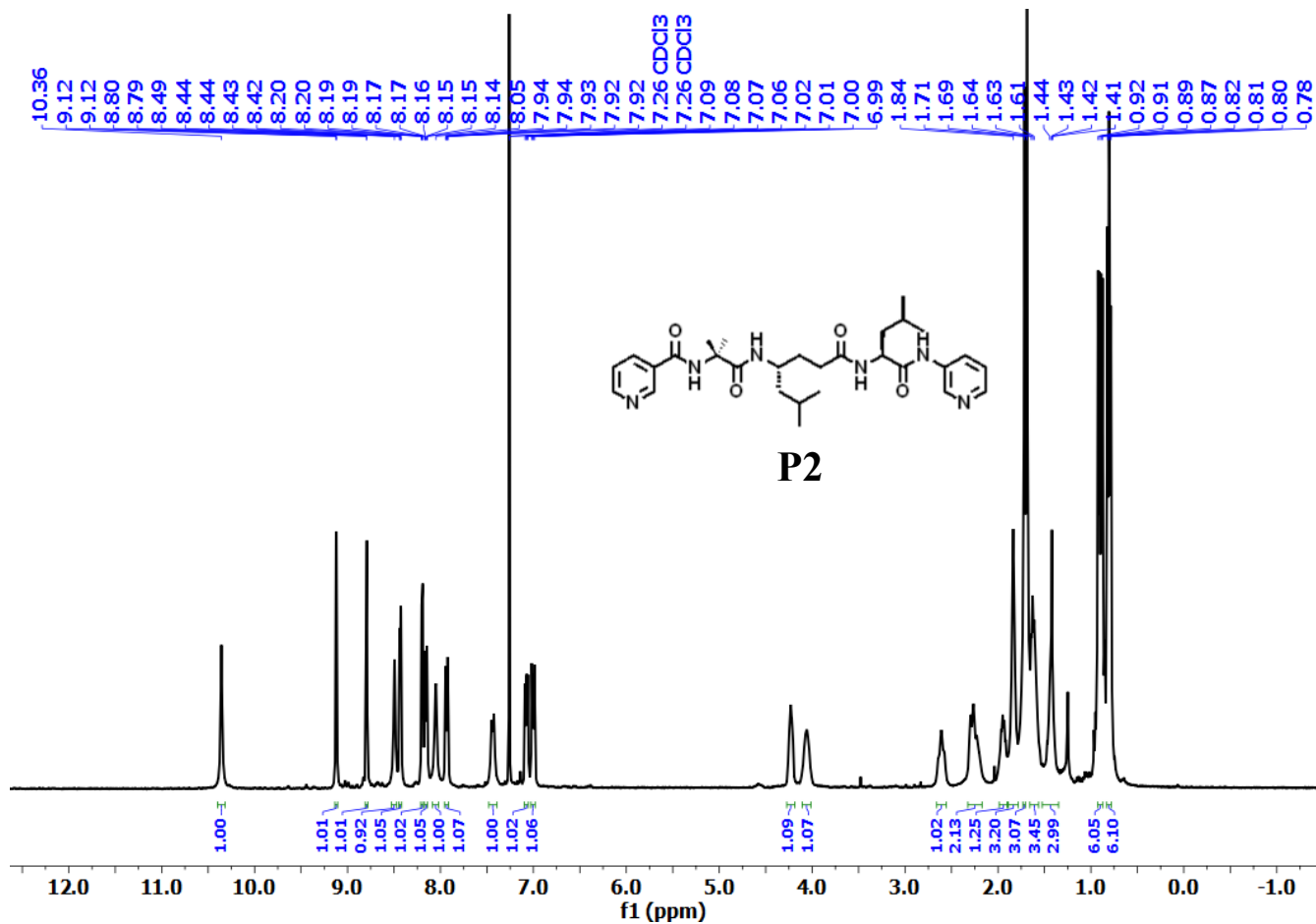
- R.; Chen, B. *J. Am. Chem. Soc.* **2012**, *134*, 8703. (c) Jiao, J.; Tan, C.; Li, Z.; Liu, Y.; Han, X.; Cui, Y. *J. Am. Chem. Soc.* **2018**, *140*, 2251. (d) Ma, L.; Falkowski, J. M.; Abney, C.; Lin, W. *Nat. Chem.* **2010**, *2*, 838. (e) Han, Z.; Wang, K.; Guo, Y.; Chen, W.; Zhang, J.; Zhang, X.; Siligardi, G.; Yang, S.; Zhou, Z.; Sun, P.; Shi, W.; Cheng, P. *Nat. Commun.* **2019**, *10*, 5117. (f) Dong, J.; Zhou, Y.; Zhang, F.; Cui, Y. *Chem. - Eur. J.* **2014**, *20*, 6455. (g) Zhao, T.; Han, J.; Jin, X.; Liu, Y.; Liu, M.; Duan, P. *Angew. Chem., Int. Ed.* **2019**, *58*, 4978. (h) Wang, X.-Z.; Sun, M.-Y.; Huang, Z.; Xie, M.; Huang, R.; Lu, H.; Zhao, Z.; Zhou, X.-P.; Li, D. *Adv. Opt. Mater.* **2021**, 2002096.
21. (a) Bandyopadhyay, A.; Gopi, H. N. *Org. Lett.* **2012**, *14*, 2770. (b) Jadhav, S. V.; Bandyopadhyay, A.; Gopi, H. N. *Org. Biomol. Chem.* **2013**, *11*, 509. (c) Veeresh, K.; Gopi, H. N. *Organic Letters.* **2019**, *21*, 4500. (d) Bandyopadhyay, A.; Jadhav, S. V.; Gopi, H. N. *Chem. Commun.* **2012**, *48*, 7170. (e) Jadhav, S. V.; Bandyopadhyay, A.; Gopi, H. N. *Org. Biomol. Chem.* **2013**, *11*, 509. (f) Misra, R.; Saseendran, A.; George, G.; K. Veeresh, K.; Raja, K. M. P.; Raghothama, S.; Hofmann, H.-J.; Gopi, H. N. *Chem. Eur. J.* **2017**, *23*, 3764.
22. (a) Baldauf, C.; Günther, R.; Hofmann, H. -J. *J. Org. Chem.* **2006**, *71*, 1200. (b) Sonti, R.; Dinesh, B.; Basuroy, K.; Raghothama, S.; Shamala, N.; Balaram, P. *Org. Lett.* **2014**, *16*, 1656. (c) Fisher, B. F.; Gellman, S. H. *J. Am. Chem. Soc.* **2016**, *138*, 10766. (d) Guo, L.; Chi, Y. G.; Almeida, A. M.; Guzei, I. A.; Parker, B. K.; Gellman, S. H. *J. Am. Chem. Soc.* **2009**, *131*, 16018.
23. (a) Misra, R.; Saseendran, A.; Dey, S.; Gopi, H. N. *Angew. Chem. Int. Ed.* **2019**, *58*, 2251. (b) Dey, S.; Misra, R.; Saseendran, A.; Pahan, S.; Gopi, H. N. *Angew. Chem. Int. Ed.* **2021**, *60*, 9863.
24. Cook, T. R.; Zheng, Y.-R.; Stang, P. J. *Chem. Rev.* **2013**, *113*, 734.
25. Venkatraman, J.; Shankaramma, S. C.; Balaram, P. *Chem. Rev.* **2001**, *101*, 3131.
26. (a) Li, J.-R.; Sculley, J.; Zhou, H.-C. *Chem. Rev.* **2012**, *112*, 869. (b) Lin, R.-B.; Xiang, S.; Zhou, W.; Chen, B. *Chem.* **2020**, *6*, 337. (c) Wang, Y.; Jin, H.; Ma, Q.; Mo, K.; Mao, H.; Feldhoff, A.; Cao, X.; Li, Y.; Pan, F.; Jiang, Z. *Angew. Chem. Int. Ed.* **2020**, *59*, 4365. (d) Li, X.; Liu, Y.; Wang, J.; Gascon, J.; Li, J.; Van der Bruggen, B. *Chem. Soc. Rev.* **2017**, *46*, 7124. (e) Lee, J. Y.; Farha, O. K.; Roberts, J.; Scheidt, K. A.; Nguyen, S. B. T.; Hupp, J. T. *Chem. Soc. Rev.* **2009**, *38*, 1450.
27. (a) Adzhubei, A.; Sternberg, M. J. E.; Makarov, A. A. *J. Mol. Biol.* **2013**, *425*, 2100. (b) Brown, A. M.; Zondlo, N. J. *Biochemistry* **2012**, *51*, 5041.

28. (a) Arold, S. T.; Leonard, P. G.; Parkinson, G. N.; Ladbury, J. E. *Prod. Natl. Acad. Sci. U. S. A.* **2010**, *107*, 15728. (b) Wang, Y.; Dutta, S.; Karlberg, H.; Devignot, S.; Weber, F.; Hao, Q.; Tan, Y. J.; Mirazimi, A.; Kotaka, M. *J. Virol.* **2012**, *86*, 12294. (c) Li, F.; Li, X. H.; Wang, Y.; Zhang, X. *Angew. Chem. Int. Ed.* **2019**, *58*, 17994. (d) Hifsudheen, M.; Mishra, R. K.; Vedhanarayanan, B.; Praveen, V. K.; Ajayaghosh, A. *Angew. Chem. Int. Ed.* **2017**, *56*, 12634.
29. (a) Meunier, A.; Singleton, M. L.; Kauffmann, B.; Granier, T.; Lautrette, G.; Ferrand, Y.; Huc, I. *Chem. Sci.* **2020**, *11*, 12178. (b) Mateus, P.; Wicher, B.; Ferrand, Y.; Huc, I. *Chem. Commun.* **2017**, *53*, 9300. (c) Yashima, E.; Ousaka, N.; Taura, D.; Shimomura, K.; Ikai, T.; Maeda, K. *Chem. Rev.* **2016**, *116*, 13752.
30. Hema, K.; Sureshan, K. M. *Angew. Chem. Int. Ed.* **2020**, *59*, 8854.
31. Sheldrick, G. M. *Acta Crystallography. Sect A.* **1990**, *46*, 467.
32. Spek, A. L. *Acta Crystallogr.* **1990**, *A46*, C34.

## 8. $^1\text{H}$ , $^{13}\text{C}$ NMR and Mass Spectra of Peptides (P1-P2):

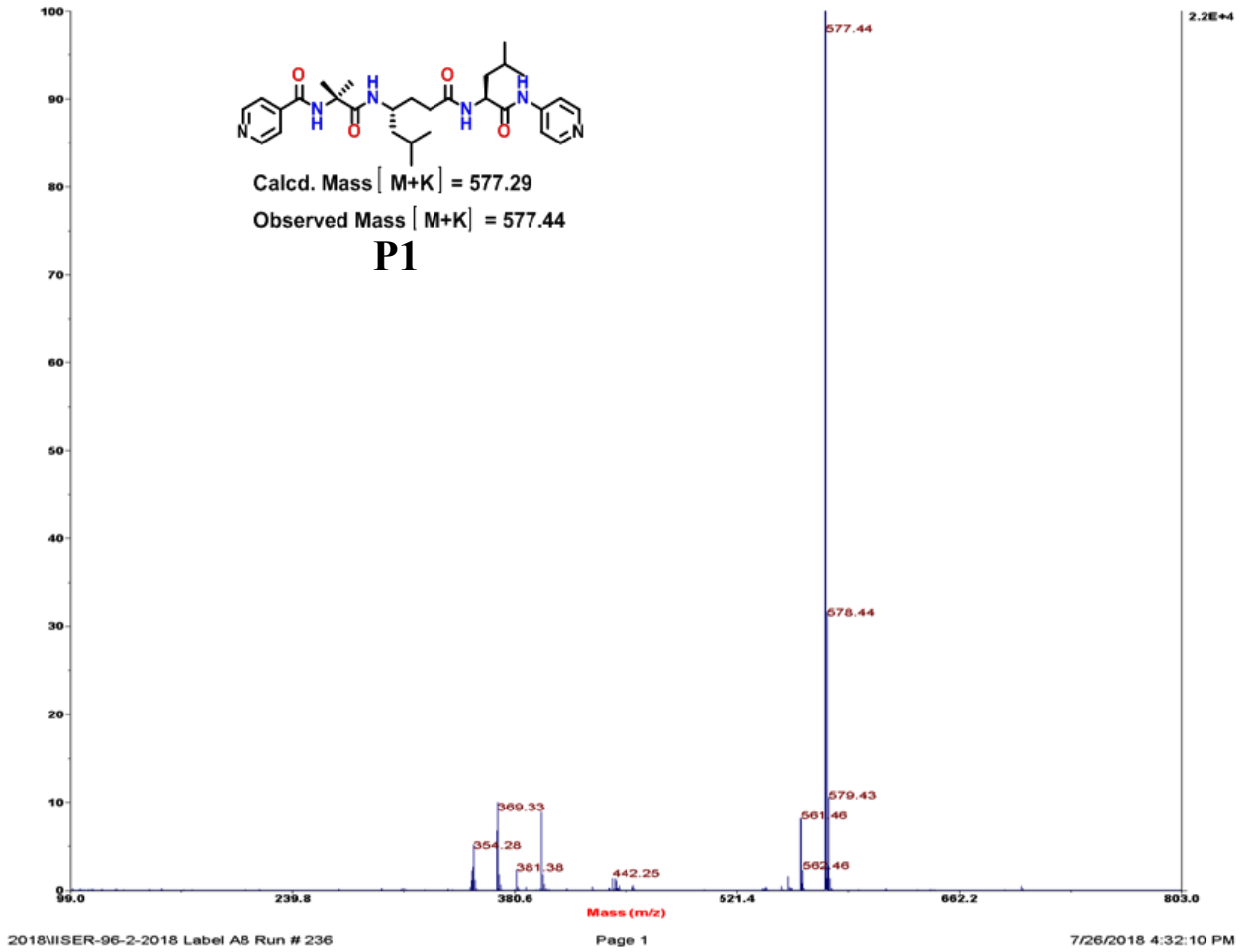






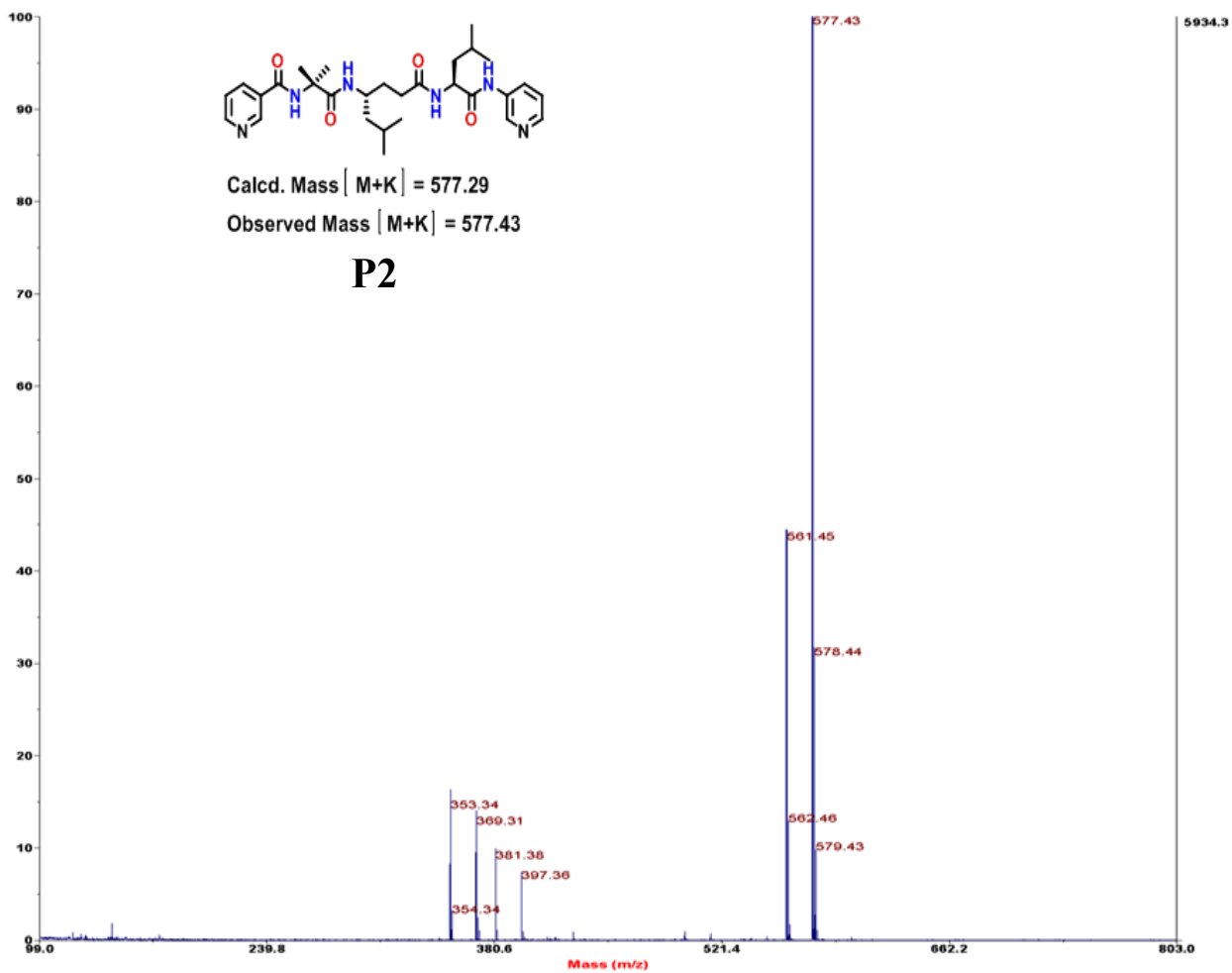
# Spectrum Report

Final - Shots 400 - IISER-96-2-2018; Run #236; Label A8



# Spectrum Report

Final - Shots 400 - IISER-96-2-2018; Run #236; Label A7



2018IISER-96-2-2018 Label A7 Run # 236

Page 1

7/26/2018 4:31:56 PM

## *Chapter 4*

### *Metal Coordinated Supramolecular Polymers from the Minimalistic Hybrid Peptide Foldamers*

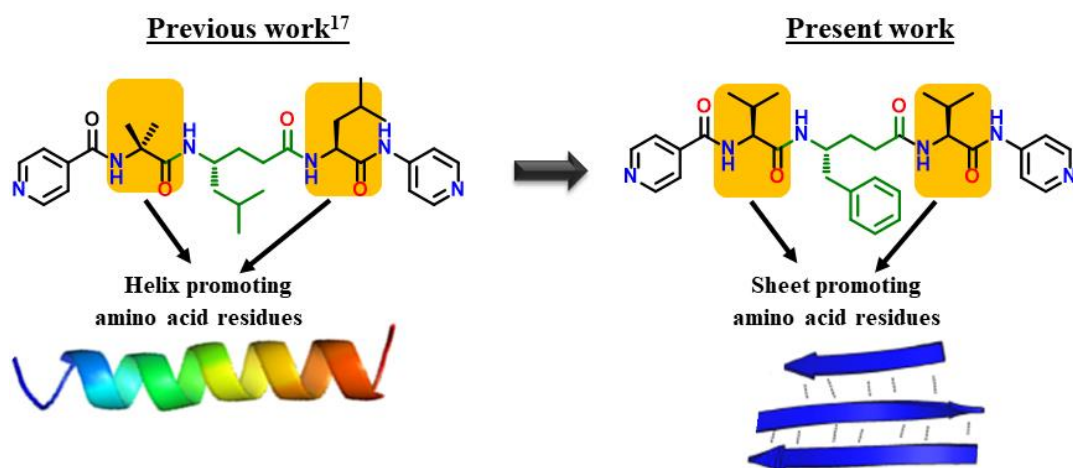
## 1. Introduction:

Supramolecular polymers in the form of Gels are cross-linked polymeric materials having properties ranging from soft and weak to hard. In 1926, Jordan-Lloyd stated that “the colloidal condition, the gel, is easier to recognize than to define”<sup>1</sup>. Based on the nature of the interaction of the components present in the gel matrix, can be classified as (1) chemical gel which is covalent bond interaction at crosslink junction and (2) supramolecular gel which is supramolecular interaction at crosslink junction. Supramolecular metallogels are the mixed combination of metal ion and gelator as a ligand which forms a coordinate bonding interaction between metal-ligand. Along with this, various non-covalent types interactions like H-bonding, hydrophobic interactions, and stacking can drive gelator molecules to produce an effective three-dimensional coordination network.<sup>2</sup> Supramolecular metallogels have been widely used for physical/chemical stimuli response, phosphorescent behavior, catalysis, redox responsive properties, and much more versatile applications<sup>3</sup>. Recently, extensive studies have been carried out to develop various multifunctional types of supramolecular metallogel depending on the metal ions and low-molecular-weight gelators (LMWGs) being used.<sup>4</sup> Irrespective of metal ions being used in metallogel, the choice of gelators can control overall the formation of metallogel and their coordination network. A large number of organic ligands, amino acids, and peptides are developed as good candidates for the gelators,<sup>5</sup> however helical peptide-based gelators are rarely examined in the literature. This is because availing the peptide folded architectures to design metal-coordinated supramolecular networks is restricted due to the scarcity of readily accessible short and stable secondary structures. The secondary structures,  $\alpha$ -helix, and  $\beta$ -sheets, play significant roles in stabilizing tertiary folds of proteins. Designing such helical structures from the short sequences of peptides without having any steric restrictions is exceptionally challenging. The structural complexity associated with a wide range of specific functional activities of proteins is always an inspiration to create synthetic mimics using natural and unnatural building blocks.<sup>6</sup> Metal ions also play a crucial role in controlling the structure and biological activity of many proteins.<sup>7</sup> Along with the design of metalloproteins, considerable efforts have also been made in the literature over the last few decades to understand the metal-coordinated supramolecular assembly of proteins<sup>8</sup> and peptides.<sup>9</sup> Metal-triggered supramolecular assembly of peptides and proteins offers a promising platform for the creation of multifunctional materials. Along with the metal binding, natural amino acids such as His, Cys, Glu, Asp, etc, a variety of artificial ligands have been

explored to design ordered supramolecular assemblies from short peptides.<sup>9a,9b,9d</sup> In addition, peptide coiled-coils<sup>10</sup> and collagen triple helices<sup>11</sup> incorporated with metal binding ligands have been designed and studied. However, the short and structured peptides have not been well explored in the literature to construct metal-mediated supramolecular architectures. The main reason for not using structured peptides in the construction of metal-mediated supramolecular assembly is that it is difficult to design protein secondary structures from the short peptide sequences without using any steric constraints. Nevertheless, various short peptides without regular secondary structures have been shown to adopt a variety of porous as well as knotted networks in the presence of metal ions.<sup>12</sup> These short peptides are entangled to form cage-like structures.

## 2. Object of the Present Work:

The metal ions which play a pivotal role in many proteins directly form metal-ligand coordination in the active site of the protein. Over the periods, attempts are made to mimic many metalloproteins and metalloenzymes. The key aspect is the design principle of protein by the choice of amino acid residues and metal-ligand coordination. In addition to naturally occurring amino acid residues, there are several artificial metal binding ligands have been explored to design ordered supramolecular assemblies in combination with amino acids and peptides.<sup>9a</sup> The synthetic oligomers derived from non-natural  $\beta$ - and  $\gamma$ -amino acid building blocks are known to form well-defined structures, similar to those found in the protein structures, and offer new openings to create self-assembled architectures.<sup>6</sup> Along with the homo-oligomers, hybrid peptides derived from mixed sequences  $(\alpha\beta)_n$ ,<sup>13</sup>  $(\alpha\gamma)_n$ ,<sup>14</sup> and  $(\beta\gamma)_n$ <sup>15</sup> have expanded the structural and functional catalog of foldamer architectures. We<sup>16</sup> and others<sup>14</sup> demonstrated the stable 12-helical secondary structures from  $\alpha,\gamma$ -hybrid peptides even in short sequences. Recently, we reported the metal-helix frameworks using short  $\alpha,\gamma$ -tripeptide 12-helices consisting of terminal pyridines and helix-promoting Aib residues in the sequence.<sup>17</sup> We hypothesized that the greater helical propensity of  $\gamma$ -amino acids can be explored to design  $\alpha,\gamma$ -hybrid peptide 12-helices with as short as three residues without having steric constraints, and these short helices with suitable metal coordinating ligands can be explored to construct supramolecular materials. To examine the possibilities of creating new metal-coordinated

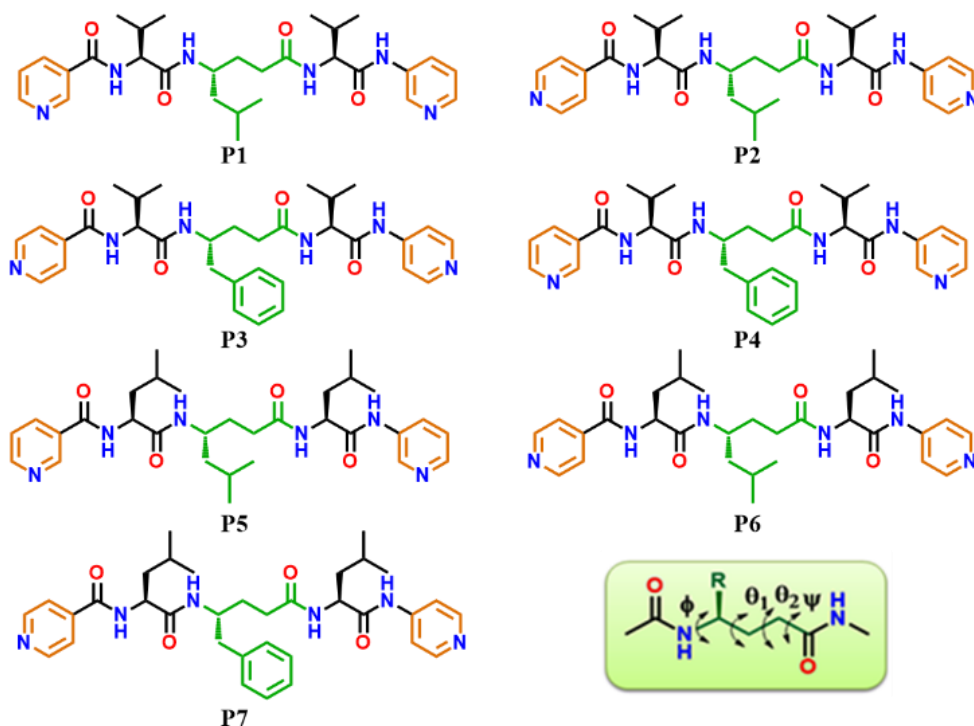


polymers of short and structured peptides, we have designed seven hybrid tripeptides with the choice of amino acid residues, and the peptide sequences are shown in Scheme 1.

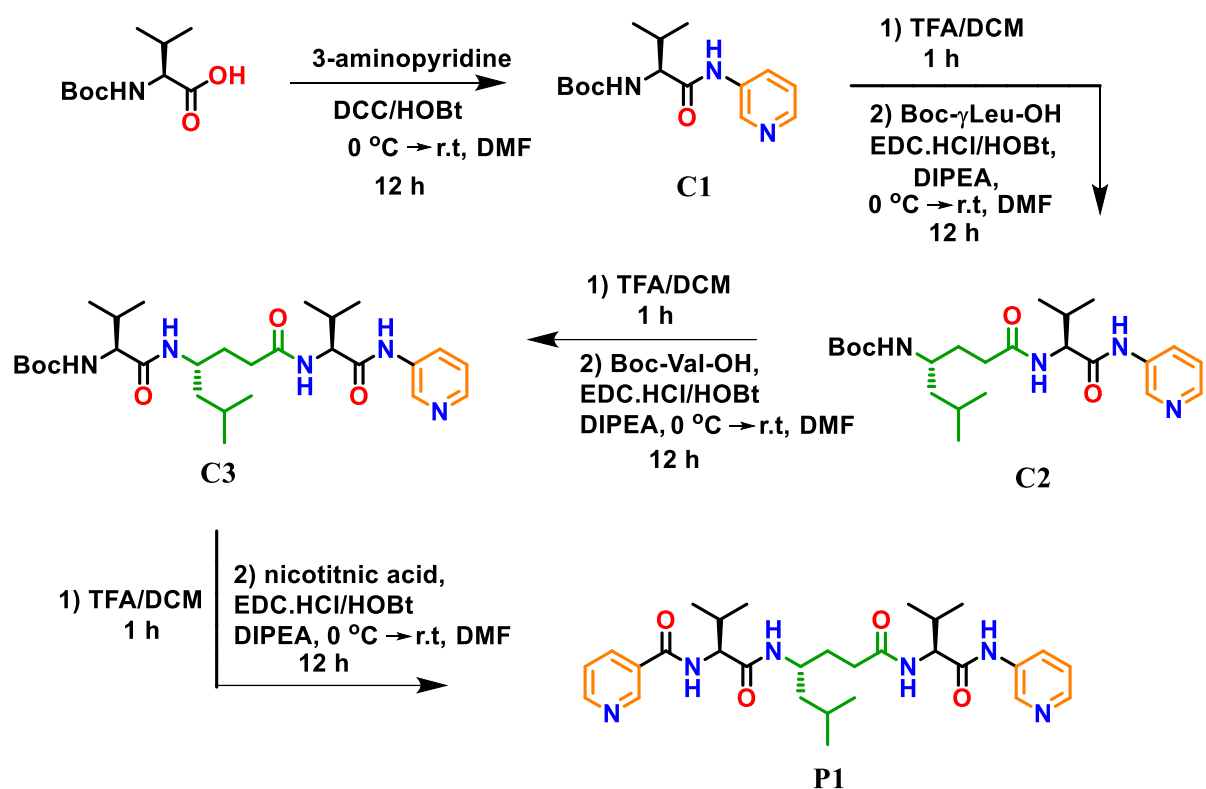
### 3. Results and Discussion:

#### 3.1. Design and Synthesis of Peptides P1-P7:

To understand the effect of amino acid residues in the short tripeptides sequence and also to examine the possibilities of creating new metal-coordinated polymers, we have designed seven hybrid tripeptides and the sequences of these peptides are shown in Scheme 1.



**Scheme 1:** Sequences of short  $\alpha,\gamma$ -hybrid tripeptides **P1-P7**. Local torsion variables of  $\gamma$ -residues are also shown.



**Scheme 2:** Synthesis of short  $\alpha,\gamma$ -hybrid tripeptide **P1**.

All tripeptides consist of  $\alpha\gamma\alpha$  sequence patterns. The C- and N-termini of all tripeptides are terminated by the metal coordinating 3-pyridyl or 4-pyridyl ligands. All tripeptides were synthesized through a standard solution phase strategy following the Boc- deprotection and coupling method and synthetic procedure as shown in Scheme 2. All peptides P2 to P7 were synthesized and purified by column chromatography following above Scheme 2 with 74% to 84% yield.

### 3.2. Crystal Structures Analysis of Peptides P1, P2, P5, P6, and P7:

As single crystal X-ray diffraction studies provide unambiguous structural information of peptides, we subjected these short hybrid peptides for crystallization in various solvent combinations. Peptides **P1**, **P2**, **P5**, **P6**, and **P7** gave single crystals upon slow evaporation of peptide solutions in various solvent combinations e.g., MeOH/H<sub>2</sub>O, CHCl<sub>3</sub>/n-heptane, and their crystal structures are shown in Figure 1. The analysis of x-ray structures reveals that all five peptides adopted right-handed 12-helix conformation in single crystals. It is worth mentioning that these tripeptides adopted helical conformations without having any sterically constrained, helix-favoring residues. Even though the  $\beta$ -branched Val residues are known to have a high propensity for  $\beta$ -sheet formation in proteins,<sup>18</sup> tripeptides **P1** and **P2** consisting of two valine residues adopted helical conformations.



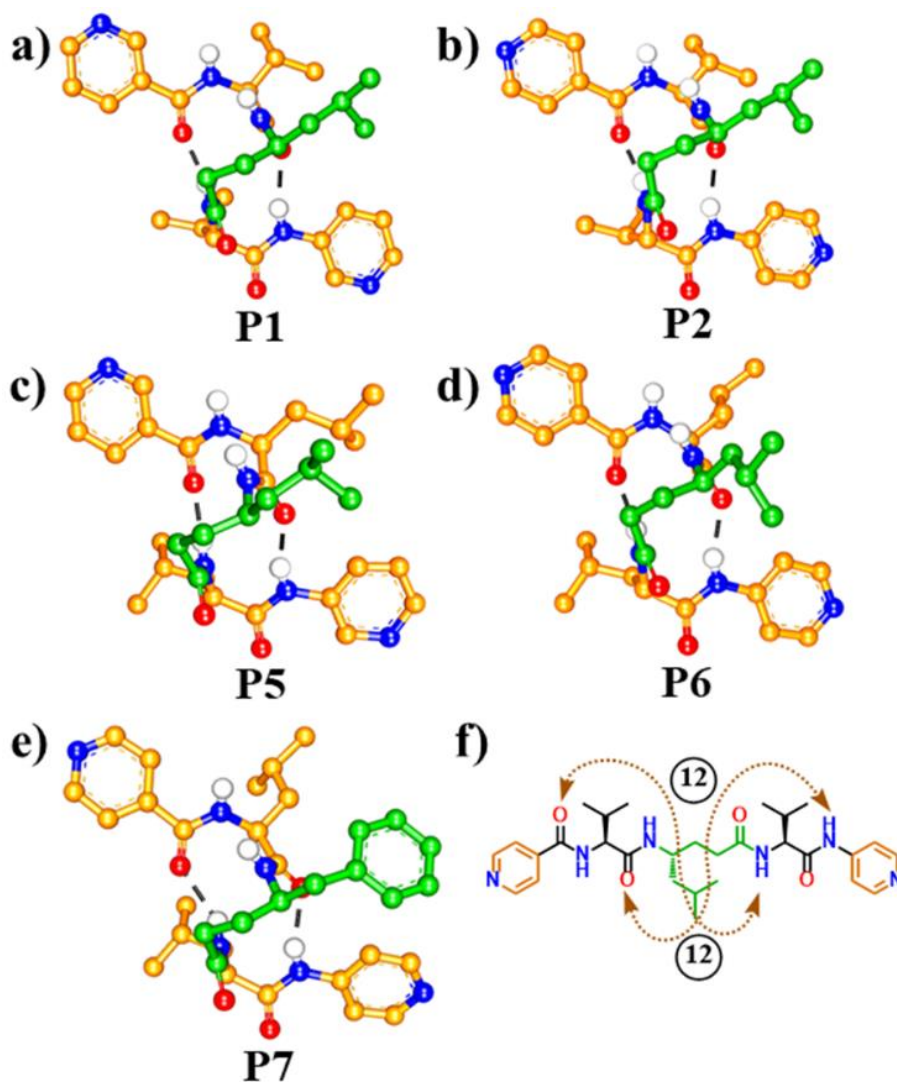


**Figure 1:** Crystal structures of (a) **P1** (b) **P2** (c) **P5** (d) **P6** and (e) **P7**. (f) H-bonding patterns of the **P2** 12-helix are also shown.

It is worth noting that the insertion of a  $\gamma$ -residue with a flexible  $-\text{CH}_2-\text{CH}_2-$  backbone at the center of a tripeptide dictates the sequence to adopt a helical conformation even in the presence of two  $\beta$ -sheet promoting residues. Similarly, other peptides **P5**, **P6**, and **P7** adopted 12-helix conformations in single crystals. The helical structures are stabilized by two consecutive 12-membered intramolecular H-bonds between CO ( $i$ ) and NH ( $i+3$ ) residues (Figure 1f). Two N-terminal amides NH groups and two C-terminal amide CO groups are exposed to intermolecular H-bonds with other helices and solvent molecules. The structural analysis reveals that the  $\gamma$ -residues adopted local *gauche*<sup>+</sup>, *gauche*<sup>+</sup> ( $g^+$ ,  $g^+$ ) conformations along  $\text{C}_\gamma-\text{C}_\beta$  and  $\text{C}_\alpha-\text{C}'(\text{O})$  bonds in all helical structures. The H-bond parameters and torsion angles of all residues of the helical peptides are tabulated in Tables S1-S2.

**Table S1: Torsion angle parameters of P1, P2, P5, P6, and P7.**

Peptide		Residue	$\phi$	$\theta_1$	$\theta_2$	$\Psi$
<b>P1</b>		Val	-69	-	-	-40
		$\gamma$ Leu	-122	44	69	-119
		Val	-64	-	-	-38
<b>P2</b>	<b>Molecule 1</b>	Val	-68	-	-	-41
		$\gamma$ Leu	-120	48	68	-121
		Val	-74	-	-	-35
	<b>Molecule 2</b>	Val	-81	-	-	-26
		$\gamma$ Leu	-117	45	63	-131
		Val	-62	-	-	-41
<b>P5</b>	<b>Molecule 1</b>	Leu	-63	-	-	-43
		$\gamma$ Leu	-115	48	66	-126
		Leu	-76	-	-	-31
<b>P5</b>	<b>Molecule 2</b>	leu	-66	-	-	-36
		$\gamma$ Leu	-119	48	61	-129
		Leu	-64	-	-	-39
<b>P6</b>	<b>Molecule 1</b>	Leu	-66	-	-	-41
		$\gamma$ Leu	-114	49	63	-129
		Leu	-79	-	-	-27
	<b>Molecule 2</b>	Leu	-71	-	-	-30
		$\gamma$ Leu	-115	47	63	-128
		Leu	-65	-	-	-41

<b>P7</b>	Leu	-83	-	-	-15
	$\gamma$ Phe	-131	46	61	-108
	Leu	-66	-	-	-43

**Table S2:** H-bond parameters of **P1**, **P2**, **P5**, **P6**, and **P7**.

Peptide	Hydrogen Bond	C=O...H-N	C=O...N-H	$\angle$ O...H-N
		in Å		in degrees
<b>P1</b>	Py CO $\leftrightarrow$ Val NH	2.08	2.93	167
	Val CO $\leftrightarrow$ NH Py	2.09	2.92	161
<b>P2 Molecule 1</b>	Py CO $\leftrightarrow$ Val NH	2.05	2.90	167
	Val CO $\leftrightarrow$ NH Py	2.08	2.91	162
<b>P2 Molecule 2</b>	Py CO $\leftrightarrow$ Val NH	2.04	2.89	169
	Val CO $\leftrightarrow$ NH Py	2.12	2.94	161
<b>P5 Molecule 1</b>	Py CO $\leftrightarrow$ Leu NH	2.02	2.89	173
	Leu CO $\leftrightarrow$ NH Py	1.97	2.82	162
<b>P5 Molecule 2</b>	Py CO $\leftrightarrow$ Leu NH	2.01	2.89	175
	Leu CO $\leftrightarrow$ NH Py	2.00	2.86	162
<b>P6 Molecule 1</b>	Py CO $\leftrightarrow$ Leu NH	2.02	2.93	172
	Leu CO $\leftrightarrow$ NH Py	1.95	2.79	159
		2.07	2.93	171

<b>P6</b> <b>Molecule 2</b>	Py CO↔Leu NH			
	Leu CO↔ NH Py	2.00	2.85	162
<b>P7</b>	Py CO↔Leu NH	2.199	2.99	151
	Leu CO↔ NH Py	2.01	2.83	156

### 3.3. Solution State Conformational Analysis of Peptide P3:

Peptides **P3** and **P4** did not give single crystals under similar conditions, however, the solution conformation of **P3** was determined through the 2D-NMR technique. The analysis of the ROESY spectrum (CD<sub>3</sub>OH at 298 K) of **P3** revealed the existence of strong NH1↔NH2 and NH3↔NH (C terminal pyridine) (dNN) NOEs.

#### 3.3.1. TOCSY Spectrum of Peptide P3:

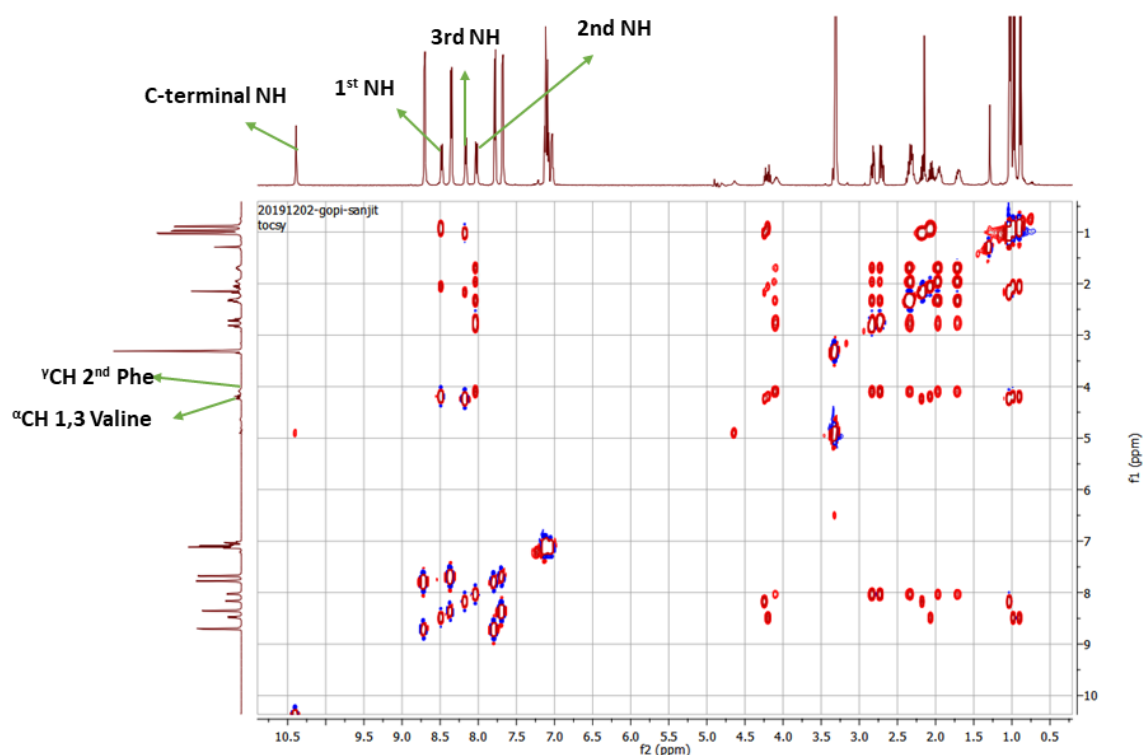


**Figure 2:** TOCSY spectra of peptide **P3** (concentration = 5 mM) in CD<sub>3</sub>OH.

### 3.3.2. NH↔NH NOEs of Peptide P3:

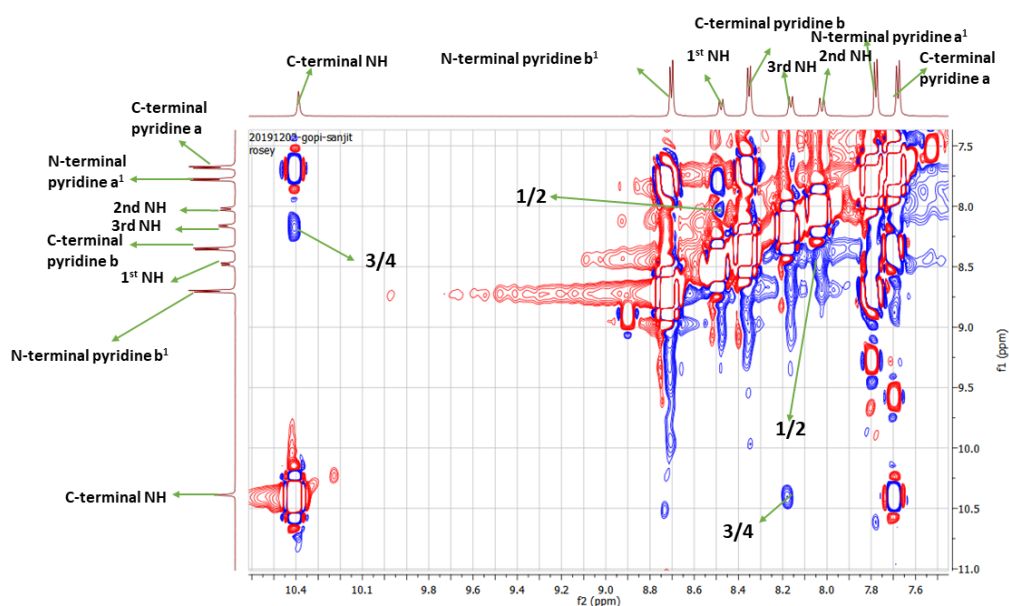


**Figure 3:** Partial ROESY spectra of **P3** (concentration = 5 mM) in CD<sub>3</sub>OH represent NH↔NHNOEs.

No NH↔NH NOEs were observed between  $\gamma$ -Leu2NH and Val3NH. Apart from the strong NH(*i*)↔NH(*i*+1), the long-range NOEs between C<sub>γ</sub>H<sub>Phe2</sub>↔C terminal amide NH and C<sub>γ</sub>H<sub>Phe</sub>↔C terminal pyridine proton Ha were also observed and shown in Figures 2-5.

### 3.3.3. C<sub>α</sub>H↔NH NOEs of Peptide P3:

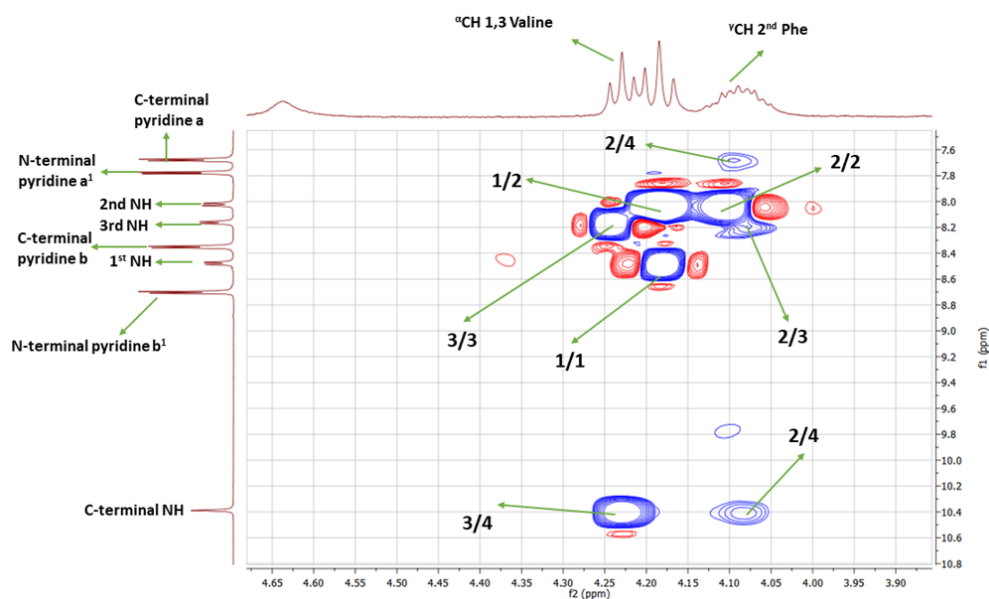
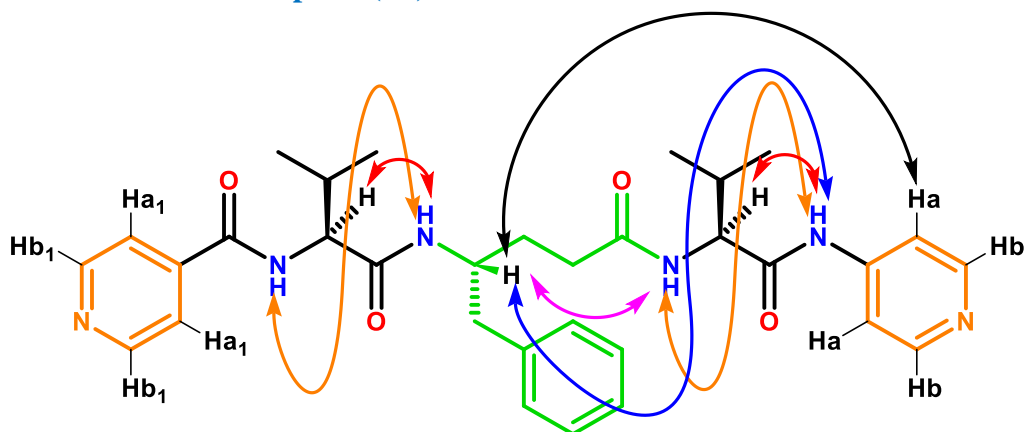


**Figure 4:** Partial ROESY spectra of **P3** (concentration = 5 mM) in CD<sub>3</sub>OH represent C<sub>α</sub>H↔NH NOEs.

### 3.3.4. NOEs Observed of Peptide (P3):



Residue	Observed NOEs Interaction
1,2 NH-NH	Medium
3,4 NH-NH	Medium
C $\alpha$ HVal(1)-2 <sup>nd</sup> NH	Strong
C $\gamma$ HPhe(2)-3 <sup>rd</sup> NH	Strong
C $\alpha$ HVal(3)-C terminal amide NH	Strong
C $\gamma$ HPhe(2)-4 <sup>th</sup> NH	Weak
C $\gamma$ HPhe(2)-C terminal Pyridine Ha proton	Weak

**Figure 5:** Observed NOEs of Peptide **P3** in CD<sub>3</sub>OH.

The observed NOEs are consistent with our previous results<sup>16c</sup> and support the helical conformation of peptide **P3** in solution. As the sequences of **P3** and **P4** are the same except for the terminal pyridine moieties, we anticipate a similar helical conformation in the peptide **P4**.

### 3.4. Metal-Peptide Gelation Studies of Peptides P1- P7:

Inspired by the diverse supramolecular architectures of metal-mediated self-assembly of proteins<sup>8</sup> peptides,<sup>9</sup> and our recent work on metal-helix frameworks,<sup>17</sup> we subjected all these short helical peptides for metal coordination using different metal salts to understand their metal-coordination properties. Upon treatment of  $\text{Ag}^+$  ( $\text{AgBF}_4$ ) in ethanol with the solution **P1** in ethanol followed by a few minutes of sonication leads to the transformation of a clear solution of peptide **P1** in ethanol into a transparent peptide silver metallogel.<sup>19</sup> Surprisingly, the gelation property of this peptide is selective for  $\text{Ag}^+$ , no metallogels were observed with other transition metal ions such as  $\text{Cu}^{2+}$ ,  $\text{Zn}^{2+}$ ,  $\text{Fe}^{2+}$ , and  $\text{Ni}^{2+}$ . The 1:1 concentration of  $\text{AgBF}_4$  and peptide **P1** was found to be the ideal stoichiometry as shown in Figure 6 for the gelation. Further, upon treatment of peptide **P2** with various metal ions, such as  $\text{Ag}^+$ ,  $\text{Cu}^{2+}$ ,  $\text{Ni}^{2+}$ ,  $\text{Zn}^{2+}$ , and  $\text{Fe}^{2+}$  peptide forms gels only with copper ions.<sup>20</sup> No gels were observed with other metal ions. To understand the stoichiometry of gelation, various concentrations of  $\text{CuCl}_2 \cdot 2\text{H}_2\text{O}$  were examined as shown in Figure 7. Though we obtained stable gels at 1:1 equivalent of peptide and metal ions, we observed the gelation behavior even at 0.25 equivalent of metal ion concentration in both peptides.

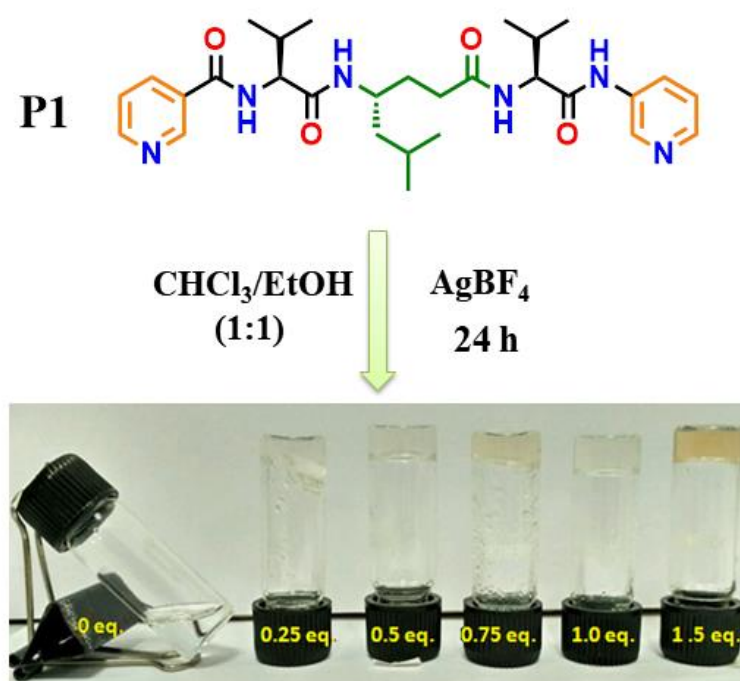


**Figure 6:** Inverted sample vial experiment to confirm the metallogel formation of the peptide **P1** at various concentrations of  $\text{AgBF}_4$ .

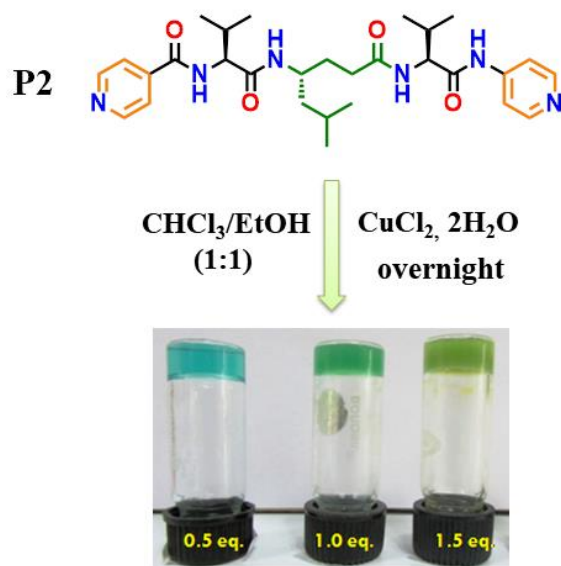


**Figure 7:** Inverted sample vial experiment to confirm the metallogel formation of the peptide **P2** at different concentrations of  $\text{CuCl}_2 \cdot 2\text{H}_2\text{O}$ .

In comparison to **P1** and **P2**, peptide **P3** forms metallogels with both  $\text{Ag}^+$  ( $\text{AgBF}_4$ ) and  $\text{Cu}^{2+}$  ( $\text{CuCl}_2 \cdot 2\text{H}_2\text{O}$ ), however, we did not observe gels with other metal ions such as  $\text{Ni}^{2+}$ ,  $\text{Zn}^{2+}$ , and  $\text{Fe}^{2+}$ . Similar to **P3**, peptide **P4** also forms metallogels with  $\text{Ag}^+$  and  $\text{Cu}^{2+}$  ions as shown in Figure 8.

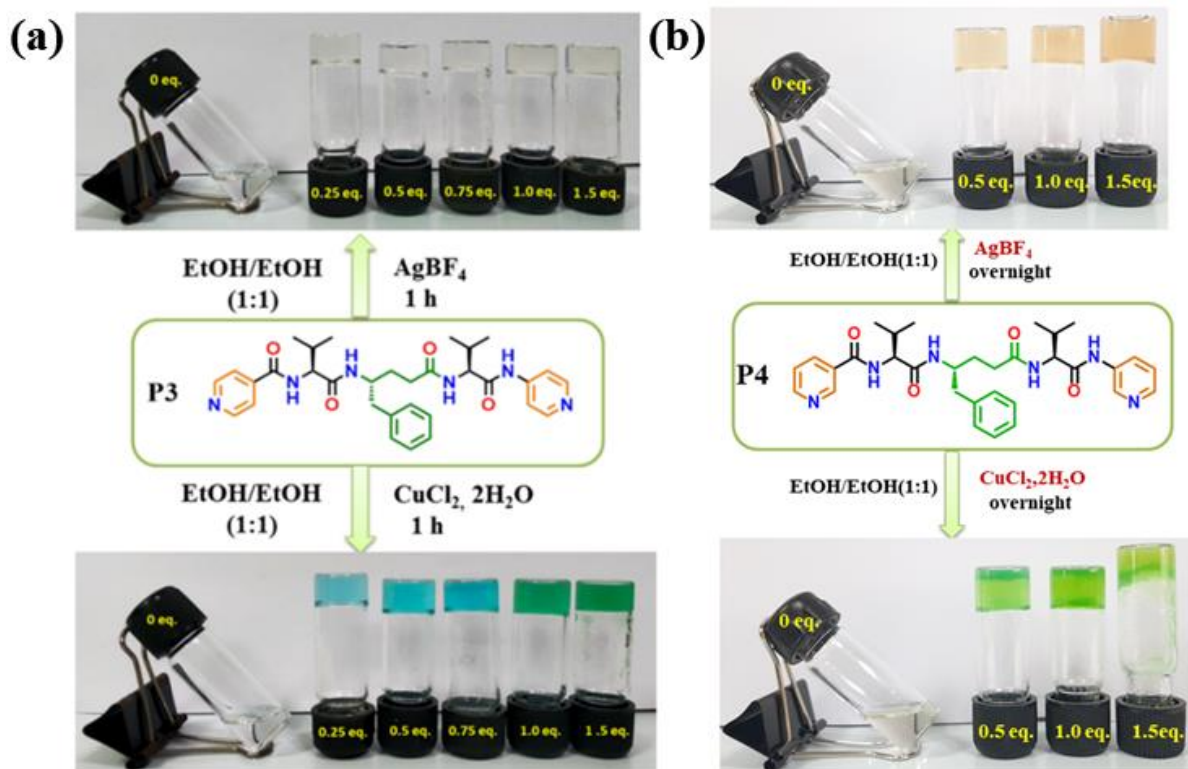


**Figure 8:** Inverted sample vial experiment to confirm the metallogel formation of the (a) peptide **P3** and (b) **P4** at different concentrations of both  $\text{AgBF}_4$  and  $\text{CuCl}_2 \cdot 2\text{H}_2\text{O}$ .



In contrast to **P1-P4**, peptides **P5-P7** did not give metallogels with any of the above-mentioned metal ions Figure 8-9. The strong gelation property of **P3** and **P4** compared to **P1** and **P2** could be attributed to the aromatic side-chain of  $\gamma$ -Phe residue, which is known for promoting self-aggregation in peptides.<sup>21</sup> Though **P7** consists of  $\gamma$ -Phe residue, however, it doesn't have Val residues in the sequence to form metallogels. Based on the experimental observation, it appears that both Val and  $\gamma$ -Phe are required for better metallogelation with silver and copper ions. Further, upon exposing the silver gels of **P1**, **P3**, and **P4** to visible light, we observed the transformation of colorless transparent gels into a brown color, indicating the formation of silver nanoparticles<sup>22</sup> from silver ions.

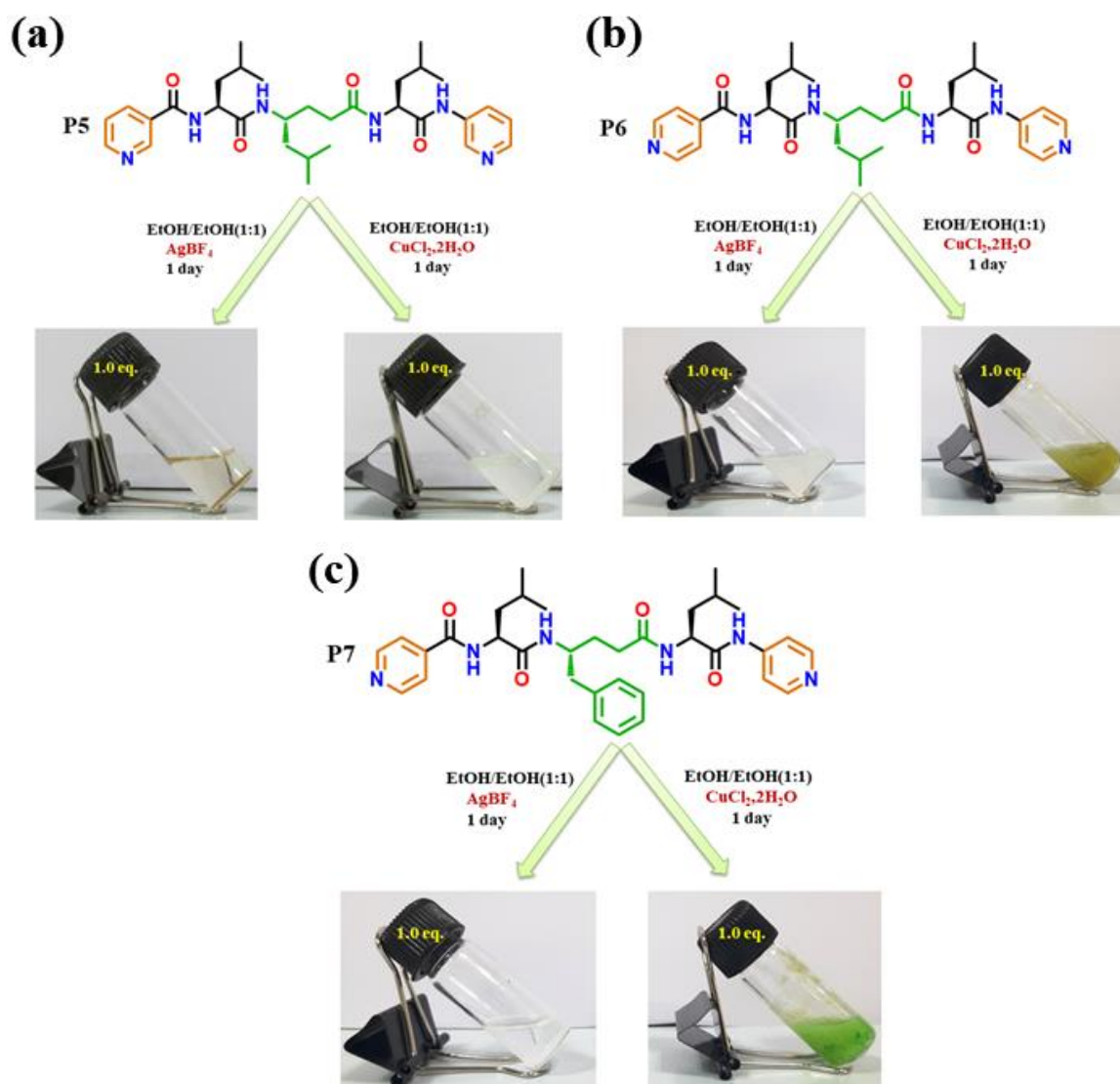


**Figure 9:** Sample vial experiment showing no metallogel formation of the (a) peptide **P5**, (b) **P6**, and (c) **P7** with both  $\text{AgBF}_4$  and  $\text{CuCl}_2 \cdot 2\text{H}_2\text{O}$  (concentration of the mixture is 15mM).

### 3.5. Investigation of Supramolecular Self-Assembly Properties of Metal-Peptide Gel:

The metal-peptide gel formation is due to the coordination network by various non-covalent interactions such as CH- $\pi$ , H-bonds, and  $\pi$ - $\pi$  interactions inspired us to look into their supramolecular self-assemblies using SEM analysis. The SEM samples were prepared by diluting the metallogel with the methanol to make little disperse of the coordination network and drop-casted onto a Si-substrate and samples were dried at room temperature. The FE-SEM analysis revealed the entangled networks of metal-coordinated peptide nanofibers for all metallogel irrespective of metal ions shown in Figure 10.

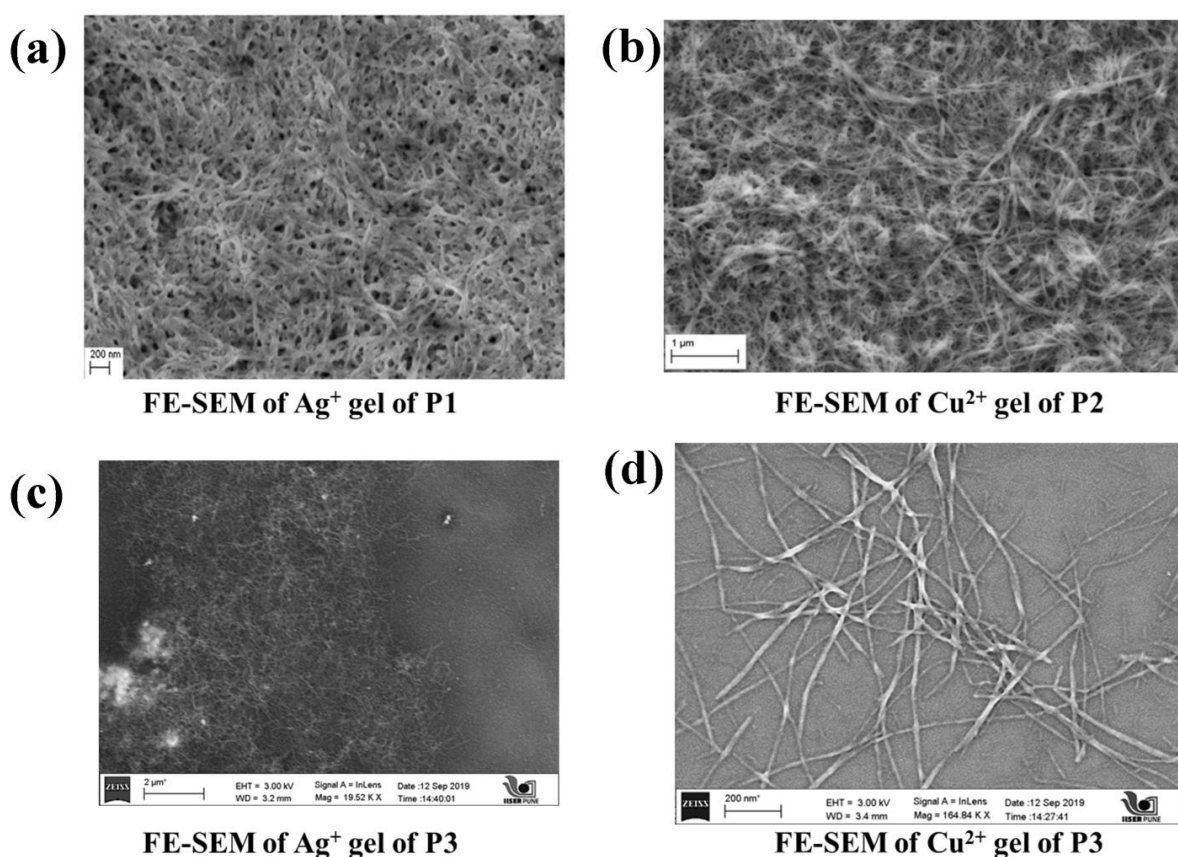


**Figure 10:** FE-SEM analysis of peptides metallogels.

Further, to gain more information on the morphology of peptide metallogels, HR-TEM measurements were performed. The HR-TEM samples were prepared by drop casting on a copper grid and then slowly evaporated at room temperature. HR-TEM analysis showed the different morphology of peptide metallogels. The silver gels of **P1** revealed the fibrillar networks of silver-coordinated peptide fibrils (Figure 11a) in HR-TEM. In comparison, **P2**

copper gels showed twisted helical morphology (Figure 11b), however, **P3** copper gels showed an entangled fibrillar network. More intriguingly, the TEM analysis of the silver gel of **P3** after 12 days of incubation showed the formation of silver nanoparticles along the fibrillar network (Figure 11c inset).

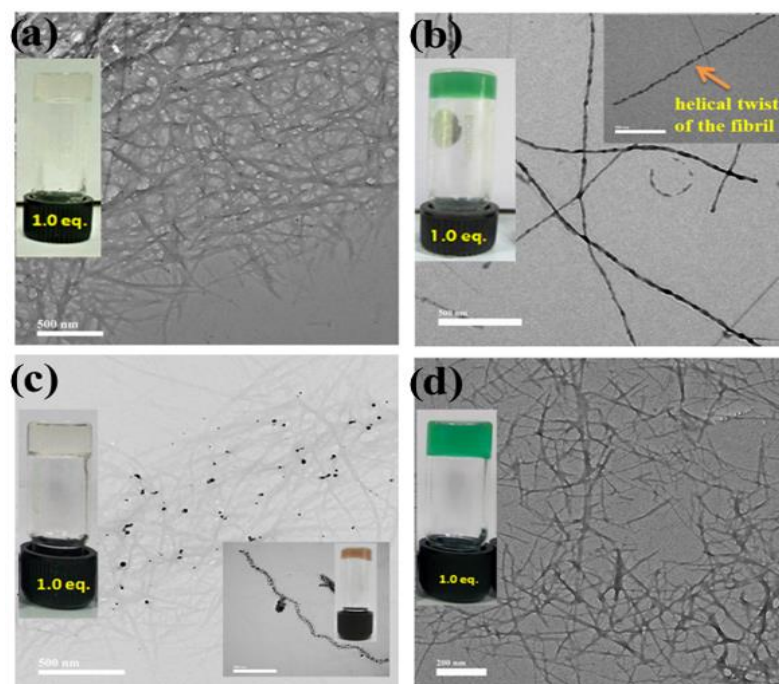
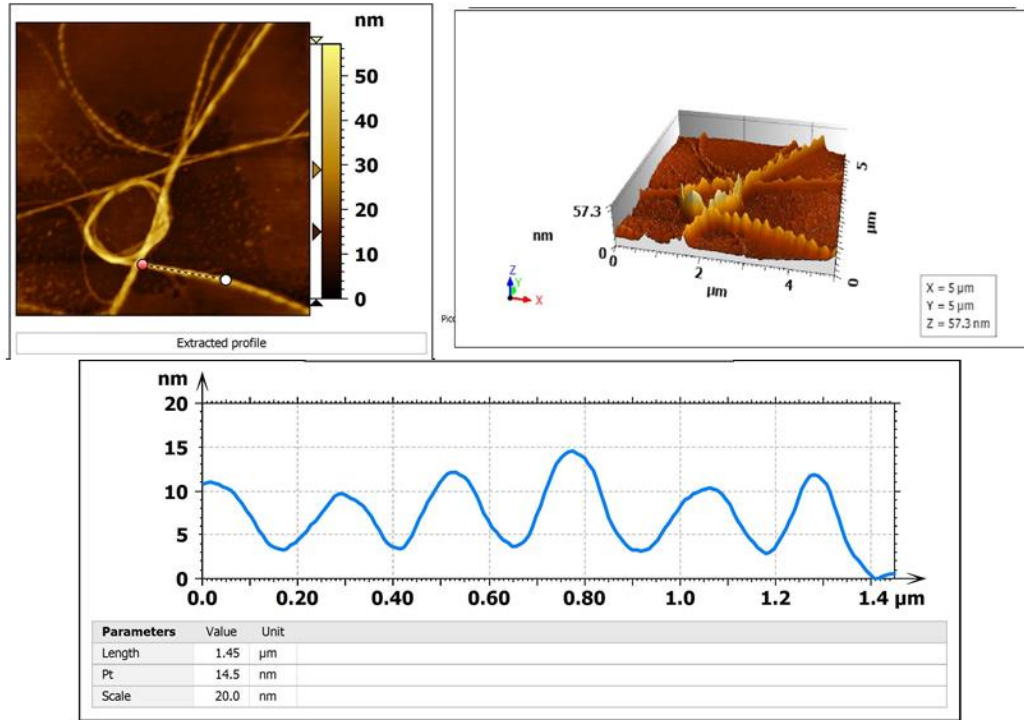


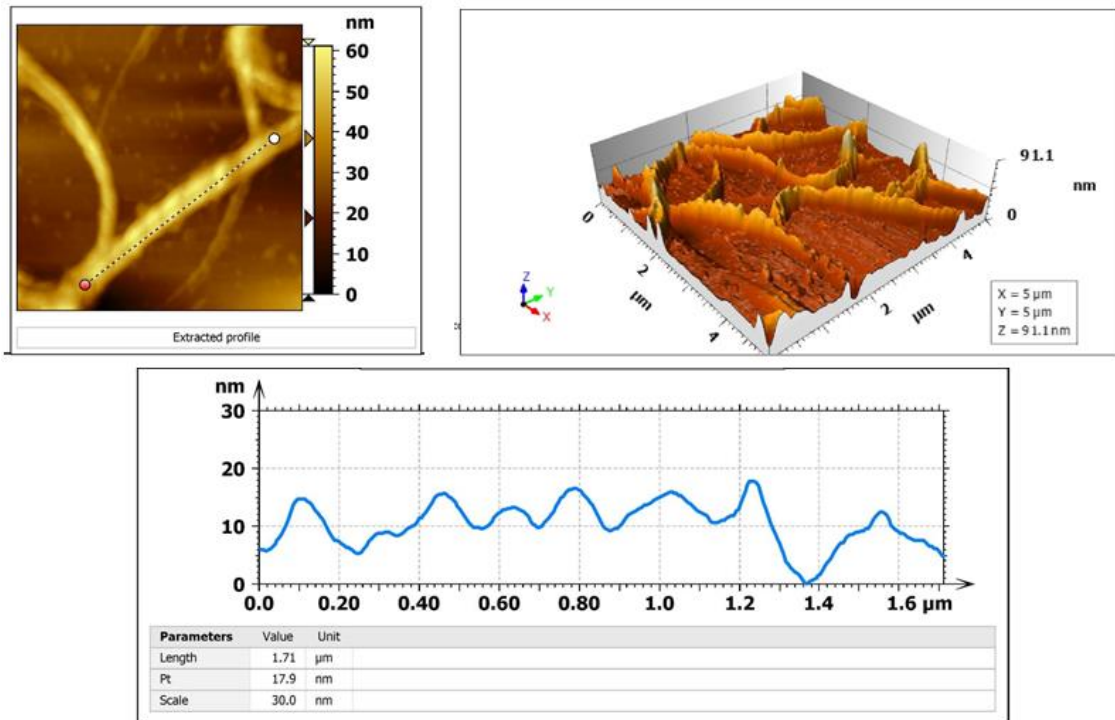
**Figure 11:** HR-TEM images of the fibrils of (a) silver metallogel **P1** and (b) copper metallogel of **P2** (observed helical twist of the fibril in the inset). HR-TEM images of the fibrils of (c) silver metallogel and (d) copper metallogel (helical arrangement of silver nanoparticles in the inset) of peptide **P3**.

Further, AFM analysis was carried out to gain more of the supramolecular self-assembly properties of peptide and peptide metallogel. The AFM studies reveal that the images of copper gels of **P3** displayed the twisted ribbons with regular periodicity, whereas silver gels of **P3** showed the elongated morphology of the fibrils in Figure 12. Both SEM and TEM analysis show similar morphology of peptide metallogel.

(a)



(b)



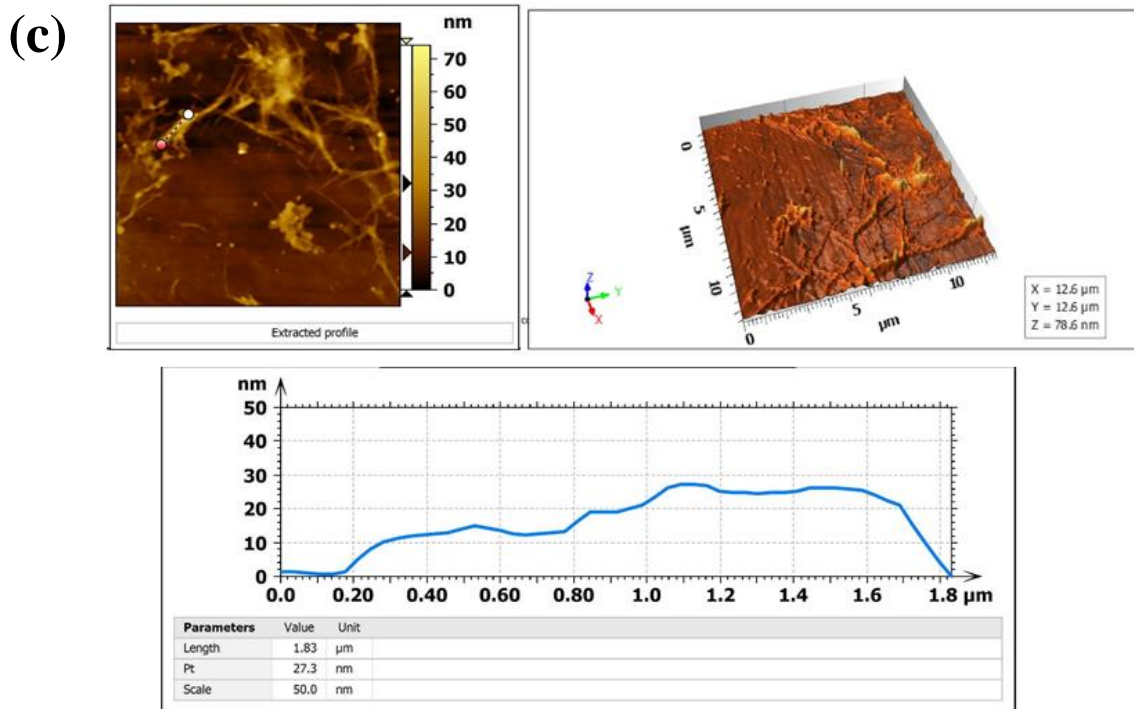


**Figure 12:** AFM images of peptide **P3** (a) alone showed the helical ribbon with regular periodicity. (b) with copper, gel displayed twisted ribbons with regular periodicity. (c) with silver gels, showed the fibrils.

### 3.6. Circular Dichroism (CD) Analysis:

In order to understand the chirality of the metallogels, we subjected CD analysis for **P2**, and **P3** shown in Figure 13. As peptides were highly robust to form metallogel. Therefore, peptide and metal salt with 25mM were added in a CD cuvette and shaken well to form metallogel. Which was further recorded for CD analysis. Both pre-metal coordinated hybrid helices and their metallogels gave the same pattern of CD signals. However, the CD signature displayed by the hybrid peptides and metallogels is different from that of  $\alpha$ -helix CD signature.<sup>23</sup>

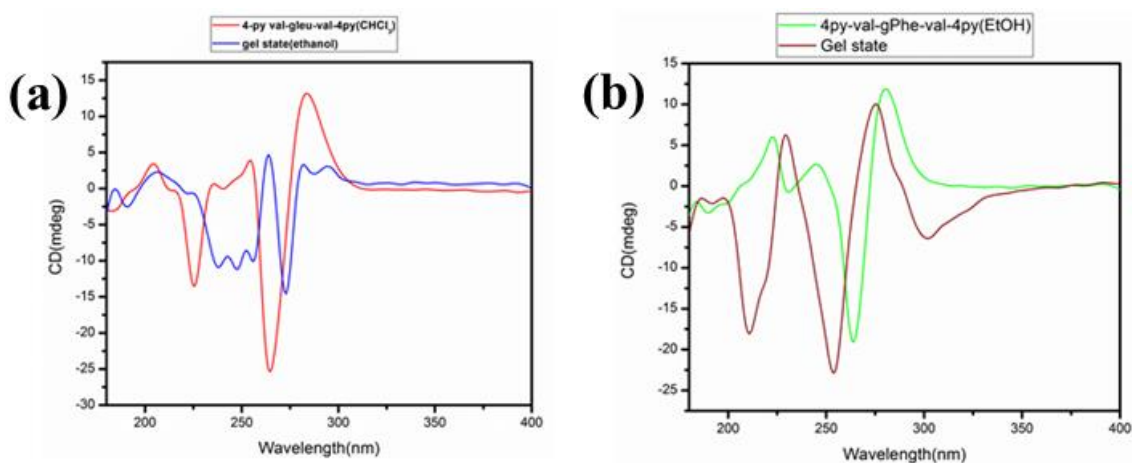


**Figure 13:** Circular Dichroism comparison study of peptide and peptide-metallogel (a) **P2** and **P2**-copper gel (b) **P3** and **P3**-silver gel.

### 3.7. Viscoelastic Property of Peptide-Metallogel:

To understand the strengths of metallogel, we carried out rheological measurements. This study provides more insight into the viscoelasticity and self-healing properties of

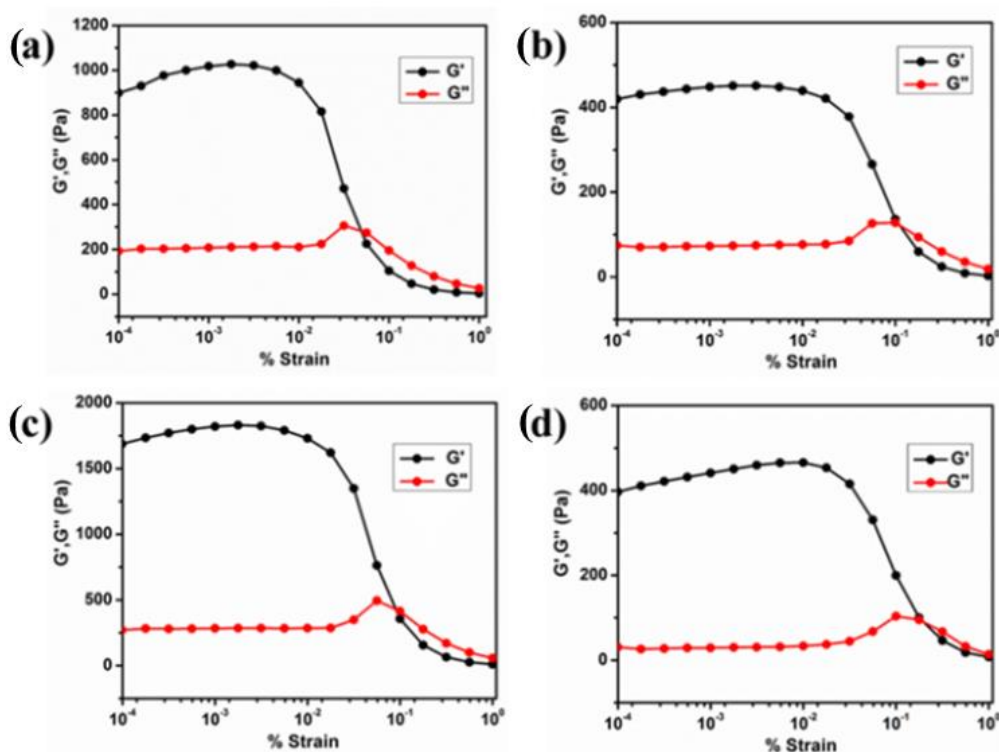


**Figure 14:** Strain sweep rheological analysis of peptides metallogels (a) **P1** with  $\text{Ag}^+$  (CGC=12 mM) (b) **P2** with  $\text{Cu}^{2+}$  (CGC=15 mM) (c) **P3** with  $\text{Ag}^+$  (CGC=10 mM) and (d) **P3** with  $\text{Cu}^{2+}$  (CGC=10 mM) at a fixed angular frequency of 1 rad/s.

metallogel. Therefore, the viscoelastic properties of the helical peptide metallogels were examined using strain-sweep and frequency-sweep experiments. In all strain-sweep experiments of metallogels,  $G'$  was found to be larger than the  $G''$ , suggesting the viscoelastic nature of the gels shown in Figure 14. In comparison, silver gels gave a substantially larger difference between  $G'$  and  $G''$ . No crossover of  $G'$  and  $G''$  was observed in the frequency sweep experiments. The constant separation of  $G'$  and  $G''$  suggests the good stability of gels. These studies indicate the strong intermolecular interactions between the peptide ligands and metal ions in the gel structure.

### 3.8. FT-IR Supports Extended Structures in Gel Matrix:

To understand the role of amino acid residues in peptide sequences for the formation of metallogel, we have carried out FT-IR analysis. The peptides having valine residues can form

peptide-metallogel(**P1**, **P2**, **P3**, and **P4**) whereas peptides containing leucine residues(**P5**, **P6**, and **P7**) fail to form peptide-metallogel instead forming metal-complex as shown in Figure 6-9. It is known that valine-containing peptides are prone to adopt beta-sheet structures and leucine-containing peptides are very prone to form helical structures.<sup>18</sup> To gain we carried out an FT-IR study to understand the particular signature of NH---O=C of **P3** before and after gelation shown in Figure 15.

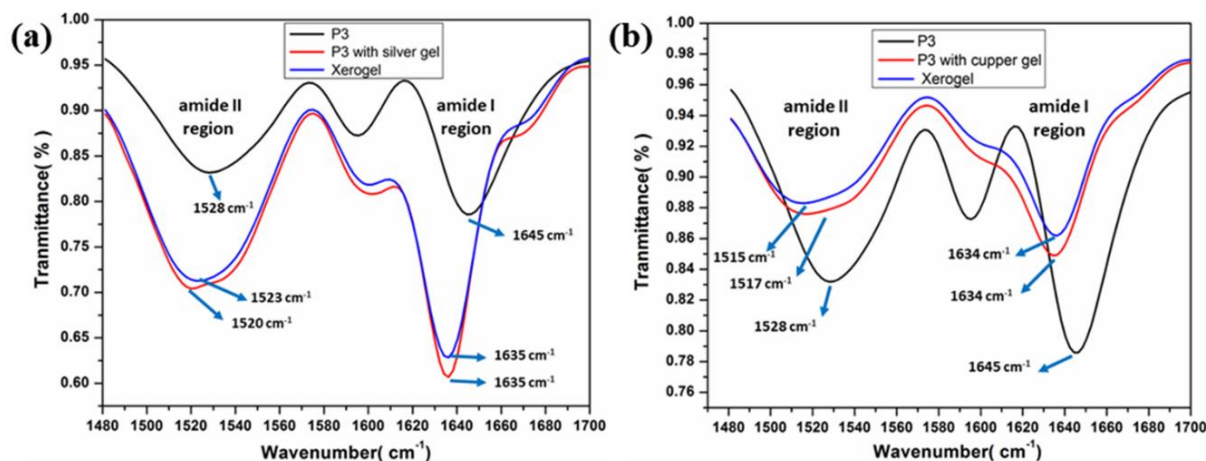


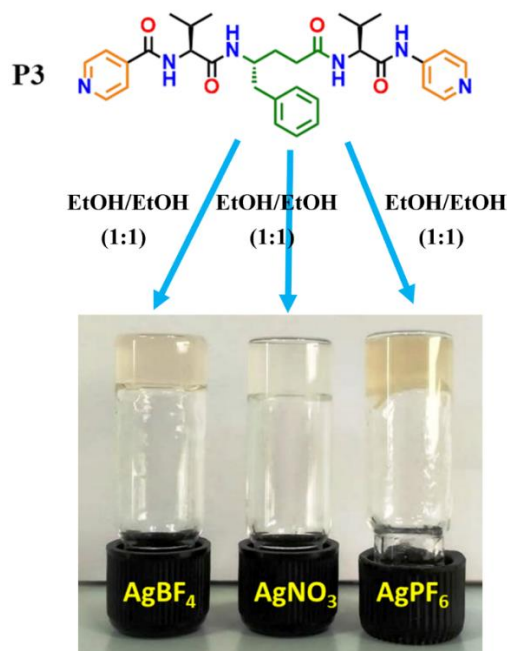
**Figure 15:** FT-IR of peptide **P3** in native form, gel state, and xerogel state. (a) **P3** with silver gel and (b) **P3** with copper gel.

The IR data analysis suggests that the **P3** in native form shows amide-I(NH---O=C) at 1645  $\text{cm}^{-1}$  and amide-II at 1528  $\text{cm}^{-1}$  which corresponds to the helical structure of **P3**. However, **P3** in silver metallogel and xerogel state both amide-I shifted to 1635  $\text{cm}^{-1}$  and 1635  $\text{cm}^{-1}$  and amide-II shifted to 1520  $\text{cm}^{-1}$  and 1523  $\text{cm}^{-1}$ . A similar trend of **P3** i.e. shifting of both amide-I and amide-II was observed in the case of copper gel i.e. amide-I shifted to 1634  $\text{cm}^{-1}$  and 1634  $\text{cm}^{-1}$  whereas amide-II shifted to 1517  $\text{cm}^{-1}$  and 1515  $\text{cm}^{-1}$ . Therefore, it was speculated that in all valine-containing ligands in their native helical form and the metallogel state, there were changes in conformation<sup>24</sup> and it is due to such structural transition peptides **P1-P4** are formed metallogel with silver and copper salt.

### 3.8. Metal-Peptide Coordinated Supramolecular Assembly:

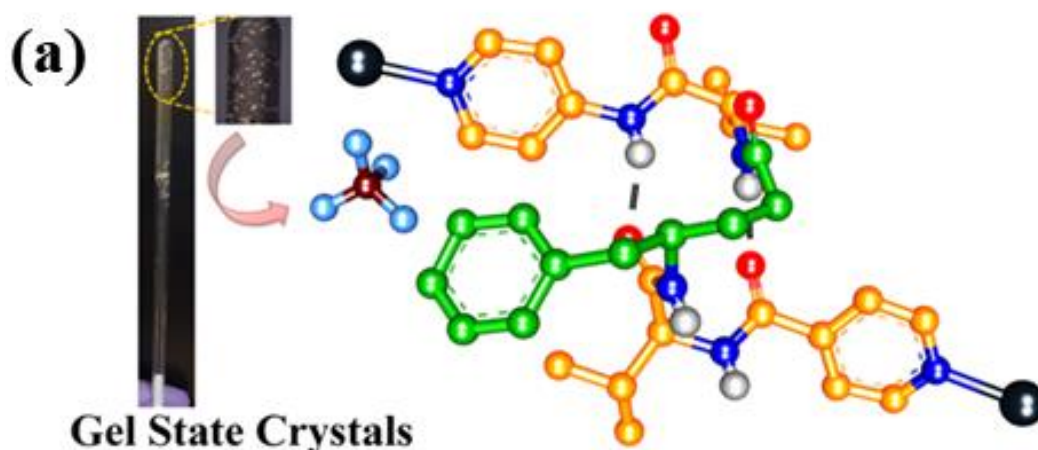
The formation of metal-coordinated helical polymers of these peptides motivated us to investigate the mechanism of the self-assembly process and the secondary structure of these hybrid peptides after metal coordination. Even though various metal-coordinated supramolecular polymers have been reported in the literature,<sup>9,10,19,20,22</sup> however the atomic-level understanding of metal-coordinated polymers remains elusive. In this context, we selected

peptide **P3** to understand the mechanism of metal-coordinated polymerization. Peptide **P3** gives silver gels upon treatment with  $\text{AgBF}_4$ ,  $\text{AgPF}_6$ , and  $\text{AgNO}_3$ . The formation of silver metallo gel by the peptide **P3** is independent of the counter ions shown in Figure 15.



**Figure 15:** Effect of counter anions: metallo gel formation of peptide **P3** with different silver salts.

However, upon incubating for a few weeks in the gel state at room temperature in the absence of visible light, silver gels derived from  $\text{AgBF}_4$  in  $\text{CD}_3\text{OH}$  yield shiny single crystals in the gel matrix (Figure 16a). These single crystals were subjected to X-ray diffraction to understand the secondary structure of metal-coordinated **P3** in its gel matrix. The structure of silver ion coordinated peptide **P3** is shown in Figure 16a.





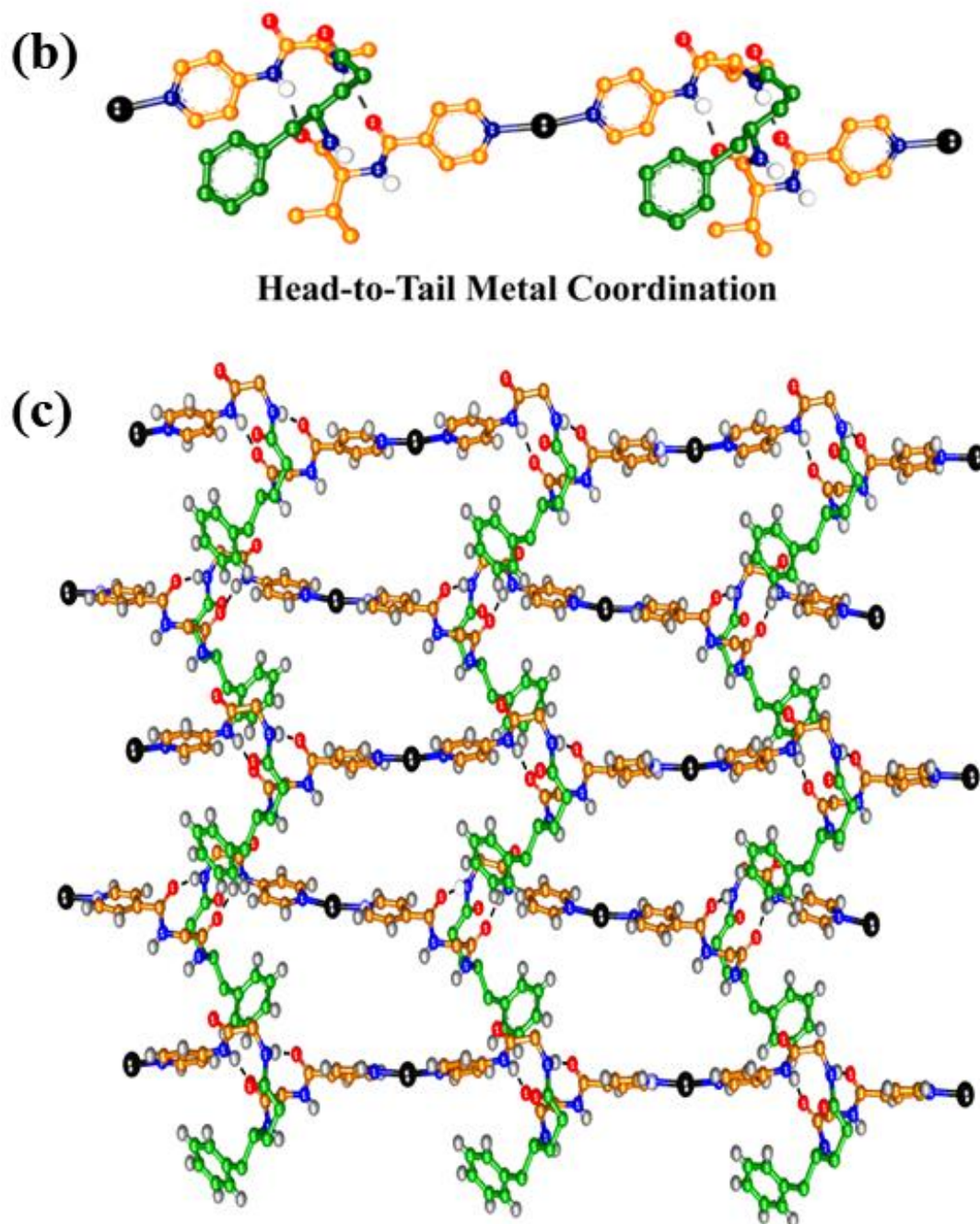


**Figure 16:** (a) Single crystals of **P3** in the silver gel matrix and the X-ray diffracted structure of silver coordinated **P3**. (b) “Head-to-Tail” silver ion coordination between the two helices was observed in the crystal packing along the b-axis. (c) Supramolecular assembly of **P3-AgBF<sub>4</sub>** complex along the a-axis.

Similar to the pre-metal coordinated structures of hybrid peptides shown in Figure 1, **P3** also adopted 12-helix conformation after the metal coordination. The structure is stabilized by two consecutive intramolecular 12-membered H-bonds between CO(*i*)→NH (*i*+3) moieties. The terminal pyridyl moieties are now engaged in silver ion coordination. The silver ion connected the two helical peptides by coordinating both C- and N-terminal pyridine of two helices in a “head-to-tail” fashion (Figure 16b and 16c) and further propagated along the *c* axis to form a supramolecular network. Instructively, the silver gel of peptide **P3** obtained upon treatment with AgPF<sub>6</sub> at 1:1 peptide and metal concentration in ethanol transformed into sol upon standing at room temperature for about 6 h. We speculate that the transformation from gel to sol is due to the difficulty in accommodating bulkier anion counterpart in the gel matrix.<sup>25</sup> Upon standing in the absence of visible light, the sol produced single crystals shown in Figure 17, and their X-ray diffraction analysis revealed that peptide **P3** again adopted 12-helix conformation.

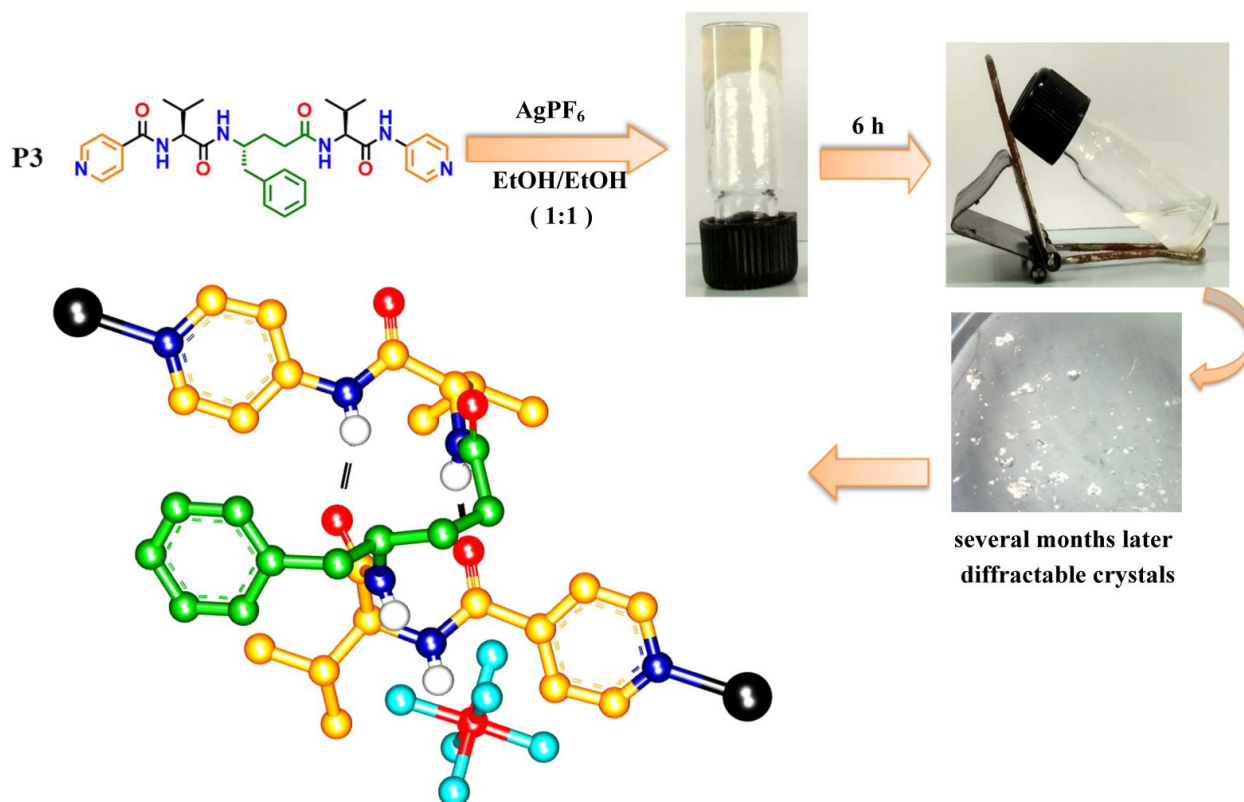


**Figure 17:** Crystal structure of **P3-AgPF<sub>6</sub>** complex.

Irrespective of the counter anion, peptide **P3** adopted 12-helix conformation. In comparison with AgBF<sub>4</sub>-mediated helical polymerization, the AgPF<sub>6</sub>-mediated coordination leads to “head-to-head” and “tail-to-tail” metal coordination as shown in Figure **18b**. Interestingly, higher-order packing along the c-axis produces a porous 3D dimensional supramolecular coordination polymer<sup>26</sup> shown in Figure **18c**.

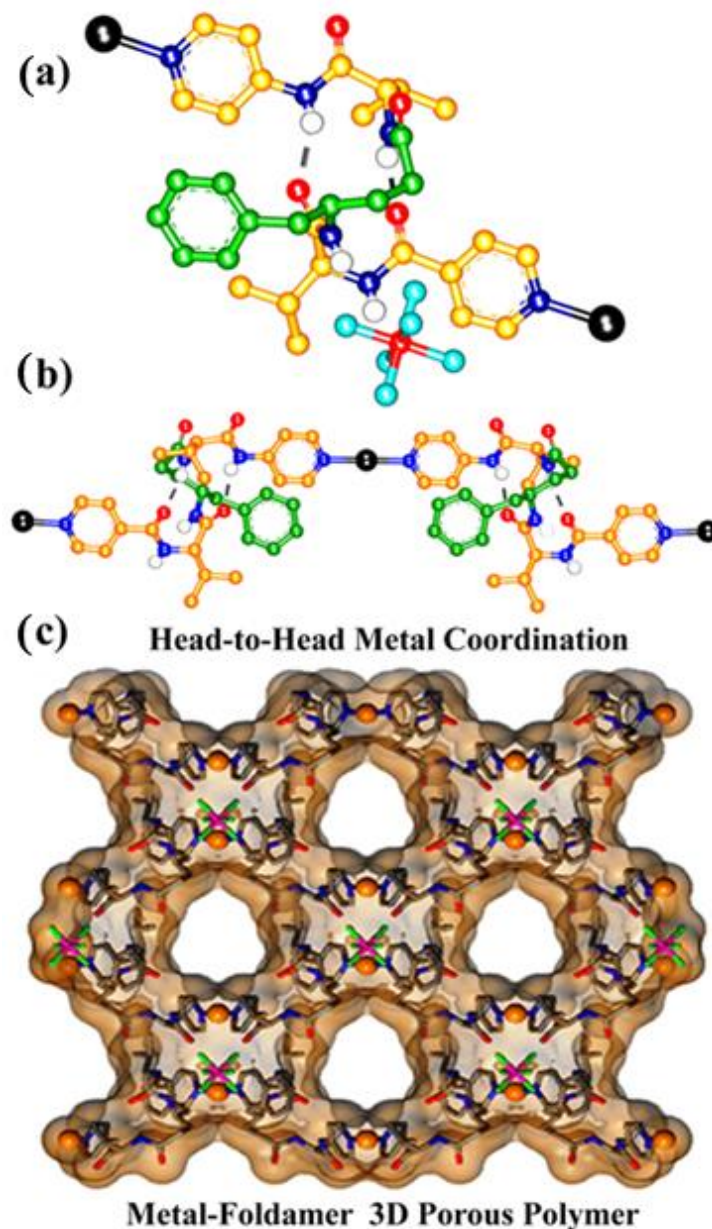


**Figure 18:** (a) The X-ray structure of silver coordinated peptide **P3**. (b) “Head-to-Head” silver ion coordination between the two helices was observed in the crystal packing along the a-axis. (c) The porous 3D supramolecular coordination polymer was observed after packing along the c-axis (the side arms of the amino acid residues are removed for clarity).

A careful crystal structure analysis of **P3-AgBF<sub>4</sub>** and **P3-AgPF<sub>6</sub>** complexes reveals that the involvement of counter anion plays a significant role to drive the helical peptide **P3** and its metal coordination direction shown in Figure 19. In the presence of AgBF<sub>4</sub>, the peptide P3 involves in a “Head-to-Tail” silver ion coordination between the two helices, and in the crystal packing the counter anion BF<sub>4</sub><sup>-</sup> forms a noncovalent interaction as like F...H-N = 2.01 Å, F...Ag = 2.76 Å, and 2[F...H-C] = 2.01 Å of aromatic pyridine units. However in the case of AgPF<sub>6</sub>, the peptide P3 involves in a “Head-to-Head” silver ion coordination between the two helices, and in the crystal packing the counter anion PF<sub>6</sub><sup>-</sup> forms a noncovalent interaction as like 4[F...H-N] = 2.01 Å, 4[F...Ag] = 2.76 Å, and 4[F...H-C] = 2.01 Å of aromatic pyridine units. It is due to more additional interaction of PF<sub>6</sub><sup>-</sup> units with the helical peptide P3 units, which could drive the peptide units to coordinate in a “Head-to-Head” fashion leading to a porous framework.

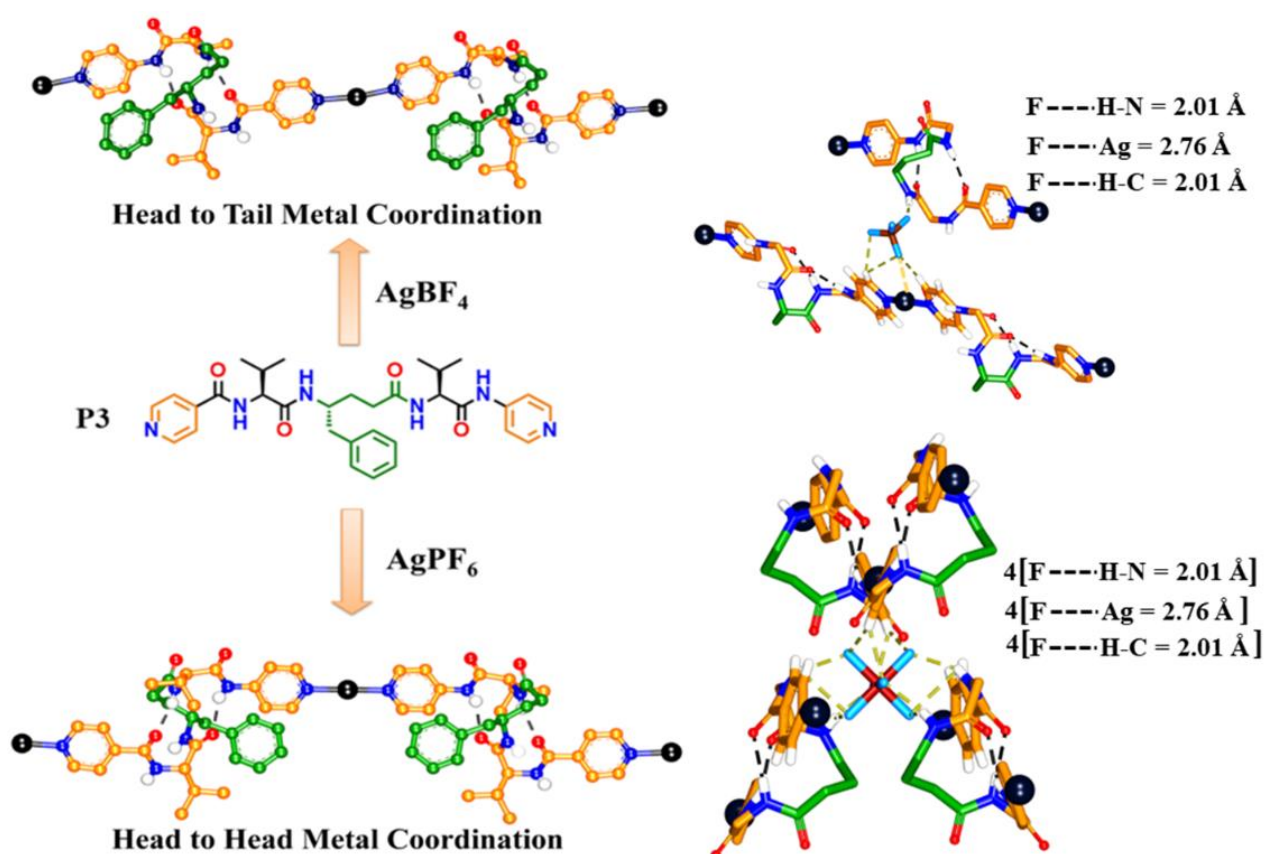


**Figure 19:** Effect of counter anion and crystal structure of **P3-Ag-salt** complexes.

The H-bond parameters and torsion angles of all residues of the helical metallo-peptides complexes are tabulated in Tables **S3-S4**.

**Table S3:** Torsion angle parameters of **P3-AgBF<sub>4</sub>** and **P3-AgPF<sub>6</sub>** complexes.

Peptide Complex	Amino-acid Residue	$\phi$	$\theta_1$	$\theta_2$	$\Psi$
<b>P3-AgBF<sub>4</sub></b>	Val	-61	-	-	-54
	$\gamma$ Phe	-123	63	61	-123
	Val	-73	-	-	-30
<b>P3-AgPF<sub>6</sub></b>	Val	-58	-	-	-51
	$\gamma$ Phe	-123	56	61	-115
	Val	-80	-	-	-22

**Table S4:** H-bond parameters of **P3-AgBF<sub>4</sub>** and **P3-AgPF<sub>6</sub>** complexes.

Complex	Hydrogen Bond	C=O...H-N	C=O...N-H	$\angle$ O...H-N
		in Å		in Degrees
<b>P3-AgBF<sub>4</sub></b>	Py CO $\leftrightarrow$ NH Val	2.06	2.92	173
	Val CO $\leftrightarrow$ NH Py	2.03	2.85	158
<b>P3-AgPF<sub>6</sub></b>	Py CO $\leftrightarrow$ NH Val	2.09	2.94	166
	Val CO $\leftrightarrow$ NH Py	2.10	2.87	150

In contrast to silver gels, we have not observed gel phase crystals of **P3** in the copper gels. As peptides **P5**, **P6**, and **P7** did not give metallogels or metal-coordinated single crystals, we did not pursue further.

## 4. Conclusion:

In conclusion, we have successfully demonstrated the metal-coordinated polymerization of short hybrid helical peptides. These  $\alpha\gamma$ -hybrid tripeptides adopted the 12-helical structures without and with metal ion coordination. Even though these short sequences contain the sheet promoting  $\beta$ -branched  $\alpha$ -residues, they preferred to adopt a helical conformation in the presence of  $\gamma$ -residues. The sequences of the peptides and the position of N in the pyridyl groups play a crucial role in metallogel formation. As metallogels have had a significant attraction in recent years due to their potential applications in various fields including, conductivity, catalysis, color, and redox activities,<sup>27</sup> these peptide metallogels may serve as ideal candidates to design new materials. Crystallization and gel formation are closely related to non-equilibrium self-assembly processes. The gels are generally metastable structures. The peptide structures in the gels may be different from the single crystal structures. Given an opportunity, these kinetically trapped metastable gel state structures slowly transformed into stable and defined structures. Further, the results reported here also demonstrate the influence of counter anions in the helical coordination polymerization and their 3-dimensional porous networks. The head-to-tail assembly of helix **P3** leads to a 2-dimensional metal-coordinated polymer while head-to-head assembly leads to a 3-dimensional porous framework. Readily accessible stable helical structures of  $\alpha,\gamma$ - hybrid peptides, their metal-driven supramolecular gelation, and 3D porous metal-helix networks reported here may serve as starting points for the construction of novel functional metal-helix frameworks with different side-chains and peptide lengths.

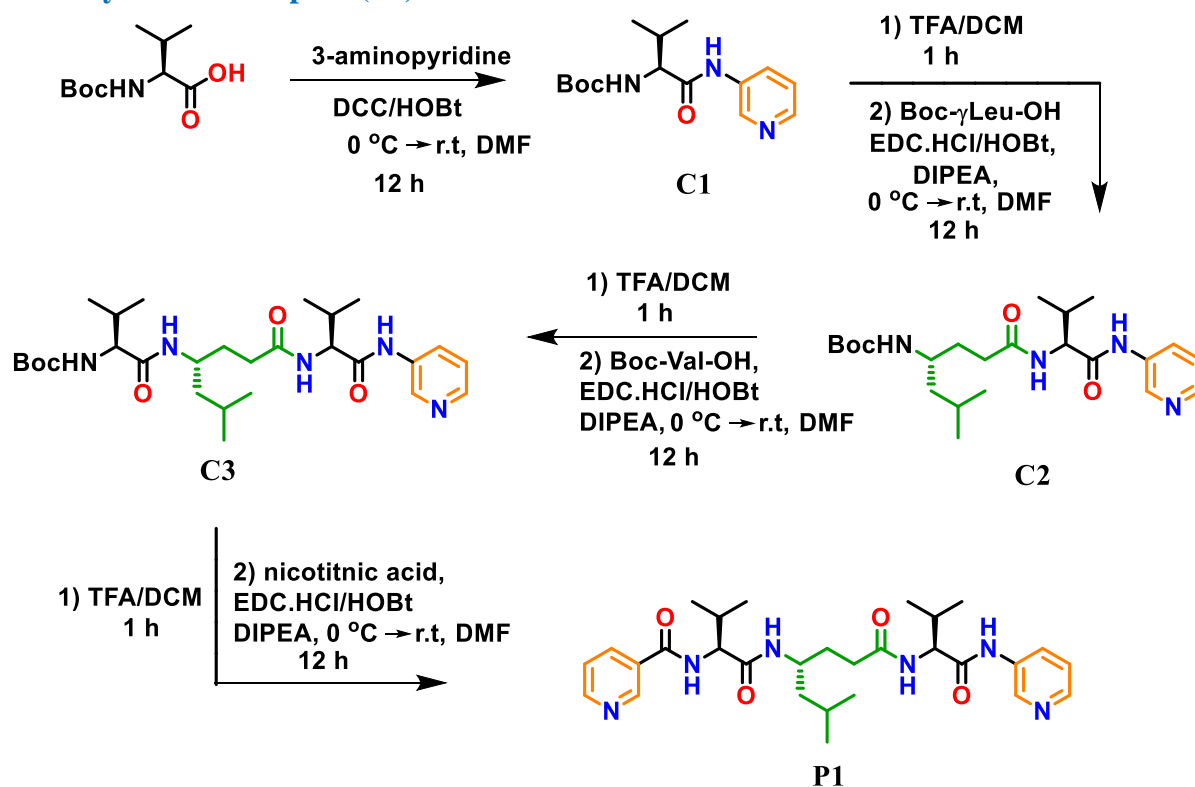
## 5. Experimental Section:

### 5.1. General Method:

All reagents were used without further purification. Column chromatography was performed on neutral alumina (100 -200 mesh). <sup>1</sup>H-NMR (400 MHz), and <sup>13</sup>C-NMR (100 MHz) were measured on a Bruker Avance 400 MHz spectrometer. Mass samples were analyzed MALDI/TOF-TOF. The X-ray data were collected at 100K temperature on a Bruker APEX(III) DUO CCD diffractometer using Mo K $\alpha$  radiation ( $\lambda = 0.71073 \text{ \AA}$ ) and Cu K $\alpha$  radiation ( $\lambda = 1.5418 \text{ \AA}$ ).

## 5.2. Procedure for the Synthesis of Peptides:

### 5.2.1. Synthesis of Peptide(P1):



**Scheme 2:** Synthesis of short  $\alpha,\gamma$ -hybrid tripeptide **P1**.

Boc-Valine-OH (10 mmol, 2.17 g) was taken in 20 mL of DMF and the solution was cooled down to 0 °C and kept in an N<sub>2</sub> atmosphere. Then DCC (10 mmol, 2.07g) and HOBt (10 mmol, 1.36 g) were added to the solution and left stirring for 5 mins. After that 3-amino pyridine (12 mmol, 1.13 g) was added to the reaction mixture and it was stirred for 12 h. Upon completion of the reaction checked by TLC, the reaction mixture was diluted with 250 ml of ethylacetate and it was filtered through a celite bed. Then, the filtrate was washed with (100 mL X 2), 10% Na<sub>2</sub>CO<sub>3</sub> solution (100 mL X 2), and then NaCl solution (100 mL X 2). The organic layer was collected and dried with anhydrous Na<sub>2</sub>SO<sub>4</sub> and concentrated under reduced pressure. The crude product was purified by column chromatography to get **C1** as a white solid (Yield- 2.54 g, 87%).

Boc deprotection of the compound **C1**(5.0 mmol, 1.47 g) was carried out by using 5 ml of each TFA and DCM (1:1) for 1 h. After that, TFA and solvent DCM were evaporated and 5-6 times DCM was added and evaporated to remove traces of TFA. The formed crude was TFA-salt of the amine of compound **C1** and to this 3 ml of DMF and 4.5 ml, of DIPEA were added to make it free amine of compound **C1**.

Boc- $\gamma$ leucine-OH (5 mmol, 1.3 g) was taken in 10 mL of DMF and the solution was cooled down to 0 °C and kept in an N<sub>2</sub> atmosphere. EDC.HCl (5 mmol, 0.96 g) and HOBt (5 mmol, 0.68 g), 2ml of DIPEA were added to the solution and the reaction mixture was stirred for 10 mins. After that, the free amine of compound C1 was added to the reaction mixture and stirred for 12 h. Upon completion of the reaction checked by TLC, the reaction mixture was diluted with 150 ml of ethyl acetate. Then, the mixture was washed with (100 mL X 2), 10% Na<sub>2</sub>CO<sub>3</sub> solution (100 mL X 2), and then NaCl solution (100 mL X 2). The organic layer was collected and dried with anhydrous Na<sub>2</sub>SO<sub>4</sub> and concentrated under reduced pressure. The crude product was purified by column chromatography to get dipeptide C2 as a white solid (Yield- 1.85 g, 85%).

Boc deprotection of dipeptide C2 (4.22 mmol, 1.85 g) was carried out by using 5 ml of each TFA and DCM (1:1) for 1 h. After that, TFA and solvent DCM were evaporated and 5-6 times DCM was added and evaporated to remove traces of TFA. The formed crude was TFA-salt of the amine of compound C2 and to this 2 ml of DMF and 3 ml, of DIPEA were added to make it free amine of dipeptide C2.

Boc-Valine-OH (5 mmol, 1.1 g) was taken in 10 mL of DMF and the solution was cooled down to 0 °C and kept in an N<sub>2</sub> atmosphere. EDC.HCl (5 mmol, 0.96 g) and HOBt (5 mmol, 0.68 g), 2 ml of DIPEA were added to the solution and the reaction mixture was stirred for 10 mins. After that, the free amine of dipeptide C2 was added to the reaction mixture and stirred for 12 h. Upon completion of the reaction monitored by TLC, the reaction mixture was diluted with 150 ml of ethyl acetate. Then, the mixture was washed with (100 mL X 2), 10% Na<sub>2</sub>CO<sub>3</sub> solution (100 mL X 2), and then NaCl solution (100 mL X 2). The organic layer was collected and dried with anhydrous Na<sub>2</sub>SO<sub>4</sub> and concentrated under reduced pressure. The crude product was purified by column chromatography to get tripeptide C3 as a white solid (Yield- 2.3 g, 85%).

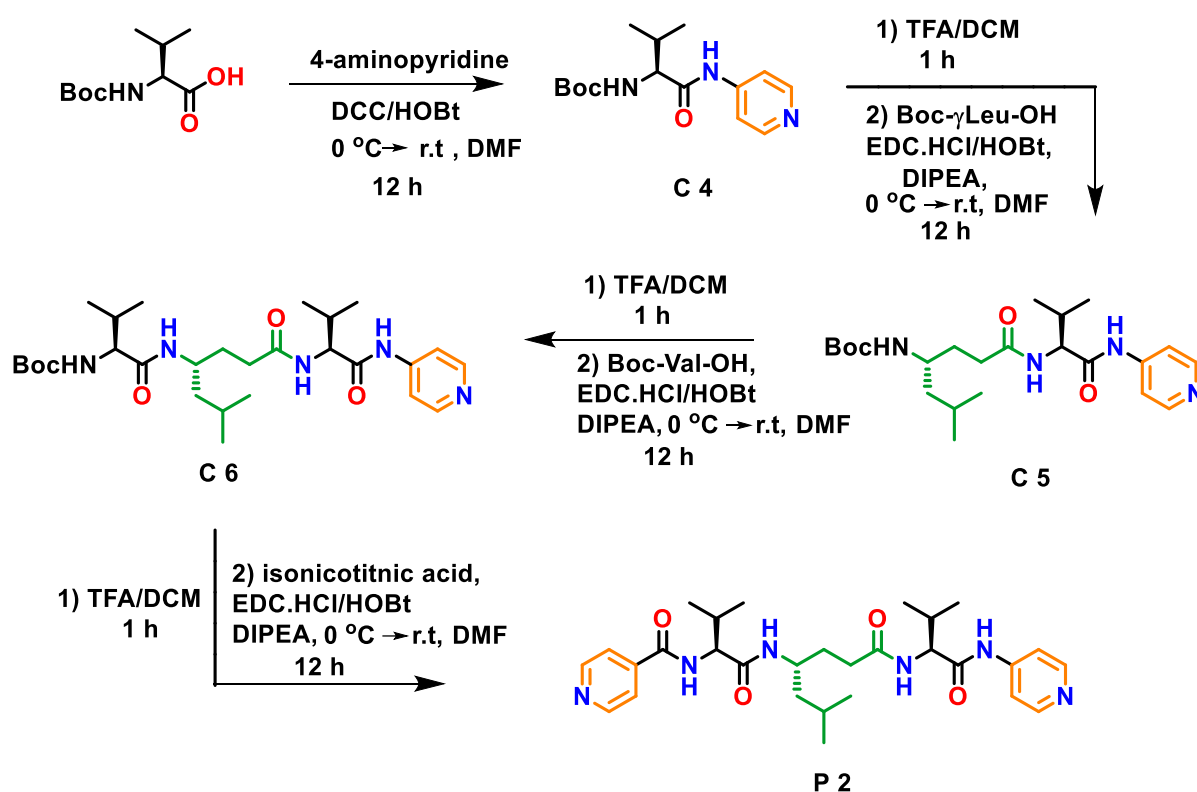
Boc deprotection of tripeptide C3 (4.3 mmol, 2.3 g) was carried out by using 5 ml of each TFA and DCM (1:1) for 1 h. After that, TFA and solvent DCM were evaporated and 5-6 times DCM was added and evaporated to remove traces of TFA. The formed crude was TFA-salt of the amine of tripeptide C3 and to this 4 ml of DMF and 4 ml, of DIPEA were added to make it free amine of tripeptide C3.

Finally, nicotinic acid (5.2 mmol, 0.64 g) dissolved in a mixture of 5 mL of DMF and 2 ml of DIPEA was added and the solution was cooled down to 0 °C and kept in an N<sub>2</sub> atmosphere.



EDC.HCl (5.2 mmol, 1.0 g) and HOBt (5.2 mmol, 0.707 g), 2 ml of DIPEA were added to the solution and the reaction mixture was stirred for 10 mins. After that, the free amine of tripeptide C3 was added to the reaction mixture and stirred for 12 h. Upon completion of the reaction monitored by TLC, the reaction mixture was diluted with 200 ml of ethyl acetate. Then, the mixture was washed with (100 mL X 2), 10% Na<sub>2</sub>CO<sub>3</sub> solution (100 mL X 2), and then NaCl solution (100 mL X 2). The organic layer was collected and dried with anhydrous Na<sub>2</sub>SO<sub>4</sub> and concentrated under reduced pressure. The crude product was purified by column chromatography to get peptide P1 as a white solid (Yield- 2.2 g, 80%).

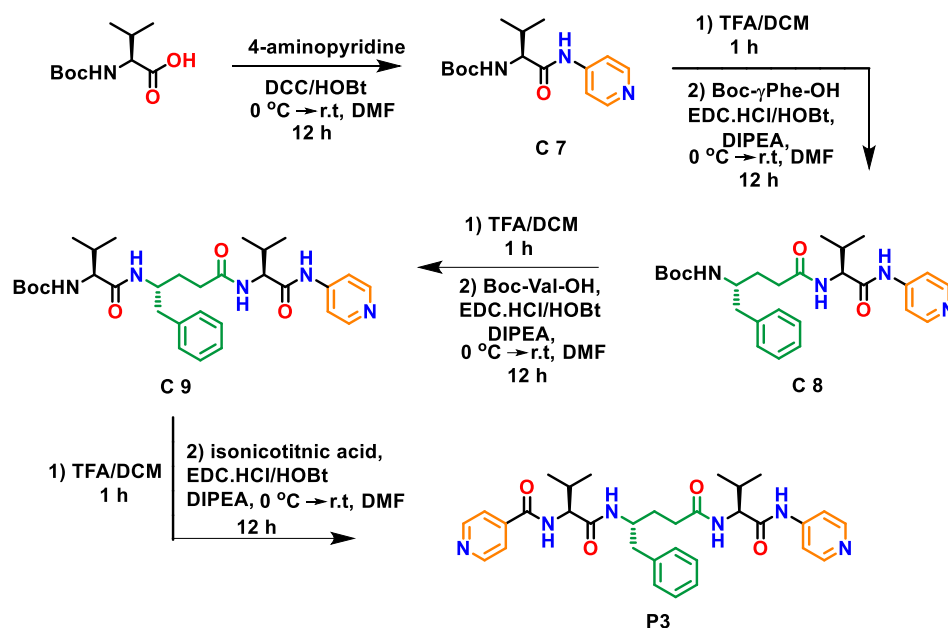
### 5.2.2. Synthesis of Peptide(P2):



**Scheme 2:** Synthesis of short  $\alpha,\gamma$ -hybrid tripeptide **P2**.

The synthesis of **P2** was carried out as described in the above scheme, following similar protocols as of **P1** (Yield- 1.5 g, 80%).

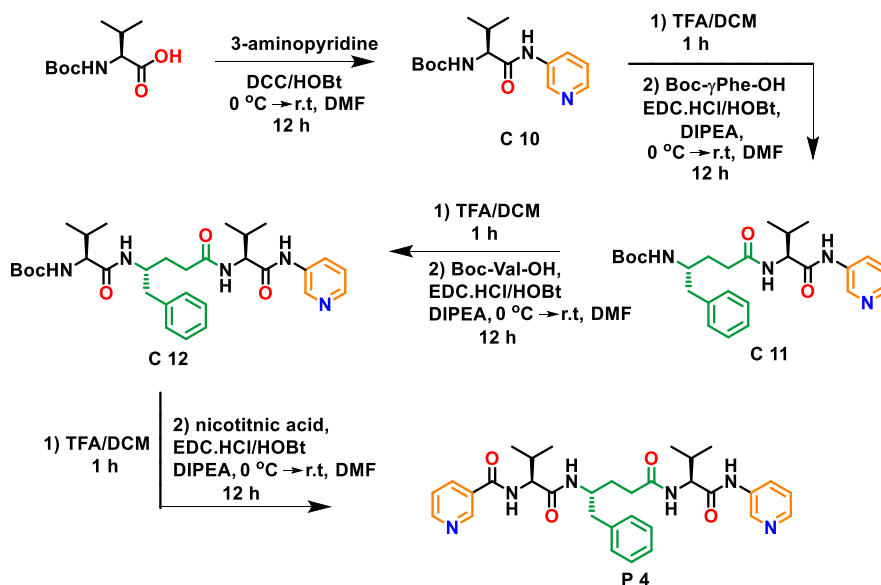
### 5.2.3. Synthesis of Peptide(P3):



**Scheme 3:** Synthesis of short  $\alpha,\gamma$ -hybrid tripeptide **P3**.

The synthesis of **P3** was carried out as described in the above scheme, following similar protocols as of **P1** (Yield- 1.8 g, 82%).

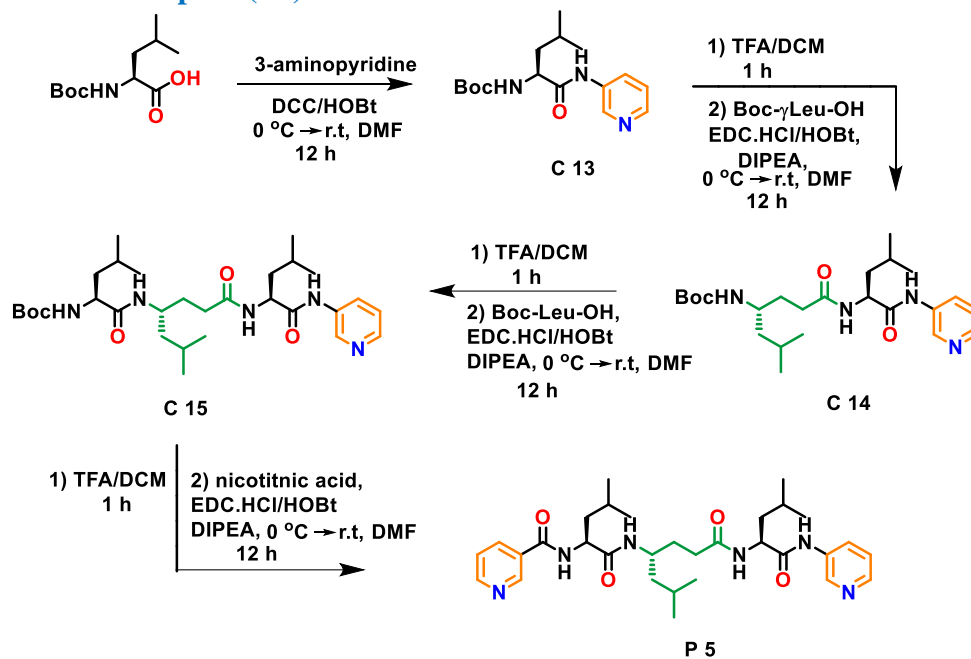
### 5.2.4. Synthesis of Peptide(P4):



**Scheme 4:** Synthesis of short  $\alpha,\gamma$ -hybrid tripeptide **P4**.

The synthesis of **P4** was carried out as described in the above scheme, following similar protocols as of **P1** (Yield- 1.4 g, 74%).

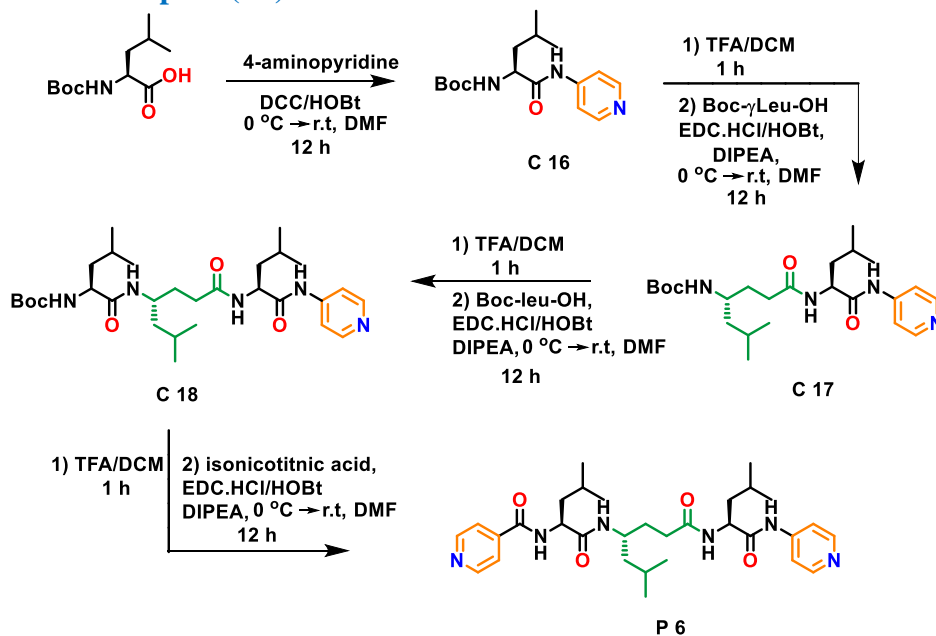
### 5.2.5. Synthesis of Peptide(P5):



**Scheme 5:** Synthesis of short  $\alpha,\gamma$ -hybrid tripeptide **P5**.

The synthesis of **P5** was carried out as described in the above scheme, following similar protocols as of **P1** (Yield- 1.2 g, 84%).

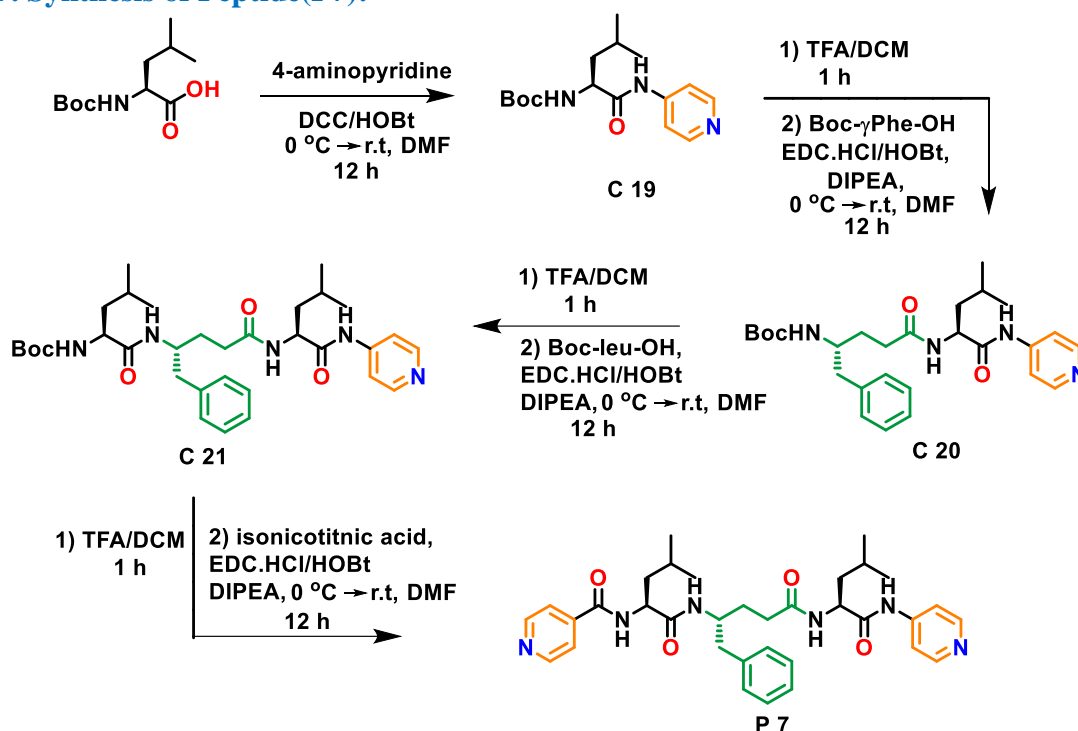
### 5.2.6. Synthesis of Peptide(P6):



**Scheme 6:** Synthesis of short  $\alpha,\gamma$ -hybrid tripeptide **P6**.

The synthesis of **P6** was carried out as described in the above scheme, following similar protocols as of **P1** (Yield- 1.1 g, 82%).

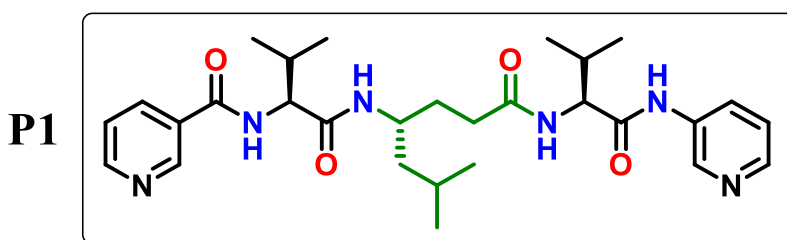
### 5.2.7. Synthesis of Peptide(P7):



**Scheme 7:** Synthesis of short  $\alpha,\gamma$ -hybrid tripeptide **P7**.

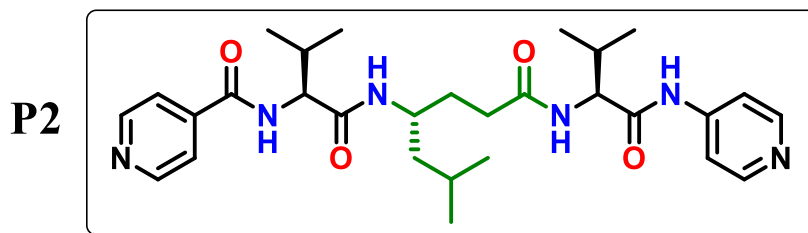
The synthesis of **P7** was carried out as described in the above scheme, following similar protocols as of **P1** (Yield- 1.0 g, 76%).

### 5.3. Characterization of Peptides(P1-P7):

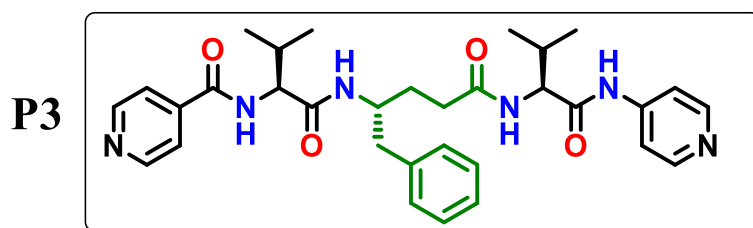


**Peptide P1:** White solid; yield 80%; <sup>1</sup>H-NMR (400 MHz, DMSO-d<sub>6</sub>)  $\delta$  10.22 (d,  $J$  = 10.7 Hz, 1H), 8.98 (dd,  $J$  = 6.5, 5.3 Hz, 1H), 8.76 – 8.70 (m, 1H), 8.66 (ddd,  $J$  = 4.7, 2.9, 1.7 Hz, 1H), 8.48 (dd,  $J$  = 13.7, 8.2 Hz, 1H), 8.21 (d,  $J$  = 4.6 Hz, 1H), 8.16 (dt,  $J$  = 8.0, 1.9 Hz, 1H), 8.05 – 7.95 (m, 2H), 7.89 – 7.71 (m, 1H), 7.50 – 7.41 (m, 1H), 7.33 – 7.24 (m, 1H), 4.24 – 4.14 (m, 2H), 3.77 (d,  $J$  = 4.3 Hz, 1H), 2.17 – 1.86 (m, 4H), 1.62 – 1.43 (m, 3H), 1.23 – 1.13 (m, 2H), 0.92 – 0.73 (m, 18H). <sup>13</sup>C-NMR (100 MHz, DMSO-d<sub>6</sub>)  $\delta$  173.01, 171.48, 171.45, 170.74, 165.97, 165.70, 152.29, 149.13, 144.74, 141.45, 136.29, 135.54, 130.36, 126.70, 124.02, 123.73, 60.11, 59.34, 44.03, 43.86, 43.54, 32.32, 31.80, 30.73, 30.33, 29.45, 24.80, 23.61,

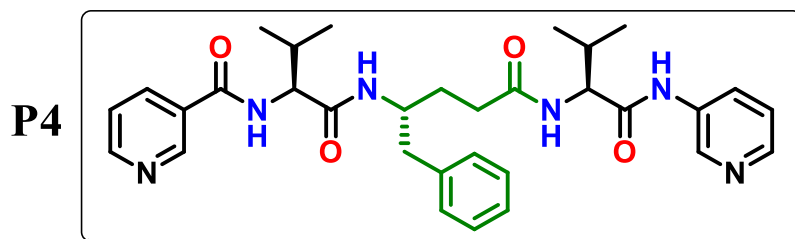
22.16, 20.04, 19.32, 19.17, 18.77. MALDI/TOF-TOF  $m/z$  calculated value for  $C_{29}H_{42}N_6O_4$   $[M+Na^+]$  is 561.32 and the observed peak is 561.44.



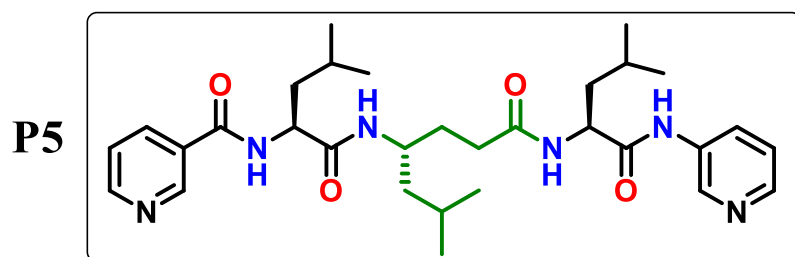
**Peptide P2:** White solid; yield 80%;  $^1H$ -NMR (400 MHz, DMSO- $d_6$ )  $\delta$  10.46 – 10.36 (m, 1H), 8.67 (t,  $J$  = 5.1 Hz, 2H), 8.61 – 8.48 (m, 1H), 8.36 (t,  $J$  = 5.6 Hz, 2H), 8.05 – 7.88 (m, 1H), 7.84 – 7.68 (m, 3H), 7.58 – 7.50 (m, 2H), 4.21 (tt,  $J$  = 8.4, 6.8 Hz, 2H), 3.77 (s, 1H), 2.21 – 2.05 (m, 3H), 1.94 (qd,  $J$  = 13.5, 6.7 Hz, 1H), 1.63 – 1.45 (m, 3H), 1.29 (dt,  $J$  = 14.4, 6.0 Hz, 1H), 1.18 – 1.10 (m, 1H), 0.91 – 0.73 (m, 18H).  $^{13}C$ -NMR (100 MHz, DMSO- $d_6$ )  $\delta$  172.96, 172.20, 170.73, 165.58, 150.80, 150.52, 145.80, 141.78, 122.03, 113.73, 60.11, 59.54, 59.20, 46.81, 44.29, 44.19, 44.00, 32.46, 32.19, 31.80, 30.77, 30.44, 30.21, 24.78, 23.65, 22.17, 20.24, 19.46, 19.26, 18.76. MALDI/TOF-TOF  $m/z$  calculated value for  $C_{29}H_{42}N_6O_4$   $[M+Na^+]$  is 561.32 and the observed peak is 561.47.



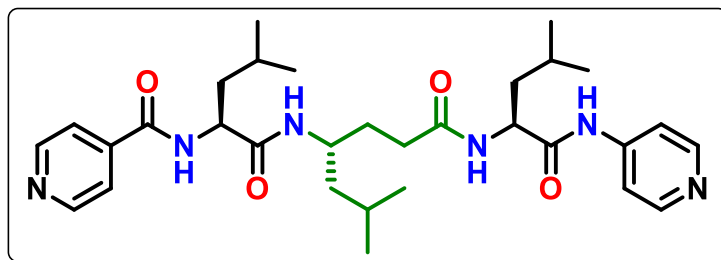
**Peptide P3:** White solid; yield 82%;  $^1H$  NMR (400 MHz, DMSO- $d_6$ )  $\delta$  10.44 (s, 1H), 8.81 – 8.62 (m, 2H), 8.52 (d,  $J$  = 8.6 Hz, 1H), 8.44 – 8.36 (m, 2H), 8.03 (d,  $J$  = 8.1 Hz, 1H), 7.95 (d,  $J$  = 8.4 Hz, 1H), 7.82 – 7.73 (m, 2H), 7.68 – 7.53 (m, 2H), 7.22 – 6.96 (m, 5H), 4.22 (q,  $J$  = 8.8, 8.2 Hz, 2H), 3.93 (s, 1H), 2.69 (qd,  $J$  = 13.6, 6.7 Hz, 2H), 2.21 (ddd,  $J$  = 19.2, 9.0, 5.7 Hz, 2H), 2.02 (dq,  $J$  = 17.3, 6.7 Hz, 2H), 1.78 – 1.49 (m, 2H), 0.92 – 0.81 (m, 12H).  $^{13}C$  NMR (100 MHz, DMSO- $d_6$ )  $\delta$  172.92, 172.28, 170.80, 165.46, 150.90, 150.61, 145.84, 141.77, 139.21, 129.73, 128.46, 126.40, 122.12, 113.81, 60.26, 59.58, 50.37, 32.39, 31.23, 30.79, 30.49, 30.31, 19.88, 19.66, 19.43, 18.88. MALDI/TOF-TOF  $m/z$  calculated value for  $C_{32}H_{40}N_6O_4$   $[M+Na]^+$  is 595.30 and the observed peak is 595.42.



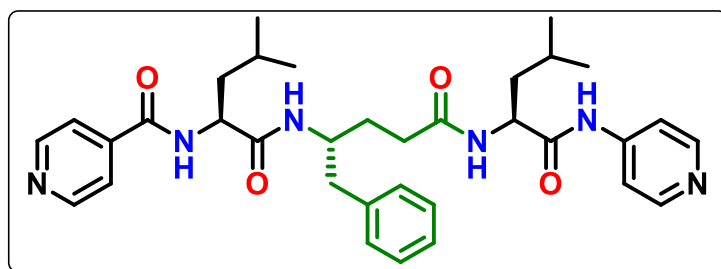
**Peptide P4:** White solid; yield 74%;  $^1\text{H-NMR}$  (400 MHz,  $\text{DMSO-d}_6$ )  $\delta$  10.27 (s, 1H), 9.01 (dd,  $J = 2.4, 0.9$  Hz, 1H), 8.79 – 8.65 (m, 2H), 8.45 (d,  $J = 8.5$  Hz, 1H), 8.29 – 8.16 (m, 2H), 8.07 – 7.96 (m, 2H), 7.92 (d,  $J = 8.6$  Hz, 1H), 7.50 (ddd,  $J = 8.0, 4.8, 0.9$  Hz, 1H), 7.37 – 7.28 (m, 1H), 7.20 – 7.02 (m, 5H), 4.28 – 4.17 (m, 2H), 3.93 (q,  $J = 8.7$  Hz, 1H), 2.69 (qd,  $J = 13.6, 6.8$  Hz, 2H), 2.31 – 2.10 (m, 2H), 2.11 – 1.94 (m, 2H), 1.62 (dddd,  $J = 37.9, 19.1, 8.4, 5.2$  Hz, 2H), 0.92 – 0.81 (m, 12H).  $^{13}\text{C-NMR}$  (101 MHz,  $\text{DMSO-d}_6$ )  $\delta$  172.86, 171.54, 170.98, 165.60, 152.36, 149.23, 144.84, 141.46, 139.24, 135.98, 135.83, 130.36, 129.73, 128.46, 126.73, 126.36, 124.14, 123.82, 60.23, 59.38, 50.33, 32.42, 30.90, 30.52, 30.33, 19.89, 19.70, 19.45, 18.91. MALDI/TOF-TOF  $m/z$  calculated value for  $\text{C}_{32}\text{H}_{40}\text{N}_6\text{O}_4$  [ $\text{M}+\text{Na}^+$ ] is 595.30 and the observed peak is 595.45.



**Peptide P5:** White solid; yield 84%;  $^1\text{H NMR}$  (400 MHz,  $\text{CDCl}_3$ )  $\delta$  10.26 (s, 1H), 9.15 (d,  $J = 2.2$  Hz, 1H), 8.78 (d,  $J = 2.7$  Hz, 1H), 8.59 – 8.50 (m, 2H), 8.24 – 8.18 (m, 3H), 7.99 (d,  $J = 7.2$  Hz, 1H), 7.91 (s, 1H), 7.77 (d,  $J = 9.0$  Hz, 2H), 7.15 (d,  $J = 4.9$  Hz, 1H), 7.07 – 7.04 (m, 1H), 4.51 (d,  $J = 6.2$  Hz, 1H), 4.37 (s, 1H), 3.91 (s, 1H), 2.35 (d,  $J = 27.8$  Hz, 2H), 2.15 (s, 2H), 2.01 – 1.90 (m, 10H), 1.74 (d,  $J = 8.2$  Hz, 2H), 1.66 – 1.52 (m, 2H), 1.37 (s, 1H), 1.08 – 1.00 (m, 12H), 0.83 – 0.79 (m, 4H).  $^{13}\text{C NMR}$  (101 MHz,  $\text{CDCl}_3$ )  $\delta$  174.39, 173.93, 173.31, 167.15, 152.32, 149.03, 144.53, 141.76, 135.61, 135.24, 131.51, 128.71, 126.99, 123.12, 55.76, 55.66, 46.57, 44.83, 40.85, 40.61, 25.26, 25.13, 25.04, 23.31, 23.23, 22.88, 22.23, 22.12, 21.62, 21.12. MALDI/TOF-TOF  $m/z$  calculated value for  $\text{C}_{32}\text{H}_{40}\text{N}_6\text{O}_4$  [ $\text{M}+\text{Na}^+$ ] is 589.35 and the observed peak is 589.52.

**P6**

**Peptide P6:** White solid; yield 82%;  $^1\text{H-NMR}$  (400 MHz, Chloroform- $d$ )  $\delta$  10.46 (d,  $J = 48.5$  Hz, 1H), 9.10 – 8.77 (m, 2H), 8.51 (dd,  $J = 11.0, 5.1$  Hz, 2H), 8.25 (t,  $J = 5.5$  Hz, 2H), 7.56 (dd,  $J = 11.8, 5.2$  Hz, 2H), 7.26 (s, 2H), 4.57 (d,  $J = 45.6$  Hz, 2H), 4.30 (s, 1H), 2.42 (s, 2H), 2.22 (s, 1H), 1.91 (s, 4H), 1.53 (d,  $J = 12.8$  Hz, 3H), 1.35 (d,  $J = 9.1$  Hz, 1H), 1.09 – 0.82 (m, 20H).  $^{13}\text{C-NMR}$  (101 MHz, DMSO- $d_6$ )  $\delta$  172.87, 172.81, 172.58, 172.49, 171.58, 164.96, 150.40, 150.32, 150.19, 145.64, 141.19, 141.17, 121.62, 121.60, 113.48, 113.39, 52.39, 52.11, 46.31, 43.87, 43.57, 40.60, 40.43, 32.08, 31.86, 31.49, 24.55, 24.49, 24.42, 24.34, 23.29, 23.23, 23.11, 23.07, 23.00, 21.83, 21.79, 21.55, 21.51. MALDI/TOF-TOF  $m/z$  calculated value for  $\text{C}_{32}\text{H}_{40}\text{N}_6\text{O}_4$  [ $\text{M}+\text{Na}^+$ ] is 589.35 and the observed peak is 588.25.

**P7**

**Peptide P7:** White solid; yield 76%;  $^1\text{H NMR}$  (400 MHz, DMSO- $d_6$ )  $\delta$  10.38 (s, 1H), 8.75 – 8.71 (m, 2H), 8.68 (d,  $J = 8.1$  Hz, 1H), 8.40 (d,  $J = 6.3$  Hz, 2H), 8.09 (d,  $J = 7.4$  Hz, 1H), 7.90 (d,  $J = 8.6$  Hz, 1H), 7.80 (d,  $J = 6.1$  Hz, 2H), 7.57 (d,  $J = 6.4$  Hz, 2H), 7.18 – 7.12 (m, 5H), 4.52 – 4.43 (m, 1H), 4.44 – 4.34 (m, 1H), 3.89 (d,  $J = 4.9$  Hz, 1H), 2.71 (d,  $J = 6.8$  Hz, 2H), 2.19 – 2.08 (m, 2H), 1.67 – 1.45 (m, 8H), 0.90 – 0.83 (m, 12H).  $^{13}\text{C NMR}$  (101 MHz, DMSO- $d_6$ )  $\delta$  172.32, 171.88, 171.00, 164.35, 149.90, 149.70, 145.12, 140.65, 138.32, 128.78, 127.56, 125.49, 121.15, 112.94, 51.85, 49.27, 31.39, 29.47, 23.96, 23.92, 22.50, 22.45, 21.17, 21.05. MALDI/TOF-TOF  $m/z$  calculated value for  $\text{C}_{32}\text{H}_{40}\text{N}_6\text{O}_4$  [ $\text{M}+\text{Na}^+$ ] is 623.33 and the observed peak is 622.72.

## 6. Appendix:

### 6.1. Crystallographic Information:

Parameters	Peptide(P1)	Peptide(P2)	Peptide(P5)
Solvent for crystallization	CDCl <sub>3</sub>	CDCl <sub>3</sub>	ACN/MeOH
Chemical formula	C <sub>29</sub> H <sub>42</sub> N <sub>6</sub> O <sub>4</sub>	C <sub>29</sub> H <sub>42</sub> N <sub>6</sub> O <sub>4</sub>	C <sub>31</sub> H <sub>46</sub> N <sub>6</sub> O <sub>4</sub>
Molecular weight	561.32	561.32	589.35
Crystal size (nm)	(0.20 × 0.12 × 0.18) nm	(0.18 × 0.11 × 0.16) nm	(0.18 × 0.16 × 0.16) nm
Radiation source	Cu Kα (λ = 1.5418Å)	Mo Kα (λ = 0.71073Å)	Mo Kα (λ = 0.71073Å)
Space group	P2 <sub>1</sub> 2 <sub>1</sub> 2 <sub>1</sub> (orthorhombic)	P2 <sub>1</sub> (monoclinic)	C2 (monoclinic)
a (Å)	15.7231(7)	9.712(5)	18.7510(8)
b (Å)	15.9965(8)	21.782(12)	16.6741(6)
c (Å)	16.980(7)	16.280(9)	21.2227(9)
α (°)	90	90	90
β (°)	90	92.771(8)	97.885(2)
γ (°)	90	90	90
h <sub>max</sub>	12	13	22
k <sub>max</sub>	19	29	19
l <sub>max</sub>	20	22	25
Volume (Å <sup>3</sup> )	4270.8(3)	3440(3)	6572.7(5)
Z	4	4	4
Density (g/cm <sup>3</sup> )(cal)	1.395	1.271	1.144
Molecules in asymmetric unit	1	2	2
F (000)	15130	8556	2440
2θ Max. (°)	137.08	57.66	50.14
μ mm <sup>-1</sup>	5.743	0.309	0.077



Reflections (cal)	7558	17516	11591
Variables	466	787	752
R (reflections)	6929	6948	10239
R <sub>factor</sub>	0.0597	0.0905	0.0860
wR2 (Reflections)	0.1623	0.2551	0.2388
Goodness-of- fit (S)	1.028	1.017	1.071
Software used	Bruker APEX(III)	Bruker APEX(III)	Bruker APEX(III)
Method used	SHELXS-97 <sup>28</sup>	SHELXS-97 <sup>28</sup>	SHELXS-97 <sup>28</sup>

Parameters	Peptide(P6)	Peptide(P7)	P3-AgBF <sub>4</sub> complex	P3-AgPF <sub>6</sub> complex
Solvent for crystallization	ACN	CHCl <sub>3</sub> /MeOH/ Toluene	CD <sub>3</sub> OH	EtOH
Chemical formula	C <sub>31</sub> H <sub>46</sub> N <sub>6</sub> O <sub>4</sub>	C <sub>34</sub> H <sub>44</sub> N <sub>6</sub> O <sub>4</sub>	C <sub>32</sub> H <sub>40</sub> Ag N <sub>6</sub> O <sub>4</sub> BF <sub>4</sub> ,	C <sub>64</sub> H <sub>80</sub> Ag <sub>2</sub> N <sub>12</sub> O <sub>8</sub> PF <sub>6</sub>
Molecular weight	589.35	623.33	789.97	848.13
Crystal size (nm)	(0.20 × 0.20 × 0.16) mm	(0.18 × 0.20 × 0.18)mm	(0.16 × 0.12 × 0.14) mm	(0.16 × 0.14 × 0.18) mm
Radiation source	Mo K $\alpha$ ( $\lambda = 0.71073\text{Å}$ )	Mo K $\alpha$ ( $\lambda = 0.71073\text{Å}$ )	Mo K $\alpha$ ( $\lambda = 0.71073\text{Å}$ )	Mo K $\alpha$ ( $\lambda = 0.71073\text{Å}$ )
Space group	C2	P2 <sub>1</sub> 2 <sub>1</sub> 2 <sub>1</sub> (orthorhombic)	P2 <sub>1</sub> (monoclinic)	C <sub>2</sub> (monoclinic)
a (Å)	19.083(3)	12.3590(9)	10.066(4)	21.196(8)
b (Å)	16.745(2)	15.9096(11)	13.261(5)	17.267(7)
c (Å)	20.733(3)	23.0887(18)	14.594(5)	13.227(5)
$\alpha$ (°)	90	90	90	90
$\beta$ (°)	95.929(4)	90	92.663(10)	121.505(10)

$\gamma(^{\circ})$	90	90	90	90
$h_{\max}$	22	14	13	26
$k_{\max}$	19	16	17	23
$l_{\max}$	22	27	16	17
Volume ( $\text{\AA}^3$ )	6590.0(19)	4539.9(6)	1946(13)	4127(3)
Z	8	4	2	2
Density ( $\text{g/cm}^3$ )(cal)	1.142	1.403	1.310	1.212
Molecules in asymmetric unit	2	1	1	2
F (000)	2448	1984	788	1550
$2\theta$ Max. ( $^{\circ}$ )	50.05	50.05	57.66	56.742
$\mu \text{ mm}^{-1}$	0.077	0.600	0.577	0.558
Reflections (cal)	11531	7953	9384	10263
Variables	752	509	438	426
R (reflections)	8026	4826	5573	6099
$R_{\text{factor}}$	0.0646	0.0697	0.1228	0.0507
wR2 (Reflections)	0.2388	0.1505	0.3366	0.1226
Goodness-of- fit (S)	1.049	1.012	1.060	1.013
Software used	Bruker APEX(III)	Bruker APEX(III)	Bruker APEX(III)	Bruker APEX(III)
Method used	SHELXS-97 <sup>28</sup>	SHELXS-97 <sup>28</sup>	SHELXS-97 <sup>28</sup>	SHELXS-97 <sup>28</sup>
Special method used	-	-		SQUEEZE of program PLATON <sup>29</sup>

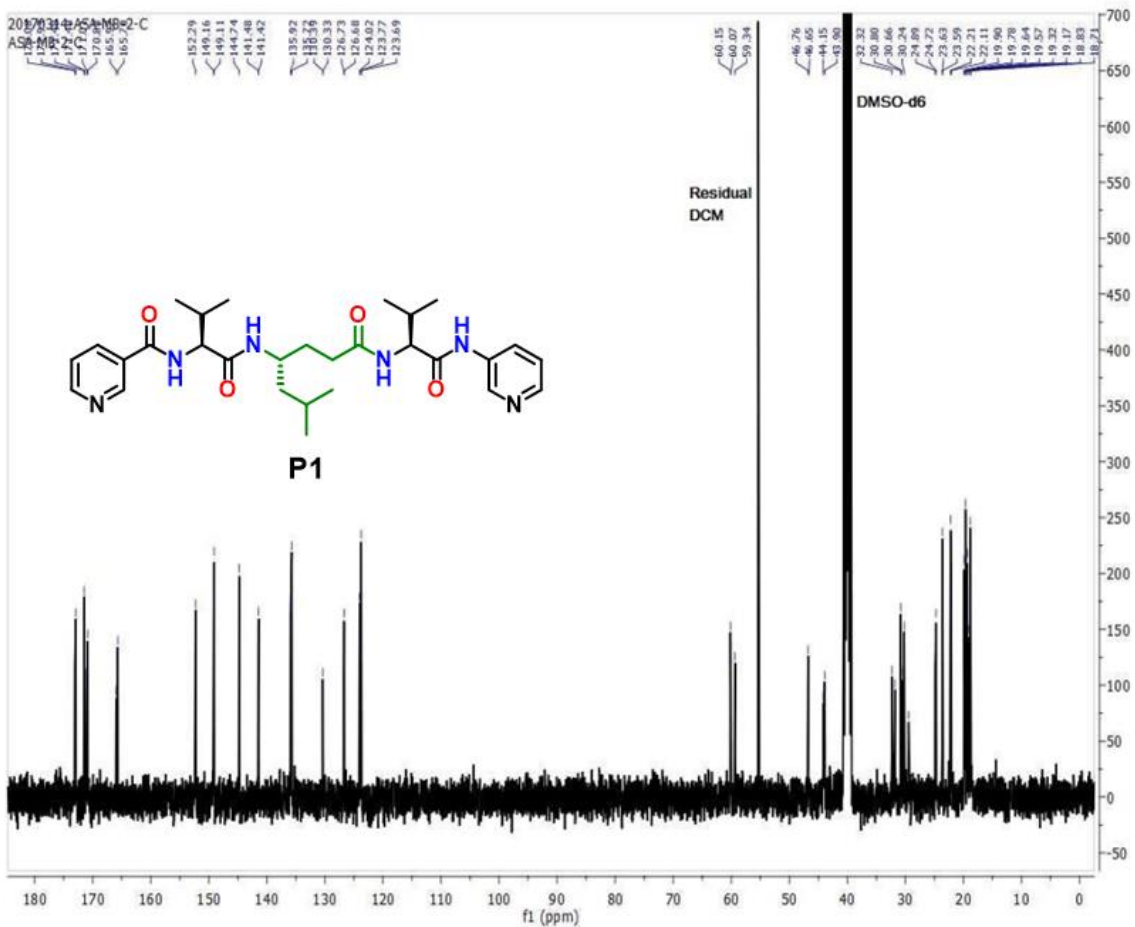
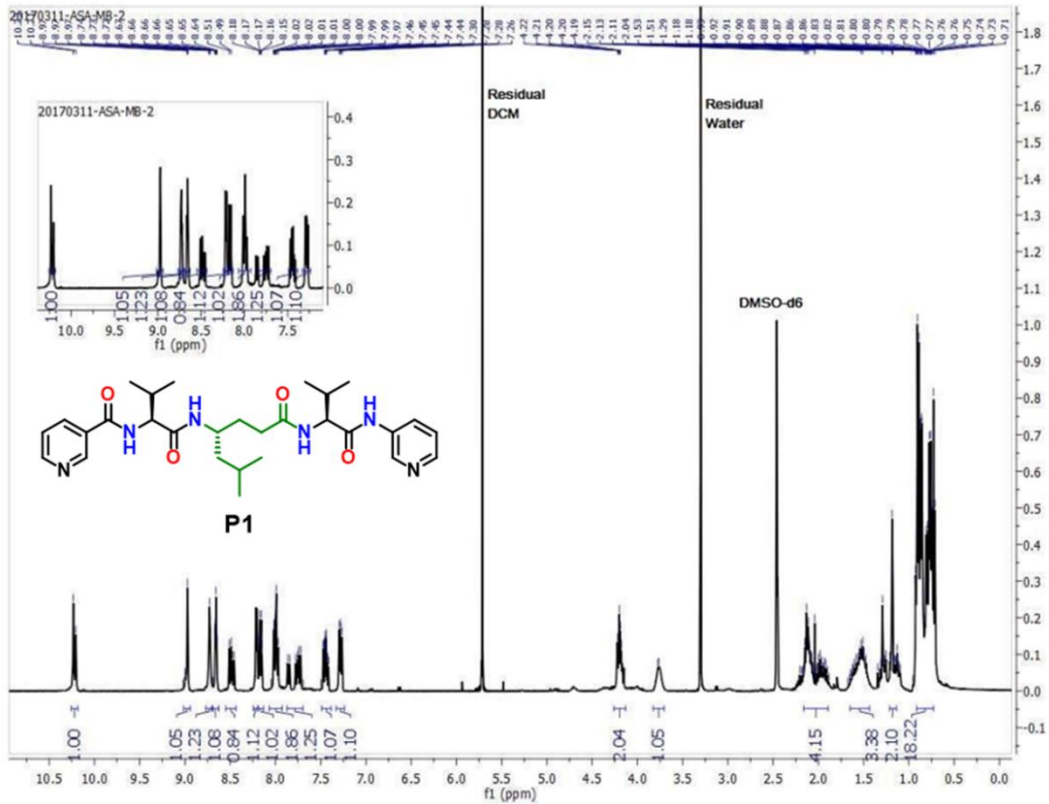
## 7. References:

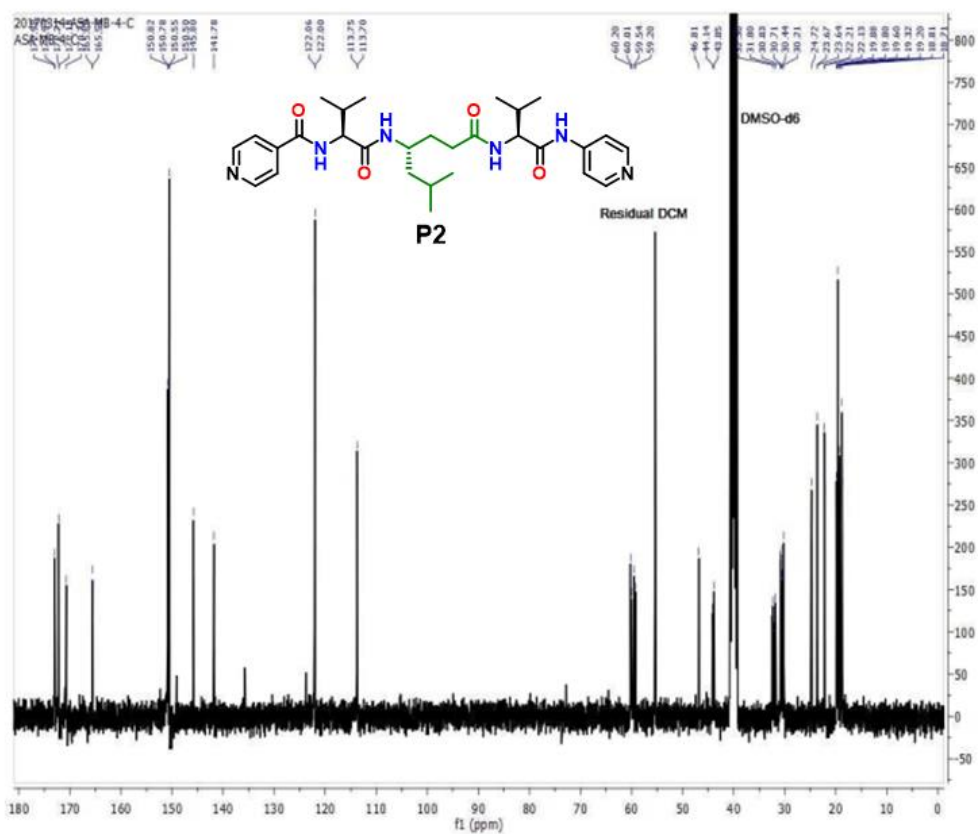
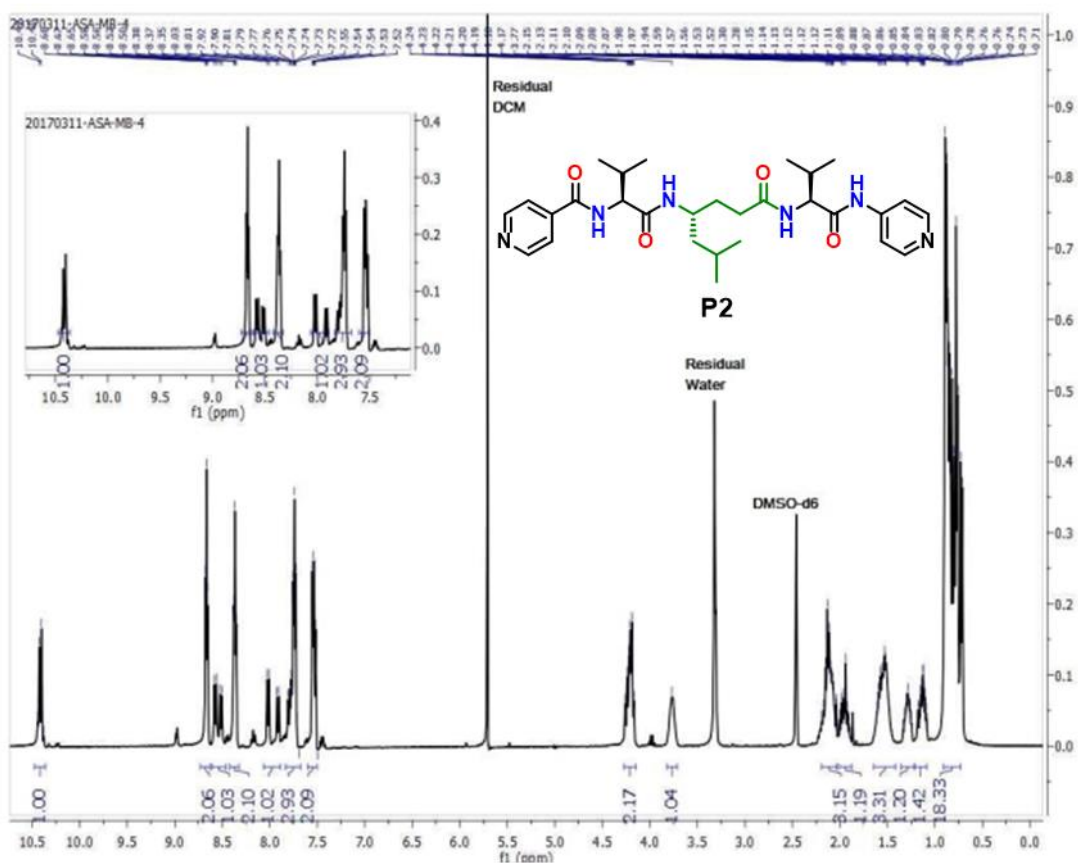
1. Lloyd, D.J.; In *Colloid Chemistry*, Alexander, J.; Ed. Chemical Catalogue Company: New York, 1926; Vol. 1.
2. (a) Kuroiwa, K.; Shibata, T.; Takada, A.; Nemoto, N.; Kimizuka, N. *J. Am. Chem. Soc.* **2004**, *126*, 2016. (b) Kuosmanen, R.; Rissanen, K.; Sievänen, E. *Chem. Soc. Rev.* **2020**, *49*, 1977.
3. (a) Tam, A. Y-Y.; Yam, V. W-W. *Chem. Soc. Rev.* **2013**, *42*, 1540. (b) Sutar, P.; Maji, T. K. *Chem. Commun.* **2016**, *52*, 8055. (c) Jones, C. D.; Steed, J. W. *Chem. Soc. Rev.* **2016**, *45*, 6546. (d) Christoff-Tempesta, T.; Lew, A. J.; Ortony, J. H. *Gels* **2018**, *4*, 40.
4. (a) Sangeetha, N. M.; Maitra, U. *Chem. Soc. Rev.* **2005**, *34*, 821. (b) Yu, G.; Yan, X.; Han, C.; Huang, F. *Chem. Soc. Rev.* **2013**, *42*, 6697. (c) Kuosmanen, R.; Rissanen, K.; Sievanen, E. *Chem. Soc. Rev.* **2020**, *49*, 1977.
5. (a) Huang, X.; Li, R.; Duan, Z.; Xu, F.; Li, H. *Soft Matter*, **2022**, *18*, 3828. (b) Sóvágó, I.; Kállay, C.; Várnagy, K. *Coord. Chem. Rev.* **2012**, *256*, 2225. (c) McEwen, H.; Du, E. Y.; Mata, J. P.; Thordarson, P.; Martin, A. *J. Mater. Chem. B* **2017**, *5*, 9412. (d) Shao, T.; Falcone, N.; Kraatz, H-B. *ACS Omega*. **2020**, *5*, 1312.
6. (a) Gellman, S. H. *Acc. Chem. Res.* **1998**, *31*, 173. (b) Goodman, C. M.; Choi, S.; Shandler, S.; DeGrado, W. F. *Nat. Chem. Bio.* **2007**, *3*, 252. (c) Guichard, G.; Huc, I.; *Chem. Commun.* **2011**, *47*, 5933. (d) Vasudev, P. G.; Chatterjee, S.; Shamala, N.; Balaram, P. *Chem. Rev.* **2011**, *111*, 657. (e) Seebach, D.; Beck, A. K.; Bierbaum, D. J. *Chem. Biodiversity* **2004**, *1*, 1111.
7. (a) Agar, J. N.; Krebs, C.; Frazzon, J. *Biochemistry* **2000**, *39*, 7856. (b) Bertini, I.; Cavallaro, G.; Rosato, A.; *Chem. Rev.* **2006**, *106*, 90. (c) Cox, E. H.; McLendon, G. L. *Curr. Opin. Chem. Biol.* **2000**, *4*, 162. (d) Permyakov, E. A. *John Wiley & Sons, Inc.* **2009**, *7*.
8. (a) Peacock, A. F. *Curr. Opin. Chem. Biol.* **2013**, *17*, 934. (b) Sontz, P. A.; Song, W. J.; Tezcan, A. F. *Curr. Opin. Chem. Biol.* **2014**, *19*, 42. (c) Rittle, J.; Field, M. J.; Green, M. T.; Tezcan, A. F. *Nat. Chem.* **2019**, *11*, 434. (d) Churchfield, L. A.; Tezcan, A. F. *Acc. Chem. Res.* **2019**, *52*, 345.
9. (a) Zou, R.; Wang, Q.; Wu, J.; Wu, J.; Schmuck, C.; Tian, H. *Chem. Soc. Rev.* **2015**, *44*, 5200. (b) Tashiro, S.; Shionoya, M. *Chem. Lett.* **2013**, *42*, 456. (c) Rufo, C. M.; Moroz, Y. S.; Moroz, O. V.; Stöhr, J.; Smith, T. A.; Hu, X.; DeGrado, W. F.; Korendovych, I. V. *Nat. Chem.* **2014**, *6*, 303. (d) Ousaka, N.; Takeyama, Y.; Iida, H.;

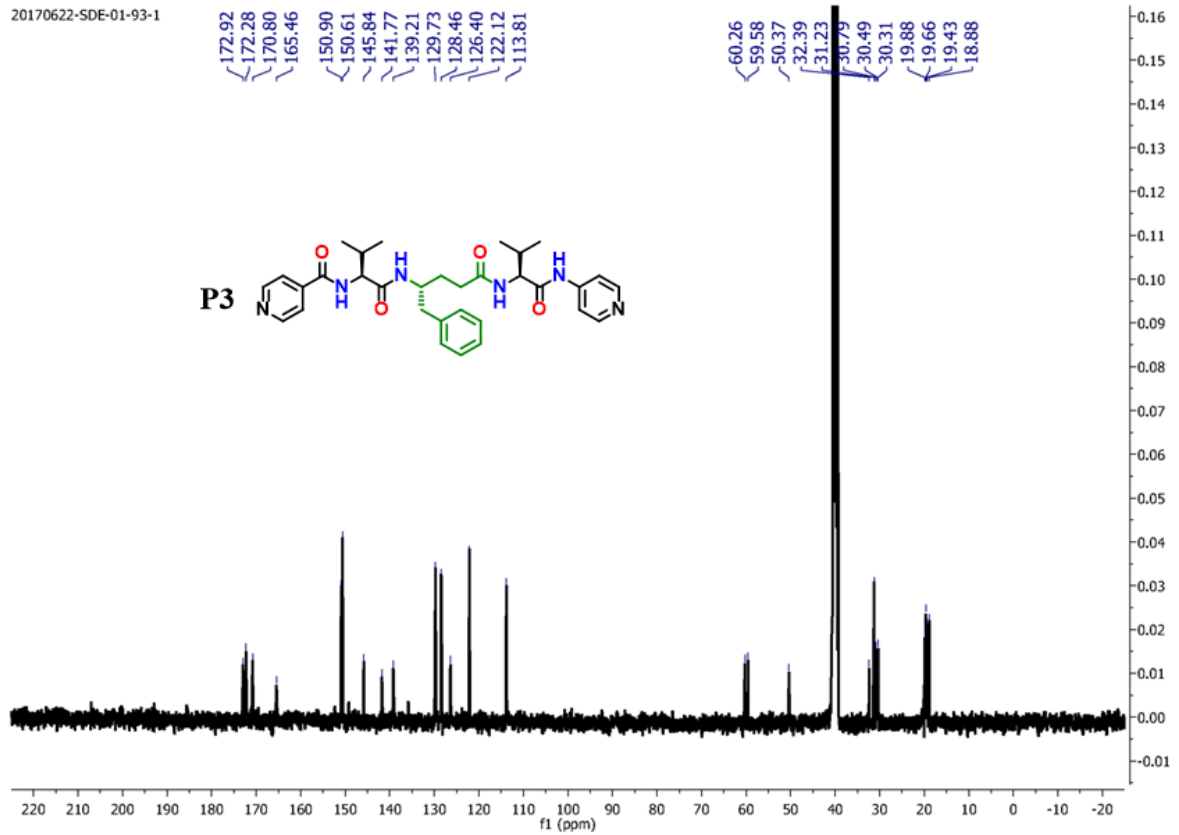
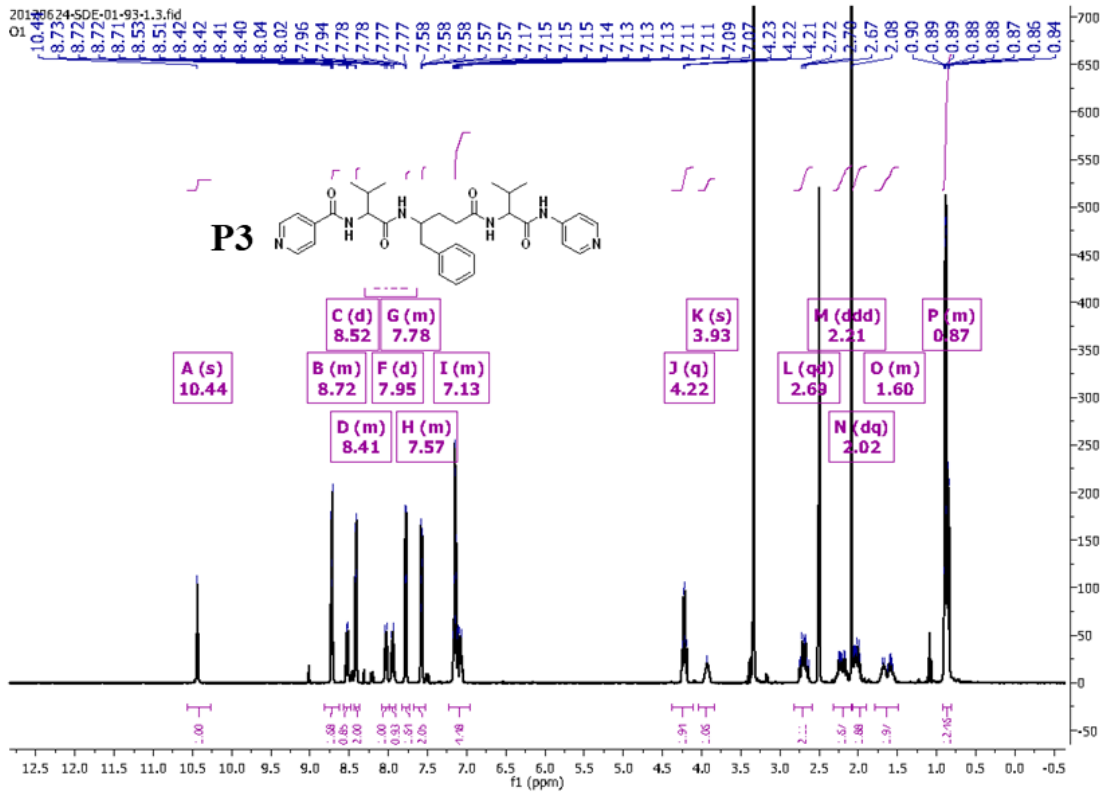
- Yashima, E. *Nat. Chem.* **2011**, *3*, 856. (e) Albrecht, M.; Stortz, P.; Engeser, M.; Schalley, C. A. *Synlett*, **2004**, 2821.
10. (a) Dublin, S. N.; Conticello, V. P. *J. Am. Chem. Soc.* **2008**, *130*, 49. (b) Anzini, P.; Xu, C.; Hughes, S.; Magnotti, E.; Jiang, T.; Hemmingsen, L.; Demeler, B.; Conticello, V.P. *J. Am. Chem. Soc.* **2013**, *135*, 10278. (c) Nambiar, M.; Wang, L. S.; Rotello, V.; Chmielewski, J. *J. Am. Chem. Soc.* **2018**, *140*, 13028. (d) Nepal, M.; Sheedlo, M. J.; Das, C.; Chmielewski, J. *J. Am. Chem. Soc.* **2016**, *138*, 11051. (e) Tavenor, N. A.; Murnin, M. J.; Horne, S.W.; *J. Am. Chem. Soc.* **2017**, *139*, 2212.
11. (a) Przybyla, D. E.; Chmielewski, J. *J. Am. Chem. Soc.* **2008**, *130*, 12610. (b) Pires, M. M.; Chmielewski, J. *J. Am. Chem. Soc.* **2009**, *131*, 2706. (c) Przybyla, D.; Chmielewski, J. *J. Am. Chem. Soc.* **2010**, *132*, 7866.
12. (a) Sawada, T.; Matsumoto, A.; Fujita, M. *Angew. Chem. Int. Ed.* **2014**, *53*, 7228. (b) Sawada, T.; Yamagami, M.; Akinaga, S.; Miyaji, T.; Fujita, M. *Chem. Asian J.* **2017**, *12*, 1715. (c) Inomata, Y.; Sawada, T.; Fujita, M. *Chem.* **2020**, *6*, 294. (d) Sawada, T.; Fujita, M. *Chem.* **2020**, *6*, 1861.
13. (a) Hayen, A.; Schmitt, M. A.; Ngassa, F. N.; Thomasson, K.A.; Gellman, S. H. *Angew. Chem. Int. Ed.* **2004**, *43*, 505. (b) Baldauf, C.; Günther, R.; Hofmann, H. -J. *Biopolymers* **2006**, *84*, 408. (c) Sharma, G. V. M.; Nagendar, P.; Jayaprakash, P.; Krishna, P. R.; Ramakrishna, K. V. S.; Kunwar, A. C. *Angew. Chem. Int. Ed.* **2005**, *44*, 5878.
14. (a) Baldauf, C.; Günther, R.; Hofmann, H. -J. *J. Org. Chem.* **2006**, *71*, 1200. (b) Sonti, R.; Dinesh, B.; Basuroy, K.; Raghothama, S.; Shamala, N.; Balaram, P. *Org. Lett.* **2014**, *16*, 1656. (c) Fisher, B. F.; Gellman, S. H. *J. Am. Chem. Soc.* **2016**, *138*, 10766. (d) L. Guo, L.; Chi, Y. G.; Almeida, A. M.; Guzei, I. A.; Parker, B. K.; Gellman, S. H. *J. Am. Chem. Soc.* **2009**, *131*, 16018.
15. (a) Guo, L.; Almeida, A. M.; Zhang, W. A.; Reidenbach, G.; Choi, S. H.; Guzei, I. A.; Gellman, S. H. *J. Am. Chem. Soc.* **2010**, *132*, 7868. (b) Grison, C. M.; Robin, S.; Aitken, D. J. *Chem. Commun.* **2016**, *52*, 7802.
16. (a) Bandyopadhyay, A.; Gopi, H. N. *Org. Lett.* **2012**, *14*, 2770. (b) Jadhav, S. V.; Bandyopadhyay, A.; Gopi, H. N. *Org. Biomol. Chem.* **2013**, *11*, 509. (c) Veeresh, K.; Gopi, H. N. *Organic Letters.* **2019**, *21*, 4500.
17. Misra, R.; Saseendran, A.; Dey, S.; Gopi, H. N. *Angew. Chem. Int. Ed.* **2019**, *58*, 2251.
18. (a) Cheng, P.-N.; Pham, J. D.; Nowick, J. S. *J. Am. Chem. Soc.* **2013**, *135*, 5477. (b) Kreutzer, A. G.; Nowick, J. S. *Acc. Chem. Res.* **2018**, *51*, 706.

19. (a) Qin, L.; Wang, P.; Guo, Y.; Chen, C.; Liu, M. *Adv. Sci.* **2015**, *2*, 1500134. (b) Kim, H.-J.; Lee, J.-H.; Lee, M. *Angew. Chem. Int. Ed.* **2005**, *44*, 5810.
20. (a) Kawano, S.-I.; Fujita, N.; Shinkai, S. *J. Am. Chem. Soc.* **2004**, *126*, 8592. (b) Offiler, C. A.; Jonesa, C. D.; Steed, J. W. *Chem. Commun.* **2017**, *53*, 2024.
21. (a) Reches, M.; Gazit, E. *Science* **2003**, *300*, 625. (b) Gazit, E. *The FASEB Journal*. **2002**, *16*, 77. (c) Do, T. D.; Kincannon, W. M.; Bowers, M. T. *J. Am. Chem. Soc.* **2015**, *137*, 10080.
22. (a) Piepenbrock, M.-O. M.; Clarke, N.; Steed, J. W. *Soft Matter* **2011**, *7*, 2412. (b) Pazos, E.; Sleep, E.; Rubert Pérez, C. M.; Lee, S. S.; Tantakitti, F.; Stupp, S. *J. Am. Chem. Soc.* **2016**, *138*, 5507.
23. (a) Grison, C. M.; Robina, S.; Aitken, D. J. *Chem. Commun.*, **2016**, *52*, 7802. (b) Shin, Y. -H.; Gellman, S. H. *J. Am. Chem. Soc.* **2018**, *140*, 1394. (c) Bandyopadhyay, A.; Jadhav, S. V.; Gopi, H. N. *Chem. Commun.*, **2012**, *48*, 7170.
24. (a) Litvinov, R. I.; Faizullin, D. A.; Zuev, Y. F.; Weisel, J. W. *Biophysical Journal* **2012**, *103*, 1020. (b) Montalvo, G.; Waegele, M. M.; Shandler, S.; Gai, F.; DeGrado, W. F. *J. Am. Chem. Soc.* **2010**, *132*, 5616.
25. (a) Lloyd, G. O.; Steed, J. W. *Nature Chemistry* **2009**, *1*, 437. (b) Steed, J. W. *Chem. Soc. Rev.* **2010**, *39*, 3686.
26. (a) Zhou, H. -C.; Long, J. R.; Yaghi, O. M. *Chem. Rev.* **2012**, *112*, 673. (b) Furukawa, H.; Cordova, K.; O'Keeffe, E. M.; Yaghi, O. M. *Science* **2013**, *341*, 1230444; (c) Zhou, H. -C.; Kitagawa, S. *Chem. Soc. Rev.* **2014**, *43*, 5415.
27. Wu, H.; Zheng, J.; Kjøniksen, A. -L.; Wang, W.; Zhang, Y.; Ma, J. *Adv. Mater.* **2019**, *31*, 1806204.
28. Sheldrick, G. M. *Acta Crystallography. Sect A.* **1990**, *46*, 467.
29. Spek, A. L. *Acta Crystallogr.* **1990**, *A46*, C34.

## 8. $^1\text{H}$ , $^{13}\text{C}$ NMR and Mass Spectra of Peptides (P1-P7):

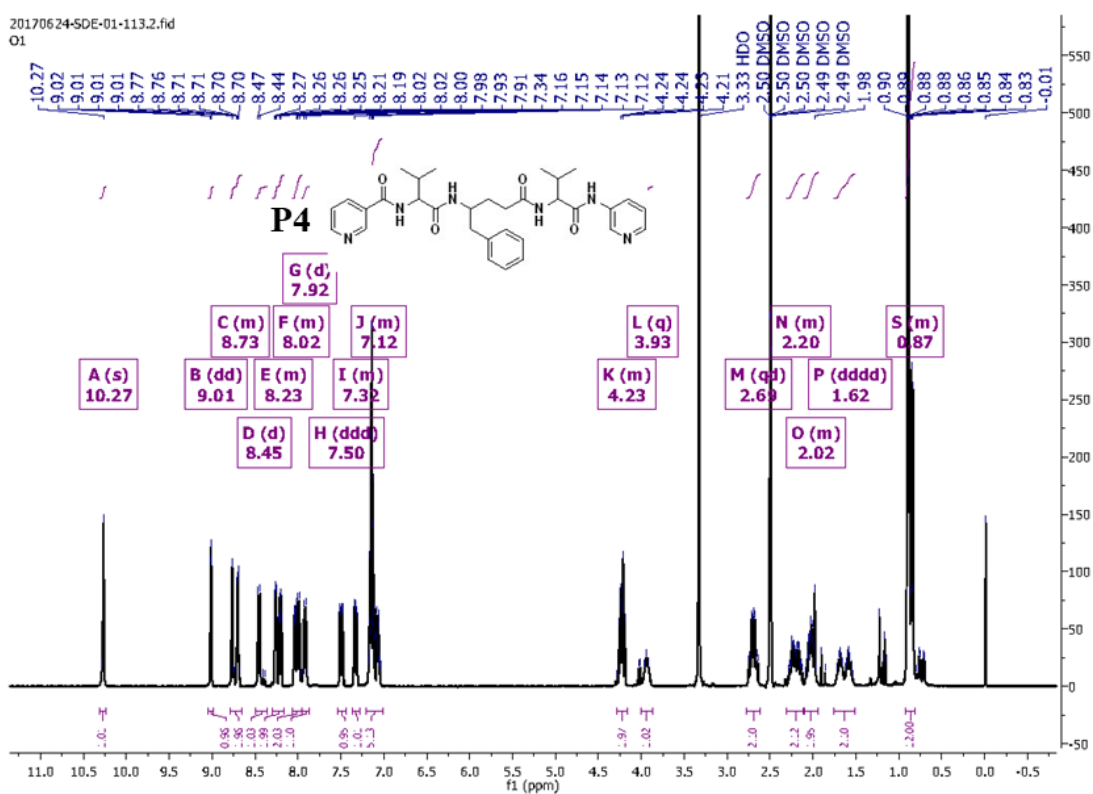




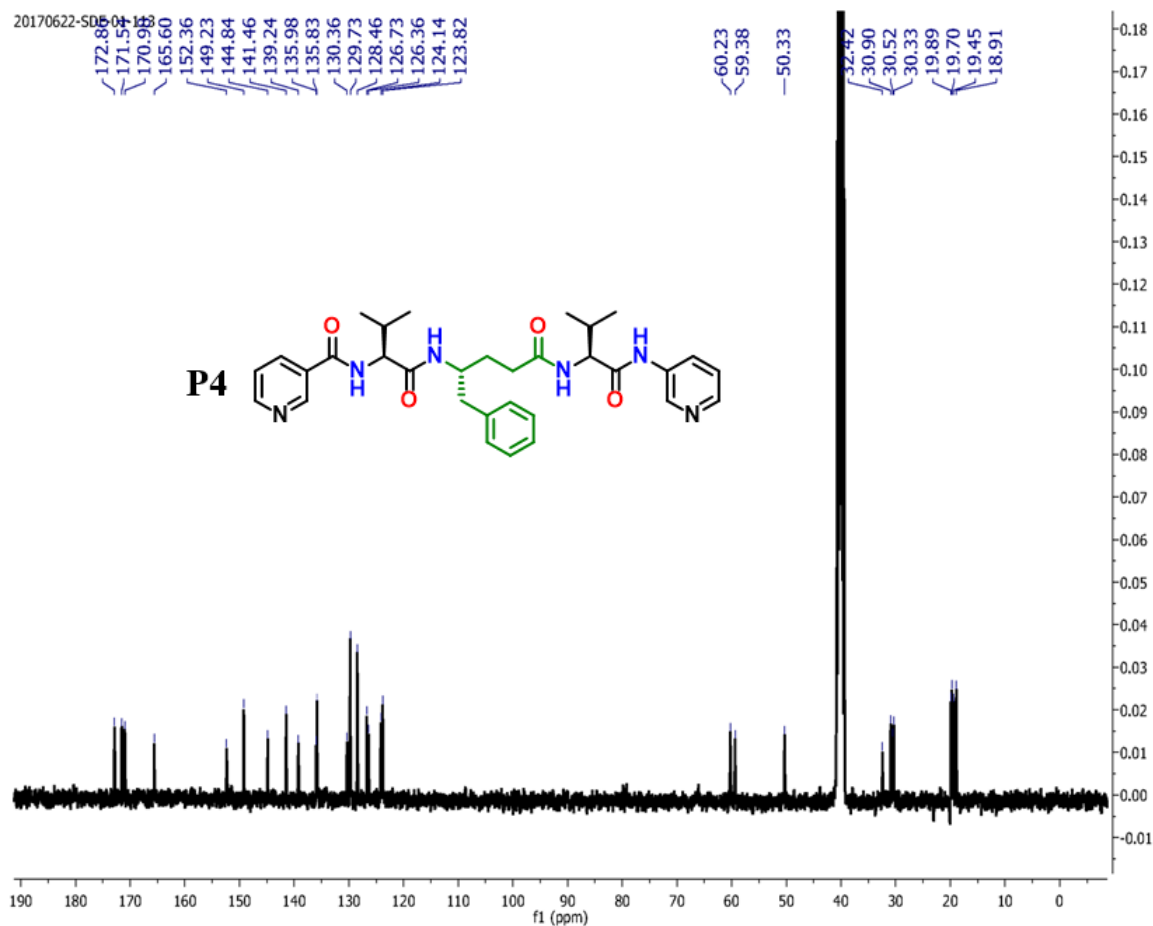


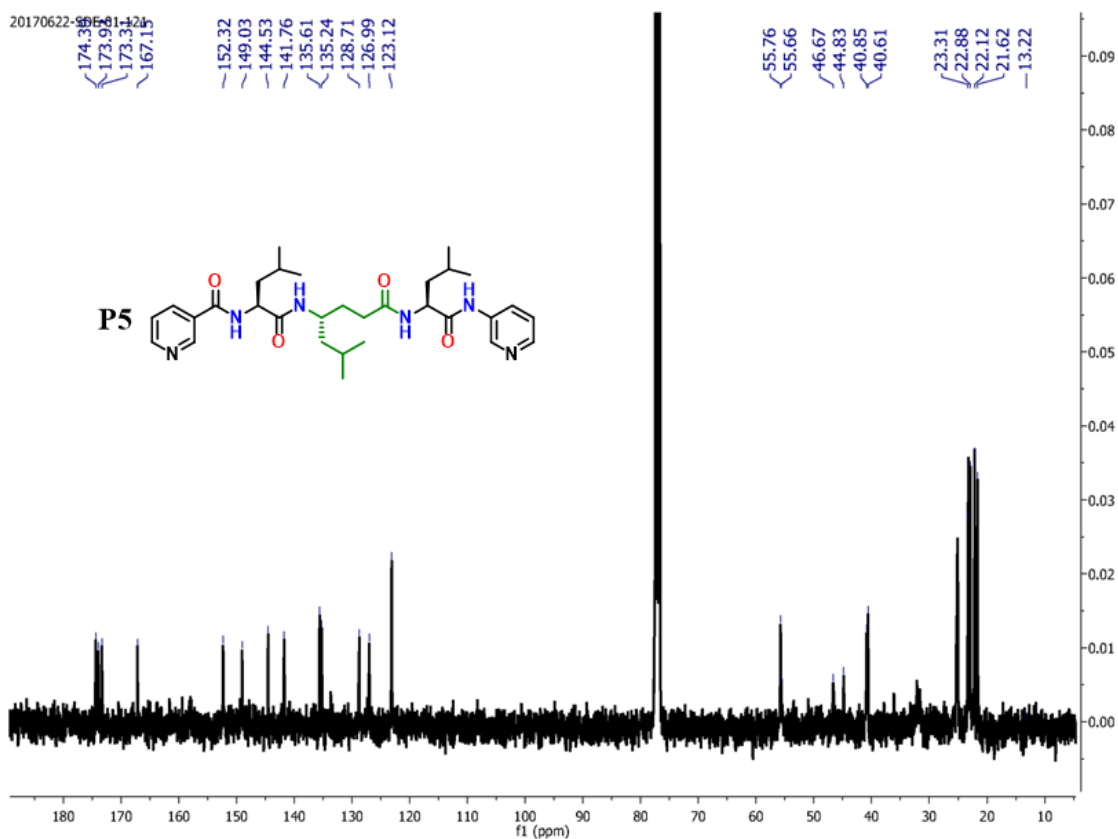
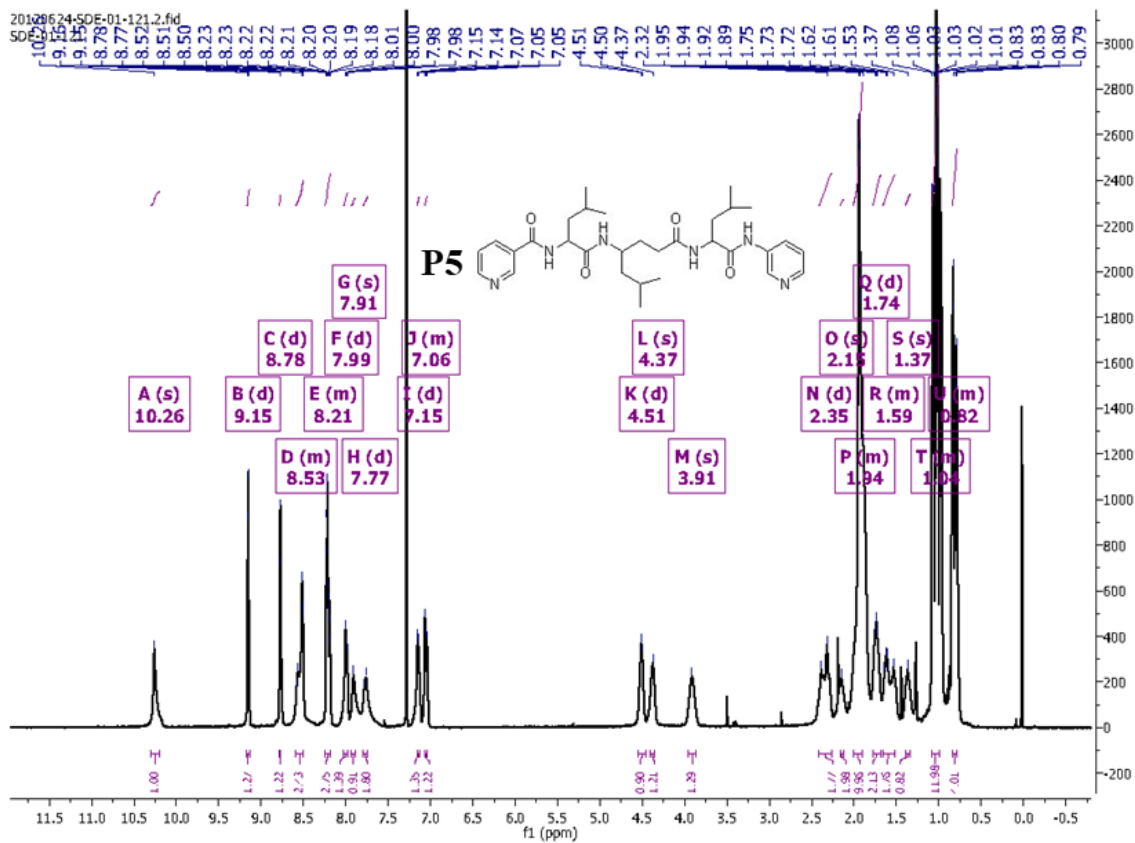


20170624-SDE-01-113.2.fid  
01

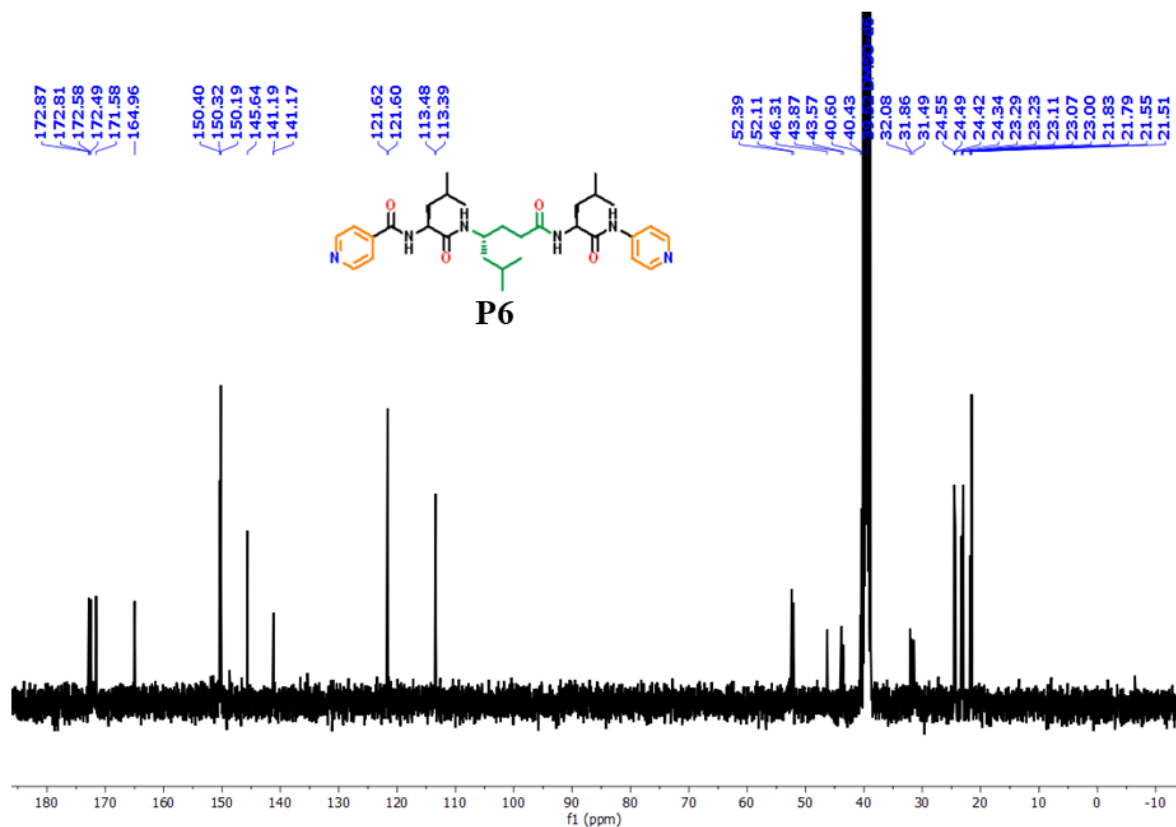
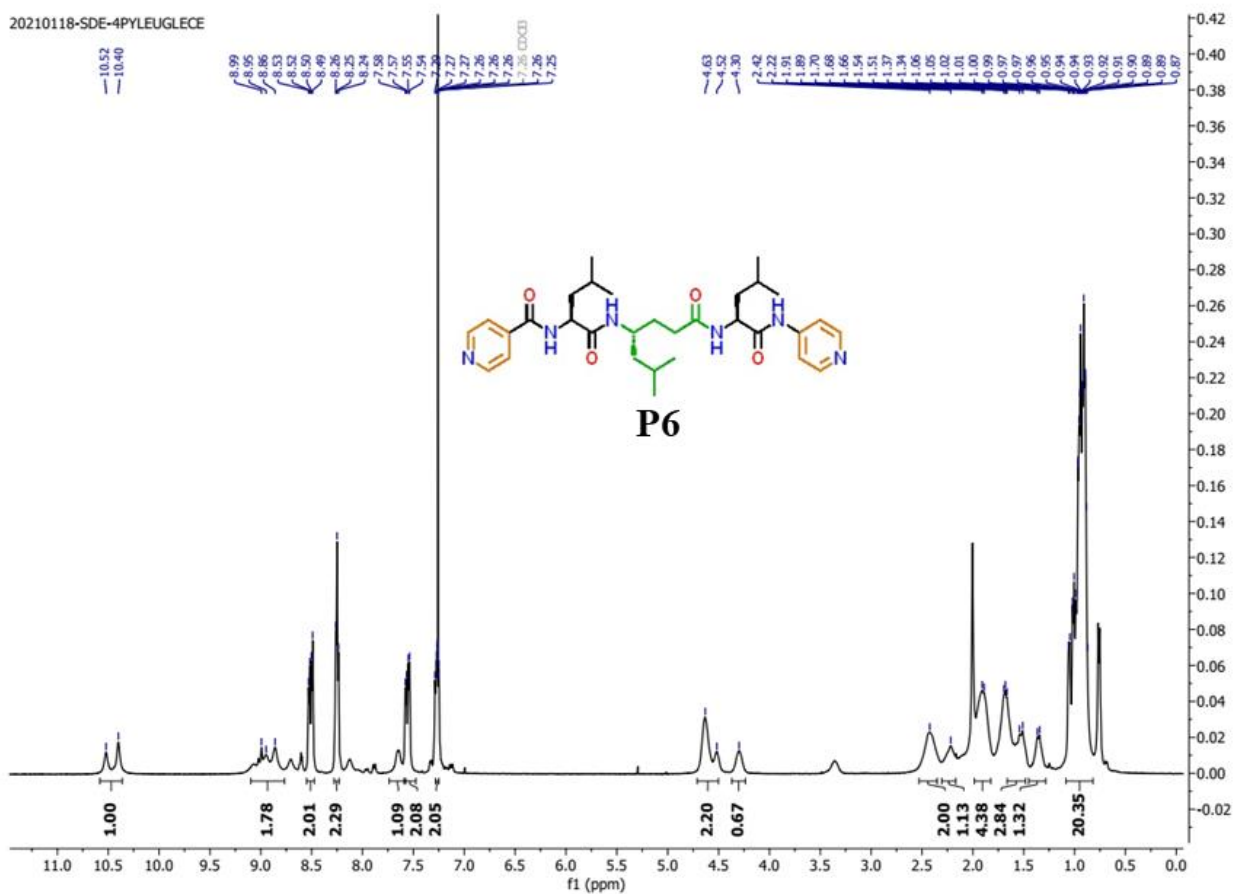


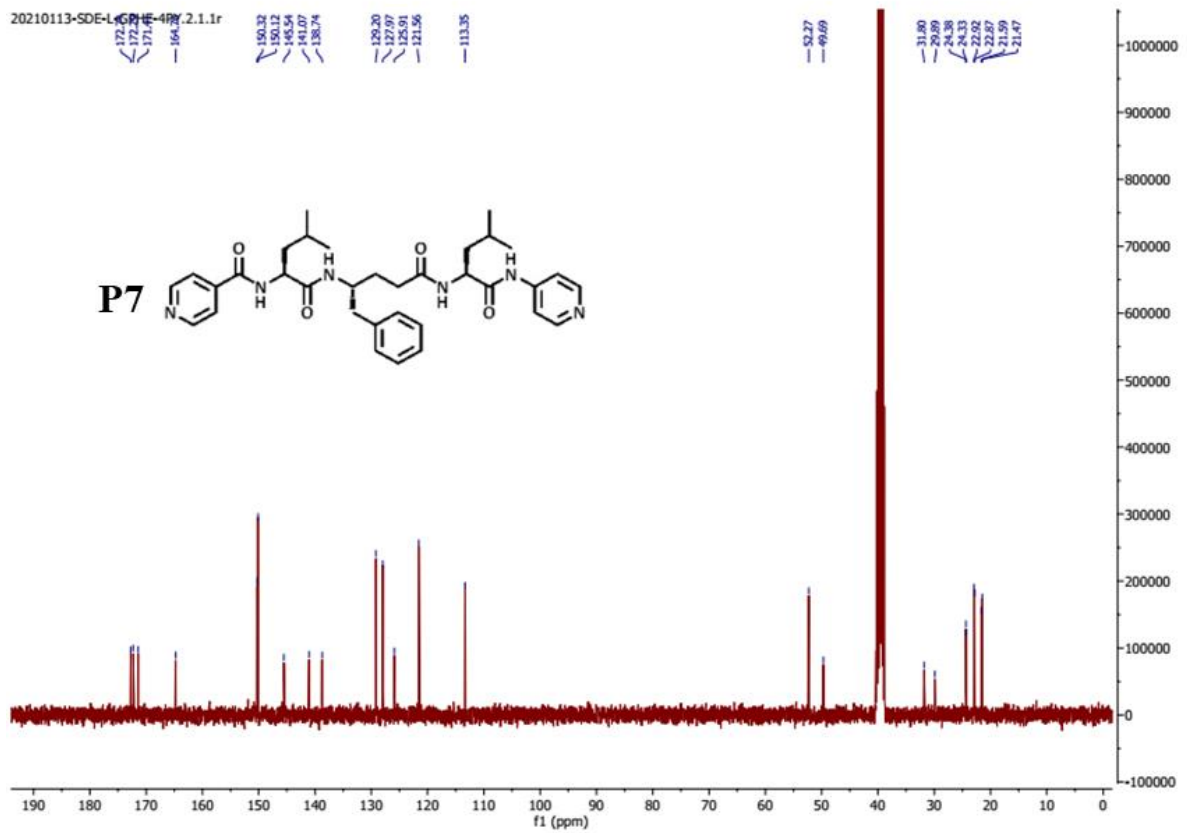
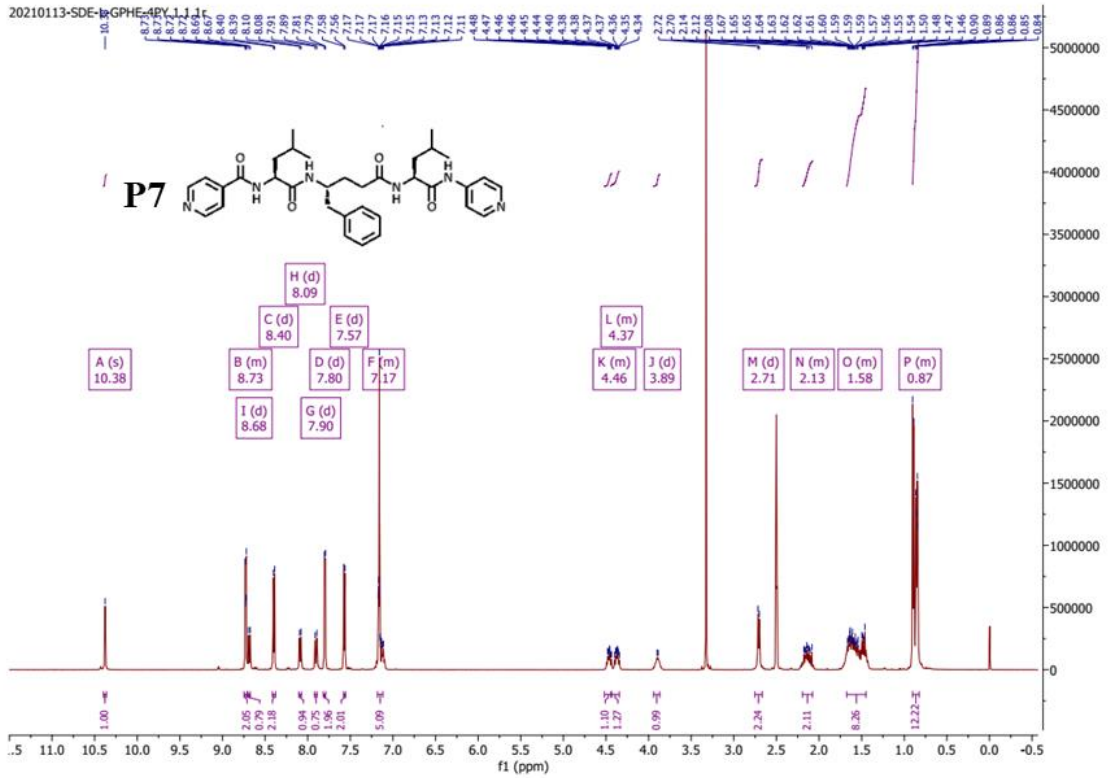
20170622-SDE





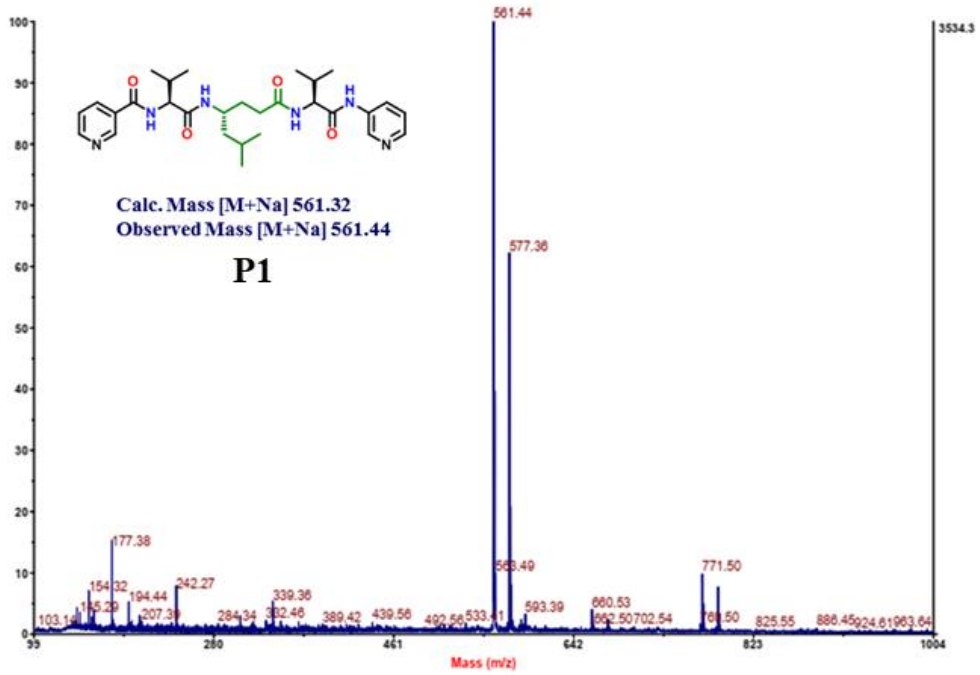
20210118-SDE-4PYLEUGLECE





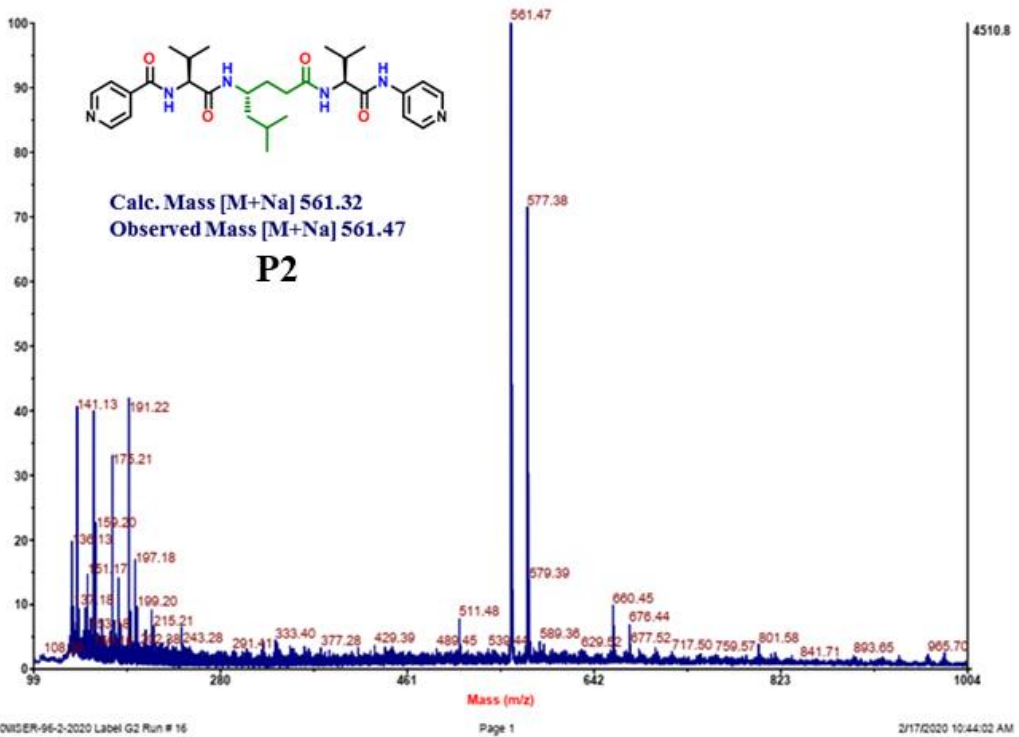
Spectrum Report

Final - Shots 400 - IISER-96-2-2020; Run #16; Label G1



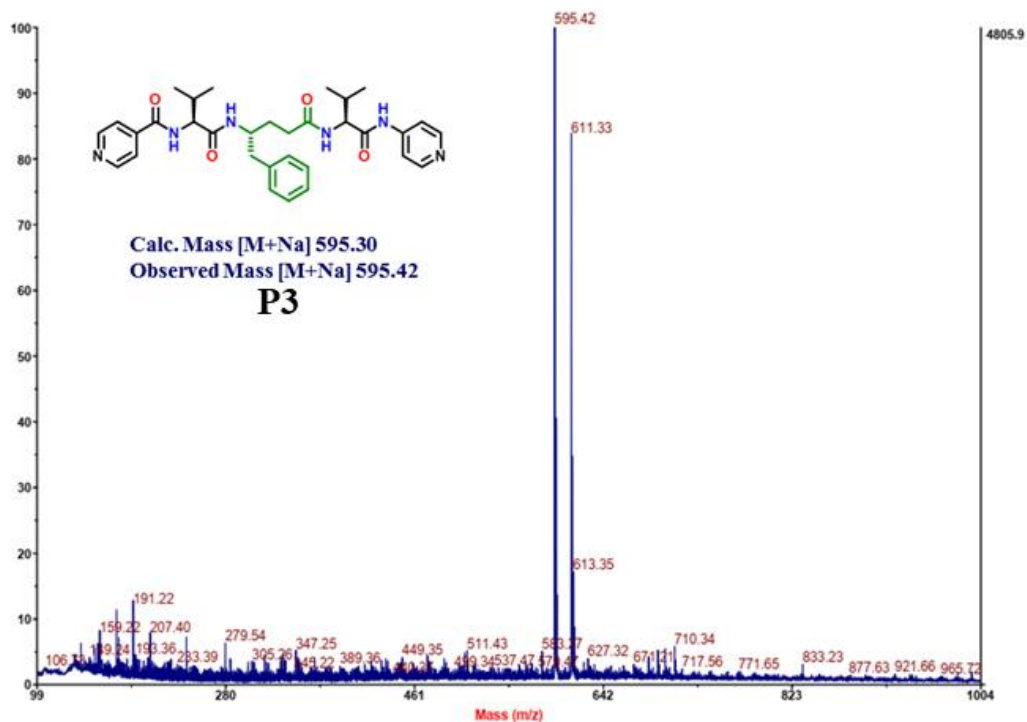
Spectrum Report

Final - Shots 400 - IISER-96-2-2020; Run #16; Label G2



### Spectrum Report

Final - Shots 400 - IISER-96-2-2020; Run #16; Label G3



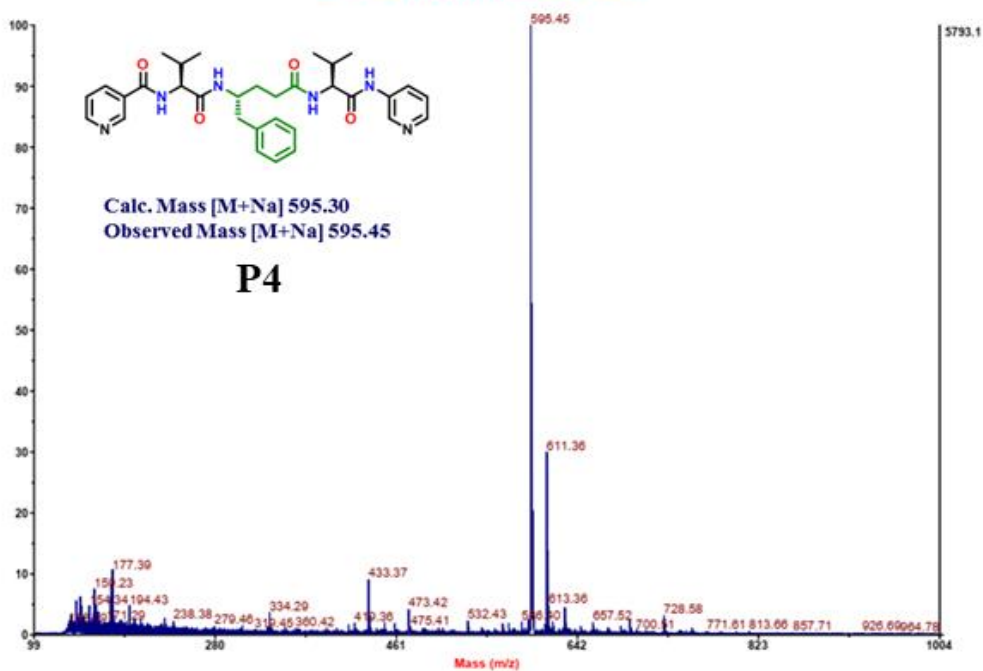
2020IISER-96-2-2020 Label G3 Run # 16

Page 1

2/17/2020 10:40:44 AM

### Spectrum Report

Final - Shots 400 - IISER-96-2-2020; Run #16; Label G4



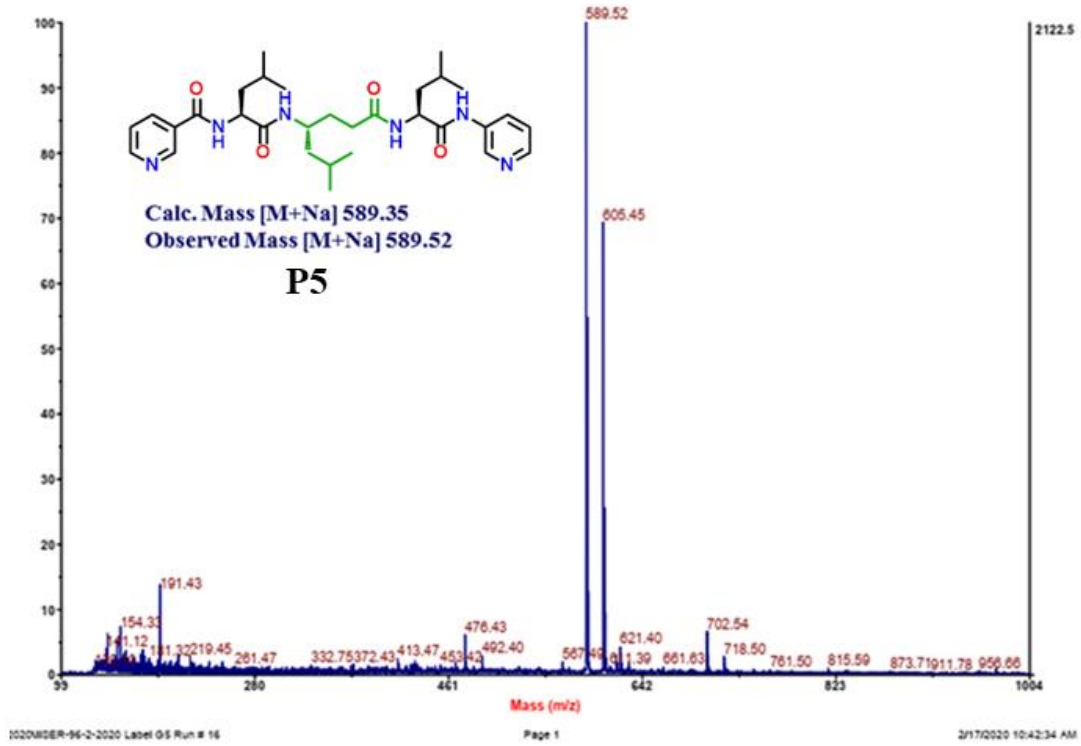
2020IISER-96-2-2020 Label G4 Run # 16

Page 1

2/17/2020 10:41:38 AM

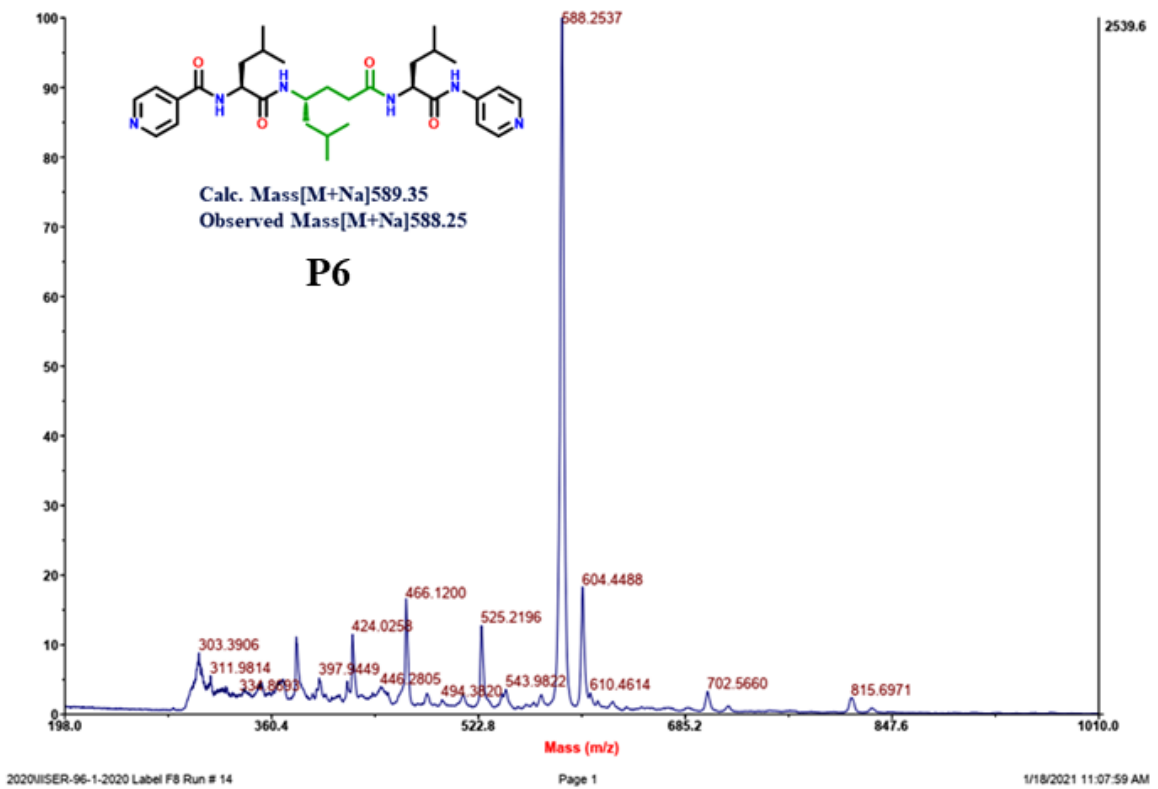
Spectrum Report

Final - Shots 400 - IISER-96-2-2020; Run #16; Label G5



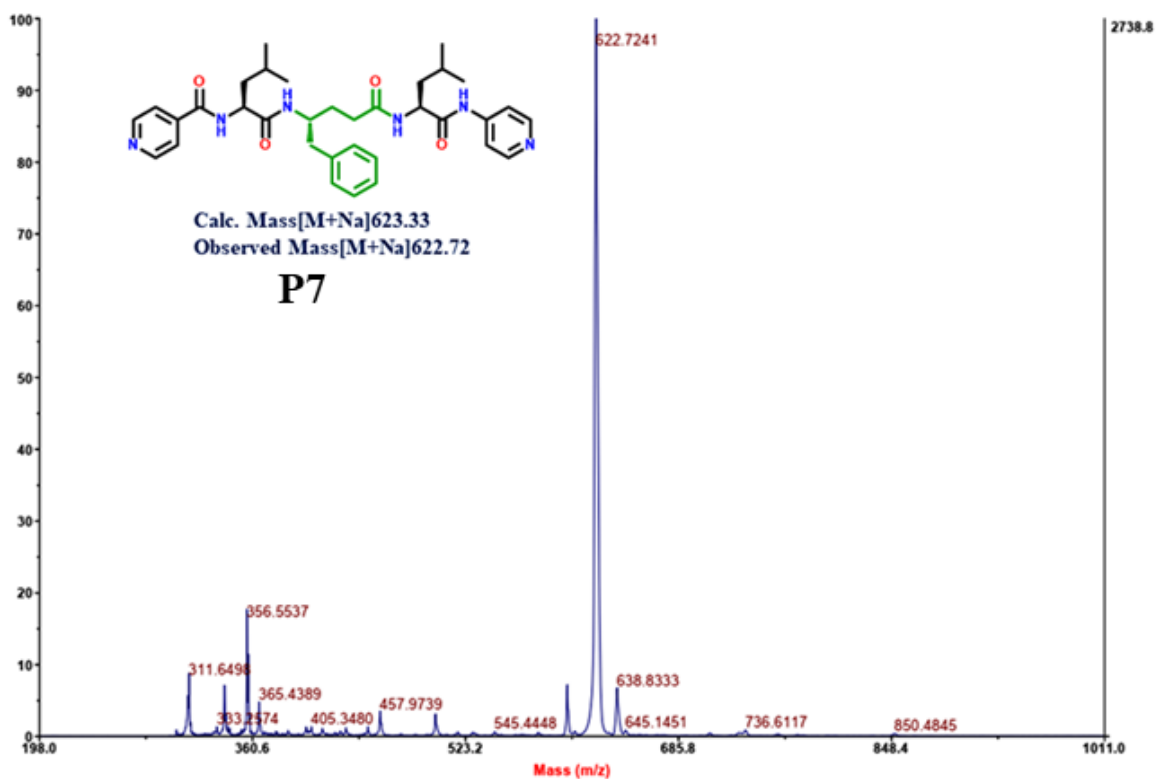
Spectrum Report

Final - Shots 2000 - IISER-96-1-2020; Run #14; Label F8



# Spectrum Report

Final - Shots 2000 - #SER.96.1.2020; Run #14; Label G6







### Metal-Coordinated Supramolecular Polymers from the Minimalistic Hybrid Peptide Foldamers

Author: Hosahudya N. Gopi, Saikat Pahan, Abhijith Saseendran, et al

Publication: Angewandte Chemie International Edition

Publisher: John Wiley and Sons

Date: Mar 17, 2021

© 2021 Wiley-VCH GmbH

#### Order Completed

Thank you for your order.

This Agreement between SANJIT DEY ("You") and John Wiley and Sons ("John Wiley and Sons") consists of your order details and the terms and conditions provided by John Wiley and Sons and Copyright Clearance Center.

License number      Reference confirmation email for license number

License date      Nov, 13 2022

#### 📄 Licensed Content

Licensed Content Publisher	John Wiley and Sons
Licensed Content Publication	Angewandte Chemie International Edition
Licensed Content Title	Metal-Coordinated Supramolecular Polymers from the Minimalistic Hybrid Peptide Foldamers
Licensed Content Author	Hosahudya N. Gopi, Saikat Pahan, Abhijith Saseendran, et al
Licensed Content Date	Mar 17, 2021
Licensed Content Volume	60
Licensed Content Issue	18
Licensed Content Pages	6

#### 📁 Order Details

Type of use	Dissertation/Thesis
Requestor type	Author of this Wiley article
Format	Print and electronic
Portion	Full article
Will you be translating?	No

#### 📄 About Your Work

Title	Construction of Ordered Self-assembled Architectures from Peptide Foldamers Composed of Non-natural Amino Acids
Institution name	INDIAN INSTITUTE OF SCIENCE EDUCATION AND RESEARCH, PUNE
Expected presentation date	May 2023

#### 📁 Additional Data

📍 Requestor Location		📄 Tax Details	
Requestor Location	Mr. SANJIT DEY Hoste-2, SER PUNE Dr. Homi Bhabha Road, Pashan Pune Pune, Maharashtra 411008 India Attn: Mr. SANJIT DEY	Publisher Tax ID	EU826007151
📄 Billing Information		\$ Price	
Billing Type	Invoice	Total	0.00 USD
Billing address	Mr. SANJIT DEY Hoste-2, SER PUNE Dr. Homi Bhabha Road, Pashan Pune Pune, India 411008 Attn: Mr. SANJIT DEY		

Would you like to purchase the full text of this article? If so, please continue on to the content ordering system located here: [Purchase PDF](#)  
 If you click on the buttons below or close this window, you will not be able to return to the content ordering system.

**Total: 0.00 USD**

[CLOSE WINDOW](#)